Beyond standard assumptions on neural excitability: when channels cooperate or capacitance varies

DISSERTATION
zur Erlangung des akademischen Grades

Doctor rerum naturalium
(Dr. rer. nat.)
im Fach Biologie (Theoretische Biologie)

eingereicht an der
Lebenswissenschaftlichen Fakultät
Humboldt-Universität zu Berlin

von

Paul Pfeiffer

M. Sc.

Präsidentin der Humboldt-Universität zu Berlin:
Prof. Dr. Julia von Blumenthal

Dekan der Lebenswissenschaftlichen Fakultät der Humboldt-Universität zu Berlin:
Prof. Dr. Dr. Christian Ulrichs

GutachterInnen:

1. Prof. Dr. Susanne Schreiber
2. Prof. Dr. Julijana Gjorgjieva
3. Prof. Dr. Dietmar Schmitz

Tag der mündlichen Prüfung: 28.10.2022

Abstract

Electrical signaling in neurons is shaped by their specialized excitable cell membranes. Commonly, it is assumed that the ion channels embedded in the membrane gate independently and that the electrical capacitance of neurons is constant. However, not all excitable membranes appear to adhere to these assumptions. On the contrary, ion channels are observed to gate cooperatively in several circumstances and also the notion of one fixed value for the specific membrane capacitance (per unit area) across neuronal membranes has been challenged recently. How these deviations from the original form of conductance-based neuron models affect the electrical properties of nerve cells has not been extensively explored and is the focus of this cumulative thesis.

In the first project, strongly cooperative voltage-gated ion channels are proposed to provide a membrane potential-based mechanism for cellular short-term memory. Based on a mathematical model of cooperative gating, it is shown that coupled channels assembled into small clusters act as an ensemble of bistable conductances. The correspondingly large memory capacity of such an ensemble yields an alternative explanation for graded forms of cell-autonomous persistent firing – a firing mode observed in several brain regions that could serve to store transient information in the activity levels of single cells. Accordingly, this mnemonic firing mode could be evoked in biological neurons by "injection" of cooperative channels via the dynamic clamp. Cooperative gating might hence present a form of cellular positive feedback that complements other memory-serving feedback mechanisms on the network level.

In the second project, a novel dynamic clamp protocol – the capacitance clamp – is developed to artificially modify capacitance in biological neurons. Experimental means to systematically investigate capacitance, a basic parameter shared by all excitable cells, had previously been missing. The technique, thoroughly tested in simulations and experiments, is shown to alter the membrane time constant and the cell impedance as expected for a capacitance change. By monitoring how capacitance thereby affects temporal integration and energetic costs of spiking in dentate gyrus granule cells, it is demonstrated how the capacitance clamp will serve as a new tool to characterize a neuron's dynamical repertoire and to understand the adaptive function of exceptional capacitance values.

Summarizing, this thesis predicts a new role for cooperative gating as an efficient neuronal memory mechanism and provides a precise and robust method to study capacitance variations in real neurons. Combined, the projects identify

computationally relevant consequences of these often neglected facets of neuronal membranes and extend the modeling and experimental techniques to further study them.

Zusammenfassung

Die elektrische Signalverarbeitung in Nervenzellen basiert auf deren erregbarer Zellmembran. Üblicherweise wird angenommen, dass die in der Membran eingebetteten leitfähigen Ionenkanäle nicht auf direkte Art gekoppelt sind und dass die Kapazität des von der Membran gebildeten Kondensators konstant ist. Allerdings scheinen diese Annahmen nicht für alle Nervenzellen zu gelten. Im Gegenteil, verschiedene Ionenkanäle "kooperieren" (im Sinne einer gekoppelten Steuerung) und auch die Vorstellung von der spezifischen Membrankapazität als eine universale biologische Konstante wurde kürzlich in Frage gestellt. Wie sich diese Abweichungen, die in der klassischen Version von Neuronenmodellen nicht abgebildet werden, auf die elektrischen Eigenschaften von Nervenzellen auswirken, ist die Ausgangsfrage der folgenden kumulativen Dissertationsschrift.

Im ersten Projekt wird gezeigt, auf welche Weise stark kooperative spannungsabhängige Ionenkanäle eine Form von zellulärem Kurzzeitspeicher für elektrische Aktivität bilden könnten. Solche kooperativen Kanäle treten in der Membran häufig in kleinen räumlich getrennte Clustern auf. Basierend auf einem mathematischen Modell wird nachgewiesen, dass solche Kanalcluster als eine bistabile Leitfähigkeit agieren. Die dadurch entstehende große Speicherkapazität eines Ensembles dieser Kanalcluster könnte von Nervenzellen für stufenloses persistentes Feuern (GPA von der englischen Bezeichnung "graded persistent activity") genutzt werden – ein Feuerverhalten, beobachtbar in verschiedenen Hirnregionen, das dazu dienen könnte, Information kurzfristig in dem Aktivitätsniveau einzelner Neuronen abzuspeichern. Entsprechend dieser Hypothese konnte, GPA, dieser mnemonische Feuermodus, in modellierten und biologischen Nervenzellen durch das Hinzufügen von kooperativen Kanälen aktiviert werden, wobei für die experimentelle Demonstration die Kanäle über die "Dynamic Clamp" Technik emuliert wurden. Kooperative Interaktionen zwischen Kanälen könnten demnach einen positiven Rückkopplungsmechanismus darstellen, der weitere Rückkopplungsschleifen für das Kurzzeitgedächtnis auf der Netzwerkebene unterstützt.

Im zweiten Projekt wird ein neues Dynamic Clamp Protokoll entwickelt, der Capacitance Clamp, das erlaubt, Änderungen der Membrankapazität in biologischen Nervenzellen zu emulieren. Eine solche experimentelle Möglichkeit, um systematisch die Rolle der Kapazität zu untersuchen, gab es bisher nicht. Eine Reihe von Tests in Simulationen und Experimenten bestätigt, dass die durch den Capacitance Clamp emulierten Kapazitätsänderungen das elektrische

Verhalten von Nervenzellen wie erwartet ändern, zum Beispiel deren Membranzeitkonstante oder deren Impedanz. Die Technik wurde anschließend in Experimenten mit Körnerzellen des *Gyrus dentatus* genutzt, um den Einfluss von Kapazität auf die zeitliche Summierung von Signalen und die energetischen Kosten von Spikes zu messen. Diese ersten Demonstrationen zeigen, wie der Capacitance Clamp in der Zukunft dazu beitragen kann, die elektrische Dynamik von Nervenzellen eingehender zu charakterisieren und die adaptive Funktion von Kapazitätsanpassungen zu verstehen.

Die zwei Hauptresultate dieser Doktorarbeit sind damit eine Hypothese über die Funktion von kooperativen Ionenkanälen als zellbasierter effizienter Gedächtnis-mechanismus und eine präzise Methode, um Kapazitätsänderungen erstmals im Experiment zu untersuchen. Die Kombination beider Projekte zeigt die Relevanz dieser oft vernachlässigten Facetten von neuronalen Membranen für die Signalverarbeitung in Nervenzellen und erweitert die Modell-basierten und experimentellen Techniken zu deren Untersuchung.

Contents

1 Introduction

Human life starts with a single cell. At birth, after a dramatic expansion in numbers and types, the human body consists of a staggering 30 trillion cells (Sender, Fuchs, and Milo 2016), with on the order of 100 billion neurons among them (Herculano-Houzel 2009). These specialized nerve cells are the main signaling units in the brain, the organ which endows the newborn with the ability to act, perceive, learn, think and feel.

A distinguishing property of neurons in human and other animal brains is their ability to process fast electrical signals via excitable membranes and to share these signals in networks with other neurons via plastic synapses. Among neurons, however, electrical properties are again highly diverse and can be linked to different signaling capabilities – a link often studied in mathematical neuron models. In this realm, the cumulative thesis presented here explores phenomena of neuronal membranes that require revising common assumptions of neural modeling: cooperative ion channels and altered cell capacitance.

A priori, it is unclear which physiological properties of neurons, sometimes dismissively deemed "biological details", are crucial to understand brain dynamics and function. Neurons differ in many aspects, but major factors are the specific combination of ion channels they express and the typical morphology they are shaped in. Systematically mapping channels and the cell membrane to equivalent electrical circuits, conductance-based neuron models can capture these differences among neuron types and characterize the associated repertoire of electrical dynamics. Models of this type reproduce a wide variety of experimentally observed firing patterns and can be used to explore the processing capabilities of neurons. A conductance-based model of a cortical pyramidal cell, for example, shows that accurately capturing the input-output mapping of this major neuron type by a net of drastically simplified "neuron units" requires a "deep" multi-layered architecture (Gidon et al. 2020; Beniaguev, Segev, and London 2021). Biological complexity of neurons hence appears as a compact mean to increase their functional repertoire.

Despite the versatility of conductance-based neuron models, their standard formulation still relies on simplifying assumptions about channel and membrane biophysics that are rarely questioned. Motivated by experimentally observed exceptions of these assumptions, this cumulative thesis explores their conse-

quences for electrical dynamics and their potential role in neuronal function in two cases.

Publication COOPMEM is based on the observation that certain ion channels cooperate (Pfeiffer et al. 2020). Direct physical feedback between them affects how they control the flow of ions across the membrane, a form of gating excluded in the standard formulation of channel dynamics by the independent gating assumption. The main contribution of this work consists in a modeling-based demonstration that small clusters of cooperative ion channels can mediate neuronal firing suited to temporarily store past inputs. Cell-autonomous short-term memory of this form has been observed in neurons from different brain regions but is challenging to explain by independent channel gating alone. The hypothesis of cooperative gating as a memory mechanism put forward here demonstrates the potential for cooperativity to build local channel networks with new dynamical and computational roles.

Publication CAPCLAMP shifts the focus from ion channels to the membrane capacitance, often treated as a biological constant and rarely considered as a determinant of neuronal dynamics (Pfeiffer et al. 2022). The central result of this work is the capacitance clamp – a closed-loop intracellular recording mode inspired by the dynamic clamp technique to emulate capacitance changes in biological neurons. Built on firm theoretical grounds, the technique is tested in simulations and demonstrated in experiments with rodent dentate gyrus granule cells. In proof-of-principle applications, the capacitance clamp is used to experimentally study how neuronal signaling and energy consumption is affected when varying capacitance – questions on exceptional capacitance values that previously could only be addressed via models and simulations.

Together, these two research articles propose how ion channel cooperativity and alteration of cell capacitance, still perceived as exceptions to the biological rule, can serve the versatile and efficient signaling of neurons and other excitable cells. To prepare the explorations of these deviations, the following background chapter first introduces standard conductance-based neuron models and the dynamic clamp technique, the two main tools used in this thesis. It then reviews evidence for neuronal membranes where channels cooperate and capacitance varies and summarizes previous work on their dynamical and functional roles. In a synthesis of these ideas, the subsequent chapter on research aims identifies and motivates the concrete questions addressed in the presented publications. The final discussion chapter critically examines the biological plausibility of cellular cooperativity-based memory and its implications on the network level, assesses future applications and limitations of the capacitance clamp technique, and presents directions to further investigate these aspects of neuronal specialization.

2 Background

2.1 Neuronal dynamics and computation

Brains flexibly control the complex behavior of animals. The major question of neuroscience is how the networks of connected neurons in a brain achieve this computationally demanding control. An additional challenge is to understand how brains perform these functions in an energy-efficient manner. In a bottom-up approach, the computations performed by a single neuron form a natural starting point to approach this question.

Neurons compute by transforming the electrical signals they receive from other cells to their own activity pattern. The main steps of this mapping, synaptic transmission, dendritic integration and non-linear spike generation, can be mathematically characterized in neuron models (Koch 1999; Brunel, Hakim, and Richardson 2014). Still, it is not fully understood, which depth of physiological details is required in a model to capture the essential dynamical and computational repertoire of a biological neuron. The following background sections prepare the ground for the exploration of two rarely questioned modeling paradigms on neuronal physiology: independence of ion channel gating and constancy of the membrane capacitance.

2.1.1 Firing patterns: dynamical repertoire of neurons

The electrical signal of a neuron is its membrane potential, the voltage difference between in- and outside of the cell. Dynamics of the membrane potential are extremely diverse among neurons; a zoo of electrophysiological phenotypes revealed by an ever-growing body of studies on single neuron dynamics. The Allen Cell Brain Atlas, for example, a large-scale recording effort, provides open access to the electrical activity of thousands of human and mouse neurons obtained in standardized stimulation protocols as illustrated in Figure 2.1 A and B (Gouwens et al. 2019). A pattern shared across neurons is the action potential, a brief millisecond-long rise of the membrane potential, which is the signal communicated to other cells. Crucial for signaling is what makes a neuron fire – its specific mapping of input into a temporal firing pattern of action potentials.

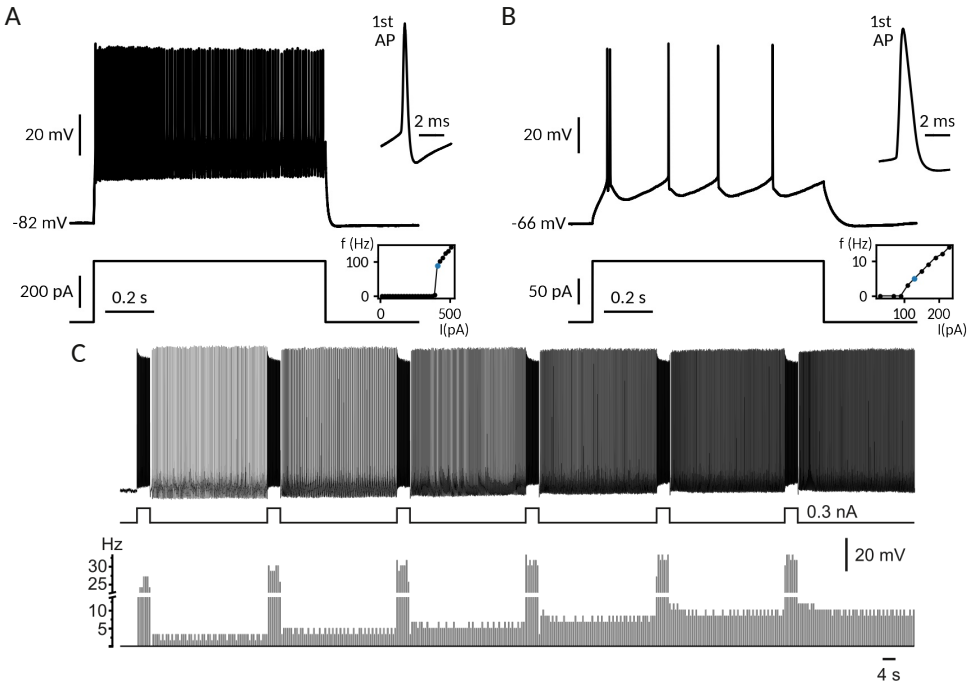

Figure 2.1: Firing patterns of neurons: **A, B** Illustration of membrane potential traces (*top*) and current stimulation (*bottom*) in recordings of a mouse (A) and a human (B) cell from the openly available brain cell database by the Allen Institute (available at celltypes.brain-map.org with IDs A: 321708130 and B: 567763632)[1]. The insights show an enlarged view of the first action potential and a frequency-current (fI) curve for different stimulation strengths. **C** Exemplary illustration of graded persistent activity obtained from principal cells in rat entorhinal cortex layer V. Different from a typical neuron, these cells continue to fire (*top*) after a transient current pulse (*middle*). Moreover, the frequency of this persistent firing is graded and can be further increased by additional pulses (*bottom*), modified from Egorov et al. 2002 with permission.

Neuronal firing patterns are investigated with respect to their biophysical origin (Hodgkin and Huxley 1952; Koch 1999), the mathematical principles governing their dynamics, and their computational role (Izhikevich 2006; Brunel, Hakim, and Richardson 2014).

A well-understood example in this regard is the experimental classification of excitability into class 1 and class 2 firing (Hodgkin 1948). In response to current stimulation, class 1 neurons begin to fire at arbitrarily low spiking frequencies

[1]While there are species-specific properties of neurons (Eyal et al. 2016; Hodge et al. 2019), the distinct firing patterns shown here are rather a signature of different neuron types present across species.

and then continuously increase their firing for larger current amplitudes. In contrast, class 2 neurons start to fire at a non-zero frequency which remains relatively constant when currents are increased further. These two excitability classes have been reproduced in biophysically grounded neuron models and have been traced back to a difference in the corresponding dynamical (bifurcation) types underlying the transition from silent rest to active spiking (Izhikevich 2006): class 1 excitability to the saddle-node-on-invariant cycle (SNIC) bifurcation and class 2 to the subcritical Hopf bifurcation (Izhikevich 2006; Hesse, Schleimer, and Schreiber 2017).

Following from these differences in neural dynamics are differences in processing. Class 1 SNIC-type neurons act as leaky integrators, summing input until a threshold for firing is reached, whereas class 2 Hopf-type neurons act as resonators, preferably responding to input with a specific frequency. Recently, the computational implications of a third dynamical type of action potential generation have received increased attention, the homoclinic orbit (HOM) bifurcation (Hesse, Schleimer, and Schreiber 2017; Hesse et al. 2022). Experimentally, neurons of the HOM-type, however, remain more difficult to identify, because they exhibit mixed characteristics of both "classical" excitability classes: their fI curves are discontinuous class 2-like when increasing the input from rest to spiking but become continuous class 1-like in the opposite direction when decreasing currents from spiking to rest. Multiple other classes of firing patterns and their dynamical underpinnings have been characterized in similar ways, for example bursting (Izhikevich 2004). While this dynamical viewpoint is one the factors motivating the development of the capacitance clamp technique in Publication CAPCLAMP, the main focus in the following lies on the underlying biophysics of neurons.

Surprisingly, the biophysical underpinning of neuronal firing patterns is often still difficult to identify or even remains elusive. One challenge is degeneracy. In the large set of ion channels governing the electrical activity of a neuron, many channel types exhibit similar overlapping functions (Goaillard and Marder 2021). As a result there are many combinations of channels that produce a specific firing pattern (Prinz, Bucher, and Marder 2004). The actual set of channels, however, can be decisive to understand how a neuron responds to perturbations like a change in temperature, potentially involving a switch of its firing type (Ratliff et al. 2021). In contrast, some firing patterns are difficult to explain at all. One intriguing example is graded persistent activity (GPA) observed in principal cells from the entorhinal cortex and perirhinal cortex (Egorov et al. 2002). These neurons continue to fire for multiple seconds after a sufficiently strong stimulation and the frequency of this persistent firing increases in a quasi-continuous manner after each stimulation (see Fig. 2.1

C). Moreover, transient strong suppression of firing decreases the frequency of persistent firing and if applied repeatedly returns the neuron to its original silent rest state. Functionwise, such neurons are hypothesized to form electrical analogue memories of previous inputs. The required multi-stability or continuous attractor, however, are difficult to attain within the standard formulation of neuron models (Fransén et al. 2006).

2.1.2 Conductance-based neuron models

Conductance-based neuron models capture the dynamics of the membrane potential by mapping an excitable cell to an equivalent electrical circuit (Koch 1999). Such an equivalent circuit model provides a set of equations that describe the temporal (and optionally spatial) evolution of the membrane potential, the state of the ion channels and the corresponding ionic currents. Its canonical form as proposed by Hodgkin and Huxley provided the first mechanistic explanation of the action potential (Hodgkin and Huxley 1952). Once termed the "closest that neurophysiologists have to Newton's laws of motion" (Gutkin and Ermentrout 2006), the Hodgkin-Huxley formalism represents the theoretical framework to understand the electrical dynamics of neurons and synapses. The following introduction to this framework focuses on its underlying assumptions about ion channels and the cellular membrane. From this re-examination, the section motivates the variations of the original Hodgkin-Huxley model explored in this thesis, namely the inclusion of cooperative interactions between channels and an altered membrane capacitance .

The assumptions linking neuronal physiology and the Hodgkin-Huxley model are best illustrated in the simple case of a *point neuron*, an idealized description of a small spherical cell. The basic circuit elements of the equivalent circuit are a capacitor representing the insulating double layer of lipids constituting the membrane itself in parallel to a set of passive and active conductors representing the ion channels embedded within (see Fig. 2.2). As the ion channels conduct ionic species with different reversal potentials, each conductor is combined in series with a corresponding battery. Additionally, a current source is added to mimic stimulation and recording of the neuron via an intracellular electrode.

According to current conservation, the sum of the currents from the membrane capacitor, the diverse ion channel conductances and the recording electrode has to be zero

$$I_C + \sum I_{g,i} + I_{\mathrm{el}} = 0.$$

The voltage-dependency of these membrane currents gives rise to the dynamics

of the membrane potential as will become apparent next.

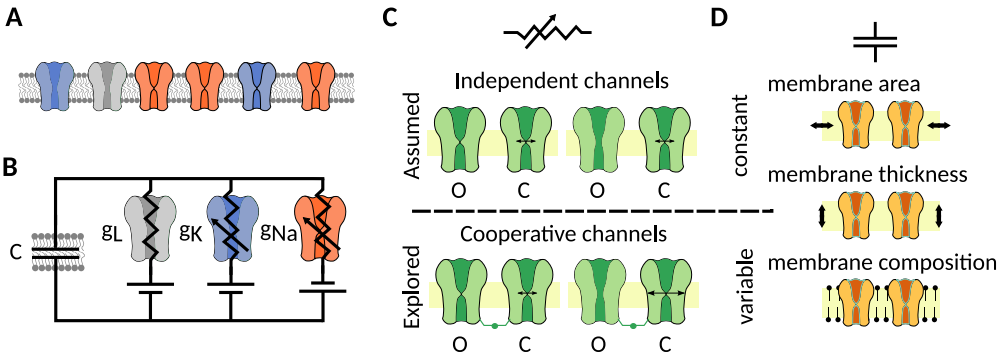

Figure 2.2: Conductance-based neuron models – standard assumptions and deviations explored in this thesis **A** Schematic of an excitable membrane with embedded ion channels. **B** Equivalent circuit model of the membrane with a capacitor and various ionic conductances (leak, potassium and sodium shown here). **C** Assumptions on conductances: Commonly assumed to gate independently, channels can cooperate, meaning that the transition between gating states, e.g. open (O) and (C), depends on the state of coupled neighbors. **D** Assumptions on capacitance: Despite biologically observed exceptions, the membrane properties determining capacitance are usually assumed to be constant or as in the case of the the membrane area are thought to be compensated by constant channel densities.

Assumptions on membrane capacitance The *capacitative current* I_C reflects the changes in the amount of charge Q_C stored on the capacitor that represents the cell membrane (Koch 1999). The capacitance value $C = \frac{Q_C}{V}$ determines how much charge Q_C has to be stored to build up a voltage difference V, the membrane potential, across the capacitor. Consequently, the capacitative current reads

$$I_C = \dot{Q}_C = (C\dot{V}) = C\dot{V} + \dot{C}V. \tag{2.1}$$

A common simplification is that the capacitance of a biological membrane is constant on the short timescales of electrical dynamics, that is $\dot{C}V \approx 0$. In most cases, this simplification appears appropriate, because the determinants of cell capacitance,

$$C = \epsilon\epsilon_0 \frac{A}{d}, \tag{2.2}$$

namely membrane surface area A, thickness d and electric permittivity $\epsilon\epsilon_0$, a material property of the membrane forming bilipid layer, are not expected to be rapidly changing (Koch 1999).

How does capacitance shape the electrical dynamics of neurons? With the above simplification, the current-balance equation becomes

$$C\dot{V} = -\sum I_{g,i} - I_{\text{el}}, \tag{2.3}$$

that is capacitance sets the rate at which the voltage changes in response to the currents flowing across the membrane. In other words, the capacitance corresponds to the "inertia" of the membrane potential; the smaller the capacitance, the faster a current can change it.

In this way, membrane capacitance enters the basic time scale of electrical dynamics, the *membrane time constant*: in a passive cell, with only a static leak conductance, the membrane potential dynamics read

$$C\dot{V} = -g_L(V - E_L) + I_{\text{el}},$$

with g_L as the leak conductance (or $R = g_L^{-1}$ as the corresponding resistance) and E_L as the leak reversal potential. In response to a step current with amplitude I_0, the charging of the membrane potential has the form

$$V(t) = E_L + \Delta V \left(1 - e^{-\frac{t}{\tau_m}}\right) \tag{2.4}$$

with $\tau_m = \frac{C}{g_L} = RC$ as the membrane time constant and $\Delta V = \frac{I_0}{g_L} = RI_0$ as the response amplitude. Hence, capacitance has a special role among the passive parameters of a cell, because it exclusively alters the temporal properties, that is only τ_m, but not ΔV. In the presence of active conductances, capacitance thus crucially influences signaling of neurons like their spiking frequency or the speed of action potential propagation down an axon (Koch 1999).

The influence of capacitance is however rarely considered, because it is commonly assumed that the capacitance per membrane area is a constant parameter. Of course, this constancy assumption does not hold for the total cell capacitance, which changes with the membrane surface area, for example in development. Neural dynamics, however, are thought to be preserved despite these capacitance changes, because area is assumed to equally scale the number of channels and therefore the channel currents, so that it can be divided out in the current-balance equation 2.3. The remaining capacitance per area, the specific membrane capacitance $C_m = \frac{C}{A}$, has been termed a "biological constant" based on measurements in membranes from a range of different cell types that consistently found a value of $\approx 0.9\ \frac{\mu\text{F}}{\text{cm}^2}$ (Gentet, Stuart, and Clements 2000). As a result, the question how capacitance shapes the firing patterns and computations of a neuron has not been extensively explored, especially in experimental neuroscience, where tools to control membrane capacitance are

lacking.

The "constant capacitance" paradigm is one of the two neuronal modeling revisited in this thesis. As discussed in more detail in the following sections, capacitance appears to be more variable than previously thought. Moreover, perturbing neural dynamics via an altered capacitance has proved to be valuable tool in theoretical neurophysiology to characterize the dynamical repertoire of a neuron. This background motivated the development of the hybrid computational-experimental capacitance clamp technique presented in Publication CAPCLAMP, the first tool to emulate and investigate capacitance changes in biological neurons (Pfeiffer et al. 2022).

Assumptions on ion channel conductances The richness of neuronal firing is provided by the diverse *ion channels*, proteins forming gated pores in the membrane controlling the flow of ions across it. In the equivalent circuit model, they are described by ohmic conductances with dynamic conductance values that represent their voltage-dependent gating,

$$I_{g,i} = \bar{g}_i m_i^{p_i} h_i^{q_i} (V - E_i), \tag{2.5}$$

$$\dot{x} = \frac{x_\infty(V) - x}{\tau_x(V)}; x \in \{m_i, h_i\}\,. \tag{2.6}$$

Originally, these dynamic gating variables were introduced in an ad-hoc fashion by Hodgkin and Huxley to capture the behavior of sodium and potassium currents measured in the giant squid axon – providing an elegant explanation for the generation and propagation of the action potential (Hodgkin and Huxley 1952; Koch 1999). Activation and inactivation variables, originally called particles, m_i and h_i reflect the state of the conductances. Their activation function $x_\infty(V)$ varies between 0 and 1. For activation particles, the function is monotonically increasing with voltage so that the corresponding conductance increases when the voltage rises, and vice versa for inactivation particles. How fast a conductance settles to a new value is described the gating time $\tau_x(V)$.

With the advent of techniques that could resolve the currents through single ion channels and reveal their molecular structure, this phenomenological neuron model could be related to the observed biophysics of ion channels (Koch 1999; Hille 2001). The gating variables were found to correspond to actual physical gates and the dynamics of the gating variables could be derived from the collective behavior of a large number of single channels. The assumptions underlying this derivation, their physiological plausibility and the implications for neural dynamics, when they are violated, are discussed next.

Single ion channels, different from the continuously varying global conductance, are discrete, stochastic, and mostly binary conductances (Hille 2001). The macromolecule forming the ion channel can take different conformations, of which some correspond to an open pore letting ions pass the membrane, whereas others obstruct current flow. Transitions between different conformations are induced by thermal noise and these molecular dynamics are quasi-instantaneous on the time scale of electrical events. Charged sensing structures within the channel make these transitions voltage-dependent, so that probability to find a channel in the conductive state depends on the membrane potential.

To connect the stochastic single channel dynamics, forming a continuous-time Markov process, to the above deterministic form for the macroscopic currents, three assumptions have to be made

1) **Channels act *independently*** that is the transitions between states in one channel are not directly altered by the states of neighboring channels. As a consequence, the dynamics of a channel ensemble can be understood by "summing" the dynamics of the single channel.

2) **The pore of a single channel is controlled by *independent* voltage-sensitive gates** that all have to be simultaneously in the appropriate open state to let the channel conduct current.

The typical kinetic scheme of a channel includes p identical activating (m-type) and q identical inactivating gates (h-type), where each gate forms a two state system

$$\mathrm{C/I} \quad \underset{\beta_x(V)}{\overset{\alpha_x(V)}{\rightleftharpoons}} \quad \mathrm{O}$$

with C/I and O denoting the closed/inactivated and the corresponding open states and $\alpha_x(V)$ and $\beta_x(V)$ as the voltage-dependent opening and respectively closing rates. Voltage-activated gates tend to be closed at low voltages ($\alpha_m(V_{\mathrm{low}}) \ll \beta_m(V_{\mathrm{low}})$), but this closed state becomes unstable when the voltage increases and the gate spends more time in the open state ($\alpha_m(V_{\mathrm{high}}) \gg \beta_m(V_{\mathrm{high}})$), whereas inactivating gates behave in the opposite manner. The probability to find a gate in the open state thus follows

$$\dot{p}_{x,\mathrm{O}} = -\alpha_x(V)p_{x,\mathrm{O}} + \beta_x(V)(1 - p_{x,\mathrm{O}}).$$

The open gate probabilities of a channel thus correspond to the activation and inactivation variables with $x_\infty(V) = \frac{\alpha_x(V)}{\alpha(V)+\beta(V)}$ as the steady-state open

probability and $\tau_x(V) = \frac{1}{\alpha(V)+\beta(V)}$ as the time scale of the gate. As the gates are independent, the final probability to find the channel in the open state is given by the product $m^p h^q$.

3) **The number of channels is sufficiently large**, so that channel noise due to the stochastic gating can be neglected. In this case, the single channel open probability is equal to the ratio of open channels to all channels. The conductance of the channel ensemble becomes $g = N_o\gamma = N\gamma m^p h^q$ with $\bar{g} = N\gamma$ as the peak conductance and γ as the single channel conductance.

From an experimental point of view, all three of these assumptions have to be seen as simplifications, because a subset of ion channels are observed to gate cooperatively against assumption 1 (Dixon et al. 2022), to exhibit more complex kinetics than independent molecular gates against assumption 2 (Aldrich, Corey, and Stevens 1983; Tytgat and Hess 1992) and to produce physiologically relevant current fluctuations in small structures against assumption 3 (White, Rubinstein, and Kay 2000; van Rossum, O'Brien, and Smith 2003). The question from a modeling perspective is then whether these deviations are relevant for neural dynamics.

This thesis explores the consequences of revising the assumption of channel independence. As reviewed in the following, experimental evidence of cooperative interactions has been accumulating and by now cases of cooperativity are known in all major classes of voltage-dependent ion channels (Dixon et al. 2022). Still, whether the direct feedback between channels has a functional role, potentially one that is difficult to fulfill with independent channels, remains an open question. The contribution of Publication COOPMEM presented here is to propose a previously neglected role of the positive feedback provided by channel cooperativity, namely memory. It demonstrates that the addition of small clusters of cooperative channels to a classic Hodgkin-Huxley type neuron model leads to a graded form of persistent neuronal firing. Thereby, cooperativity appears as an alternative mechanism for GPA, the experimentally observed firing pattern hypothesized to mediate cell-autonomous short-term memory shown in Figure 2.1 C that has been challenging to explain via independent channels alone.

The Hodgkin-Huxley formalism as the basis of exploring neural dynamics
The equivalent circuit description based on the above membrane model is the basic framework to include more of the known biology of neurons. An important structural extension is for example to include neuronal morphology by resistively

linking multiple compartments each modeled like the above point neuron (Koch 1999), the basis to study computations in the dendrites of neurons. Current dynamics can be extended in multifold ways, such as including the dependence of channel conductances on intracellular calcium (Koch 1999; Schutter and Smolen 1999), the activity-dependent changes of ion concentrations controlling the reversal potentials (Contreras et al. 2021), or even genetic mechanisms that regulate the expression of ion channels (O'Leary et al. 2014). These extended Hodgkin-Huxley neuron models demonstrate the relevance of this various biological processes for neuronal function and computation (Sidiropoulou, Pissadaki, and Poirazi 2006). This thesis follows the route of a model-driven exploration into the role of neuronal complexity, but in the "opposite" direction, taking a closer look at the basic assumptions on membrane biology.

To summarize, conductance-based neuron models can be derived from the electrical functions of ion channels and biological membranes. In the majority of neuron models, channels are assumed to gate independently and the cell capacitance is assumed to be a constant despite experimental evidence for deviations from these assumptions. Adapting neuron models to incorporate and study such deviations, this thesis contributes to the question how neural dynamics change when channels cooperate or capacitance varies. Before a more in-depth background on channel cooperativity and membrane capacitance, the experimental technique complementing the theoretical approach used in this thesis is introduced: the dynamic clamp technique, a hybrid of computational modeling and intracellular recordings.

2.1.3 Dynamic clamp

In the quest to understand the electrical activity of a neuron, conductance-based models and standard intracellular recordings play complementary roles. Intracellular recordings reveal the electrical phenotype of a neuron with all its biophysical intricacies, but experimental control over cellular components like ion channels or synapses is challenging. In conductance-based neuron models, in contrast, each cellular parameter can be controlled and its role can be investigated in detail via simulations or mathematical analysis, but these simulated cells are necessarily simplified and incomplete in comparison to their biological counterpart.

For conductances, this gap between full physiology accessible in experiment and full control accessible in modeling has been bridged by a recording mode termed the *dynamic clamp* (Sharp et al. 1993; Robinson 1994; Prinz, Abbott, and Marder 2004). The dynamic clamp exploits that current injection in closed-loop with voltage recording can emulate the presence of a modeled conductance in a

biological neuron. In this way, experimenters have full control over the individual parameters of a conductance, like its resistance and its gating kinetics, and can investigate the role of these properties in the complex environment of a real cell. In the following section, the dynamic clamp technique is explained to prepare its application in studying cooperative ion channels in Publication COOPMEM. In addition, the idea to extend the underlying closed-loop approach to parameters beyond conductances is introduced which motivated the development of the capacitance clamp in Publication CAPCLAMP.

Intracellular recordings: current and voltage clamp

Intracellular recordings from neurons and other excitable cells have been crucial to understand neurophysiology and develop conductance-based models. A recording electrode is inserted into a cell and allows an experimenter to measure the membrane potential and inject currents. Whereas early electrodes were actual metal wires and recordings could only be obtained from large cellular structures like the giant squid axon (≈ 0.5 mm), modern electrodes consist of glass pipettes with very fine tips (≈ 1 μm) filled with ionic solutions and recordings guided by microscopy can be made from small structures in the micrometer range like the soma of insect neurons (Murthy and Turner 2013) and dendrites or synaptic terminals in mammalian neurons (Davie et al. 2006).

The two standard recording modes for intracellular recordings are *current-clamp* and *voltage-clamp*. In current-clamp, the basic recording form, the experimenter defines the current stimulus to be injected and observes the voltage response. A typical current-clamp experiment is the injection of step currents with increasing amplitudes to observe firing of action potentials (see Fig. 2.1). In voltage-clamp, developed as a complementary mode for the current-clamp, the experimenter instead defines a temporal form for the voltage, which is enforced by a closed loop that counteracts voltage deviations from this predefined form by the current through the electrode. In an ideal voltage clamp, the experimenter can thus measure the dynamics of the intrinsic membrane currents, because they are the inverted version injected current. Again, a typical voltage-clamp experiment consists in stepping the voltage from for example a low to a high value, while pharmacologically blocking all but one ion channel type, to trigger conductance changes and study the channel kinetics (a simulated voltage clamp experiment with cooperative channels is shown in Figures 1 and 2 of Publication COOPMEM). Taken together, the standard recording modes offer either a global view of the whole membrane dynamics or a detailed view of individual channel kinetics, but cannot observe both at the same time.

To understand the link of the individual channel kinetics to the combined

membrane potential dynamics, data from both current- and voltage-clamp can be combined to infer ion channel kinetics, peak conductances and other cellular parameters for an *in-silico* conductance-based model of the recorded cell (type). In a simulated cell, the contribution of each channel current as well as the resulting membrane potential dynamics can be visualized simultaneously, bridging the gap between the two experimental recording modes. Additionally, the behavior of the modeled cell can be studied under controlled synaptic input – the physiologically relevant neuronal input – which cannot be experimentally mimicked by current-clamp stimulation alone due to the associated conductance changes. Finally, in the model, the role of all cellular properties can be characterized in detail, including those that are difficult or impossible to modify and control experimentally like for example the half activation voltage of a channel. However, even when carefully fitted, every neuron model is incomplete with respect to its biological counterpart – it might for example neglect important channel types or lack information about their spatial distribution – limiting the conclusions that can be drawn from modeling alone.

Emulation of modeled conductances in biological neurons

To further narrow this gap between modeled and biological neurons, a third recording mode, the *dynamic clamp*, has been developed. The dynamic clamp allows experimenters to emulate the presence of a virtual conductance, simulated and under full control, in a recorded neuron, biological and preserving its full dynamics (Sharp et al. 1993; Robinson 1994). Like the voltage clamp, the dynamic clamp relies on a fast closed loop between voltage measurement and current injection, but with the difference that the mapping of voltage to current is calculated online in real-time by a computer provisioned with a model of an ionic conductance, a setup schematically shown in Figure 6 of Publication COOPMEM.

Each sampling interval, the computer receives the present membrane potential, uses it in combination with the conductance model to calculate the current that flows through it and then sends a corresponding command to update the current through the recording electrode. If the sampling frequency is high enough to track the membrane potential and the kinetics of the modeled channel, the current through the electrode accurately mimics the channel current. As a result, the neuron displays voltage dynamics as if it had expressed this simulated conductance in its physical membrane. In the words of the first review about this technique, "the dynamic clamp uses biological neurons as simulators" to reveal the effects of a modeled conductance the experimenters are interested in (Sharp et al. 1993).

"Conductance injection" via the dynamic clamp allows experimenters to perturb and study neurons in a more physiological way than possible via the current clamp. This can be illustrated by the basic case of an altered leak current, $I_L = -\Delta g_L(V - E_L)$, a current controlled by various neuromodulators. Mimicking the altered leak current by a fixed additional current in current clamp is severely limited, because it ignores its voltage dependency. In a dynamic setting, where the membrane potential changes, it thus fails to reproduce other relevant consequences of an altered leak, like for example faster or slower charging due to the modified membrane time constant $\tau_m = \frac{C}{g_L}$ and possible changes in the firing type of a neuron (Kirst et al. 2015; Hesse, Schleimer, and Schreiber 2017; Hesse et al. 2022). The same argument holds for mimicking any conductance by a predefined waveform, be it a time-dependent synaptic conductance or an active ion channel type with voltage-dependent gates. In contrast, the dynamic clamp captures the full physiological effects of a conductance by the continuous update of the conductance state and the injected current via the recorded voltages.

Applications of the dynamic clamp

Applications of the dynamic clamp can address a broad range of questions from mechanisms of cell-intrinsic excitability to synaptic interactions between neurons and the surrounding network, often in ways that are difficult or even impossible to achieve with other experimental tools[2].

In the realm of cell-intrinsic dynamics, the dynamic clamp can be seen as a virtual and flexible form of a genetic knock-in experiment which adds an ion channel of interest to a cell to observe its impact on the electrical dynamics (Dorval, Christini, and White 2001). Such a virtual "knock-in" has been used for example to add potassium conductances with long gating time constants to neurons from the stomatogastric ganglion of crabs, which confirmed that they can support cellular short-term memory as suggested by previous modeling studies in simplified cell models (Turrigiano, Marder, and Abbott 1996).

In principle, the dynamic clamp can also "knock-out" an existing conductance by reversing the sign of the injected current. In practice, this is difficult, because any mismatch between the modeled and the actual channel kinetics leaves behind a "negative" conductance that can destabilize the membrane potential. Still, virtual "knock-out"s have been successfully used to study channels where pharmacological tools to selectively block it were missing, e.g., persistent sodium

[2]For a comprehensive overview of applications of the dynamic clamp, see the edited collection in *Dynamic-Clamp* (Bal and Destexhe 2009).

currents and their role for action potential generation (Vervaeke et al. 2006; Bal and Destexhe 2009).

The other class of conductances studied via the dynamic clamp are synaptic conductances. In a basic setting, artificial synapses offer a more physiological way to excite or inhibit a neuron than the widespread practice of current pulse injection. But artificial synapses further allow experimenters to "control" the network a neuron is embedded in. In small networks, artificial synapses can connect previously unconnected neurons, replace blocked synapses in a controlled fashion[3](Morozova, Newstein, and Marder 2022) or link simulated neurons to the biological ones (Prinz, Abbott, and Marder 2004). In larger networks, the dynamic clamp can recreate *in-vivo* network activity resembling the one in a brain of an alive awake animal in a neuron recorded *in-vitro* from an extracted brain slice where many connections are severed and network activity is reduced (Destexhe, Rudolph, and Paré 2003). The possibility to mimic a physiological in-vivo like network state in the experimentally much simpler setting of a brain slice recording is an important contribution of the dynamic clamp, which demonstrates that neurons embedded in an active network operate very differently from those in isolation (Chance, Abbott, and Reyes 2002; Prescott et al. 2008).

Limitations and requirements on hard- and software

Although a powerful experimental tool, the mimicry of a conductance modification via the dynamic clamp is technically challenging and limited in comparison to its full physiological implications. To decide whether the dynamic clamp is suited for a research question, thus requires awareness of both hard- and software requirements as well as the limitations inherent to the technique.

A basic demand for dynamic clamp is a well-timed and sufficiently fast closed-loop between voltage measurement and current injection. The loop interval should be considerably shorter than the fastest voltage changes in the recorded cell as well as the shortest gating time constant of the modeled conductance. Whether a loop interval is sufficient can first be evaluated in simulations (Bettencourt et al. 2008) and then in the best case is experimentally verified by increasing the sampling frequency and ensuring that measured properties like the shape of a spike remain unchanged (Robinson 1994). In addition, the computer or dedicated chip simulating the channel has to provide the updated conductance and current in hard real-time (that is at the times defined by the sampling and injection process). The main obstacle in a modern computer is not

[3]Both applications require simultaneous recordings from two or more neurons.

the time to compute the updates, but rather the guaranteed time of executing the update, which is why dedicated real-time operating systems should be used (Patel et al. 2017).

The other prerequisite are accurate voltage measurements. From random recording noise to systematic electrode artifacts, multiple sources can distort the sampled voltage value from the actual membrane potential (Brette and Destexhe 2012). In the classic open loop setting of the current clamp, such measurement errors "only" affect the recorded, but not the actual dynamics of the cell. In the closed-loop setting of the dynamic clamp, however, where erroneous voltage values are fed back to the cell, they can alter the dynamical course of the cell and potentially destabilize it (Bal and Destexhe 2009). An important error source is the recording electrode itself, which forms an electrical device with a distributed capacitance and resistance (often non-linear), so that the electrode voltage is a filtered version of the membrane potential. Amplifiers provide different mechanisms to "compensate" an electrode and minimize these artifacts, but the majority relies on the assumption that the electrode acts like a linear RC circuit. A recent promising technique to further reduce electrode artifacts and improve dynamic clamp experiments is active electrode compensation (AEC), which estimates a model for the currently used electrode by a test protocol and can then infer the actual membrane potential (Brette et al. 2008).

Putting aside technical requirements, even a perfectly operated dynamic clamp is constraint in emulating biological conductances (Sharp et al. 1993). Spatially, the modeled conductance is located at the recording site, typically the soma of a neuron – a constraint known as space clamp inherent to all clamping techniques. For site-specific channel injection, the space clamp can be overcome by corresponding dendritic or axonal recordings, but for any distributed conductance like synaptic input it implies that the dynamic clamp can only approximate its effects. Another dimension of biological ion channels challenging for the dynamic clamp is their selectivity for one or multiple ion types. For calcium-selective channels, for example, dynamic clamp via an electrode with the typical potassium-based recording solution cannot emulate changes of the intracellular calcium concentration. Therefore secondary effects of calcium channels like blocking other channels or altering gene expression are not captured by the dynamic clamp (Prinz, Abbott, and Marder 2004).

Beyond conductances: dynamic clamp for other virtual cellular components

The wide range of dynamic clamp applications shows that its challenges can be met and that the control over virtual conductances in biological neurons has become an important tool to investigate the role of ion channels and synapses.

Given the advantages of this hybrid computational-experimental approach, one could ask whether the same technique can also be used to to study other determinants of neural dynamics beyond conductances like membrane capacitance, neuronal morphology, ion channel pumps or changes of the cellular environment, e.g., dynamic ionic concentrations. Components affecting the electrical behavior of a cell eventually express themselves via modified currents, so that it appears reasonable to elucidate whether they can be emulated via the same dynamic clamp principle of a closed-loop control of current injection used for artificial conductances. In other words, can one establish a practical dynamic clamp protocol to virtually lower the reversal potential of potassium or artificially increase membrane capacitance?

Before further examining the membrane capacitance parameter and preparing tackling this question in Publication CAPCLAMP, the next section focuses on cooperative channels, an aspect neglected in most conductance models, including those used in hybrid dynamic clamp simulations.

2.2 Cooperative ion channels

A central, but repeatedly questioned tenet of conductance-based neuron models is the assumption that voltage-gated ion channels gate independently. Independent gating implies that channels cannot *directly* alter the physical state of other channels, but only interact *indirectly* via the current-induced changes of the membrane potential. Independent gating is a theoretically convenient assumption, because it simplifies the link of the microscopic single channel activity to the macroscopic behavior of a large ensemble. However, it appears at odds with the interactive nature of channel proteins which provide specialized structures to sense a wide variety of physical modalities (pressure, light, neurochemicals, etc.). Correspondingly, since the advent of methods to observe channels in small ensembles, experimental evidence has accumulated for cooperative gating, including for certain types of voltage-gated sodium, potassium and calcium channels present in neurons and heart cells (Dixon et al. 2022).

Despite growing evidence for ion channel cooperativity, its impact on electrical signaling remains poorly understood. Theoretical attempts to incorporate channels that violate the independent gating assumption into neuron models and to study their functional role are rare. In Publication COOPMEM of this thesis, a neuron model with both independent action-potential generating channels and clusters of cooperative channels is introduced to study whether channel coupling can support bistable firing patterns and thereby cell-intrinsic memory. In the following section, as a background to this investigation, experimental methods

to detect cooperative gating are reviewed, as well as biophysical mechanisms that could mediate channel coupling. Current hypotheses on the role of such a direct inter-channel feedback are formulated and models of cooperative gating are introduced to study this mechanism.

2.2.1 Experimental evidence of cooperative gating

Cooperativity between voltage-gated ion channels is still perceived as a rather rare and inconsequential mode of gating. The by now extensive body of experimental work on such interactions suggests that on the contrary cooperativity might be widespread and critical to understand various aspects of electrical excitability (Dixon et al. 2022). Cases of cooperativity have been reported for the central families of voltage-gated sodium- (Iwasa et al. 1986; Clatot et al. 2017), potassium- (Kim et al. 2014) and calcium-selective channels (Navedo et al. 2010; Moreno et al. 2016) that are expressed both in heart (Navedo et al. 2010; Clatot et al. 2017) and brain tissue (Moreno et al. 2016), including human cells (Kim et al. 2014).

Moreover, cooperative gating is not constrained to voltage-gated ion channels. It is also observed in various ligand-binding channels like acteylcholine-activated receptors in muscle (Keleshian et al. 2000) and even in mechanosensitive potassium channels of bacteria (Grage et al. 2011). The essential prerequisites for cooperativity, namely close spatial arrangement of channels and physical interactions, might hence be general properties of the larger class of membrane pore-forming proteins.

Methods to detect cooperative gating

Experimental methods to detect ion channel cooperativity rely on measuring channel currents and screening the current dynamics for deviations from the predictions of independent gating. Channel currents are measured via voltage clamp (see Section 2.1.3) and can either be monitored in a small membrane patch with a few channels or in a whole cell with a large ensemble of channels (typically > 1000). In a small membrane patch, the opening and closing of single channels can be directly observed as step-like jumps in the current trace. This pattern constitutes a stochastic process that can be compared to the dynamics expected from a collection of independently-gating channels. For a whole cell, the large number of stochastic channels results in a macroscopic current, whose fluctuations can be analyzed to search for fingerprints of cooperativity.

Small membrane patches: channel-state distribution, dwell-time analysis and full state space models

Channel state distribution The simplest scenario to detect cooperativity is a membrane patch with two channels - a case first analyzed in pairs of toxin-modified sodium channels (Iwasa et al. 1986). If the two channels gate independently and identically with one open and one closed conformation, occurring with probability p and $1-p$ respectively, the time spent in a state with zero, one, or two open channels is distributed binomially

$$P(0) = (1-p)^2, P(1) = 2p(1-p), P(2) = p^2.$$

Significant deviations from a binomial distribution thus signal either the presence of coupled gating or differences among the channels. If differences among channels can be excluded through further experiments, the deviations also reveal the nature of the coupled gating. Positive cooperativity is indicated by an increased prevalence of simultaneously open channels: after one channel switches to the open configuration, the positive coupling increases the chance of its neighbor opening as well and once both channels are open they mutually stabilize each other. Whereas positively cooperating channels tend to be in the same state, both closed or both open, negatively cooperating channels compete by mutual inhibiting each other, indicated by a state distribution with a higher peak for the state with one open channel.

Detection of cooperative interactions by the stationary channel state distribution alone is limited and has been extended in different ways. A minor extension is to the case of inactivating channels. Such channels, like for example the sodium channel $Na_v1.5$, transiently open in response to an increase of the membrane potential, but then inactivate to a second, more stable closed configuration. In the stationary regime, inactivating channels are hence non-conductive, which prevents to sample the state distribution. Instead, repeated runs are used to determine the time-dependent channel state distribution $\mathbf{P}(t) = (P_0(t), P_1(t), P_2(t))$, which can again be screened for non-binomial features (Clatot et al. 2017; Hichri, Selimi, and Kucera 2020). It is important to note that the presence of the inactivating state does not affect the derivation of the binomial distribution, because each channel still has only two observable states, open and shut (combining closed and inactivated).

Dwell-time analysis Dwell-time describes the time period during which an ensemble of channels occupies a certain state. In the channel state distribution, this time domain information is discarded such as the duration of transitions

between states, e.g., how long it takes until a channel opens. Conditional dwell-time analysis compares the timing of such transitions conditioned on the number of already open channels to screen for signs of coupled gating (Keleshian et al. 1994). When channels gate independently, the conditional dwell times in a given channel state are identical, because the transition rates are independent of the state of other channels. Deviations, in contrast, indicate that the channel cooperate. In membrane patches with two ATP-sensitive potassium channels, for example, the mean dwell time in the closed state was shown to be shorter when the neighboring channel was closed than when it was open. In other words, the opening of one channel stabilized the close configuration of its neighbor, a case of negative cooperativity (Choi and Licht 2012).

State space models The statistical measures to detect cooperativity, reviewed so far, are model-independent. This makes them generally applicable, but limits their insight into more specific questions about the coupling of channels like which gating transitions are affected. Such questions can be answered via formulating channel models (for more details see the following section on "Models of cooperative gating"): if the state space of a channel type is known, i.e., its (potential multiple) closed and open conformations, this determines the state space model for a collection of two or more channels. For independent gating, the transition rates in the multi-channel model follow directly from those in the single channel model. Consequently, deviations from this expected transition rates in the experimentally observed channel traces can be used to detect cooperativity. In addition, such an analysis can pinpoint which exact transition rates are affected and by how much. Such an approach has, for example, been used to demonstrate that cooperative interactions between nicotinic receptors can increase both the binding affinity of a closed channel to the ligand, but also its transition rate to the open conducting state (Keleshian et al. 2000).

In addition to providing more information, state space descriptions of cooperative channels have the further advantage that they can be incorporated into conductance-based neuron models. In this way, the role of their coupled gating for the global voltage dynamics of a cell can be characterized (Naundorf, Wolf, and Volgushev 2006; Zarubin, Zhuchkova, and Schreiber 2012).

Macroscopic fingerprints of cooperative channels "Fingerprints" of cooperative gating can also be detected on the macroscopic level with currents recorded in a whole-cell configuration containing thousands of channels. One of the first indications for cooperative gating stems from the analysis of the current fluctuations in a membrane patch with thousands of sodium channels (Neumcke

and Stämpfli 1983). When N identical channels gate independently, the mean I and variance σ_I^2 of the macroscopic current are sums of the mean single channel current pi (where p is the open probability and i the unitary channel current) and respectively its variance $p(1-p)i^2$. The variance and the mean of the macroscopic current hence follow a parabolic relationship (Sigworth 1980)

$$\sigma_I^2 = I(i - \frac{I}{N}).$$

For an ensemble of *independent* channels, measuring this mean-variance relationship thus provides information about microscopic properties including their number and their conductance. When channels cooperate, however, this relationship is altered (Liu and Dilger 1993; Choi 2014). How exactly mean and variance are linked in the case of coupled gating depends on the form of their interaction. In general, positively cooperative channels increase the variance, because they prefer similar states corresponding to an effective reduction of the number of independent units. Vice-versa, when channels are negatively cooperative, the variance is expected to be reduced.

An interesting case of macroscopic evidence for cooperative gating is negative dominance. This phenomenon is observed with the sodium channel $Na_v1.5$ and thought to contribute to severe heart diseases (Keller et al. 2005). When the wild-type (WT) version of this channel is expressed at equal levels with a genetic variant known to exhibit reduced activity, the resulting currents are reduced by about 75% with respect to a cell with only WT channels – an apparent dominance of the less active variant. The additional observation that these channels form dimers (pairs) in the membrane led to the hypothesis that the negative dominance is mediated by cooperative interactions in heterodimers, pairs containing both a WT and a variant channel (Clatot et al. 2017). Indeed, microscopic state space models of such interacting pairs show that the altered gating scheme of the variant channel can significantly reduce the time of its WT neighbor spent in the open conductive state (Hichri, Selimi, and Kucera 2020).

Biophysical mechanisms of cooperative gating

Despite the growing evidence for cooperative gating from the statistical analysis of channel currents, there is relatively little known about the underlying biophysical mechanisms mediating the interaction. One essential requirement for any coupling mechanism is spatial clustering of channels, which is observed in multiple channel types and has been proposed to rely on stochastic self-assembly where channels transported to the membrane preferentially locate close to other channels (Sato et al. 2019). Potential coupling mechanisms then fall into two

categories: *allosteric* coupling mediated by mechanic links between channels and local forms of *indirect* coupling mediated by an intermediate process.

Allosterically coupled channels might either form direct links or require additional proteins as bridging units. For direct links, subunits of two different channels have to be able to connect. For example, nicotinic acetylcholine receptors have been observed to form dimers and even oligomers, pairs or larger groups of channels whose δ subunits connect via disulfide or other non-identified covalent bonds (Schindler, Spillecke, and Neumann 1984; Yeramian, Trautmann, and Claverie 1986). In other cases, the channels require an additional bridging protein, like calmodulin connecting intracellular termini of $Ca_V1.3$ channels (Moreno et al. 2016) or 14-3-3 in sodium $Na_V1.5$ channels (Hichri, Selimi, and Kucera 2020). The tight structural association of two or multiple channels also couples them functionally – the opening of one channel exerts forces onto its its neighbor(s) that can prime or suppress conformational changes. Although a detailed understanding of the relevant forces is still missing, the functional role of the structural links has been confirmed by experimentally modifying them. For example, $Ca_V1.3$ gate independently in the absence of the bridge protein calmodulin, but replacing this bridge by an artificial link restores cooperativity (Moreno et al. 2016).

In the case of indirect coupling, the conformational change of one channel affects the neighbor despite the lack of a direct structural link, for example through a secondary process triggered by the ionic currents. In this case, channels in principle gate independently, but appear to cooperate because their gating modifies each others immediate environment – a localized version of the concerted gating directed by the membrane potential. Hypotheses in this direction comprise a local modification of the membrane potential by altered surface charges (electrically charged parts of a channel protein) after a conformational switch (Keleshian et al. 2000), ephaptic coupling mediated by the electric field that the ionic current through an open channel generates (Hichri, Selimi, and Kucera 2020), or mechanical forces induced via stretching the membrane (Ursell et al. 2007).

The nature of the coupling mechanism constraints how many channels can interact and gate cooperatively. In the case of allosteric coupling, the number of interaction sites restricts the number of partner channels. For one interaction point, channels can only form dimers, whereas for two or more interaction sites they could assemble into oligomers, small networks of channels forming a macrochannel. Indirect coupling mechanisms, in contrast, might mediate a broader interaction, a form of all-to-all coupling within a cluster. Indirect coupling is likely heterogeneous, because interaction strength is expected to decrease sharply with inter-channel distance. Both coupling mechanisms could

also be at play at the same time, as proposed for the previously considered example of $Ca_V1.3$ channels (Moreno et al. 2016). These channels appear in spatial clusters of around ten channels, but the allosteric binding sites for the bridge protein calmodulin are unique to each channel, restricting the resulting positive cooperativity to dimers. To enable bridging, calmodulin, however, has to be activated by binding of two calcium ions, implying a further form of indirect coupling: open channels in the cluster increase the local calcium concentration, which allows channels to dimerize and thereby activate faster.

2.2.2 Implications of cooperative gating for electrical activity

The functional implications of cooperatively-gating channels are only starting to be understood. As cooperativity influences the basic properties of ion channels, e.g., shifting activity to another range of membrane potentials, it is expected to affect, at least quantitatively, the electrical signaling of neurons. An intriguing question is whether there are consequences of cooperative gating that extend the computational repertoire of a neuron beyond what is efficient or even possible with independent channels.

Sensitivity

Cooperative gating constitutes a direct feedback loop between channel proteins, a motif common to many cellular processes. Among these processes, one role of positive feedback to increase sensitivity as illustrated by the classic example of allosteric binding of oxygen to the four binding sites of the transporting protein hemoglobin (Pauling 1935). The signal-response curve of oxygen concentration versus bound oxygen is steeper than expected for independent binding, because one bound oxygen molecule facilitates the binding of further oxygen molecules. Correspondingly, for positively cooperating voltage-gated channels, the activation curve of voltage versus open probability is predicted to get steeper and shifted to lower voltages (Liu and Dilger 1993; Zarubin, Zhuchkova, and Schreiber 2012), which has been confirmed experimentally (Kim et al. 2014; Moreno et al. 2016). Coupling of calcium channels, for example, is observed to strengthen ionic currents present in the heart (Navedo et al. 2010) and the brain (Moreno et al. 2016). Aberrant cooperativity in turn can lead to a pathological sensitivity and excessive channel activity; a condition implicated in heart arrhythmia (Sato et al. 2018) as well as epilepsy (Kim et al. 2014).

Increased sensitivity of cooperative channels to voltage changes might also be beneficial for the signaling capabilities of neurons. When a cell approaches its spiking threshold, modeling suggests that strongly coupled sodium channels

open in a highly synchronous fashion. This synchronous opening could underlie the fast onset of action potentials observed in cortical neurons (Gutkin and Ermentrout 2006; Naundorf, Wolf, and Volgushev 2006; Öz, Huang, and Wolf 2015) and extend the range of high stimulus frequencies these cells can encode in their spike trains (Huang, Volgushev, and Wolf 2012). This idea remains controversial. A contrary proposal, in agreement with independent gating, explains the observed fast spike onset of an AP recorded at the soma by backpropagation from an axon initial segment equipped with *uncoupled* sodium channels (McCormick, Shu, and Yu 2007). However, in contrast to cooperative channels, this morphological effect cannot increase the encoding capabilities of a neuron, because those rely on the actual spike generating mechanism (Öz, Huang, and Wolf 2015) (but see (Brette 2013) for more complex morphological effects). Concluding, the proposed role of sodium channel cooperativity in spike generation, although awaiting further experimental tests, illustrates the potential for channel interactions to alter neuronal information processing.

Memory/bistability

A central role of positive feedback, so far neglected for cooperative channels, is memory. Persistent switches in gene expression (Burrill and Silver 2010) and long-term modification of synaptic strengths (Crick 1984; Lisman 1985) rely on positive feedback loops that make these molecular systems bi- or multi-stable. Similarly, network models of short-term or working memory exploit positive feedback via synaptic reverberation between neurons (Zylberberg and Strowbridge 2017). In a strongly recurrently connected ensemble of excitatory cells, activity triggered by a short external stimulus persists because spikes "loop" through the network keeping it in the active state until a inhibitory pulse switches them back to the silent state. Such delay activity is indeed observed when animals perform working memory tasks (Goldman-Rakic 1995; Lundqvist, Herman, and Miller 2018), but whether it relies solely on a network mechanism is an open question (Major and Tank 2004).

Interestingly, persistent spiking can also be evoked in single neurons that are synaptically isolated (Egorov et al. 2002). As mutual excitation of neurons is excluded in these cases, the underlying feedback loops behind such bistable firing patterns have to be cell-intrinsic. One candidate is the indirect feedback between calcium channels and calcium-activated channels. Feedback of this form can form a self-sustaining cycle where calcium inflow during one spike activates depolarizing channels to trigger the next spike (Debanne, Inglebert, and Russier 2019). This poses the question whether cooperative channels can similarly self-sustain neuronal activity to serve cell-intrinsic memory.

To summarize, the direct feedback mechanisms between cooperative channels are relevant to understand excitable cell physiology. Relevance for neuronal computations, while suggested by the common functions of feedback loops like increased sensitivity or eventually bistability, remains hypothetical at this point. As cooperativity is hard to detect and even more difficult to control experimentally, modeling of coupled channels is crucial to identify dynamics where their direct feedback plays a role.

2.2.3 Models of cooperative gating

To model cooperativity among ion channels, the natural starting point is the description of a single channel. In the state space description of a channel, cooperative interactions are incorporated by transition rates that depend on the state of neighboring channels. This inter-dependence means that – different from the treatment in the standard Hodgkin-Huxley neuron – the dynamics of an ensemble of channels cannot longer be derived directly from the single channel level. In the following, the *voltage-shift* model of cooperative gating is introduced (Naundorf, Wolf, and Volgushev 2006), which is used in Publication COOPMEM to study the emergent dynamics in clusters of interacting channels. To connect the heuristic voltage-shift model with the biophysical level of channel gating, the cooperative alteration of transition rates is first explained for the simple case of a cluster of two channels following the treatment in (Hichri, Selimi, and Kucera 2020).

State space model of two cooperatively-gating channels

The state space of a channel pair consists of the combinatorial set of single channel states. This simple combination implicitly assumes that the channel interaction only affects transitions between existent states and does neither create new stable configurations nor destroys existing ones. For a two state channel with an open state O and a closed state C, the dimer state space is therefore {CC, OC, CO, OO}.

In the case of independently-gating channels, the transition rates of the single channel

$$\mathrm{C} \underset{\beta(V)}{\overset{\alpha(V)}{\rightleftharpoons}} \mathrm{O}$$

determine the corresponding rates in the dimer state space

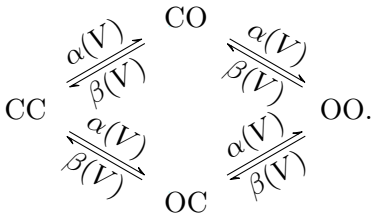

When channels gate cooperatively, the transition rates change, but not in an arbitrary fashion. The altered transition rates have to correspond to the altered energy landscape of the dimer, where the channel interactions can affect both the energy of the combined states and/or the energetic barriers between them. This correspondence is described by the Arrhenius law, which relates the transition rate from a state i to a state j with the height of the energy barrier Δ_{ij} measured from the point of view of the states energy level,

$$r_{ij} = \kappa \frac{kT}{h} e^{-\Delta_{ij}/kT},$$

where T is the temperature, k is the Boltzmann constant, h is the Planck constant and κ is a molecule dependent transmission coeffcient. Consequently, cooperativity has concerted effects on the transition rates of the channel pair:

1. If cooperative/channel interactions alter the *energy of a state i* by an amount δE, the height of the energetic barrier to leave the state changes by the same amount and *all "exit" rates* from this state are scaled as $r\prime_{ij} = e^{\delta E/kT} r_{ij}$.
2. If cooperative/channel interactions alter the *energetic barrier between two states i and j* by an amount $\delta\Delta$, then *both forward and backward rates* are scaled as $\frac{r\prime_{ij}}{r_{ij}} = \frac{r\prime_{ji}}{r_{ji}} = e^{-\delta\Delta/kT}$.

As an illustration, consider the effects of channel interactions in a dimer with raised energy of the OC and CO state. In comparison to two independently-gating channels, such a dimer is expected to spend less time in the OC/CO state because its higher energy makes it less stable. Exemplary, the channel state distribution is derived for an energy increase by $\delta E = kT$ and equal opening and closing rates $\alpha = \beta = 1$ ms^{-1} for the single channel. In isolation, the channel is thus expected to have an open probability of $p_O = 0.5$ With the correspondingly increased transition rates from the OC and CO state, the dimer state space scheme then reads

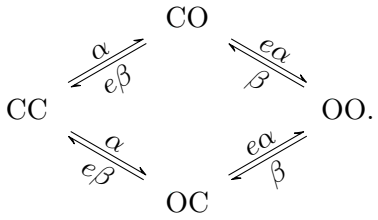

Lumping the states OC and CO with one open channel together because they cannot be distinguished from each other, the dynamics of the dimer state distribution are

$$\begin{aligned}
\frac{\mathrm{d}p_{\mathrm{CC}}}{\mathrm{d}t} &= -2 \cdot 1\mathrm{ms}^{-1} p_{\mathrm{CC}} + e \cdot 1\mathrm{ms}^{-1} p_{\mathrm{OC}}, \\
\frac{\mathrm{d}p_{\mathrm{OC}}}{\mathrm{d}t} &= 1\mathrm{ms}^{-1} p_{\mathrm{CC}} - 2e \cdot 1\mathrm{ms}^{-1} p_{\mathrm{OC}} + 1\mathrm{ms}^{-1} p_{\mathrm{OO}}, \\
\frac{\mathrm{d}p_{\mathrm{OO}}}{\mathrm{d}t} &= e \cdot 1\mathrm{ms}^{-1} p_{\mathrm{OC}} - 1\mathrm{ms}^{-1} p_{\mathrm{OO}}.
\end{aligned}$$

The stationary distribution $\dot{\mathbf{p}}_0 \stackrel{!}{=} 0$ is

$$\mathbf{p}_0 = \begin{pmatrix} p_{\mathrm{CC},0} \\ p_{\mathrm{OC},0} \\ p_{\mathrm{OO},0} \end{pmatrix} = \frac{1}{2(1+e)} \begin{pmatrix} e \\ 2 \\ e \end{pmatrix} \approx \begin{pmatrix} 0.37 \\ 0.26 \\ 0.37 \end{pmatrix}$$

confirming the reduced occurrence of the OC state and the resulting deviation from the binomial distribution $\mathbf{p}_{\mathrm{indp.}} = (0.25, 0.5, 0.25)$. The increased tendency of the interacting channels to be in the same state technically implies positive cooperativity. Still, channels coupled in this way exhibit no increased activity, because they have the same individual open probability $p_{\mathrm{O}} = p_{\mathrm{OO}} + 0.5 p_{\mathrm{OC}} = 0.5$ as an isolated channel.

Modeling coupled gating by a virtual membrane potential change

Detailed state space models are a good choice to investigate cooperative gating between two channels in the controlled setting of a voltage clamp experiment, but they are less suited to study the behavior of larger channel ensembles in the dynamic setting of an evolving membrane potential. When the number of channels in an ensemble increases, the number of ensemble states grows rapidly as well as the transitions between them. This growth of the state space poses two challenges. First, experimentally inferring the large number of (voltage-dependent) transition rates becomes difficult. Second, numerical simulations

quickly get computationally expensive. Consequently, questions about the role of cooperative gating on spike generation in neurons (Naundorf, Wolf, and Volgushev 2006; Zarubin, Zhuchkova, and Schreiber 2012) or rhythmic activity in heart cells (Sato et al. 2018) have instead relied on simpler heuristic models.

Next, the *voltage-shift model*, a cooperative gating model originally developed for sodium channels introduced by Naundorf et al. (Naundorf, Wolf, and Volgushev 2006), is reviewed. As explained earlier, Naundorf et al. were interested in the question of whether cooperative interactions could synchronize the opening of sodium channels and create sharper spike onsets (see previous section on "Implications of cooperative gating for electrical activity").

To introduce coupled gating, they allowed the voltage-dependent transition rates to also vary with the state of other coupled channels by adding an "effective" voltage shift for each open connected neighbor. Specifically, starting from an established sodium channel model, they modified the opening $\alpha(V)$ and closing rates $\beta(V)$ between the open O and closed C state, which for the ith channel in a cluster of N then read

$$\alpha_i(V, \{\sigma_k\}_{k\neq i}) = \alpha\left(V + j\sum_{k\neq i}\sigma_k\right), \beta_i(V, \{\sigma_k\}_{k\neq i}) = \beta\left(V + j\sum_{k\neq i}\sigma_k\right), \tag{2.7}$$

The important parameter controlling cooperativity is the coupling strength j which determines the "virtual" voltage shift that occurs when a neighboring channel switches from the closed ($\sigma = 0$) to the open state ($\sigma = 1$)[4]. Crucially, when the coupling is positive $j > 0$ mV and the channel is voltage-activated like in the case of sodium channels, the rates at the shifted voltage result in an increased opening and a decreased closing rate. Therefore, a closed channel in the presence of an open neighbor has a higher activation and is also biased to the open configuration (see Fig. 1 of Publication COOPMEM). This bias increases with each open channel, so that the gating of channels coupled in this way indeed becomes more synchronized as expected for positive cooperativity.

From a theoretical point of view, the voltage-shift model is attractive because it is flexible enough to reproduce different aspects of cooperative gating while it

[4]Here, a homogeneous coupling strength is assumed, but generally, it could vary for different channel pairs, e.g., because the interaction is distance-dependent. In this case, the uniform coupling strength j in Equation 2.7 is replaced by individual coupling strengths j_{ik} for each coupled channel pair. Most interaction types are symmetric, i.e., $j_{ik} = j_{ki}$ (e.g. ephaptic coupling, coupling via membrane stretches or allosteric coupling between identical channels with identical bindings sites), but in principle asymmetric coupling $j_{ik} \neq j_{ki}$ could occur, for example between different channel types.

remains amenable to analysis. Reversing the sign of the coupling ($j < 0$ mV), for example, leads to negative cooperativity, where the opening of one channel suppresses the tendency of other channels to open as well, overall reducing their activity – a scenario that has been studied for potassium and calcium channels in a simple neuron model (Zarubin, Zhuchkova, and Schreiber 2012). Furthermore, the voltage-shift model can also be applied to inactivating channels, i.e., those with an activation function decreasing with voltage. Due to the reversed activation function, the effect of the sign of the coupling parameter is opposite in this case: for a positive coupling coefficient, opening of one channel stabilizes the closed state of adjacent channels.

The simple functional form of the voltage-shift model is suited to include cooperative channels into simulations of neurons with multiple conductances. Previous studies considered the case of a large ensemble containing thousands of identical all-to-all coupled channels (Naundorf, Wolf, and Volgushev 2006; Zarubin, Zhuchkova, and Schreiber 2012). As the classical form of the macroscopic gating dynamics from the Hodgkin-Huxley model is no longer valid in this case due to the interdependence of cooperative channels, other approaches have to be used. One way to simulate the conductance of the cooperative ensemble is to directly use the stochastic dynamics of the microscopic state description, which can be combined with the otherwise deterministic dynamics of the membrane potential and the independent channel populations (Zarubin, Zhuchkova, and Schreiber 2012; Anderson, Ermentrout, and Thomas 2015). Alternatively, macroscopic dynamics can be derived using a mean field ansatz, where the exact number of open neighboring channels N_o is replaced by its expected mean (Naundorf, Wolf, and Volgushev 2006; Zarubin, Zhuchkova, and Schreiber 2012). The expected ensemble activation, the mean open probability, then follows recursive dynamics in the form

$$\frac{\mathrm{d}m}{\mathrm{d}t} = \frac{m(V + mJ) - m}{\tau_m(V + mJ)}$$

where $J = (N-1)j$ is the maximal voltage shift that a channel can experience and $m(V)$ and $\tau_m(V)$ are the activation function and respectively gating time scale of the single channel. As expected, the steady-state activation of the ensemble $m_{\mathrm{coop}}(V)$ then differs from the one of the single channel, it can for example become steeper reflecting the increased activity of positively cooperating channels (see Fig. 1 of Publication COOPMEM).

An important aspect missing in previous work using the voltage-shift model is the experimentally observed spatial clustering. Clustering suggests that coupled gating is constrained to small groups of channels. Publication COOPMEM

combines modeling such channel clusters with the question of cooperativity as a cellular memory function, suggesting that such memory is not only possible in small clusters, but that clustering eventually increases memory capacity.

After the current section prepared the ground for this exploration of deviations from the assumption of independent channel gating, the following examines the assumption of membrane capacitance as a constant cell parameter.

2.3 Membrane capacitance

A basic parameter of cellular excitability, often overseen in comparison to the diverse and dynamic ion channels, is membrane capacitance. Splitting the world of a cell in an in- and outside, a membrane creates the spatial structure required for the maintenance of life, including the membrane potential underlying neuronal signaling. Acting as a capacitor, the membrane controls the rate of change in the membrane potential in response to a current. As the membrane potential in turn orchestrates the opening and closing of ion channels, capacitance has broad and significant implications for signaling and processing properties of neurons (Koch 1999).

Still, capacitance is rarely studied. The observation of similar specific membrane capacitance values, the capacitance per area, across different neuron types lead to a seldomly questioned assumption of capacitance as a universal biological constant. Natural variations of capacitance with cell size are thought to be inconsequential, because they are assumed to be compensated by changes in ionic conductances. Critically reviewing these assumptions, the following section motivates why studying capacitance in experiment or theory might yield interesting insights into neuronal dynamics. Finally, the challenge to control capacitance in biological neurons leads to the idea of the capacitance clamp, the dynamic clamp extension to virtual capacitance changes developed in Publication CAPCLAMP.

2.3.1 How capacitance shapes electrical dynamics of neurons

Capacitance, as shown in the section on "Conductance-based neuron models", sets the membrane time constant, the central time scale for the membrane potential dynamics. In this role as a general clock, capacitance affects both single neurons as well as networks by determining the response time to incoming signals and the velocity of action potentials traveling down an axon. Such effects correspond to the expectation of capacitance as a "neuronal metronome" (e.g. action potentials propagate faster at smaller capacitances). The combined non-linear dynamics of membrane potential and active ion channels, however,

are predicted to result in seemingly paradoxical behavior like a sudden doubling of spiking frequency when capacitance is increased (and the dynamics would actually be expected to become slower). Identification of such "critical" capacitance values is of particular interest, because the underlying dynamical transitions are expected to mark switches in a neurons computational abilities.

A very brief history of capacitance and time (constants)

Timing is essential in neuronal signaling. How fast can a neuron respond to a change in its input? What is the minimum time interval that a neuron requires to discriminate two successive inputs? How long can a neuron keep a record of past input? The electrical activity of single neurons is known to exhibit a large dynamic range spanning the sub-millisecond regime up to seconds, further expanded by recurrent network connections into minutes and more. While active ionic mechanisms are a major factor, the temporal properties also depend on the passive membrane properties, namely on the membrane time constant and thereby on capacitance.

The membrane time constant τ_m is highly variable among neurons from $<$1 ms up to 100 ms[5]] reflecting different signaling needs (Tripathy et al. 2014). In addition, heterogeneity of time constants in a network appears to be advantageous for processing of temporal stimuli like speech (Perez-Nieves et al. 2021). Neurons can adapt $\tau_m = RC$ via altering either membrane resistance R or capacitance C. A major difference is that membrane resistance determines both the amplitude and the timing of a voltage response to a current, whereas the membrane capacitance solely determines the timing (see Eq. 2.4). Investigating the effects of the membrane time constant in an isolated fashion hence requires a mean to control capacitance – a simple task in computational modeling, but a challenging one in experiment.

It is important to note that response times of neurons are generally not limited by the membrane time constant, but rather by capacitance itself (Koch, Rapp, and Segev 1996). In a morphologically extended neuron, the response to a step current consists of an infinite sum of exponentials with timescales of which only the slowest is the membrane time constant. But all the time scales are proportional to the specific membrane capacitance. As a result the rise time of a post-synaptic potential in the dendritic tree can be significantly faster than the membrane time constant, but still remains limited by the capacitance.

[5]See the electrophysiology properties collected by NeuroElectro at `https://neuroelectro.org/ephys_prop/4/`

Concerted action of ion channels

Although a passive electrical component, capacitance determines the active behavior of a neuron: the propagation speed of an action potential in an unmyelinated axon is proportional to the inverse of the specific membrane capacitance $1/C_m$ (Koch 1999) and the same scaling applies to the frequency of repetitive spiking, at least for class 1 SNIC-type neurons with fast channel dynamics (Izhikevich 2006). In these examples, the relatively simple dependence on capacitance stems from a quasi-separation of between regimes of active and passive dynamics. In the case of repetitive firing (and in the absence of slow ion channels), ion channels open and close rapidly during the spike, determining its short duration. But these fast channels are in an almost stationary regime during the comparatively long recharging until the next spike, which hence mainly depends on capacitance.

In general, however, more complex scenarios are possible, where the influence of capacitance on the spike shape and the underlying currents, ignored in the above argument, can become decisive and qualitatively switch the firing behavior of a neuron. For example, changing capacitance can turn one class of bursting neuron models (firing bouts of spikes with intermittent long breaks) into regularly firing ones (Franci, Drion, and Sepulchre 2018). Such a switch demonstrates that a change of capacitance can perturb the dynamic balance of ionic currents: when the membrane potential changes more slowly or rapidly in response to a current from one conductance, the relative timing of voltage-dependent activation of another conductance might change and as a result the complete course of the membrane potential takes another shape.

Capacitance as a bifurcation parameter Importantly, in this way capacitance can significantly affect how neurons transition from rest to regular spiking – a transition called "spike onset" type whose nature is known to determine basic signaling properties. One possible switch is a change between the two classical excitability classes briefly introduced in Section 2.1.1. This transition from class 1 to class 2 excitability is associated to the Bogdanov-Takens bifurcation which induces the aforementioned change from an integration to a resonating mode (Izhikevich 2006). Another interesting switch of this kind, termed saddle-node-loop bifurcation, consists in a transition from a SNIC-type to a HOM-type. The SNL bifurcation underlies the above mentioned counterintuitive doubling of spiking frequency as a result of *increasing* capacitance which is usually expected to slow down membrane potential dynamics (Hesse, Schleimer, and Schreiber 2017). Neurons in the HOM regime further exhibit a bistability between a silent rest and an active firing state as well as an increased tendency

to synchronize. Taken together, the effects of capacitance changes can extend beyond mere slowing or acceleration of voltage dynamics to switching between computationally distinct types of spiking.

Probing capacitance in this regard is especially informative for understanding effects of other variables that similarly affect the relative ratio of timescales of the membrane potential and the ion channels (Hesse, Schleimer, and Schreiber 2017). For example, the effects of a larger capacitance, which increases the membrane time constant, share aspects with the effects of a higher temperature, which primarily decreases the gating time constants of ion channels. Accordingly, higher temperatures have already observed to induce a switch to the HOM regime of spiking in hippocampal CA1 neurons (Hesse et al. 2022).

One might ask why theoreticians consider capacitance when studying bifurcations in neuronal dynamics despite the prevailing view that it is constant. The answer lies in the fact that capacitance together with leak conductance and input current are universal parameters of neural dynamics, present in every excitable cell (Kirst et al. 2015). Observing how firing patterns change when varying capacitance hence provides a canonical dimension of characterizing a neuron's dynamics and the specific set of present ion channels.

2.3.2 Capacitance – constant or variable?

The broad implications of capacitance suggest that its value is an important determinant of neural function. Whereas there is general agreement that neurons specialize for their respective function through cell-specific and adaptive expression of ion channels, there is less certainty about how capacitance varies among and within cells and which biophysical mechanisms underlie the regulation of membrane properties determining capacitance.

Measuring membrane capacitance Capacitance characterization, required to answer these questions, is a standard step in electrophysiology and an important prerequisite for neuronal modeling (Golowasch et al. 2009). Typically, experimenters are interested in the *total membrane capacitance* C and use either current-clamp and voltage-clamp protocols to estimate it. If in addition, a morphological reconstruction of the neuron is used to measure its surface area A, the *specific membrane capacitance* $C_m = \frac{C}{A}$ can be inferred. In current-clamp, a step current of amplitude I_0 is injected and capacitance can be estimated by extracting the response amplitude ΔV and membrane time constant τ_m from the exponential charging curve of the membrane potential (see Eq. 2.4)

$$C = \frac{\tau_m}{R} = \frac{\tau_m}{R} = \tau_m \frac{I_0}{\Delta V}.$$

In voltage-clamp, a voltage step of amplitude V_0 is used and capacitance is estimated by using the transient part of the clamping current $I_C(t)$ to calculate how much charge ΔQ accumulated on the membrane

$$C = \frac{\Delta Q}{V_0} = \frac{\int I_C(t)\mathrm{d}t}{V_0}.$$

Still, accurate capacitance measurements are difficult. The above methods are only valid in a compact isopotential cell, whereas most neurons have extensive dendritic trees and correspondingly a large distributed electronic structure. In voltage clamp, compartments further away from the clamped one exhibit smaller voltage changes, resulting in reduced capacitance estimates (Golowasch et al. 2009; Taylor 2012). In current-clamp, the total membrane capacitance can still be estimated, but this requires careful exponential "peeling": the voltage response becomes a sum of exponentials and only the slowest timescale corresponds to the membrane time constant (as explained in more detail in Publication CAPCLAMP17). An alternative is to directly reproduce the observed voltage response by optimizing the specific membrane capacitance and other passive membrane parameters in a multicompartment simulation of the reconstructed morphology (Nörenberg et al. 2010; Eyal et al. 2016). Here, challenges are the reconstruction of small structures like spines in the dendrites and choosing assumptions on the heterogeneity of parameters across the morphology. In addition to the difficulty of a non-compact morphology, another factor is that capacitance measurements rely on the assumption of a passive membrane. The activation of voltage-gated ion channels can thus affect capacitance estimates and should be minimized or controlled for (White and Hooper 2013).

Given these difficulties, it is still an open question how variable capacitance is among neurons and whether this variability has functional implications. As indicated in the review of the assumptions underlying neuronal modeling in the section "Conductance-based neuron models", the predominant view is that unavoidable variations due to surface area are compensated by ionic conductances and that the specific membrane capacitance is uniform among biological membranes. However, this view is challenged by a number of reported exceptions, which are reviewed in the following based on the membrane properties determining capacitance, namely surface area, thickness and lipid composition (see Eq. 2.2 and Fig. 1 of Publication CAPCLAMP).

Capacitance changes with the size of a neuron The dependence of capacitance on area implies that capacitance naturally varies between neurons with

different morphologies and within a cell during development. For example, studying developmental trajectories of neurons in the rat brain, capacitance was observed to increase by a factor of ≈ 2 during the first two postnatal weeks (Dufour et al. 2014). This increase of capacitance was however accompanied by a decrease of membrane resistance, so that the membrane time constant $\tau_m = RC$ remained relatively constant. Based on such measurements, it is usually assumed that capacitance increases due to changes in surface area are naturally compensated by increased channel numbers.

Still, the area dependence of capacitance might play a role in cases where a compensation by ion channels is too slow, complex or costly. An example of changes in area and capacitance that are appears too fast to be countered by channel expression is swelling of neurons due to activity-dependent changes of ionic concentrations, for example, during seizures (Amzica and Neckelmann 1999). Moreover, the simple argument that neural dynamics are preserved by a simultaneous increase of membrane capacitance and conductances cannot hold for dendritic growth, because dendrites tend to have a different channel densities in comparison to the soma (Nusser 2012). The regulation of firing in the presence of additional dendritic capacitative load therefore posits more elaborate mechanisms linking capacitance and conductances than merely a constant channel density, e.g., processes that set cellular excitability by activity-dependent channel expression (Gorur-Shandilya, Marder, and O'Leary 2020). Finally, even when neural dynamics can be preserved, it is to be expected that the increased capacitance in larger cells leads to a rise in ionic currents and therefore higher energetic costs of spiking (Hasenstaub et al. 2010; Sengupta et al. 2010; Stemmler et al. 2011).

Specific capacitance depends on membrane thickness and composition - constant or adaptive? Whereas membrane area is an extrinsic determinant of capacitance, true intrinsic adaptations would be expected to affect the specific membrane capacitance, the capacitance per area. Whether biological membranes with their multifold functions are flexible enough to differ in thickness or composition in ways that significantly change the specific membrane capacitance is an open question.

As the specific membrane capacitance is required to formulate neuronal models, considerable experimental efforts have been made to measure it. Early measurements combined electrophysiology and microscopy to determine both cell capacitance and surface area of a whole cell and found a range of values from 0.6 to 3 $\frac{\mu\mathrm{F}}{\mathrm{cm}^2}$ (Koch 1999). These measurements, however, yielded large uncertainties and as a global measure could not resolve potential differences in

specific membrane capacitance between neuronal compartments. More accuracy and spatial resolution can be achieved by estimating the specific membrane capacitance of a nucleated patch "pulled" from the membrane of a neuron. The nucleated patch technique has been applied in an influential study by Gentet, Stuart, and Clements which found a value of 0.9 $\frac{\mu F}{cm^2}$ in three different cell types. Based on these findings, the authors suggested that the specific membrane capacitance, "is, to a first approximation, a 'biological constant' "(Gentet, Stuart, and Clements 2000, p.320). In modeling, this value, conveniently simplified to 1.0 $\frac{\mu F}{cm^2}$, is correspondingly treated as a universal constant and capacitance variations have rarely been considered.

When Eyal et al. explored the electrophysiological properties of pyramidal cells from human neocortex, it was hence especially surprising that one unique feature in these neurons was a reduced specific membrane capacitance of 0.5 $\frac{\mu F}{cm^2}$ (Eyal et al. 2016). This value was first discovered in the process of estimating parameters for a conductance-based models of these cells and then corroborated by the above mentioned nucleated patch technique. Based on simulations, the authors proposed that this reduction of capacitance could be a compensatory measure for the large size of human cells, for example to facilitate the integration of synaptic inputs. The finding is not without controversy: a similar characterization of pyramidal cells from a different layer in human neocortex, layer 5 instead of layer 2/3, yielded specific capacitance estimates of 0.9 $\frac{\mu F}{cm^2}$, the same value as in mouse and rat cells. Concluding, more research is needed to characterize neuronal membranes in different animals and brain regions before accepting the paradigm of a universally constant specific membrane capacitance.

Mechanisms of altered capacitance

Support for possible alterations of specific capacitance also comes from new hypothesis on how its determinants – membrane thickness and composition – could be altered. A prominent known case of increasing the effective thickness of membranes is myelination: repeated wrapping of axons in sheaths of membrane by Schwann cells (Hartline and Colman 2007; Castelfranco and Hartline 2015; Cohen et al. 2020). The correspondingly reduced capacitance, as well as the high resistance, is a prerequisite for the "saltatory" conduction mode of myelinated axons, yielding a multifold increase of propagation speed compared to unmyelinated axons of the same diameter (Swadlow and Waxman 2012; Cohen et al. 2020). Myelination has only been observed in axons, but increases of effective membrane thickness could be a more general mechanism to reduce capacitance. In particular, perineuronal nets (PNNs) – structures in the extracellular space surrounding neurons – have been observed to decrease the (total) capacitance

of inhibitory interneurons, potentially by "thickening" the membrane via tight association. The actual thickness of membranes, in contrast, appears to be relatively constant; for example mice and human neurons both have 5-6 nm thick membranes (Eyal et al. 2016). The reduction of the specific capacitance in human cells thus hints at a reduced electric permittivity due to differences in the lipids and proteins composing these membranes (Niles, Levis, and Cohen 1988; Eyal et al. 2016).

2.3.3 Experimental modification of capacitance

In modeling, capacitance modification is simple, allowing theoreticians both to explore the consequences of exceptional capacitance values as well as to exploit changing capacitance as a tool to better characterize neuronal dynamics. Ideally, these predictions could also be tested in biological neurons by a tool to experimentally modify capacitance in a controlled fashion. In today's repertoire of electrophysiology, however, such a tool is missing.

Experimental means to physically interact with biological membranes are actively researched and might eventually provide access to membrane capacitance. For example, focused ultrasound is an interesting candidate for non-invasive stimulation of neurons and its excitatory effects are hypothesized to be mediated via fast changes of membrane capacitance caused by rapidly expanding and contracting membrane thickness (Plaksin, Shoham, and Kimmel 2014). Alternatively, persistent capacitance changes could be achieved by merging biological membranes with artificial components, for example electroactive polymers that alter the native dielectric properties and/or the thickness of a membrane (Liu et al. 2020). However, such techniques are still under investigation and might affect ionic conductances.

In the case of ionic conductances, pharmacological and genetic techniques to modify ion channels are complemented by the insertion of virtual channels via the dynamic clamp technique (see Section "Dynamic Clamp"). Similarly precise control as offered by the dynamic clamp for these virtual channels would also be desirable for the membrane capacitance. The idea of a virtual change of membrane capacitance via the dynamic clamp is the goal of Publication CAPCLAMP.

3 Research aims

The overarching question behind the work presented in this thesis is how aspects of the biophysics of a single neuron affect its dynamical and signaling repertoire. As introduced in the background section, it approaches this question by exploring two assumptions on the biophysics of biological membranes, the independent channel assumption and the notion of membrane capacitance as a biological constant. In this context, this cumulative thesis addresses the following specific questions:

1) How does positive feedback inherent to cooperative interactions among ion channels in small clusters alter their collective dynamics? And, given the often observed role of positive feedback for memory, whether such clusters can mediate multi-stable firing patterns suited for cell-intrinsic memory functions?

2) How can the dynamic clamp technique, originally developed to inject artificial conductances in biological neurons, be extended to modify the capacitance of a cell? And which new ways such a capacitance clamp opens to to study neuronal dynamics?

Publication COOPMEM: Dynamics of small clusters of cooperative ion channels

The first question of this thesis, which dynamics emerge in a small cluster of cooperative ion channels, is motivated by the fact that despite solid experimental evidence for coupled gating in various channel types, the functional role of such interactions remains unclear. The hypothesis that a small cluster of cooperative channels can act as a bistable macrochannel is based on the analogy to a magnet. In a magnet ("the cluster"), the magnetic fields of individual atoms ("conductance states of the channels") can be directed by a transient external field ("membrane potential"), but then keep this direction ("multistability") by mutually aligning to the direction of the neighbors ("cooperative gating"). Regarding function, bistable clusters of cooperative channels could then serve as a basic cellular memory unit – just like magnets in a hard drive. More precisely, they could conduct currents that reflect previous activity levels of a cell. This

might explain firing patterns of cell-intrinsic memory like graded persistent firing that have been difficult to understand so far.

Experimentally, detecting ion channel cooperativity remains challenging, not to mention controlled modulation of the underlying channel interactions. Here, a computational approach is taken. To this end, the project builds on the voltage-shift model for cooperative gating proposed in earlier computational studies (Naundorf, Wolf, and Volgushev 2006; Zarubin, Zhuchkova, and Schreiber 2012) but adds an important biophysical constraint, namely the spatial clustering of channels, where cooperative interactions are restricted within a cluster. The resulting cluster model is used to investigate various aspects of cluster dynamics, especially bistability and the related cell-intrinsic memory hypothesis:

- How do the emergent dynamics of a cluster depend on the kinetics (activation function, gating time constant) of its constituent channels and the degree of cooperativity? Given that bistability is expected to require strong interactions, can the necessary coupling strengths be derived from the channel parameters?
- What is the role of channel noise? As experimentally observed clusters only contain a small number of channels (≈ 10), the stochastic nature of gating – spontaneous transitions between channel states – cannot be neglected. In particular, channel noise could mean that clusters must have a minimum size to act as reliable memory elements.
- How do the firing patterns of a neuron equipped with the basic channel repertoire required for the generation of action potentials (independently-gating sodium and potassium channels) change when an ensemble of clusters of cooperative channels is added to its membrane? In particular, could such a neuron exhibit bi- or multistable firing patterns like graded persistent activity in the absence of synaptic network interactions?

Approaches to these questions presented in the second article of this thesis use a mean-field analysis and detailed stochastic simulations to characterize the cluster dynamics. To demonstrate the potential memory function, the conditions for the emergence of graded persistent activity are first explored in simulations of a conductance-based neuron model equipped with clusters of cooperative channels. This demonstration is validated in biological neurons making use of the "classic" dynamic clamp technique to add virtual cooperative channels to rodent pyramidal cells.

Publication CAPCLAMP: A dynamic clamp protocol to modify membrane capacitance

The second part of this thesis addresses the question whether it is possible to extend the dynamic clamp to artificial capacitance modification. This idea of a capacitance clamp (CapClamp) is motivated by the success of this technique in its "classic" form. The ability to study hybrids of biological neurons and artificial computer-controlled conductances has enabled electrophysiologists and modelers to study neuronal dynamics in ways that were otherwise impossible as demonstrated by the dynamic clamp experiments reviewed in the previous section. It appears natural to ask whether the flexibility of the closed-loop between voltage sampling, a custom computer program, and current injection underlying the dynamic clamp can also be used to artificially alter membrane capacitance.

Membrane capacitance is interesting, because it is a basic parameter shared by all excitable cells that is still rarely considered. Commonly assumed to be constant in mature neurons, the role of exceptional capacitance values remains little understood. Capacitance is the only neuronal parameter that exclusively changes the membrane time constant – a property that has been exploited in theoretical studies to investigate computationally-relevant switches between excitability classes. Importantly, while theory suggests that capacitance is an interesting parameter to study, experimental tools to alter it in a controlled fashion have been missing.

The simple effect of an altered capacitance, namely to change the rate of change in the membrane potential in response to a current, makes a capacitance clamp in principle conceivable: it would require clamping currents calculated such that the membrane potential changes either faster (targeting an increase of capacitance) or slower (targeting a decrease) than with the cell's original physical capacitance. This thesis intends to mathematically derive these clamping currents from the form of the membrane potential dynamics in conductance-based neuron models and thereby clarify questions decisive for turning the capacitance clamp into a practical tool applicable in experiments.

- Which knowledge about the recorded cell does the experimenter need to clamp its capacitance? As discussed in the previous section, adding artificial conductances by the "classic" dynamic clamp is possible without prior knowledge, but knocking out existent ones – while theoretically possible, requires a very accurate model of its gating dynamics often not available in practice.

- What are the hardware requirements to clamp a cell's capacitance? Again,

in the case of virtual conductances, one prerequisite is that the dynamic clamp loop interval has to be shorter than the channel gating time constants, which can be challenging for fast channel types e.g Na^+.

- Are there limitations to the range of capacitances a cell can be clamped at? And how accurately does a clamped cell, given that its physical capacitance will not be altered, mimic the behavior of a cell undergoing a real capacitance change? In particular, does the combined system of a biological cell and the capacitance clamp behave as expected close to critical capacitance values where transitions are expected, potentially involving fast dynamics?

- Are there constraints on the cell types to which the capacitance clamp can be applied? Most biological neurons have elaborate morphologies with branching axons and extended dendritic trees, so that membrane capacitance is a spatially distributed quantity. Can the capacitance clamp act locally in such cells or is it constrained to small, electronically compact cells where the spatial dimension is negligible?

To answer these questions, Publication CAPCLAMP takes various approaches to test and validate the capacitance clamp both in simulations and experiments. Simulations of conductance-based neuron models, including both spatially simple one-compartment and biologically more realistic multi-compartment ones, have the advantage that the actual dynamics of a neuron clamped at a given capacitance can be simply contrasted with the expected ones (that is those of the same model with an altered capacitance parameter). While a similar approach is impossible for a biological neuron, basic expectations on measurable quantities can be formulated to examine the capacitance clamp experimentally, e.g., on the dependence of the membrane time constant(s) on capacitance. Finally, once having established the capacitance clamp in this way, this thesis aims to illustrate proof-of-concept applications demonstrating its value as a new tool for electrophysiology.

4 Publications

4.1 COOPMEM – Clusters of cooperative ion channels enable a membrane-potential-based mechanism for short-term memory

Paul Pfeiffer, Alexei V. Egorov, Franziska Lorenz, Jan-Hendrik Schleimer, Andreas Draguhn, and Susanne Schreiber (Feb. 2020). "Clusters of Cooperative Ion Channels Enable a Membrane-Potential-Based Mechanism for Short-Term Memory". In: *eLife* 9, e49974. ISSN: 2050-084X. DOI: 10.7554/eLife.49974

Supplementary figure(s) follow directly after the main article.

eLIFE elifesciences.org

RESEARCH ARTICLE

Clusters of cooperative ion channels enable a membrane-potential-based mechanism for short-term memory

Paul Pfeiffer[1,2]*, Alexei V Egorov[3], Franziska Lorenz[3], Jan-Hendrik Schleimer[1,2], Andreas Draguhn[3], Susanne Schreiber[1,2]*

[1]Institute for Theoretical Biology, Humboldt-Universität zu Berlin, Berlin, Germany; [2]Bernstein Center for Computational Neuroscience, Humboldt-Universität zu Berlin, Berlin, Germany; [3]Institute of Physiology and Pathophysiology, Heidelberg University, Heidelberg, Germany

Abstract Across biological systems, cooperativity between proteins enables fast actions, supralinear responses, and long-lasting molecular switches. In the nervous system, however, the function of cooperative interactions between voltage-dependent ionic channels remains largely unknown. Based on mathematical modeling, we here demonstrate that clusters of strongly cooperative ion channels can plausibly form bistable conductances. Consequently, clusters are permanently switched on by neuronal spiking, switched off by strong hyperpolarization, and remain in their state for seconds after stimulation. The resulting short-term memory of the membrane potential allows to generate persistent firing when clusters of cooperative channels are present together with non-cooperative spike-generating conductances. Dynamic clamp experiments in rodent cortical neurons confirm that channel cooperativity can robustly induce graded persistent activity – a single-cell based, multistable mnemonic firing mode experimentally observed in several brain regions. We therefore propose that ion channel cooperativity constitutes an efficient cell-intrinsic implementation for short-term memories at the voltage level.

***For correspondence:** pfeiffpa@hu-berlin.de (PP); s.schreiber@hu-berlin.de (SS)

Competing interests: The authors declare that no competing interests exist.

Funding: See page 24

Received: 05 July 2019
Accepted: 14 January 2020
Published: 07 February 2020

Reviewing editor: José D Faraldo-Gómez, National Heart, Lung and Blood Institute, National Institutes of Health, United States

Introduction

Cooperative molecular interactions are ubiquitous in biology and guide cellular processes from sensing to memory formation (***Bray et al., 1998***; ***Burrill and Silver, 2010***). They are found not only in the simplest organisms like bacteria, but also in higher organisms including mammals (***Stefan and Le Novère, 2013***). Evidence increases that also ion channels of excitable membranes in the heart and the nervous system, including the mammalian brain, can exhibit cooperative properties (***Choi, 2014***; ***Molina et al., 2006***; ***Grage et al., 2011***; ***Kim et al., 2014***; ***Gianoli et al., 2017***; ***Navedo et al., 2010***; ***Dixon et al., 2015***; ***Moreno et al., 2016***; ***Clatot et al., 2017***; ***Vivas et al., 2017***). Nevertheless, the majority of neuron models relies on the independent gating assumption: channels communicate indirectly via the common membrane potential, but do not directly influence each other. Thus, it is an open question how cooperative channels affect the electrical dynamics - and therefore the computations - of a neuron.

Experimentally, ion channel cooperativity has been studied in various channel types with key roles in the nervous system such as potassium (***Molina et al., 2006***; ***Kim et al., 2014***), sodium (***Iwasa et al., 1986***; ***Undrovinas et al., 1992***; ***Clatot et al., 2017***), HCN (***Dekker and Yellen, 2006***) and calcium channels (***Dixon et al., 2015***; ***Moreno et al., 2016***). However, most studies have focused on the demonstration of cooperative gating in small ensembles of channels and avoided the complex dynamics of the neuron as a whole. An exception is the study of cooperative calcium channels in rodent hippocampal neurons, where optical control of channel coupling has revealed that the

spontaneous firing rate rises when channels cooperate (**Moreno et al., 2016**). With such control of channel interactions, future experiments have the means to test hypothesis on the function of cooperativity.

So far, a few computational studies predict effects of cooperativity. Along these lines, cooperative sodium channels have been suggested to underlie the rapid initiation and low variability of spiking onset in cortical neurons (**Naundorf et al., 2006**; **Huang et al., 2012**; for an alternative mechanism see **Yu et al., 2008**) and mild cooperative interactions in potassium and calcium channels have been shown to modify the steepness of a channel's activation curve and modulate neural excitability (**Zarubin et al., 2012**). Furthermore, cardiac alternans, a pathological condition of unstable heart contractions, has been linked to strong degrees of coupling among cooperative calcium channels (**Sato et al., 2018**). These studies demonstrate that cooperative channels can significantly alter cellular firing properties with a range of effects from advantageous to pathological depending on the interplay with other currents in the cell.

Here, we show in simulations and mathematical analysis that small clusters of cooperative channels with simple and generic activation dynamics can induce a multistability of the membrane potential and demonstrate that this multistability enables a form of cellular memory. Our central observation is that the mutually enhancing nature of cooperative gating favors joint opening and closing of channels, and, more importantly, results in a hysteresis of their gating behavior. We demonstrate that such cooperative channels - when arranged in clusters and located in membranes with 'normal' independent conductances that mediate spiking - can induce graded persistent neural activity: spiking that persists after transient suprathreshold depolarization and represents successive inputs with increasing persistent firing rates. Taken together, we propose that cooperativity of a few ion channels is an elegant way to implement a cell-intrinsic memory directly reflected in a cell's firing. In principle, ion channel cooperativity could thus efficiently complement network-based mechanisms of persistent activation and thereby contribute to decision making (accumulation of evidence) and working memory. Overall, the emergence of memory in a cluster of coupled, yet in isolation memoryless channels suggests a more general design principle: cooperativity serves to dynamically build functionally rich macrochannels from simpler channels.

In the following, we first dissect the mechanism and compare the gating of independent versus cooperative ion channel clusters. We then add clusters of cooperative channels to a simple neuron model with non-cooperative, spike-generating sodium and potassium channels, proving the ability of ion channel cooperativity to mediate graded persistent activity. Finally, we use the dynamic clamp technique to experimentally endow perirhinal cortex neurons with 'virtual' cooperative ion channels and show that stable persistent activity can be robustly induced, rendering ion channel cooperativity an efficient and plausible mechanism for cellular voltage memory.

Results

Although the mechanisms of cooperative interactions among ion channels are still not fully understood on the molecular level, it can be assumed that ion channels need to be in spatial proximity to directly interact and gate in a cooperative manner (**Gutkin and Ermentrout, 2006**). Matching this assumption, cooperativity is often found in channels that form small clusters (**Molina et al., 2006**; **Choi, 2014**; **Navedo et al., 2010**; **Moreno et al., 2016**). For our study, we therefore assume that the cooperative channels are distributed in multiple clusters and limit cooperative interactions to channels within the same cluster. In this regard, we deviate from previous theoretical studies, where all-to-all interactions between channels in a membrane have been investigated (**Naundorf et al., 2006**; **Zarubin et al., 2012**; **Huang et al., 2012**). To understand the underlying principles, we begin with a comparison of gating properties in a cluster of cooperative versus non-cooperative ion channels.

Gating of a cluster of cooperative channels

A cluster is assumed to comprise S voltage-gated channels of the same type, whose individual activation curve is a monotonically increasing, yet saturating function of voltage. To ensure the generality of the analysis, we make no further assumptions on other channel properties like their ionic nature and therefore simply refer to them as 'channels'. Cooperative interactions are chosen to be enhancing, that is the opening of a channel in the cluster increases the opening probabilities of all

other $S-1$ channels. This increase in opening probability is implemented phenomenologically by shifting the channels' activation curves to lower voltages for each new opening of a neighbor. The size of the shift j induced by one new opening is a measure of the coupling between channels in the cluster (***Naundorf et al., 2006***; ***Zarubin et al., 2012***; ***Huang et al., 2012***). An important determinant for the cluster dynamics is the maximal shift $J=(S-1)j$, which a channel experiences, when all neighbors are in the open state (***Figure 1A***). Variation of this interaction strength from independent (J = 0 mV) to strongly cooperative (J = 70 mV) yields the activation curve of a cluster of S channels. Clearly, an isolated channel and channels in an independent ensemble have the same activation curve. Mild cooperative interactions, however, increase the channel activity and make the activation curve steeper. Beyond a critical coupling, the activation curve 'bends over', which characterizes the regime of strong cooperativity (***Figure 1B***).

Simulating a simple voltage clamp experiment in a membrane patch containing a cluster of six channels demonstrates fundamental differences between the gating of independent and cooperative clusters: The conductance dynamics of a cluster of independent channels is identical to the sum of its individual, independent components. Therefore, the single channel opening probability dictates the most probable cluster state (defined by the channel activation curve and the voltage) and the cluster conductance fluctuates around this state following a binomial distribution (***Figure 1C***, top). At the half-activation voltage, the cluster average is at half of its total conductance. Fluctuations in the total cluster conductance are relatively fast (due to channel gating time constants of ≈ 1 ms).

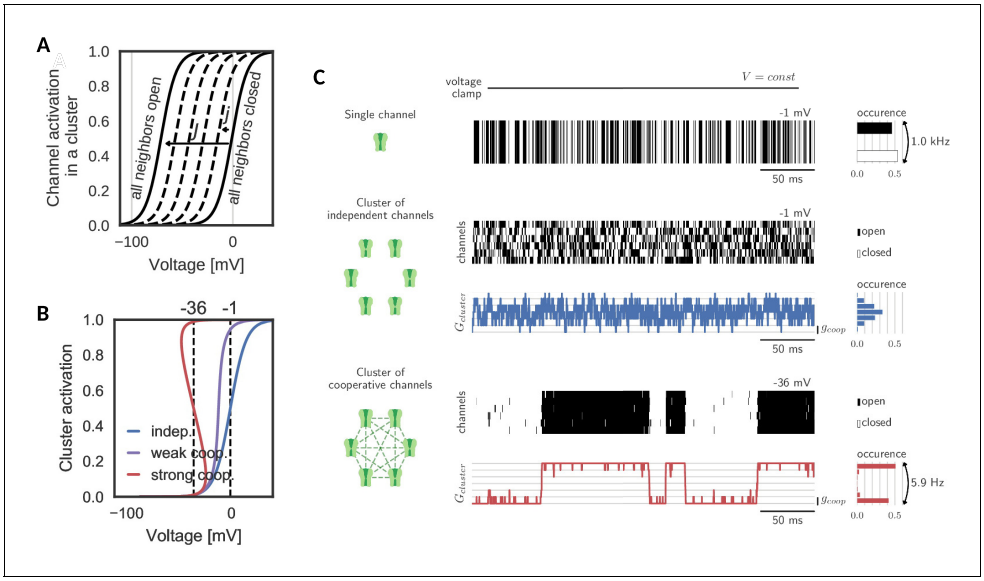

Figure 1. Gating of a cluster of cooperative channels. (**A**) Model of cooperative gating: the activation of a channel in a cluster depends on the state of the surrounding channels. Opening of a neighboring channel leads to a shift of the activation curve by the coupling strength *j*. When all neighbors are closed, the activation coincides with the one of an isolated channel, whereas when all neighbors are open, the activation undergoes the maximal shift *J*. (**B**) Cluster activation: cooperative interactions inside a cluster increase the channel activity, so that the activation curve becomes steeper (weak coop.). Above a critical coupling strength, the activation starts to 'bend over' (strong coop.); whether a channel is open or closed is determined mostly by the state of its surrounding channels. Activation curve based on a self-consistency relation, for details see Materials and methods. (**C**) *Top*: Simulation of a voltage clamp experiment with an isolated two-state channel shows fast, random switching between the conducting (black) and non-conducting (white) state. Operated at the half-activation potential $V_{0.5}$, the channel spends about half of the time in the open state. *Middle*: In a cluster of independent channels, their asynchronous gating results in a fluctuation of the cluster conductance around half of the total conductance. *Bottom*: Cooperative channels have a strong preference for the state of the surrounding channels. In a cluster, they open and close in synchrony acting like a macrochannel. Its slow switching frequency demonstrates the stability of the open and closed cluster state. As the cooperative channels are more active compared to the independent ones, they are clamped at more hyperpolarized voltages: −1 mV (independent) and 36 mV (cooperative). The details of the jump process simulation are given in the section Materials and methods and parameters are summarized in ***Table 1***.

The picture changes when ion channel cooperativity is introduced. Assuming strong interactions, all channels in a cluster gate open and close quasi-simultaneously (at a voltage level within the regime where the activation curve 'bends over'). Intuitively, this coordination within a cluster can be easily understood: the opening of ion channels strongly enhances the probability of their neighbors to open. Similarly, the closing of channels reduces the probability of their neighbors to remain open, so that gating dynamics largely synchronize. The distribution of total cluster conductance now deviates from the unimodal, binomial distribution of clusters with independent channels: it becomes bimodal reflecting the alternation between a fully closed and a fully open cluster state (***Figure 1C***, bottom). Note that the bistability is accompanied by a novel slow time scale; the cluster switches between the all-open or all-closed states at a drastically reduced rate (6 Hz) compared to its constituting channels when independent (1000 Hz). Effectively, the bistability and the slow switching let the cluster of cooperative channels appear as one slow macrochannel (***Blunck et al., 1998***).

Hysteresis and bistable gating

The new, slow timescale also changes the response of the cluster to a pulsatile stimulation protocol. During a sufficiently strong depolarizing pulse, all channels in both the cooperative and independent cluster open. Once the pulse is over and voltage returns to baseline, the cluster of independent channels follows and channels swiftly return to the closed state. In the case of the cooperative cluster, however, channels in the cluster remain open, despite the return of the clamped voltage value to its original value before the pulse onset. The strong channel interactions introduce what we would like to term 'stickiness': the cluster 'sticks' to its new open state (even when voltage levels are back to 'normal') and can only be released from this state by a sufficiently strong hyperpolarization (***Figure 2A***). In other words, cooperative gating induces hysteresis and hence allows channels in a cluster, which are fast switching in isolation, to represent (i.e. 'remember') voltage values that occurred multiple hundred milliseconds ago.

The hysteresis in gating arises from the bistability of the cluster. Before the depolarizing pulse, the channels in the cluster are closed, which is a stable cluster state, because the single channel is not activated at this membrane potential and there is no facilitation between closed channels. During the pulse, channels open, and this open cluster configuration is stable at the baseline voltage, because the strong coupling allows the channels to secure each other in the open state. Only when the voltage is lowered further, it overcomes the mutual facilitation and the channels close again.

The bistability reflects those effective cluster activation curves that 'bend over' (***Figure 2B***). Consequently, cluster size, channel coupling and the shape of the isolated channel's activation curve determine the voltage range of bistability. Both an increase in channel coupling j and cluster size S can lead to a stronger overall cooperativity strength J, which is the product of the two. Bistability arises from a critical overall cooperativity strength J_{crit}, which depends on the shape of the single channel activation. With increasing J, the bistable range broadens and extends to more hyperpolarized voltages (***Figure 2C***). Correspondingly, for a cluster with more channels and/or strong coupling, which both result in a larger J, the voltage pulse to close the cluster has to be stronger in order to leave the bistable range.

Due to their self-excitatory effect, channels in a cooperative cluster can be compared to neurons in a recurrently connected network: if the external input is low, the neurons are silent, but during a short stimulation they switch to a very active state, which they sustain after the stimulation by recurrent self-excitation. Such networks have been proposed to underlie the short-term storage of stimuli in working memory (***Durstewitz et al., 2000***). This poses the question, whether in a similar way, a cluster of cooperative channels can act as a memory unit for a single neuron. In order to address this question, we first need to better understand the emerging slow timescale of switches between cluster states in the cooperative regime.

Prolonged lifetimes of the open and closed cluster state

As we have seen, hysteresis allows clusters to act as a voltage memory. After high voltages, they remain open and after low voltages, they remain closed. Eventually, however, a cluster spontaneously switches its state - in a quasi-synchronous fashion all channels open or close (***Figure 3A***). These switches originate in channel noise, stochastic gating of individual channels. If multiple channels coincide in their spontaneous gating, their neighbors quickly follow. Both opening and closing of

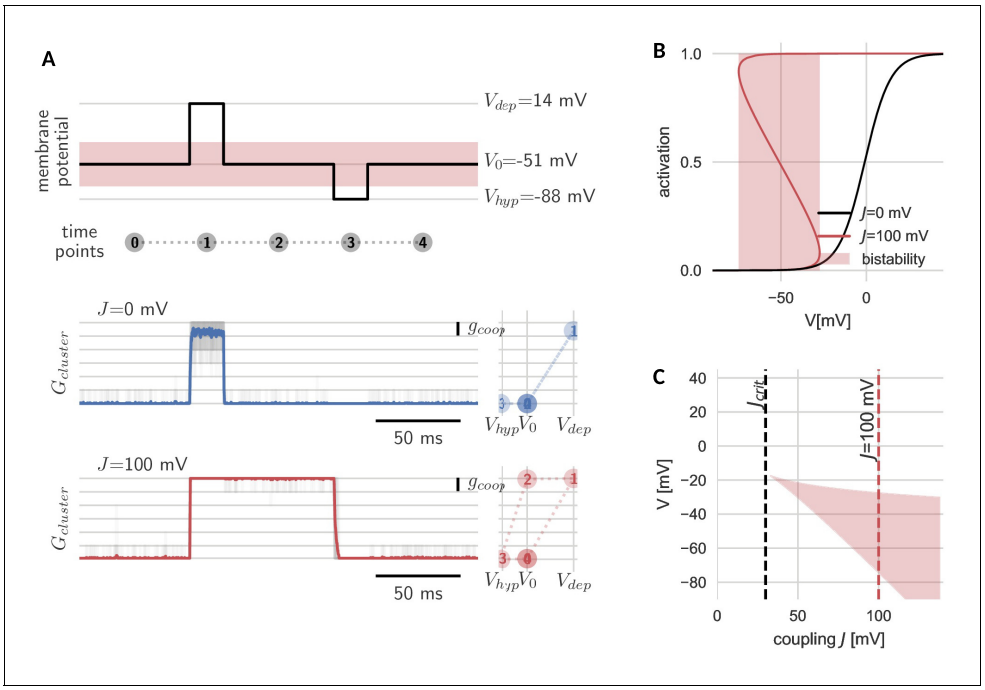

Figure 2. Hysteresis and bistability of a cluster of cooperative channels. (**A**) Probing an initially closed cluster (time point 0), both independent (blue) and cooperative (red) channels open in response to a depolarizing voltage pulse (1). However, returning to the base line voltage (2), independent channels rapidly close again, whereas a cluster of cooperative channels 'sticks' to the open configuration. Only a strong hyperpolarizing pulse (3) can close the cooperative channels and restore the initial condition (4). Tracking membrane potential versus conductance during the pulse protocol (right panels), the hysteresis in gating for the cooperative channels becomes apparent; whether the cluster is open or closed at baseline voltage depends on the previous voltage pulse. The transparent lines correspond to 20 repetitions of the pulse protocol and the solid lines are the respective means. (**B**) Strong coupling among channels changes the activation in a cluster (red) with respect to an isolated channel (black) and induces a voltage regime of bistability (red shaded). (**C**) Clusters only become bistable beyond a critical coupling strength (black dashed) and for increasing coupling, the bistable range extends to lower voltages. Cluster and channel parameters are summarized in ***Table 1***.

channels spread by cooperative coupling; in a spiral of facilitation build-up or, reversely, in a spiral of facilitation loss (***Figure 3—figure supplement 1***). These gating avalanches, however, cannot be triggered by single or few channels, so that the life times of a cluster can be orders of magnitude longer than those of the single channel.

Figure 3 shows the lifetimes of the open and closed states - exemplary in a cluster with five channels - as a function of voltage. These lifetimes are defined as the time $\tau_{O\to C}$ it takes, once all channels are open until all channels are closed again, and vice versa for $\tau_{C\to O}$. In the center of the bistable range, both open and closed cluster state are very robust against channel fluctuations with mean residence times in the range of seconds (***Figure 3A***). However, at the verges of the bistable range, channel noise corrupts the stability. At low voltages, an open cluster switches back to the closed state within $\approx$ 10 ms, whereas at high voltages, within in the same time, a closed cluster spontaneously opens. Thus, for a persistent representation of recent voltage history, the middle voltage range offers the longest memory lifetimes: here both the probability to lose an open cluster state and to lose a closed cluster state are low - a prerequisite for encoding of previous voltages in a persisting cluster state (***Figure 3A***). The lifetimes in this voltage range define the memory timescale τ_{max} of the cluster, that is the time during which a cluster of cooperative ion channels can act as a reliable memory device. For completeness, ***Figure 3B*** shows the numerically derived center of the bistable range V_{max} and the memory timescale τ_{max} for clusters of different sizes and with different channel-channel coupling j. We find that both, larger cluster size and stronger channel coupling, favor bistability. Although quantitative data on cooperative interactions is scarce, we note that for a cluster of eight channels coupled with strength j = 17 mV, the mid-voltage of the bistable range decreases to -60

mV and the average lifetime of the open and closed state exceeds hundreds of seconds, rending this paradigm suitable for persistent activation in the context of short-term memory.

In general, our analysis shows that, as expected, larger and more strongly coupled clusters have a more hyperpolarized operation voltage and longer life times. Even for clusters with the same maximal shift J (that is hyperboles in ***Figure 3B***), we observe a pronounced increase in lifetime with cluster size. In other words, large clusters of weakly coupled channels tend to be more stable than small clusters of strongly coupled ones. This observation is explained by a reduction of effective channel noise when more channels are added to a cluster.

Clusters as cellular memory units can mediate persistent spiking

The analysis so far showed that clusters of cooperative ion channels can implement a memory of recent voltage levels in their opening state. Next, we demonstrate how this property - when exhibited by small clusters of channels not even directly involved in the generation of spikes - can lead to persistent neuronal activity that does not require further network input. Interestingly, we find that clusters of cooperative channels can even solve the computationally harder problem required for a graded form of persistent activity. In this graded form, the neuron can signal previous input strength and input duration in the frequency of long-term stable firing. Hence, we propose that ion channel cooperativity offers a generic mechanism for cellular memory.

Neural signaling events lead to controllable, persistent cluster switches

To this end, we extend a Hodgkin-Huxley type neuron model including (independent) sodium and potassium channels by a set of 100 small clusters of cooperative channels with the generic activation kinetics described above (for details on the neuron model, see Materials and methods). On the ionic nature of the latter, we assume for the moment that they conduct a depolarizing current like for

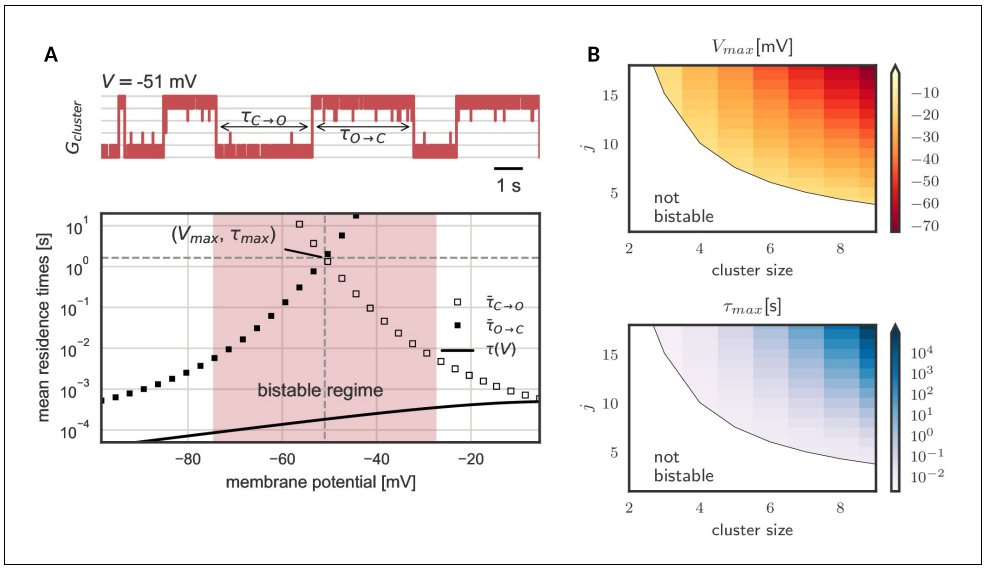

Figure 3. Prolonged life times of cluster states in the bistable regime. (**A**) *Top*: Voltage-clamped in the bistable regime, a cluster of five cooperative channels can stay in the open or closed state for multiple seconds until it spontaneously switches. The noise source are spontaneous single channel gating events, visible as the fast fluctuations around the stable states. *Bottom*: Entering the bistable regime, the residence times in the open and closed state increase over multiple orders of magnitude. The point of maximal stability (V_{max}, τ_{max}) is located at the center; here, a cluster is expected to stay open or closed for seconds, exceeding by far the single channel time constant $\tau(V)$ (black line). Mean life times are derived from a first passage analysis, see Materials and methods. (**B**) Stability of the open and closed cluster configuration depend on the cluster size and the intra channel coupling j. Larger clusters with stronger intra-channel coupling can be stable for multiple seconds and their bistable range moves to more hyperpolarized voltages. Note that small clusters with weak coupling are not bistable (white region). Cluster and channel parameters are summarized in ***Table 1***.
The online version of this article includes the following figure supplement(s) for figure 3:

Figure supplement 1. Channel noise can open and close a cluster.

example calcium channels, which are a potential candidate (**Moreno et al., 2016**). For the small number of cooperative channels, we simulate their stochastic gating, whereas for the other ionic currents, we use a deterministic simulation.

Stimulating the model cell with transient input pulses elicits spiking at a rate that increases with the stimulus amplitude (**Figure 4**). Correspondingly, the stimulation amplitude determines the response of the cooperative channels: At low input amplitudes (and consequently low ensuing firing rates), few channels in the clusters open transiently, but close again rapidly (**Figure 4A**, top trace). When the pulse is over, the cell falls silent and does not generate spikes. In contrast, if the firing rate during the pulse is large enough, in a subset of clusters all channels open. Moreover, in agreement with our above observations, these clusters now remain open when the input pulse is over (**Figure 4A**, middle and bottom traces). This additional depolarizing conductance suffices to keep the cell in a firing modus and the model neuron exhibits firing activity that persists beyond the presentation of the stimulus pulse.

Furthermore, the larger the amplitude of the stimulating pulse, the larger the persistent firing rate following the pulse (owing to the persistent opening of more clusters). As every cluster of cooperative channels has a stable open and closed configuration, the population conductance across all clusters allows for a quasi-continuous range of persistent currents. When all cluster are open, the maximal current is reached and the persistent firing rate saturates ($\approx$ 15 Hz). According to the gating properties of cooperative channel clusters, sufficiently hyperpolarizing pulses should be able to close clusters and hence 'reset' the memory of the previous pulse by annihilation of the persistent activity. Indeed, **Figure 4B** shows that a hyperpolarizing pulse cancels persistent activity.

In order to ensure maximal stability when there are no inputs to the neuron, the center of the cluster bistability (-70 mV) coincides with the resting potential (-67 mV). The limited extent of the bistable range from around -90 mV to -50 mV allows the clusters to react to spikes or strong inhibition. For the occurrence of graded levels of persistent activity, we choose channels that do not open instantaneously during a spike. Otherwise, a single spike would open all clusters at once. In contrast, for slower channels with a time constant exceeding the width of a single action potential (>10 ms), only a small ratio of the closed channels opens per spike, so that the conductance gradually increases. The channels considered here are even more inert ($\approx$ 100 ms), comparable to slow adaptation currents that require multiple spikes to fully develop (**Benda and Herz, 2003**). Similarly, clusters of inert channels require multiple spikes in fast succession to switch to the open state (minimum of $\approx$ 20 Hz, see **Figure 4C**). In this way, persistent activity at low frequencies cannot open further clusters and remains stable. Similarly, we find that the slow channels make the clusters robust against fluctuation-driven firing (**Schreiber et al., 2009**) - action potentials triggered by noise in the membrane potential (see **Figure 4—figure supplement 2**). Finally, the cell is slightly depolarized, so that it spikes in the absence of a stimulus when several clusters are open (see **Figure 4C**). Even when there are too few open clusters to induce spiking, they still increase the membrane potential and leave a form of 'silent' memory (not shown).

Interestingly, the bistable clusters also support an 'inverse' form of neuronal memory - persistent activity activated by hyperpolarization and silenced by strong depolarization. For this other form, the cooperative channel dynamics are the same, but they are required to conduct a hyperpolarizing current like for example potassium channels. Then, open clusters act as an additional standing leak current and prevent the cell from firing. Permanently closing the clusters by a hyperpolarizing pulse relieves the cell from this additional leak and allows persistent firing. However, when the cell is stimulated to spike strongly, the clusters return to the open state, restore the standing leak and again silence the cell (see **Figure 4—figure supplement 1**). Similarly to depolarization-activated persistent activity, the memory relies on the cooperative dynamics of the channels, but how the neuron makes use of this memory changes with their ionic nature.

Cooperative channels mediate graded persistent activity

Graded persistent activity is an intriguing, cell-intrinsic feature of some neurons that has been reported in vitro under carbachol in the entorhinal cortex, the perirhinal cortex and the amygdala (**Egorov et al., 2002**; **Navaroli et al., 2012**; **Egorov et al., 2006**). These neurons fire at high frequency in response to depolarizing current pulses and continue to fire stably when the stimulus is over. The persistent firing rate is lower than the one during the pulse and increases with each new

pulse presented. Hyperpolarizing pulses lead to graded decreases in firing rate and finally end the persistent activity, seemingly resetting the cell. While other mechanisms reproducing this firing mode have been suggested in the literature (**Loewenstein and Sompolinsky, 2003**; **Fransén et al., 2006**), we here add a novel candidate and show that cooperative clusters allow to capture essential properties of graded persistent activity.

In analogy to the experimental paradigm used by **Egorov et al. (2002)**, our neuron model was subjected to a series of depolarizing current pulses. **Figure 5A** shows the persistent firing after the first pulse as well as the increase of the frequency after each pulse. The persistent frequency was stable for at least one minute (data not shown). The role of the clusters as the underlying memory variable becomes apparent in the step-like evolution of their conductance, which increases during the pulses and stays constant in between. In this simulation, we observe four distinct stable persistent frequencies (from about 3 Hz to 10 Hz). At 10 Hz, further depolarizing pulses fail to increase the frequency of persistent firing. This saturation is reached, when all clusters have been switched to the open state. In addition, we confirmed that persistent firing can be gradually turned off by hyperpolarizing pulses (**Figure 5B**).

We further investigated which other channel properties - next to strong cooperativity - are essential for the graded nature of persistent activity (**Figure 5—figure supplement 1**). We concentrated on the time constant and the conductance of the channels. Fast channels, as discussed in the previous section, are less suited than slow channels. The slow channels ensure that clusters gradually open during stimulated fast spiking and halt during slow spiking, so that the persistent firing remains stable. The conductance of the channels has to be at an appropriate intermediate level: sufficient to drive the neuron over threshold, but limited to provide persistent firing frequencies of maximal 10–15 Hz. Otherwise, faster spiking can open further clusters and the persistent activity increases, so that it is no longer stable.

Concluding, a small set of cooperative clusters of ion channels - when combined with 'normal', non-cooperative potassium and sodium channels (responsible for the generation of action potentials) - can reproduce the computationally relevant feature of graded persistent activity.

Cooperative channels induce a switch to mnenomic firing in perirhinal cortex neurons

Last but not least, we test the cooperativity mechanism experimentally. Our simulations indicate that clusters of cooperative ion channels can enable the mnemonic firing mode of graded persistent activity in a simple point neuron. In biological neurons, however, other ionic currents, morphological effects or noise could interfere with the action of the cooperative channels and undermine their role as memory units. Thus, we employed the dynamic clamp technique (**Sharp et al., 1993**; **Prinz et al., 2004**) to equip perirhinal cortex (PR) neurons in-vitro with the same cooperative clusters used in our models, acting as 'virtual channels' in real cells (**Figure 6**). PR neurons have been shown to exhibit graded persistent activity under activation of muscarinic acetylcholine receptors (**Navaroli et al., 2012**). Consequently, we applied no carbachol, so that any form of persistent activity observed in the recorded PR neurons stems from the clusters of cooperative channels introduced via dynamic clamp. Accordingly, all recordings were performed in the presence of a synaptic blocker to exclude network contributions. For details of experiments, see Materials and methods.

The dynamic clamp technique allowed us to control the cluster size, channel interactions and channel kinetics of the artificial conductances during the experiment. Like in the model neuron simulations, we adapted the cluster parameters so that the bistability range fitted to the properties of the recorded cell.The resting potential determined the center of the bistable range, whereas the spike shape set boundaries for the bistable range. Voltage values during afterhyperpolarization lied above the lower boundary (to prevent reset by a spike's afterhyperpolarization), but the upstroke of the action potential exceeded the upper boundary of the bistable range.

Stable recordings with cooperative channel dynamics added via dynamic clamp were obtained for three PR neurons. Under cooperative conditions, all cells exhibited persistent activity in response to current stimulation with pulses (**Figure 6C**). Persisting activity following pulses was graded, that is the persistent firing rate increased with each presented pulse. As in the mathematical model, hyperpolarizing pulses lowered the rate of persistent activity and when applied multiple times, silenced it

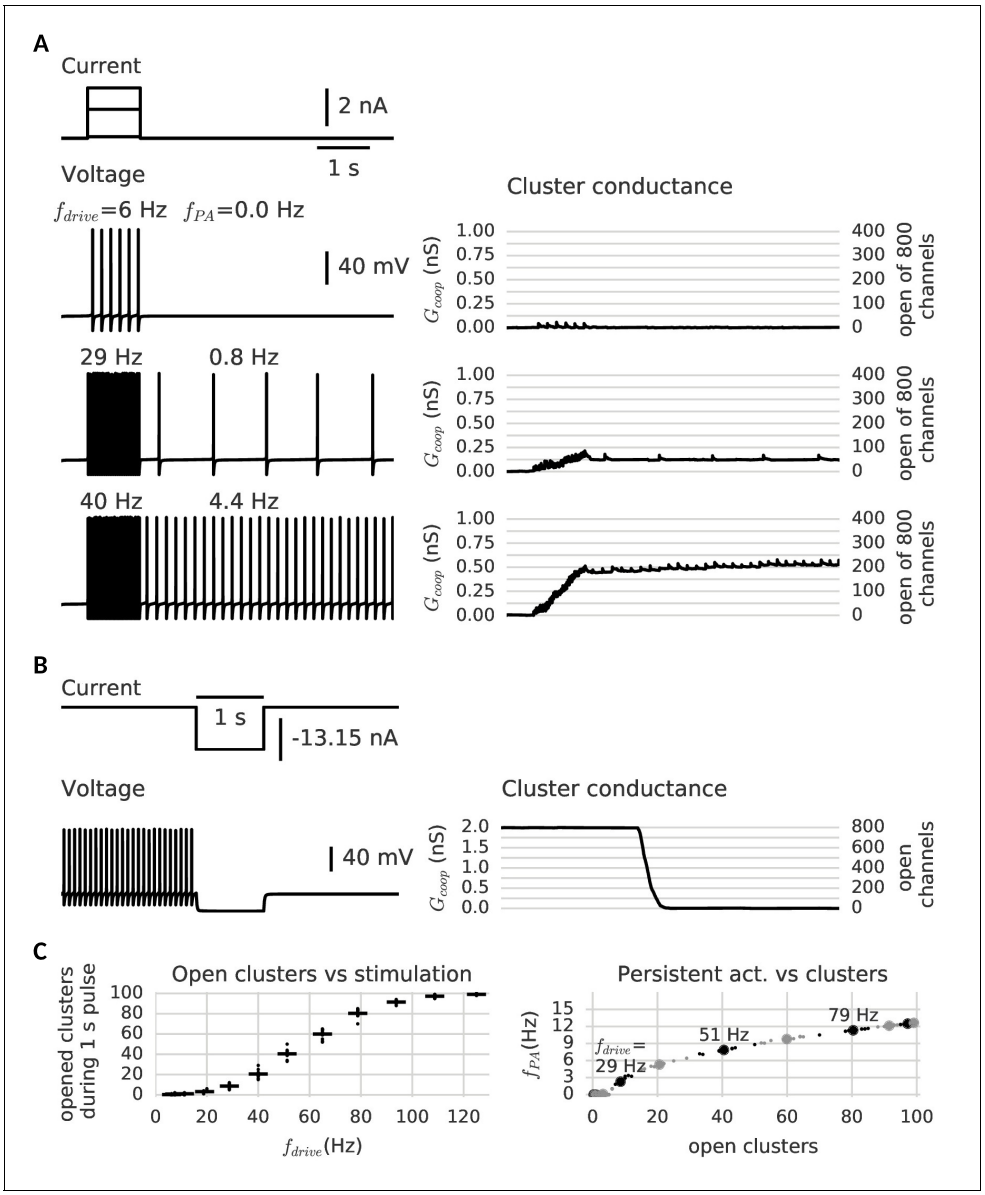

Figure 4. Clusters of cooperative channels mediate persistent activity at different levels in a model neuron. (**A**) Current stimulation with different amplitudes to test the response of clusters to different firing rates. *Left*: Voltage traces demonstrating stimulated firing at increasing frequencies. Whereas the neuron returns to rest after a low amplitude stimulation, after a stronger drive the neuron continues to spike at a stable frequency f_{PA}, which increases with the frequency of the stimulated firing f_{drive}. *Right*: Persistent activity is mediated by the conductance of the clusters, which builds up during high-frequency spiking and remains stable during low-frequency spiking and at rest. (**B**) A strong hyperpolarizing step closes the clusters and stops persistent firing. (**C**) *Left*: The cooperative clusters track the input strength; more clusters open when the cell fires at higher frequencies. Firing below 20 Hz, however, does not open clusters. The number of open clusters can differ across trials (black dots) because of stochastic channel gating. *Right*: Persistent activity increases with the number of open clusters, thereby allowing the neuron to represent the input strength after the stimulus has ended, for example 3 Hz after 29 Hz firing and 9 Hz after 51 Hz firing. Big dots denote the mean for each stimulation strength, small dots the individual trials. The simulation procedure is described in Materials and methods and parameters are summarized in ***Table 1***.

The online version of this article includes the following figure supplement(s) for figure 4:

Figure supplement 1. Depending on their reversal potential, clusters of cooperative channels can mediate de- or hyperpolarization-activated persistent activity.

Figure supplement 2. Clusters are robust against noise in the membrane potential.

(*Figure 6D*). In the control conditions (identical, yet non-cooperative channel clusters), no persistent firing could be evoked (*Figure 6—figure supplement 1*).

Periods of stimulation were followed by a slow afterhyperpolarization (sAHP) in both control and cooperative conditions, which for paradigms with cooperative gating generated a 3–4 s lasting refractory period between the stimulation and the self-sustained firing. Interestingly (and in agreement with mathematical modelling), the persistent activity 'unfolded' despite these intrinsically generated dynamics. We note that such sAHP were not expected in the original recordings of carbachol-induced persistent activity (*Egorov et al., 2002*), as carbachol blocks sAHPs.

Taken together, the experimental data support the hypothesis that cooperative ion channels can mediate cellular persistent activity. The persistent dynamics are very robust and could be easily evoked without further knowledge of the intrinsic properties of the recorded cells, such as the multitude of other ionic currents, complex cell morphology, and the presence of channel noise.

Discussion

Despite a large body of evidence for cooperative interactions between channels pivotal to the nervous system (*Iwasa et al., 1986*; *Dekker and Yellen, 2006*; *Kim et al., 2014*; *Choi, 2014*; *Dixon et al., 2015*; *Moreno et al., 2016*; *Clatot et al., 2017*), it is unknown which function coupled channels have for neural dynamics and computation. Based on a mathematical analysis, we show in this study that a cluster of cooperative channels can gate with hysteresis and find, in both simulations and experiments, that multiple such clusters embedded in the membrane of a neuron mediate mnemonic firing like persistent activity. Therefore, we suggest that ion channel cooperativity might serve as a cell-intrinsic memory mechanism at the voltage level.

From synaptic learning, adaption of the immune system to epigenetics, many biological memory systems are founded on strong positive autofeedback (*Lisman, 1985*; *Burrill and Silver, 2010*). Feedback loops are ubiquitous in biology (*Thomas and D'Ari, 1990*); they amplify signals as in calcium-induced calcium release and enhance sensitivity in controlling protein function by multisite phosphorylation. In particular, strong feedback enables bistability and memory as in networks of recurrently connected neurons (*Amit, 1990*; *Durstewitz et al., 2000*). Here, we exploit the same principles for voltage-gated ion channels, where cooperativity can act as a strong auto-feedback and enables clusters of channels to act as bistable macrochannels with a memory of previous voltage levels.

Bistability and memory of a cooperative channel cluster

Our gating analysis shows that clusters only become bistable, when channels cooperate strongly. We suggest two criteria to detect this strong coupling regime: a bimodal distribution of cluster conductance states and a hysteresis in gating. Along these lines, experimental evidence for the strong coupling regime comes from cooperative calcium channels in the heart (*Navedo et al., 2010*). Although these channels couple weakly for the majority of clusters, a few clusters are bistable, switching between the all open and the all closed state, which implies the presence of strong coupling.

Our study of channel noise confirms that also small clusters exhibit a robust hysteresis and can be used for neuronal memory. Cooperativity is inherently local - only close-by channels can interact - and is therefore restricted to small assemblies of channels (*Gutkin and Ermentrout, 2006*). In these small clusters, spontaneous channel fluctuations become a prominent source of noise, a phenomenon occluded by the assumption of all-to-all coupling in previous studies (*Naundorf et al., 2006*; *Zarubin et al., 2012*). In contrast, the clustered model here captures channel noise and therefore predicts that the lifetime of the open and closed cluster state decreases in smaller clusters. However, we find that experimentally observed cluster sizes of about 10 channels (*Moreno et al., 2016*) - each gating in the millisecond range - suffice for memory on the timescale of seconds. Consequently, also small clusters offer a robust memory and, in contrast to one large cluster with only two states, the ensemble of small clusters yields a more versatile response and has a larger memory capacity.

Ion channel cooperativity as a mechanism for graded persistent activity

Neurons can exploit these hysteretic cluster macrochannels as a short-term, analogue memory of recent voltage history - spikes open clusters and strong hyperpolarization closes them. In particular,

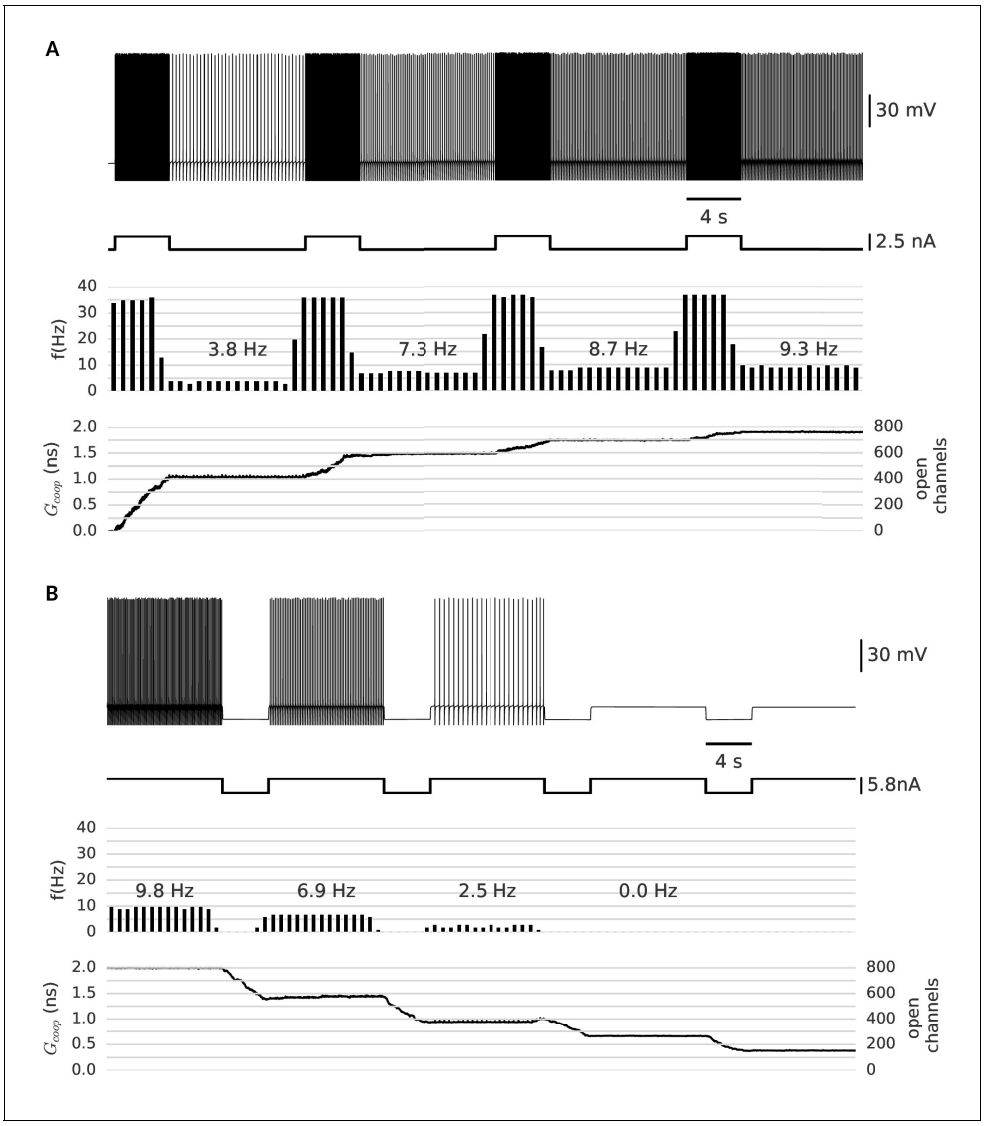

Figure 5. Clusters of strongly cooperative ion channels mediate graded persistent activity in a simple neuron model. (**A**) Repeated stimulation drives fast spiking in the neuron, which is followed by self-sustained, stable low-frequency activity at increasing rates (top). With each pulse, the driven, fast spiking switches more clusters to the open state and adds further stable conductances (bottom). The built-up conductance allows a persistent current to flow and sustains activity beyond stimulation. (**B**) In the same manner, strong hyperpolarization closes the clusters and allows to reduce the frequency of persistent activity until finally the cells stops firing. The simulation procedure is described in Materials and methods and parameters are summarized in ***Table 1***.

The online version of this article includes the following figure supplement(s) for figure 5:

Figure supplement 1. Memory dynamics with different properties of cooperative channels.

the ensemble of clusters can differentiate stimulation strength - very strong or prolonged firing opens more clusters - so that the level of persistent firing depends on the stimulation history. In this way, the collection of cooperative clusters offers the memory capacity required for forms of graded persistent activity previously observed in neurons from entorhinal (***Egorov et al., 2002***), perirhinal (***Navaroli et al., 2012***) and prefrontal cortices (***Winograd et al., 2008***), as well as the amygdala (***Egorov et al., 2006***).

Our analysis predicts the following prerequisites for persistent activity. First, the cooperative channels should have a bistable range which comprises the resting membrane potential and whose borders set the voltage activity needed to switch the persistent activity on and off (see ***Figure 3*** and ***Figure 4***). In this way, as our dynamic clamp experiments in the perirhinal cortex showed, the memory is robust for multiple seconds and can be reliably controlled via neural activity. Second, for *graded* persistent activity, the channels should have a slow time constant, on the order 50–100 ms matching the maximal persistent firing frequency. Slow cooperative channels enable a gradual opening of individual clusters during stimulation, prevent progressing excitation during the persistent period and make the clusters more robust against fluctuation-driven spikes. If the time constant was too fast, all clusters would open with the voltage elevation of the first action potential and, consequently, only one persistent response state (i.e. all clusters open) would be possible.

The type of ion conducted by cooperative channels, however, is less constrained. In principle, persistent activity can be mediated by both depolarizing and hyperpolarizing cooperative channels like calcium or potassium channels, respectively (see ***Figure 4—figure supplement 1***). If clusters consist of depolarizing calcium channels, persistent activity starts after strong spiking as observed by Egorov in the entorhinal cortex (***Egorov et al., 2002***). If on the other hand, clusters consist of hyperpolarizing potassium channels, persistent activity starts after strong hyperpolarization - similar to hyperpolarization-activated GPA as reported by Winograd in prefrontal cortices (***Winograd et al., 2008***). Independent of the ion type, we expect that the cooperative channels are separate from the action potential-generating sodium and potassium channels, or at least form only a small subgroup therein. This separation would prevent memory from interfering with the action potential, the first based on persistent currents and the latter on regenerative, memoryless currents.

Experimental evidence and comparison to other model of persistent activity

To date, it is not known, whether neurons exhibiting graded persistent activity express cooperative ion channels. However, in mammalian cells from the hippocampus, a cooperative variant of CaV1.3, a calcium channel wide spread in the brain, has been demonstrated to provide persistent depolarizing currents and increase the firing rates of hippocampal neurons (***Moreno et al., 2016***). Other candidates implicated in persistent activity, the transient receptor potential cation (TRPC) channels (***Zhang et al., 2011***), are known to cluster and therefore provide the spatial proximity required for cooperativity (***Nilius and Owsianik, 2011***). However, a recent study showed that graded persistent activity in the entorhinal cortex of mice does not require TRPC channels (***Egorov et al., 2019***). Generally, the channels required for persistent activity are still under debate. As our work demonstrates, only a small fraction of channels has to be cooperative to produce persistent activity, so that they might be easily overlooked, especially if cooperativity depends on other intracellular regulators like calmodulin (***Moreno et al., 2016***).

As a model of persistent activity, cooperativity shares positive feedback as the core principle with other hypothesis like calcium modulated conductances, but differs in several aspects. The central difference is that coupled channels have an inherent, direct feedback mechanism - one channel opening facilitates another - whereas independent channels require an indirect interaction. Accordingly, previous studies suggested a feedback cycle of spiking, calcium inflow and a calcium modulated conductance as the basis of persistent spiking (***Rodriguez et al., 2018***). A direct consequence is that memory in the case of calcium modulated channels requires spiking, whereas cooperative clusters could also implement a silent memory - a long lasting change of excitability after stimulation. However, silent memories are also possible in extended models of calcium modulation, where a rise in calcium triggers persistent conductance changes through intracellular signaling (***Fransén et al., 2006***; ***Winograd et al., 2008***). Another difference is that models based on calcium modulation naturally address the finding that blocking calcium channels or strong calcium buffering prevents persistent activity (***Egorov et al., 2002***; ***Cui and Strowbridge, 2018***). For the cooperativity hypothesis, this central role of calcium could imply a calcium regulated coupling, like in the case of calcified calmodulin mediated channel interactions (***Moreno et al., 2016***).

As mediators of graded persistent activity, clusters of cooperative channels could be the computational substrate of important cognitive processes such as short term memory and evidence accumulation (***Zylberberg and Strowbridge, 2017***). Beyond graded persistent activity, the cluster

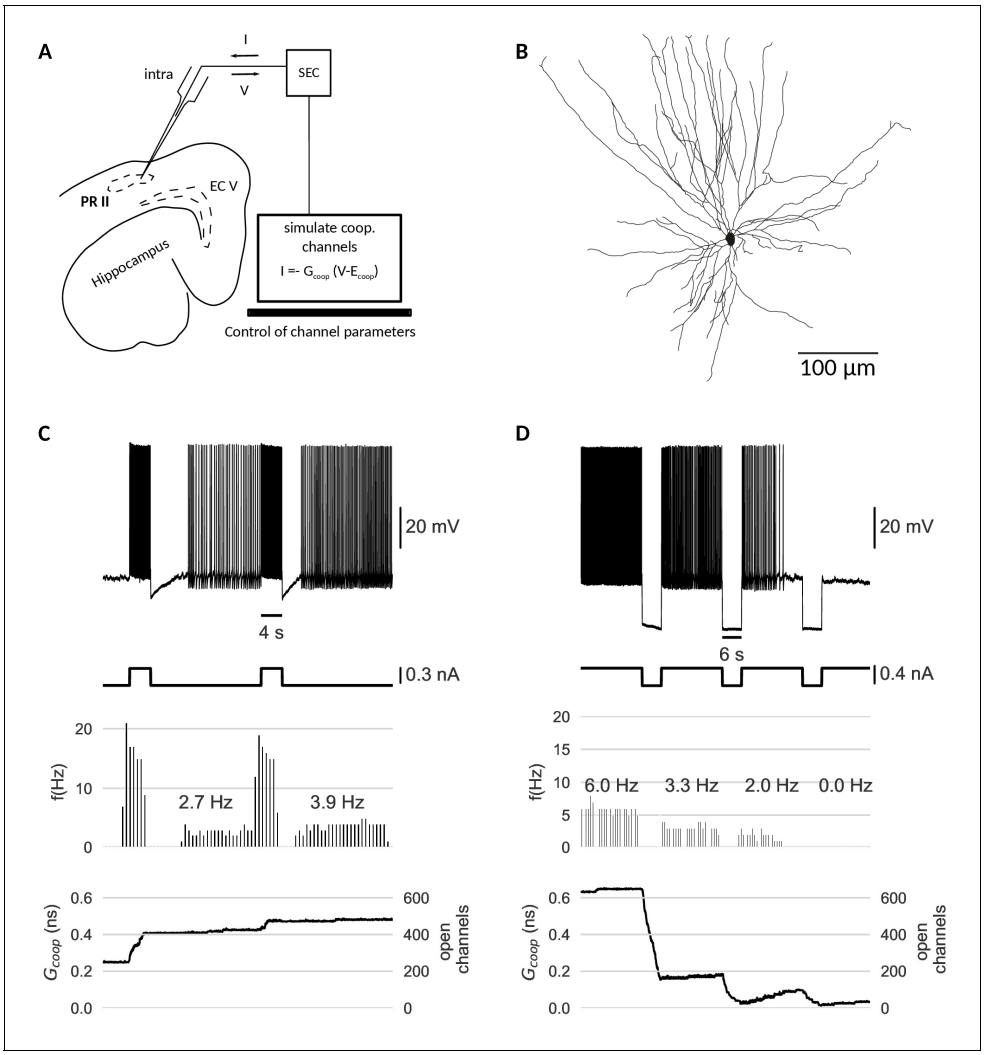

Figure 6. Dynamic clamp experiment. (**A**) Intracellular recording of a perirhinal cortex neuron in dynamic clamp mode. The computer simulates the state of clusters of cooperative channels given the measured membrane potentials and emulates the effect of their conductance to the neuron's activity by inserting a corresponding current. (**B**) Neurolucida drawing of the recorded neuron. (**C**) Graded persistent activity of the recorded neuron mediated by the multi stable conductance of the clusters of cooperative channels. (**D**) Hyperpolarization brings the cell back to rest via intermediate levels of persistent firing. In control recordings with identical, yet- independent channels, no persistent firing was observed (***Figure 6—figure supplement 1***). Slice preparation, electrophysiological setup and the dynamic clamp emulation of the clusters are described in Material and methods. Cluster parameters are summarized in ***Table 1***.

The online version of this article includes the following figure supplement(s) for figure 6:

Figure supplement 1. Cooperative interactions are necessary to mediate graded persistent activity.

bistability may serve other plasticity mechanism of intrinsic excitability such as dendritic attenuation or boosting of synaptic inputs (***Marder et al., 1996***; ***Debanne et al., 2019***).

Cooperativity dynamically regulates the computational repertoire of ion channels

An attractive feature of cooperative channels is the computational flexibility. For a cell-intrinsic memory on demand, biophysical modulators could turn on and off the cluster bistability. Bistability only emerges, when the channels are coupled strongly and the cluster consists of a sufficient number of

channels. Thus, one regulatory mechanism could be to change the coupling as in the case of calcium regulated cooperativity (**Moreno et al., 2016**). Another regulatory mechanism could be to control clustering of channels, which is subject to factors like neural activity (**Misonou et al., 2004**), extracellular pH (**Sumino et al., 2014**), ionic concentrations (**Eisenach et al., 2014**) and lipid signaling (**Hilgemann et al., 2018**). As a composite of multiple channels, a cluster macrochannel is a more flexible conductance than its 'hard-coded' parts.

The emergence of memory in a cluster of cooperative, but memoryless channels suggests a general role of ion channel cooperativity. Cooperative interactions guide the formation of novel macrochannels with a gating repertoire absent at the single channel level. At the level of the neuron, the common membrane potential orchestrates sodium and potassium channel gating to generate the spike. In the same way, cooperativity could orchestrate gating in small channel assemblies to enrich neural dynamics. Correspondingly, it has been suggested that different TRP channels from heteromultimeres to create a wide variety of functions (**Nilius and Owsianik, 2011**). Another example of a heterogenous cluster is the assembly of BK and CaV, 1.3 channels (**Berkefeld et al., 2006**; **Vivas et al., 2017**). A quantitative understanding of these channel complexes requires detailed experimental characterization of the channel couplings like in **Sato et al. (2018)**. Still, simple coupling models like the one presented here already reveal the potential of cooperativity to provide emergent gating functions.

In summary, clusters of cooperative channels broaden the computational repertoire of neurons. Extrapolating from the current study on cell-intrinsic memory, ion channel cooperativity can mediate direct feedback loops between channels and therefore could allow to form macrochannels with novel gating dynamics. If, additionally, neuromodulation can control cooperative interactions, ion channel cooperativity provides an extremely versatile cell-intrinsic mechanism to enrich and regulate neural activity.

Materials and methods

Neuron and channel model

Isolated ion channel model

We assume that the cooperative channels have a single activation gate and model their gating dynamics in isolation according to the calcium channel dynamics from the Morris-Lecar model (**Morris and Lecar, 1981**).

The activation kinetics are

$$\frac{\mathrm{d}m}{\mathrm{d}t} = \frac{m(V) - m}{\tau(V)} \tag{1}$$

where the steady state activation is

$$m(V) = \frac{1}{2}\left(1 + \tanh\left(\frac{V - V_{1/2}}{k}\right)\right), \tag{2}$$

and the activation time constant reads

$$\tau(V) = \tau \cosh^{-1}\left(\frac{V - V_m}{\sigma}\right). \tag{3}$$

Correspondingly, the channel has two states, open (O) and closed (C) and their kinetics reads

$$C \underset{\beta(v)}{\overset{\alpha(v)}{\rightleftharpoons}} O,$$

with opening rate

$$\alpha(V) = \frac{m(V)}{\tau(V)},$$

and closing rate

$$\beta(V) = \frac{1 - m(V)}{\tau(V)}.$$

The channels have a single channel conductance g_{coop} and reversal potential E_{coop}. Original parameters are $E_{coop} = 100\mathrm{mV}$, $V_{1/2} = -1\mathrm{mV}$, $k = 15\mathrm{mV}$, $\tau = 0.05\mathrm{ms}$, $V_m = -1\mathrm{mV}$ and $\sigma = 30\mathrm{mV}$, see ***Zarubin et al. (2012)***. Unless reported otherwise, we choose a single channel conductance of $g_{coop} = 2.5\mathrm{pS}$ as reported for calcium channels (***Church and Stanley, 1996***). Modifications of these parameters are summarized in ***Table 1***.

Cooperativity model

In order to capture cooperative interactions among channels, we model the activation of a channel as dependent on both the membrane potential and the state of near-by channels (***Naundorf et al., 2006***). Specifically, we assume that the activation $\widetilde{m}$ of a channel among o open neighbours has the form

$$\widetilde{m}(V, o) = m(V + oj). \tag{4}$$

where j is the *coupling strength between two channels*. Therefore, if the coupling is positive $j>0$, opening of a neighbouring channel shifts the activation curve towards lower membrane potentials. As a result, a channel with open neighbours has itself an increased open probability, see ***Figure 1A***.

For the time constant, we posit that the same shift applies,

$$\widetilde{\tau}(V, o) = \tau(V + oj). \tag{5}$$

Cluster model

Next, we introduce the experimentally observed clustering of the channels. We presume that only channels in the same cluster are close enough to cooperate, so that channels in different clusters gate independently. For a cluster, a characteristic measure of cooperativity is the *maximal shift* J, which corresponds to the shift of the activation curve when all neighbours of a channel are open. Under the simplifying assumption of constant coupling strength j among all channels, the maximal shift in a cluster of size S amounts to $J = (S-1)j$.

A note on comparing coupling strengths with previous studies: We choose J for the maximal shift in accordance with the notation of ***Zarubin et al. (2012)***. In contrast, Naundorf et al used J to denote the coupling strength between two channels, which in the work presented here is j (***Naundorf et al., 2006***).

In a cluster of size S with o open channels, all $S - o$ closed channels open with rate

$$\widetilde{\alpha}(V, o) = \alpha(V + oj)$$

and all o open channels, having only $o - 1$ open neighbours, close with rate

$$\widetilde{\beta}(V, o-1) = \beta(V + (o-1)j).$$

Instead of tracking the cluster state in terms of each constituting channel, we can also view the cluster as a macrochannel. For S two-state channels, this macrochannel has $S+1$ conductance states, from all channels closed to all channels open. In a small time interval, at most one channel opens or closes, so that transitions are restricted to adjacent cluster states with a difference of one open channel,

$$o \underset{\beta_{o+1,o}(v)}{\overset{\alpha_{o,o+1}(v)}{\rightleftharpoons}} o+1.$$

The macrochannel rates result from the number of channels that are possible candidates for the transition and the single channel transition rate. Therefore, in a cluster with o open channels, the opening of one of the other $S - o$ closed channels happens with rate

$$\alpha_{o,o+1}(V) = (S - o)\alpha(V + oj). \tag{6}$$

Correspondingly, from a state with $o+1$ open channels, the closing of one of the open channels each having o open neighbours reads

$$\beta_{o+1,o}(V) = (o+1)\beta(V+oj). \tag{7}$$

Figure 1C shows simulated traces of clusters and demonstrates their behaviour as macrochannels.

Neuron model

We used a conductance-based neuron model with a single isopotential compartment,

$$C\frac{\mathrm{d}V}{\mathrm{d}t} = I_{\mathrm{app}} - I_{\mathrm{cluster}} - I_V, \tag{8}$$

where I_{cluster} is the current through the clusters of cooperative channels, I_V summarizes the other channel currents, I_{app} is a stimulus current and C is the capacitance of the membrane.

Cluster current

We model the cooperative channels arranged in N clusters, each composed of S identical channels. Then, the current through all clusters is determined by the total number of open channels O_{coop} among all clusters,

$$I_{cluster} = g_{coop}O_{\mathrm{coop}}(V - E_{coop}), \tag{9}$$

where E_{coop} denotes the reversal potential of the considered ions. For most of the article, we assume that the cooperative channels conduct a depolarising current with $E_{coop} = 100mV$ (e.g. Ca2+ or Na+). In ***Figure 4—figure supplement 1***, we then consider the case of a hyperpolarising current with $E_{coop} = -100mV$ (e.g. K+).

In a description, where each channels is tracked, O_{coop} simply counts the number of channels in the open state. In the alternative macrochannel description of the clusters, the total number of open channels is obtained from the number of macrochannels in the different conductance states, so

$$O_{\mathrm{coop}} = \sum_{o=0}^{S} \gamma_o o,$$

where γ_o is the number of clusters with o open channels. This occupancy vector γ can also be used to capture the distribution of conductance states of a single cluster over time (***Figure 1C***).

As opposed to the other ionic conductances, the dynamics of the clusters is modeled on the level of the underlying jump process generated by the single-channel gating events. Such a detailed description is necessary to account for the fact that cooperative interactions reduce the number of independent stochastic units and therefore increase fluctuations ($1/\sqrt{N}$ as opposed to $1/\sqrt{SN}$ ***White et al., 2000***). Effectively, the N clusters represent the independent units, so that with around 100 clusters, a jump process description is adequate to account for the discrete nature of the fluctuations.

Leak and action potential mediating currents

We choose a type 1 neuron model to account for the continuous low-frequency firing range as observed in graded persistent activity (***Egorov et al., 2002***). The model presented is a version of the Traub-Miles model (***Benda, 2002***), which comprises action potential generating potassium and sodium currents and a leak current,

$$I_V = A(I_{Na} + I_K + I_L).$$

The original model is formulated with conductance densities and is independent of the neuron surface area A. In the present model, the cluster conductance is defined in absolute terms, because it stems from a concrete number of channels with a fixed conductance. Correspondingly, we turn the remaining currents and the capacitance into absolute quantities by choosing a surface area, for details see Choosing a neuron surface. The capacitance density is $\bar{C} = 1\mu F/\mathrm{cm}^2$.

In the following, all gating variables have first order kinetics of the form

$$\dot{x} = \alpha_x(V)(1-x) - \beta_x(V)x. \tag{10}$$

Sodium current

$$I_{Na} = \bar{g}_{Na} m^3 h (V - E_{Na})$$

with $\bar{g}_{Na} = 100\frac{\mathrm{mS}}{\mathrm{cm}^2}$, $E_{Na} = 48\mathrm{mV}$ and gating variables m and h with rates

$$\alpha_m(V) = 0.32\mathrm{kHz}(V/\mathrm{mV} + 54)/(1 - \exp(-0.25(V/\mathrm{mV} + 54))),$$

$$\beta_m(V) = 0.28\mathrm{kHz}(V/\mathrm{mV} + 27)/(\exp(0.2(V/\mathrm{mV} + 27)) - 1),$$

$$\alpha_h(V) = 0.128\mathrm{kHz}\exp(-(V/\mathrm{mV} + 50)/18),$$

$$\beta_h(V) = 4.0\mathrm{kHz}/(\exp(-0.2(V/\mathrm{mV} + 27)) + 1).$$

Potassium current

$$I_K = \bar{g}_K n^4 (V - E_K)$$

with $\bar{g}_K = 200\frac{\mathrm{mS}}{\mathrm{cm}^2}$, $E_K = -82\mathrm{mV}$ and gating variable n with rates

$$\alpha_n(V) = 0.032\mathrm{kHz}(V/\mathrm{mV} + 52)/(1 - \exp(-0.2(V/\mathrm{mV} + 52))),$$

$$\beta_n(V) = 0.5\mathrm{kHz}\exp(-(V/\mathrm{mV} + 57)/40).$$

Leak current

$$I_L = \bar{g}_L (V - E_L)$$

with $\bar{g}_L = 0.1\frac{\mathrm{mS}}{\mathrm{cm}^2}$ and $E_L = -67\mathrm{mV}$.

Choosing a neuron surface

When we fix the peak conductances of the other ionic currents, the contribution of the cluster current for a fixed number of cooperative channels depend on the neuron area A. For example, for a small neuron area, the cluster conductance becomes relatively larger and could drive faster persistent spiking than for a large neuron area. In choosing a neuron area, we try to meet two characteristics of graded persistent activity, namely its low-frequency range and its quasi-continuous nature.

Specifically, the frequency of persistent firing is usually located in the low-frequency range below 15 Hz, which sets a limit to the conductance of the clusters. In terms of conductance densities, we find that close to rheobase $I_{app} = 0.105\mu\mathrm{A}/\mathrm{cm}^2$ and with a reversal potential $E_{coop} = 100\mathrm{mV}$ common for Ca_{2+} channels, a cooperative channel conductance density of about $\bar{g}_{\mathrm{coop}} \approx 0.0004\frac{\mathrm{mS}}{\mathrm{cm}^2}$ is sufficient to drive spiking at about 10 Hz.

Furthermore, the levels of persistent firing are assumed to be quasi-continuous, which requires a large number of clusters with a small conductance. In all simulations, we assumed about 100 clusters, which in principle allow 100 levels of persistent firing. In a frequency range of up to 10 Hz, this would correspond roughly to a frequency resolution of 0.1 Hz, which lies below the experimentally observed grading of about 0.5 Hz (***Fransén et al., 2006***). Furthermore, the clusters have to be of a certain size to be bistable on the timescales of seconds, as shown in ***Figure 3***. Hence, for a high number of clusters N = 100 with size S = 8 and a typical single channel conductance $g = 2.5\mathrm{pS}$, the total cooperative channel conductance is $g_{\mathrm{coop}} = 2\mu\mathrm{S}$.

Therefore, we arrive at a required surface area of,

$$A = \frac{g_{\mathrm{coop}}}{\bar{g}_{\mathrm{coop}}} = 0.005\mathrm{cm}^2,$$

which is a large neuron area compared to typical neuron surface areas as reported in literature (e.g. ***Ambros-Ingerson and Holmes, 2005***). This large membrane area also explains the rather high currents that are needed to excite and hyperpolarise the neuron. In principle, a smaller neuron area could be reached by smaller cluster numbers, smaller cluster sizes, a lower reversal potential or an increase of the firing range.

Stimulation with a white noise current

We investigate how robust the clusters are against noise in the membrane potential (***Schreiber et al., 2009***). In particular, we mimic fluctuating synaptic input to the neuron, a major noise source, by injecting a white noise current with standard deviation σ_I and time resolution dt_{noise},

$$I_{noise}(t) = \sum_k i_k (H(t - k\ \mathrm{dt}_{noise}) - H(t - (k+1)\mathrm{dt}_{noise}));\ i_k \mathrm{from} \mathcal{N}(0, \sigma_I^2),$$

where $H(x)$ is the Heaviside step function and $\mathcal{N}(0, \sigma_I^2)$ denotes a normal distribution with zero mean and variance σ_I^2.

We choose a time resolution of $\mathrm{dt}_{noise} = 0.5ms$, oriented at the temporal width of synaptic currents, and then vary the noise intensity (see ***Figure 4—figure supplement 2***). Note that the simulation step size is much smaller than the temporal resolution of the noise (see Simulation of the neuron model).

Overview of cluster and cooperative channel parameters.

Simulation and analysis of cluster dynamics

Mean channel activation in a cluster

In a large cluster of cooperative channels, the number of open channels is expected to coincide with its mean $\bar{o} = m_{\mathrm{coop}}(V)S$, where $m_{\mathrm{coop}}(V)$ is the average activation of the channels in the cooperative ensemble. Moreover, the average activation reflects how much the open neighbours shift the activation curve,

$$m_{\mathrm{coop}}(V) = m(V + \bar{o}j),$$

where we use ***Equation 4*** for the cooperativity altered activation and $m(V)$ is the single channel activation function. A rewrite of the shift term $\bar{o}j = m_{\mathrm{coop}}(V)Sj \approx m_{\mathrm{coop}}(V)J$ results in a self-consistency relation (***Naundorf et al., 2006***, Supplementary Notes 2),

$$m_{\mathrm{coop}}(V) = m(V + m_{\mathrm{coop}}(V)J). \tag{11}$$

We numerically solve ***Equation 11*** for a range of membrane potentials to obtain the activation curves $m_{\mathrm{coop}}(V)$ for different couplings J. As discussed in the results on cluster dynamics, the activation becomes bistable for sufficiently strong coupling $J > J_{crit}$ (***Figure 1***).

The critical coupling strength depends on the form of the single channel activation $m(V)$. For the activation curve in ***Equation 4***, it reads (derivation below)

$$J_{crit} = 2k.$$

Hence, the critical coupling J_{crit} coincides with the width of the activation curve. Put differently, bistability emerges, when cooperative facilitation by the neighbouring open channels can keep a channel open despite a low membrane potential at which the channel would usually be closed. Thus, when all neighbours are open, the shift has to exceed the width of a channel's activation curve (***Figure 1A***).

Derivation of the critical coupling strength

For the derivation of the critical coupling strength, we follow the argument of ***Huang et al. (2012)***, (***Equations 4-10***). They consider cooperative sodium channels and are interested in the coupling strength, where the channel activation becomes a step function. This coupling strength in principle also induces bistability; the steps in the activation curve occur at the edges of the bistable range. However, sodium channels transit to the inactivated state when they are open and thus they cannot be bistable.

If a bistable range exists, the number of solutions of the self-consistency ***Equation 11*** has to change from one to three (bistable) and back to one again, when the voltage is increased. From this observation, we can deduce a condition in the coupling strength J. Namely, each solution m_c corresponds to an intersection of the left and right hand of ***Equation 11***,

$$m_c = m(V + m_c J)$$

and for the voltages where the number of solutions change, these intersections have to be tangential, that is

$$\frac{\mathrm{d}}{\mathrm{d}m_c} m_c = \frac{\mathrm{d}}{\mathrm{d}m_c} m(V + m_c J)$$

$$\Rightarrow \quad 1 = \frac{J}{2k}\left(1 - (2m(V + m_c J) - 1)^2\right).$$

Here, we use that $\frac{\mathrm{d}m(V)}{\mathrm{d}V} = \frac{1}{2k}\left(1 - (2m(V) - 1)^2\right)$. Again using the self-consistency relation $m_c = m(V + m_c J)$, we observe that the solution has to obey

$$\frac{J}{k} m_c^2 - \frac{J}{k} m_c + \frac{1}{2} = 0.$$

Finally, as the solution has to be real, bistability sets the following condition on J : $\left(\frac{J}{k}\right)^2 - 2\frac{J}{k} \geq 0 \Rightarrow J \geq 2k = J_{crit}$.

Mean first passage times between cluster states

In order to study the stability of the open and closed cluster state, we calculate the mean first passage times between these two states. We employ the macrochannel description, where for a cluster of size S the dynamics form a continuous-time Markov process with transition matrix

$$Q_{ij}(V) = \delta_{i,j+1}\alpha_{i-1,i}(V) + \delta_{i,j-1}\beta_{i+1,i}(V);\ 0 \leq i,j \leq S.$$

$Q_{ij}(V)$ denotes the voltage-dependent transition rate from cluster state j to i and summarizes the opening and closing rates from ***Equation 6 and 7***.

Over a small time interval, the transition rates become transition probabilities and the continuous Markov chain can be discretized. That is, choosing a small time interval Δt, such that for all i,j it holds $Q_{ij}\Delta t \ll 1$, the transition probabilities are $P_{ij} = Q_{ij}\Delta t$ for $i \neq j$ and $P_{ii} = 1 - \sum_{j \neq i} P_{ji}$. For a discrete Markov chain, the mean first passage steps K (with K_{ij} denoting the mean number of steps required to reach state i from state j)) can be obtained by solving the system of equations given by ***Allen (2010)***, see p.69)

$$K = E + (K - diag(K))P,$$

where E is a $(S+1) \times (S+1)$ matrix of ones. Multiplication with the time interval recovers the mean first passage times $M = K\Delta t$.

For the stability of a bistable cluster, the mean first passage times between the open and closed state are of particular interest: the average time $\bar{\tau}_{O \to C}$ it takes until a cluster spontaneously switches from the state with all channels open to the one with all channels closed or vice versa $\bar{\tau}_{C \to O}$. In terms of M, they read $\bar{\tau}_{O \to C} = M_{0,S}$ and $\bar{\tau}_{C \to O} = M_{S,0}$. ***Figure 3A*** depicts the mean residence times as a function of the membrane voltage.

Numerical simulation of cluster dynamics

For the simulation of the cluster dynamics at a constant membrane potential, we use both a fixed time step method and the Gillespie algorithm (***Gillespie, 1977***).

In the fixed time step method, we track the state of each channel in the cluster. For each time step, we look up the number of open channels, evaluate the corresponding opening and closing rates and obtain the transition probabilites by multiplying the rates with the time step. Finally, a

random number generator is used to update the state of the channels according to the transition probabilities. This method is used for the cluster simulations in ***Figure 1*** and ***Figure 2***.

For the application of the Gillespie algorithm (***Gillespie, 1977***), we switch to the macrochannel description, where the states only specify the number of open channels, but ignore the configuration of the individual channels. Specifically, for clusters of size S, the $S+1$ conductance states represent the species in the Gillespie algorithm, whereas the $2S$ transitions between adjacent cluster states with their respective rates form the reactions.

Simulation of the neuron model

In the neuron model, the coupled dynamics of the continuous variables, voltage (***Equation 8***) and gating variables (***Equation 10***), and the jump process of the cooperative channels form a hybrid stochastic system (***Anderson et al., 2015***). For the simulation of spiking activity, we use brute, a custom written fixed time step algorithm.

BRUTE algorithm

The brute algorithm tracks the state of each channel and uses a fixed time method to update their states. In order to take into account the cooperative interactions among channels in one cluster, it considers each cluster separately and calculates the opening and closing rate of the channels therein. For N clusters of size S, the channel states can be cast into a matrix $C \in \{0,1\}^{N\times S}$, which the algorithm updates in each time step.

In the following, the membrane potential and the continuous gating variables are summarized in $\mathbf{x}$ and the current time is t. Channel states are encoded as 0 (closed) or 1 (open). Then, in pseudo code, the update algorithm with time step Δt is

1. Initialize: set $t = t_0$, set the initial membrane potential and gating variables $\mathbf{x}_0$ and set the initial channel states $C \in \{0,1\}^{N\times S}$

Table 1. Cluster and cooperative channel parameters.
N: number of clusters, S: cluster size, J: overall coupling, j: channel-channel coupling, $V_{0.5}$: half activation, k: width of the channel activation, τ: time constant of the channel with maximum at attained at V_m and width σ, g_{coop}: single channel conductance and E_{coop}: reversal potential.

Figure	N	S	J	j	$V_{0.5}$	k	τ	V_m	σ	g_{coop}	E_{coop}
			mV	mV	mV	mV	ms	mV	mV	pS	mV
Figure 1 (independent)	1	6	0	0	−1	15	0.5	−1	30	-	-
Figure 1 (weak coop.)	1	6	22.5	4.5	−1	15	0.5	−1	30	-	-
Figure 1 (strong coop.)	1	6	70	14	−1	15	0.5	−1	30	-	-
Figure 2 (independent)	1	6	0	0	−1	15	0.5	−1	30	-	-
Figure 2 (cooperative)	1	6	100	20	−1	15	0.5	−1	30	-	-
Figure 3	1	5	100	25	−1	15	0.5	−1	30	-	-
Figure 4	100	8	80	11.4	−30	10	120	−30	20	2.5	100
Figure 5	100	8	80	11.4	−30	10	120	−30	20	2.5	100
Figure 6c	90	8	101.5	14.5	−10	15	100	−10	30	1	100
Figure 3—figure supplement 1	1	5	100	25	−1	15	0.5	−1	30	-	-
Figure 4—figure supplement 1A	100	8	80	11.4	−30	10	120	−30	20	2.5	100
Figure 4—figure supplement 1B	100	8	80	11.4	−30	10	120	−30	20	10	−100
Figure 4—figure supplement 2	100	8	80	11.4	−30	10	120	−30	20	2.5	100
Figure 5—figure supplement 1A,B	100	8	80	11.4	−30	10	10–240	−30	20	2.5	100
Figure 5—figure supplement 1C,D	100	8	80	11.4	−30	10	120	−30	20	0.5–10	100
Figure 6—figure supplement 1 (independent channels, red)	90	8	0	0	−10	15	100	−10	30	1	100
Figure 6—figure supplement 1 (cooperative channels, black)	90	8	101.5	14.5	−10	15	100	−10	30	1	100

2. Generate an array of random numbers $r \in [0,1]^{N \times S}$
3. Numerically integrate voltage and gating variables dynamics (***Equation 8***; 10) until $t + \Delta t$
4. Update each cluster, that is each row i of C as follows

    1. calculate the number of open channels $o_i = \sum_j C_{ij}$
    2. update each channel C_{ij}
        - if $C_{ij} = 1$ and $r_{ij} < \beta(V, o_i - 1)\Delta t$ then $C_{ij} = 0$
        - else if $C_{ij} = 0$ and $r_{ij} < \alpha(V, o)\Delta t$ then $C_{ij} = 1$
5. Increment t by Δt and check if simulation is finished, otherwise continue with step 2

In all simulations, we chose a time step $\Delta t = 0.25us$. At this small time resolution, we observed a convergence of the cluster dynamics. A python implementation of the algorithm with a simple example is available at https://itbgit.biologie.hu-berlin.de/cooperativity/brutelib.git (copy archived at https://github.com/elifesciences-publications/49974-brutelib).

Dynamic clamp experiment

Preparations of mouse brain slices

Dynamic clamp experiments were conducted with horizontal mouse brain slices (300–450 µm thick) containing the hippocampus, entorhinal and perirhinal cortices. Brain slices were obtained from male C57BL/6N mice (4–8 weeks old, 20–25 g) using standard proceedings (***Roth et al., 2016***). Mice were purchased from Charles River Laboratories (Sulzfeld, Germany, Strain Code: 027) and were taken care of in the Interfaculty Biomedical Research Facility in Heidelberg. Housing was provided in Makrolon II cages with a maximum of three animals and tissue nesting material made of cellulose. Animals had ad libitum access to food and water. All experimental protocols were conducted in compliance with German law and with the approval of the state government of Baden-Württemberg (Project T100/15).

In order to minimize the stress of euthanasia, mice were sedated by exposure to CO_2 in a rising concentration (20–30 l/h sourced from a compressed gas cylinder) until the animal fell unconscious. Mice were subsequently killed by decapitation and the brain was quickly removed and transferred to 4˚C cold, carbogen buffered (95% O_2, 5% CO_2 at pH 7.4) artificial cerebrospinal fluid (ACSF) containing the following (in mM): 124 NaCl, 3 KCl, 1.8 $MgSO_4$, 1.6 $CaCl_2$, 10 glucose, 1.25 NaH_2PO_4, 26 NaH_2CO_3. Brain slices were cut using a vibratome (Leica VT1200S, Nussloch, Germany). Then, slices were transferred to a Haas-type interface chamber (***Haas et al., 1979***), perfused with ACSF at a rate of 1.2–1.4 ml/min at 34 ±1˚C. Slices rested for at least 2 hr before electrophysiological recordings.

Electrophysiological recordings

Single-cell recordings were obtained from principal neurons of the perirhinal cortex layer II. These neurons show graded persistent firing under activation of muscarinic cholinergic receptors (***Navaroli et al., 2012***).

The recordings were obtained with sharp microelectrodes (tip resistance 100–130 MΩ) pulled from 1.0 mm borosilicate glass capillaries (Harvard Apparatus, Cambridge, UK, Cat. No. 30–0019) on a DMZ Universal Electrode Puller (Zeitz, Martinsried, Germany) and filled with 2 M K-acetate that in some cases contained 1% biocytin.

Recorded signals were low-pass filtered at 10 kHz, amplified x10 using an SEC-05X amplifier (npi electronic, Tamm, Germany) and digitized at 20 kHz with an analog to digital converter (MICRO 1401 mkII ADC, CED, Cambridge, UK). Signals were visualized and saved using Spike2 software (CED, Cambridge, UK). All intracellular recordings were conducted in bridge mode and bridge balance was monitored and adjusted during experiments.

Positive and negative current pulses (duration and amplitudes controlled by Spike2 Software and SEC-05X amplifier) were applied via the recording electrode to determine input resistance and firing properties. Input resistance was estimated during the experiment and later calculated off-line using Matlab software (The Mathworks, Natick, MA). Resting membrane potential was calculated by subtracting the potential offset after withdrawal from the cell at the end of the recording.

All cells selected for measurements had an input resistance above 20 MΩ, a stable membrane potential throughout the recording and exhibited firing properties of principal neurons. Membrane potential of neurons was controlled by manually adjustable DC current injection through the

recording electrode to determine the current needed for intended firing frequencies and depolarisation near threshold.

To prevent spontaneous network activity in slices, all experiments were performed in the presence of ionotropic glutamate receptor blockers 6-cyano-7-nitroquinoxaline-2,3-dione (CNQX, 30 µM, Cat. No. 1045) and DL-2-amino-5-phosphonovaleric acid (APV, 10 µM, Cat. No. 0105) obtained from Tocris (Bristol, UK). Drugs were bath applied by continuous perfusion. Biocytin (Cat. No. B4261) was obtained from Sigma-Aldrich (Taufkirchen, Germany).

Biocytin staining

After recordings the slice was fixed in 4% PFA in phosphate buffer (PB) at 4˚C for 90 min and then stored in phosphate buffered saline (PBS) at 4˚C until further processing. It was washed 3 × 15 min to remove excess PFA and incubated with Avidin - Alexa Fluor 488 conjugate (1:1000; Life Technologies, Carlsbad, CA) diluted in PBS containing 5% normal goat serum and 0.2% Triton X at room temperature under light protection for 2 hr. The slice was then washed in PBS for 15 min, incubated with 4,6-diamidino-2-phenylindole (DAPI; 1:10,000; Carl Roth, Germany) in H_2O for 3 min, washed again in PBS (15 min) all at room temperature and afterwards embedded in Mowiol 4–88 (Sigma-Aldrich, Taufkichen, Germany).

Fluorescence images were acquired with a Nikon A1+ Confocal Microscope (Nikon, Düsseldorf, Germany) and reconstruction of the neuron was obtained from z-stack confocal images using Neurolucida tracing software (MBF Bioscience, Williston, VT).

Dynamic clamp

Data acquisition and dynamic clamp loop were controlled by RELACS, V0.9.8, RRID:SCR_017280. The feedback loop run at a frequency of 20 kHz and consisted of sampling the membrane potential, updating the state of the clusters of cooperative channels and injection of the corresponding current (***Equation 9***). The software allowed online adjustments of the following model parameters:

- the channel to channel coupling strength j
- cluster number N and cluster size S
- single channel conductance g_{coop} and reversal potential E_{coop}
- parameters of the channel kinetics, namely maximum of the time constant τ and the half-activation voltage $V_{1/2}$

Real time cluster update in the dynamic clamp loop

In order to meet the real time requirement imposed by dynamic clamp, we employ the macrochannel description of the clusters (see Cluster model). In each time step, the macrochannel description updates the cluster population in the $S+1$ conductance states of a cluster by evaluating the $2S$ possible transitions. This provides a huge reduction of transitions, when compared to the $N \cdot S$ state update required to each channel.

In pseudo code, the update algorithm works as follows:

1. Initialize: set initial cluster population $\gamma_0 \in \{0, ..., N\}^{S+1}$
2. Get currently measured membrane potential V
3. Generate two arrays of random numbers $r^{open} \in [0,1]^S$ and $r^{close} \in [0,1]^S$ for the $2S$ opening and closing reactions
4. Calculate propensities of the $2S$ reactions via the macrochannel transition rates in ***Equation 6*** and ***Equation 7***.
   - $\lambda_o^{open} = \gamma_o \alpha_{o,o+1}(V)$ for $o \in \{0, S-1\}$
   - $\lambda_o^{close} = \gamma_{o+1} \beta_{o+1,o}(V)$ for $o \in \{0, S-1\}$
5. Update cluster populations
   - S opening reactions: if $r_o^{open} < \lambda_o^{open} \Delta t$ then increase γ_{o+1} by one and decrease γ_o by 1
   - S closing reactions: if $r_o^{close} < \lambda_o^{close} \Delta t$ then increase γ_o by one and decrease γ_{o+1} by 1
6. Wait until the time interval Δt has passed and continue at step 2

The successive update of the cluster populations can lead to a problem for states, which have a population of one and where both the opening and the closing reaction happen. In our solution, we

chose to assure a positive population for all states and reject the closing reaction in such a case. In an offline comparison with the exact Gillespie algorithm, we tested that our update algorithm accurately captured the evolution of the clusters despite this slight bias toward opening reactions.

The algorithm with instructions how to use it in the recording software RELACS is available at https://itbgit.biologie.hu-berlin.de/cooperativity/dynamic_clamp_model (copy archived at https://github.com/elifesciences-publications/49974-dynamic_clamp_model).

Experimental protocol

In all recordings, we first measured the f-I curve of the neuron and determined the resting potential and the form of the action potentials. With these neuron properties at hand, we chose the model parameters for the dynamic clamp experiment. First, we aimed at a total conductance of the cooperative channels, that allowed a current to flow sufficient for about 10 Hz persistent firing. Correspondingly, we chose the number of cooperative channels, given that channel conductance and reversal potential were orientated at values from calcium channels. Second, we split the channels into clusters such that we obtained both a large number of clusters and a sufficient cluster size for long-term stability. Third, we adjusted the bistable regime of the clusters such that its center coincided with the resting potential and its borders remain far below the spike peak. To this end, we selected the appropriate coupling strength and half-activation voltage of the channels.

We used the stimulation protocol of consecutive pulses, either depolarising or hyperpolarising, to test for graded persistent activity. Pulses had a length of 4–6 s with a period of about 25 s. Often, we saw channels opening persistently during the depolarising pulses, but no persistent activity. In these cases, we would increase the baseline current to bring the neurons closer to threshold. Additionally, we run control protocols with zero coupling to test whether the cell displayed no persistent activity in the absence of cooperativity (***Figure 6—figure supplement 1***).

Analysis

First, we categorised the recordings according to the amplitude and the number of pulses, for example UP-4 for a series of four depolarising pulses or DOWN-1 for one hyperpolarising pulse. Then, the inter spike intervals were analysed during and after the pulses as well as before and after the pulse protocol. For the inter spike intervals, we excluded the first 1000 ms of each interval to account for transient currents. Next, we defined a simple success criteria for a protocol: during an UP (DOWN) protocol, the frequency of persistent firing increases (decreases) with each pulse. During increase or decrease successive periods of silence were allowed to include runs where the persistent firing would only start after for example the second pulse. From the three recorded cells, we got successful runs of every protocol: DOWN-1 (two successful/3 total), DOWN-3 (2/2), DOWN-4 (6/8). UP-1 (7/15), UP-3 (1/1), UP-4 (4/7). An overview of all protocols is available at https://gin.g-node.org/ppfeiffer/cooperative_channels_in_biological_neurons_via_dynamic_clamp, together with the raw data and python scripts for analysis.

For the presented recordings, the model parameters are summarized in ***Table 1***.

Acknowledgements

This work was supported by BMBF (01GQ0901, 01GQ1403), DFG (GRK 1589/2), SFB1134, A01, and Volkswagen Foundation (SmartStart). We are grateful to Jan Benda for his dedicated support with dynamic clamp. We thank Fabian Santi and Dominik Spicher for fruitful contributions during an earlier stage of the project. Finally, we thank Nelson Niemeyer for valuable feedback on the final form of the manuscript.

We acknowledge support by the German Research Foundation (DFG) and the Open Access Publication Fund of Humboldt-Universität zu Berlin.

Additional information

Funding

Funder	Grant reference number	Author
Bundesministerium für Bildung und Forschung	01GQ0901	Susanne Schreiber
Bundesministerium für Bildung und Forschung	01GQ1403	Susanne Schreiber Jan-Hendrik Schleimer
Deutsche Forschungsgemeinschaft	GRK 1589/2	Paul Pfeiffer Susanne Schreiber
Volkswagen Foundation	SmartStart2	Paul Pfeiffer
Deutsche Forschungsgemeinschaft	SFB1134,AO1	Alexei V Egorov Franziska Lorenz Andreas Draguhn

The funders had no role in study design, data collection and interpretation, or the decision to submit the work for publication.

Author contributions

Paul Pfeiffer, Conceptualization, Data curation, Software, Formal analysis, Funding acquisition, Validation, Investigation, Visualization, Methodology; Alexei V Egorov, Supervision, Investigation, Methodology; Franziska Lorenz, Data curation, Software, Investigation, Methodology; Jan-Hendrik Schleimer, Conceptualization, Software, Formal analysis, Supervision, Validation, Methodology; Andreas Draguhn, Resources, Supervision, Funding acquisition, Methodology, Project administration; Susanne Schreiber, Conceptualization, Resources, Formal analysis, Supervision, Funding acquisition, Investigation, Visualization, Methodology, Project administration

Author ORCIDs

Paul Pfeiffer https://orcid.org/0000-0001-5324-5886
Alexei V Egorov https://orcid.org/0000-0003-4899-8407
Susanne Schreiber https://orcid.org/0000-0003-3913-5650

Ethics

Animal experimentation: All experimental protocols were conducted in compliance with German law and with the approval of the state government of Baden-Württemberg (Project T100/15).

Decision letter and Author response

Decision letter https://doi.org/10.7554/eLife.49974.sa1
Author response https://doi.org/10.7554/eLife.49974.sa2

Additional files

Supplementary files

- Transparent reporting form

Data availability

The model for the cooperative ion channels and the neuron are described in the manuscript. Software for simulation of the cooperative channels is provided in git repositories linked in the manuscript (https://itbgit.biologie.hu-berlin.de/cooperativity/brutelib; copy archived athttps://github.com/elifesciences-publications/49974-brutelib; and https://itbgit.biologie.hu-berlin.de/cooperativity/dynamic_clamp_model; copy archived at https://github.com/elifesciences-publications/49974-dynamic_clamp_model). The recordings and analysis obtained in the dynamic clamp experiments are explained in the manuscript and are publicly available at https://gin.g-node.org/doi/cooperative_channels_in_biological_neurons_via_dynamic_clamp.

The following dataset was generated:

Author(s)	Year	Dataset title	Dataset URL	Database and Identifier
Pfeiffer P, Egorov A, Lorenz F, Schleimer J, Draguhn A, Schreiber S	2019	Clusters of cooperative ion channels enable a membrane potential-based mechanism for short-term memory	https://doi.org/10.12751/g-node.08853e	G-Node, 10.12751/g-node.08853e

References

Allen LJS. 2010. *An Introduction to Stochastic Processes with Applications to Biology*. Chapman & Hall/CRC.

Ambros-Ingerson J, Holmes WR. 2005. Analysis and comparison of morphological reconstructions of hippocampal field CA1 pyramidal cells. *Hippocampus* **15**:302–315. DOI: https://doi.org/10.1002/hipo.20051, PMID: 15490464

Amit DJ. 1990. Attractor neural networks and biological reality: associative memory and learning. *Future Generation Computer Systems* **6**:111–119. DOI: https://doi.org/10.1016/0167-739X(90)90027-B

Anderson DF, Ermentrout B, Thomas PJ. 2015. Stochastic representations of ion channel kinetics and exact stochastic simulation of neuronal dynamics. *Journal of Computational Neuroscience* **38**:67–82. DOI: https://doi.org/10.1007/s10827-014-0528-2, PMID: 25408289

Benda J. 2002. *Single Neuron Dynamics - Models Linking Theory and Experiment*. Humboldt-Universität zu Berlin.

Benda J, Herz AV. 2003. A universal model for spike-frequency adaptation. *Neural Computation* **15**:2523–2564. DOI: https://doi.org/10.1162/089976603322385063, PMID: 14577853

Berkefeld H, Sailer CA, Bildl W, Rohde V, Thumfart JO, Eble S, Klugbauer N, Reisinger E, Bischofberger J, Oliver D, Knaus HG, Schulte U, Fakler B. 2006. BKCa-Cav channel complexes mediate rapid and localized Ca2+-activated K+ signaling. *Science* **314**:615–620. DOI: https://doi.org/10.1126/science.1132915, PMID: 17068255

Blunck R, Kirst U, Riessner T, Hansen U. 1998. How powerful is the dwell-time analysis of multichannel records? *Journal of Membrane Biology* **165**:19–35. DOI: https://doi.org/10.1007/s002329900417, PMID: 9705979

Bray D, Levin MD, Morton-Firth CJ. 1998. Receptor clustering as a cellular mechanism to control sensitivity. *Nature* **393**:85–88. DOI: https://doi.org/10.1038/30018, PMID: 9590695

Burrill DR, Silver PA. 2010. Making cellular memories. *Cell* **140**:13–18. DOI: https://doi.org/10.1016/j.cell.2009.12.034, PMID: 20085698

Choi KH. 2014. Cooperative gating between ion channels. *General Physiology and Biophysics* **33**:1–12. DOI: https://doi.org/10.4149/gpb_2013076, PMID: 24177017

Church PJ, Stanley EF. 1996. Single L-type calcium channel conductance with physiological levels of calcium in chick ciliary ganglion neurons. *The Journal of Physiology* **496**:59–68. DOI: https://doi.org/10.1113/jphysiol.1996.sp021665, PMID: 8910196

Clatot J, Hoshi M, Wan X, Liu H, Jain A, Shinlapawittayatorn K, Marionneau C, Ficker E, Ha T, Deschênes I. 2017. Voltage-gated sodium channels assemble and gate as dimers. *Nature Communications* **8**:2077. DOI: https://doi.org/10.1038/s41467-017-02262-0, PMID: 29233994

Cui ED, Strowbridge BW. 2018. Modulation of Ether-à-Go-Go related gene (ERG) Current governs intrinsic persistent activity in rodent neocortical pyramidal cells. *The Journal of Neuroscience* **38**:423–440. DOI: https://doi.org/10.1523/JNEUROSCI.1774-17.2017, PMID: 29175952

Debanne D, Inglebert Y, Russier M. 2019. Plasticity of intrinsic neuronal excitability. *Current Opinion in Neurobiology* **54**:73–82. DOI: https://doi.org/10.1016/j.conb.2018.09.001

Dekker JP, Yellen G. 2006. Cooperative gating between single HCN pacemaker channels. *The Journal of General Physiology* **128**:561–567. DOI: https://doi.org/10.1085/jgp.200609599, PMID: 17043149

Dixon RE, Moreno CM, Yuan C, Opitz-Araya X, Binder MD, Navedo MF, Santana LF. 2015. Graded Ca2+/calmodulin-dependent coupling of voltage-gated CaV1.2 channels. *eLife* **4**:e05608. DOI: https://doi.org/10.7554/eLife.05608

Durstewitz D, Seamans JK, Sejnowski TJ. 2000. Neurocomputational models of working memory. *Nature Neuroscience* **3**:1184–1191. DOI: https://doi.org/10.1038/81460, PMID: 11127836

Egorov AV, Hamam BN, Fransén E, Hasselmo ME, Alonso AA. 2002. Graded persistent activity in entorhinal cortex neurons. *Nature* **420**:173–178. DOI: https://doi.org/10.1038/nature01171, PMID: 12432392

Egorov AV, Unsicker K, von Bohlen und Halbach O. 2006. Muscarinic control of graded persistent activity in lateral amygdala neurons. *European Journal of Neuroscience* **24**:3183–3194. DOI: https://doi.org/10.1111/j.1460-9568.2006.05200.x, PMID: 17156379

Egorov AV, Schumacher D, Medert R, Birnbaumer L, Freichel M, Draguhn A. 2019. TRPC channels are not required for graded persistent activity in entorhinal cortex neurons. *Hippocampus* **29**:1038–1048. DOI: https://doi.org/10.1002/hipo.23094, PMID: 31002217

Eisenach C, Papanatsiou M, Hillert EK, Blatt MR. 2014. Clustering of the K+ channel GORK of Arabidopsis parallels its gating by extracellular K+. *The Plant Journal : For Cell and Molecular Biology* **78**:203–214. DOI: https://doi.org/10.1111/tpj.12471, PMID: 24517091

Fransén E, Tahvildari B, Egorov AV, Hasselmo ME, Alonso AA. 2006. Mechanism of graded persistent cellular activity of entorhinal cortex layer v neurons. *Neuron* **49**:735–746. DOI: https://doi.org/10.1016/j.neuron.2006.01.036, PMID: 16504948

Gianoli F, Risler T, Kozlov AS. 2017. Lipid bilayer mediates ion-channel cooperativity in a model of hair-cell mechanotransduction. *PNAS* **114**:E11010–E11019. DOI: https://doi.org/10.1073/pnas.1713135114
Gillespie DT. 1977. Exact stochastic simulation of coupled chemical reactions. *The Journal of Physical Chemistry* **81**:2340–2361. DOI: https://doi.org/10.1021/j100540a008
Grage SL, Keleshian AM, Turdzeladze T, Battle AR, Tay WC, May RP, Holt SA, Contera SA, Haertlein M, Moulin M, Pal P, Rohde PR, Forsyth VT, Watts A, Huang KC, Ulrich AS, Martinac B. 2011. Bilayer-mediated clustering and functional interaction of MscL channels. *Biophysical Journal* **100**:1252–1260. DOI: https://doi.org/10.1016/j.bpj.2011.01.023, PMID: 21354398
Gutkin B, Ermentrout GB. 2006. Spikes too kinky in the cortex? *Nature* **440**:999–1000. DOI: https://doi.org/10.1038/440999a
Haas HL, Schaerer B, Vosmansky M. 1979. A simple perfusion chamber for the study of nervous tissue slices in vitro. *Journal of Neuroscience Methods* **1**:323–325. DOI: https://doi.org/10.1016/0165-0270(79)90021-9, PMID: 544974
Hilgemann DW, Dai G, Collins A, Lariccia V, Magi S, Deisl C, Fine M. 2018. Lipid signaling to membrane proteins: from second messengers to membrane domains and adapter-free endocytosis. *The Journal of General Physiology* **150**:211–224. DOI: https://doi.org/10.1085/jgp.201711875, PMID: 29326133
Huang M, Volgushev M, Wolf F. 2012. A small fraction of strongly cooperative sodium channels boosts neuronal encoding of high frequencies. *PLOS ONE* **7**:e37629. DOI: https://doi.org/10.1371/journal.pone.0037629, PMID: 22666374
Iwasa K, Ehrenstein G, Moran N, Jia M. 1986. Evidence for interactions between batrachotoxin-modified channels in hybrid neuroblastoma cells. *Biophysical Journal* **50**:531–537. DOI: https://doi.org/10.1016/S0006-3495(86)83491-9, PMID: 2428414
Kim GE, Kronengold J, Barcia G, Quraishi IH, Martin HC, Blair E, Taylor JC, Dulac O, Colleaux L, Nabbout R, Kaczmarek LK. 2014. Human slack potassium channel mutations increase positive cooperativity between individual channels. *Cell Reports* **9**:1661–1672. DOI: https://doi.org/10.1016/j.celrep.2014.11.015, PMID: 25482562
Lisman JE. 1985. A mechanism for memory storage insensitive to molecular turnover: a bistable autophosphorylating kinase. *PNAS* **82**:3055–3057. DOI: https://doi.org/10.1073/pnas.82.9.3055, PMID: 2986148
Loewenstein Y, Sompolinsky H. 2003. Temporal integration by calcium dynamics in a model neuron. *Nature Neuroscience* **6**:961–967. DOI: https://doi.org/10.1038/nn1109, PMID: 12937421
Marder E, Abbott LF, Turrigiano GG, Liu Z, Golowasch J. 1996. Memory from the dynamics of intrinsic membrane currents. *PNAS* **93**:13481–13486. DOI: https://doi.org/10.1073/pnas.93.24.13481, PMID: 8942960
Misonou H, Mohapatra DP, Park EW, Leung V, Zhen D, Misonou K, Anderson AE, Trimmer JS. 2004. Regulation of ion channel localization and phosphorylation by neuronal activity. *Nature Neuroscience* **7**:711–718. DOI: https://doi.org/10.1038/nn1260, PMID: 15195093
Molina ML, Barrera FN, Fernández AM, Poveda JA, Renart ML, Encinar JA, Riquelme G, González-Ros JM. 2006. Clustering and coupled gating modulate the activity in KcsA, a potassium channel model. *Journal of Biological Chemistry* **281**:18837–18848. DOI: https://doi.org/10.1074/jbc.M600342200, PMID: 16670090
Moreno CM, Dixon RE, Tajada S, Yuan C, Opitz-Araya X, Binder MD, Santana LF. 2016. Ca(2+) entry into neurons is facilitated by cooperative gating of clustered CaV1.3 channels. *eLife* **5**:e15744. DOI: https://doi.org/10.7554/eLife.15744, PMID: 27187148
Morris C, Lecar H. 1981. Voltage oscillations in the barnacle giant muscle fiber. *Biophysical Journal* **35**:193–213. DOI: https://doi.org/10.1016/S0006-3495(81)84782-0
Naundorf B, Wolf F, Volgushev M. 2006. Unique features of action potential initiation in cortical neurons. *Nature* **440**:1060–1063. DOI: https://doi.org/10.1038/nature04610, PMID: 16625198
Navaroli VL, Zhao Y, Boguszewski P, Brown TH. 2012. Muscarinic receptor activation enables persistent firing in pyramidal neurons from superficial layers of dorsal perirhinal cortex. *Hippocampus* **22**:1392–1404. DOI: https://doi.org/10.1002/hipo.20975, PMID: 21956787
Navedo MF, Cheng EP, Yuan C, Votaw S, Molkentin JD, Scott JD, Santana LF. 2010. Increased coupled gating of L-type Ca2+ channels during hypertension and timothy syndrome. *Circulation Research* **106**:748–756. DOI: https://doi.org/10.1161/CIRCRESAHA.109.213363, PMID: 20110531
Nilius B, Owsianik G. 2011. The transient receptor potential family of ion channels. *Genome Biology* **12**:218. DOI: https://doi.org/10.1186/gb-2011-12-3-218, PMID: 21401968
Prinz AA, Abbott LF, Marder E. 2004. The dynamic clamp comes of age. *Trends in Neurosciences* **27**:218–224. DOI: https://doi.org/10.1016/j.tins.2004.02.004, PMID: 15046881
Rodriguez G, Sarazin M, Clemente A, Holden S, Paz JT, Delord B. 2018. Conditional bistability, a generic cellular mnemonic mechanism for robust and flexible working memory computations. *The Journal of Neuroscience* **38**:5209–5219. DOI: https://doi.org/10.1523/JNEUROSCI.1992-17.2017, PMID: 29712783
Roth FC, Beyer KM, Both M, Draguhn A, Egorov AV. 2016. Downstream effects of hippocampal sharp wave ripple oscillations on medial entorhinal cortex layer V neurons in vitro. *Hippocampus* **26**:1493–1508. DOI: https://doi.org/10.1002/hipo.22623, PMID: 27479916
Sato D, Dixon RE, Santana LF, Navedo MF. 2018. A model for cooperative gating of L-type Ca2+ channels and its effects on cardiac alternans dynamics. *PLOS Computational Biology* **14**:e1005906. DOI: https://doi.org/10.1371/journal.pcbi.1005906
Schreiber S, Samengo I, Herz AVM. 2009. Two distinct mechanisms shape the reliability of neural responses. *Journal of Neurophysiology* **101**:2239–2251. DOI: https://doi.org/10.1152/jn.90711.2008

Sharp AA, O'Neil MB, Abbott LF, Marder E. 1993. The dynamic clamp: artificial conductances in biological neurons. *Trends in Neurosciences* **16**:389–394. DOI: https://doi.org/10.1016/0166-2236(93)90004-6, PMID: 7504352

Stefan MI, Le Novère N. 2013. Cooperative binding. *PLOS Computational Biology* **9**:e1003106. DOI: https://doi.org/10.1371/journal.pcbi.1003106, PMID: 23843752

Sumino A, Yamamoto D, Iwamoto M, Dewa T, Oiki S. 2014. Gating-Associated Clustering-Dispersion dynamics of the KcsA potassium channel in a lipid membrane. *The Journal of Physical Chemistry Letters* **5**:578–584. DOI: https://doi.org/10.1021/jz402491t, PMID: 26276612

Thomas R, D'Ari R. 1990. *Biological Feedback*. CRC Press.

Undrovinas AI, Fleidervish IA, Makielski JC. 1992. Inward sodium current at resting potentials in single cardiac myocytes induced by the ischemic metabolite lysophosphatidylcholine. *Circulation Research* **71**:1231–1241. DOI: https://doi.org/10.1161/01.RES.71.5.1231, PMID: 1327577

Vivas O, Moreno CM, Santana LF, Hille B. 2017. Proximal clustering between BK and $Ca_V1.3$ channels promotes functional coupling and BK channel activation at low voltage. *eLife* **6**:e28029. DOI: https://doi.org/10.7554/eLife.28029, PMID: 28665272

White JA, Rubinstein JT, Kay AR. 2000. Channel noise in neurons. *Trends in Neurosciences* **23**:131–137. DOI: https://doi.org/10.1016/S0166-2236(99)01521-0

Winograd M, Destexhe A, Sanchez-Vives MV. 2008. Hyperpolarization-activated graded persistent activity in the prefrontal cortex. *PNAS* **105**:7298–7303. DOI: https://doi.org/10.1073/pnas.0800360105, PMID: 18474856

Yu Y, Shu Y, McCormick DA. 2008. Cortical action potential backpropagation explains spike threshold variability and rapid-onset kinetics. *Journal of Neuroscience* **28**:7260–7272. DOI: https://doi.org/10.1523/JNEUROSCI.1613-08.2008, PMID: 18632930

Zarubin D, Zhuchkova E, Schreiber S. 2012. Effects of cooperative ion-channel interactions on the dynamics of excitable membranes. *Physical Review E* **85**:061904. DOI: https://doi.org/10.1103/PhysRevE.85.061904

Zhang Z, Reboreda A, Alonso A, Barker PA, Séguéla P. 2011. TRPC channels underlie cholinergic plateau potentials and persistent activity in entorhinal cortex. *Hippocampus* **21**:386–397. DOI: https://doi.org/10.1002/hipo.20755

Zylberberg J, Strowbridge BW. 2017. Mechanisms of persistent activity in cortical circuits: possible neural substrates for working memory. *Annual Review of Neuroscience* **40**:603–627. DOI: https://doi.org/10.1146/annurev-neuro-070815-014006, PMID: 28772102

Supplementary figures for Publication COOPMEM

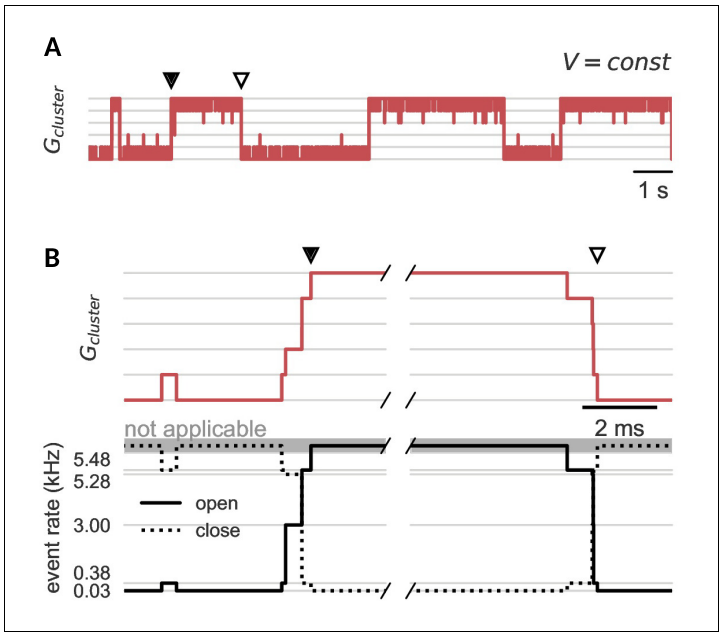

Figure 3—figure supplement 1. Channel noise can open and close a cluster. (**A**) Clamped at a fixed voltage in the bistable regime, a cluster of cooperative channels slowly switches between the open and closed state. In both cases, when a cluster opens (black dot) or closes (white dot), this quasi-synchronous gating of all channels is triggered by channel noise and amplified by cooperativity. (**B**) Zoom on the exemplary opening (left) and closing (right) events in *A*. The cooperative interactions spread single channel switches by changing the rates for the next opening (solid) or closing (dashed) event. Either channels open and facilitate further openings or channels close and decrease the facilitation of their neighbors. Note that the cluster is stable against single channel gating events; when only one channel opens, the increased opening rate (0.03 kHz to 0.38 kHz) is still ten-fold smaller than the closing rate (5.48 kHz). Cluster parameters are summarized in ***Table 1***.

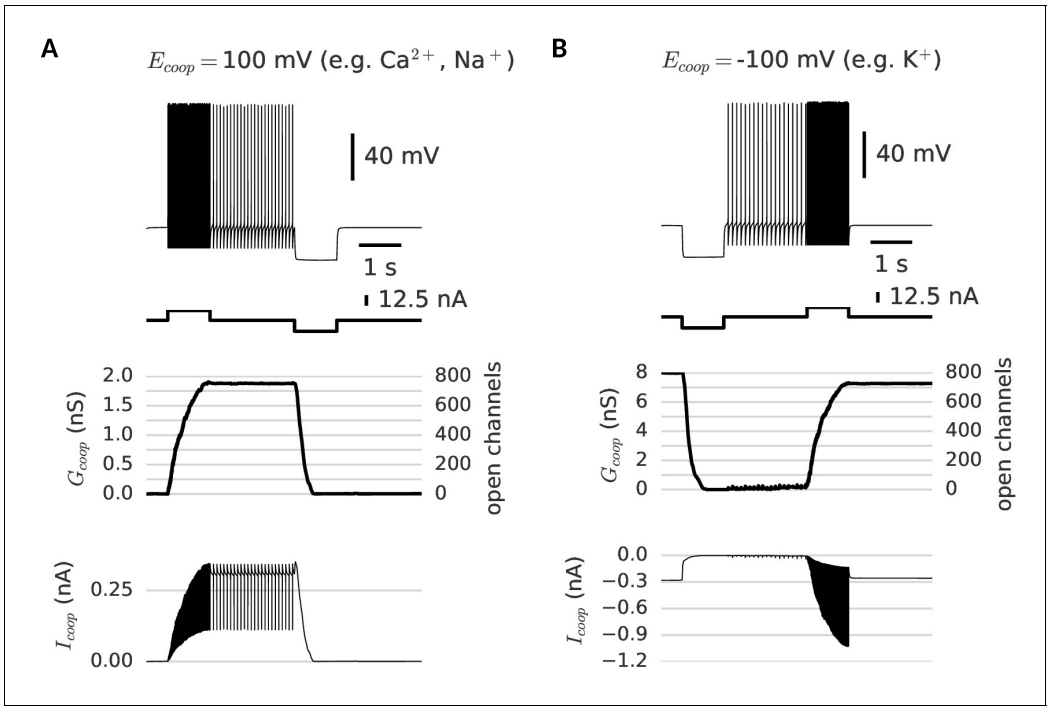

Figure 4—figure supplement 1. Depending on their reversal potential, clusters of cooperative channels can mediate de- or hyperpolarization-activated persistent activity. (**A**) Depolarization-activated persistent activity. After stimulated spiking, the neuron continues to spike, because of the depolarizing current (E_{coop}=100 mV) through the persistently open clusters (bottom trace). (**B**) Hyperpolarization-activated persistent activity. A very distinct mnemonic firing behavior is possible with clusters of cooperative channels that have the same dynamics as the ones in *A*, but conduct a hyperpolarizing current (E_{coop}=-100mV). When such clusters are open initially, they provide a standing leak current that prevents the neuron from firing (bottom trace). A strong hyperpolarizing pulse persistently closes the clusters and thereby activates low-frequency spiking. Strong stimulated spiking reopens the clusters and hence silences the neuron. For a summary of cluster parameters, see ***Table 1***.

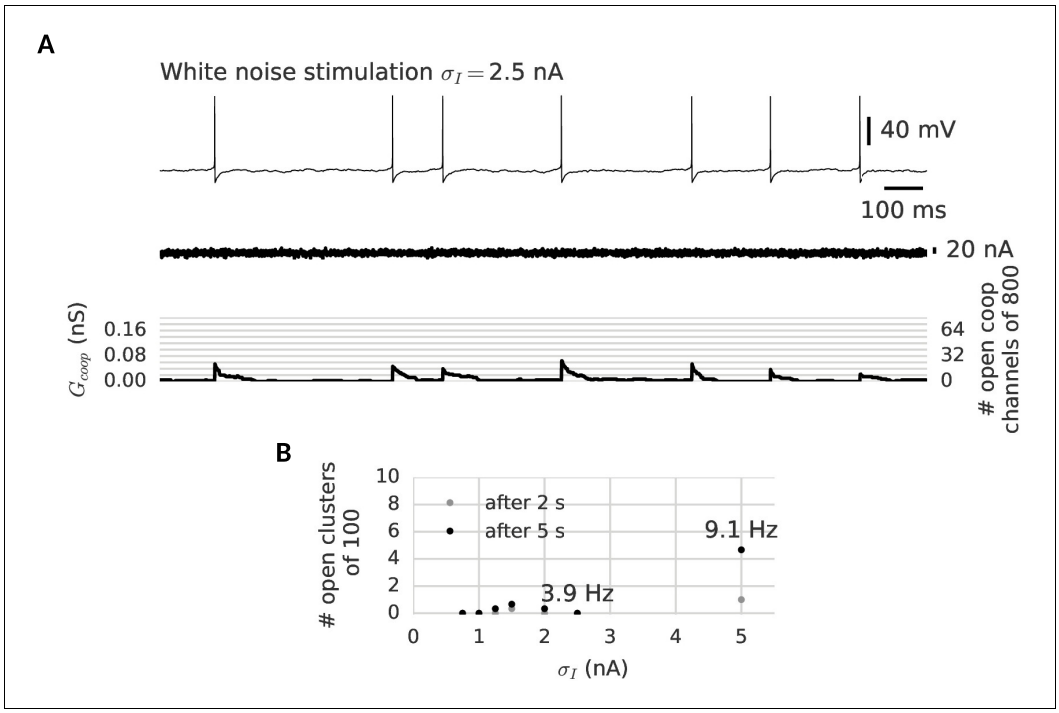

Figure 4—figure supplement 2. Clusters are robust against noise in the membrane potential. (**A**) A neuron is stimulated for 2 s with a white noise current (middle) to induce membrane potential fluctuations and spontaneous spikes (top). Despite the noisy membrane potential, the clusters remain in their closed state (bottom). Even spontaneous spikes only open a few channels transiently in each cluster and cannot switch a whole cluster persistently to the open state (**B**) The clusters remain closed after exposure to 5 s of noise stimulation. Only an unphysiologically high noise level leads to the opening a few clusters by spontaneous firing at around 10 Hz (see indicated firing frequencies). For details on the white noise stimulation see Materials and methods. There are 100 clusters of eight cooperative channels each. Further parameters are summarized in ***Table 1***.

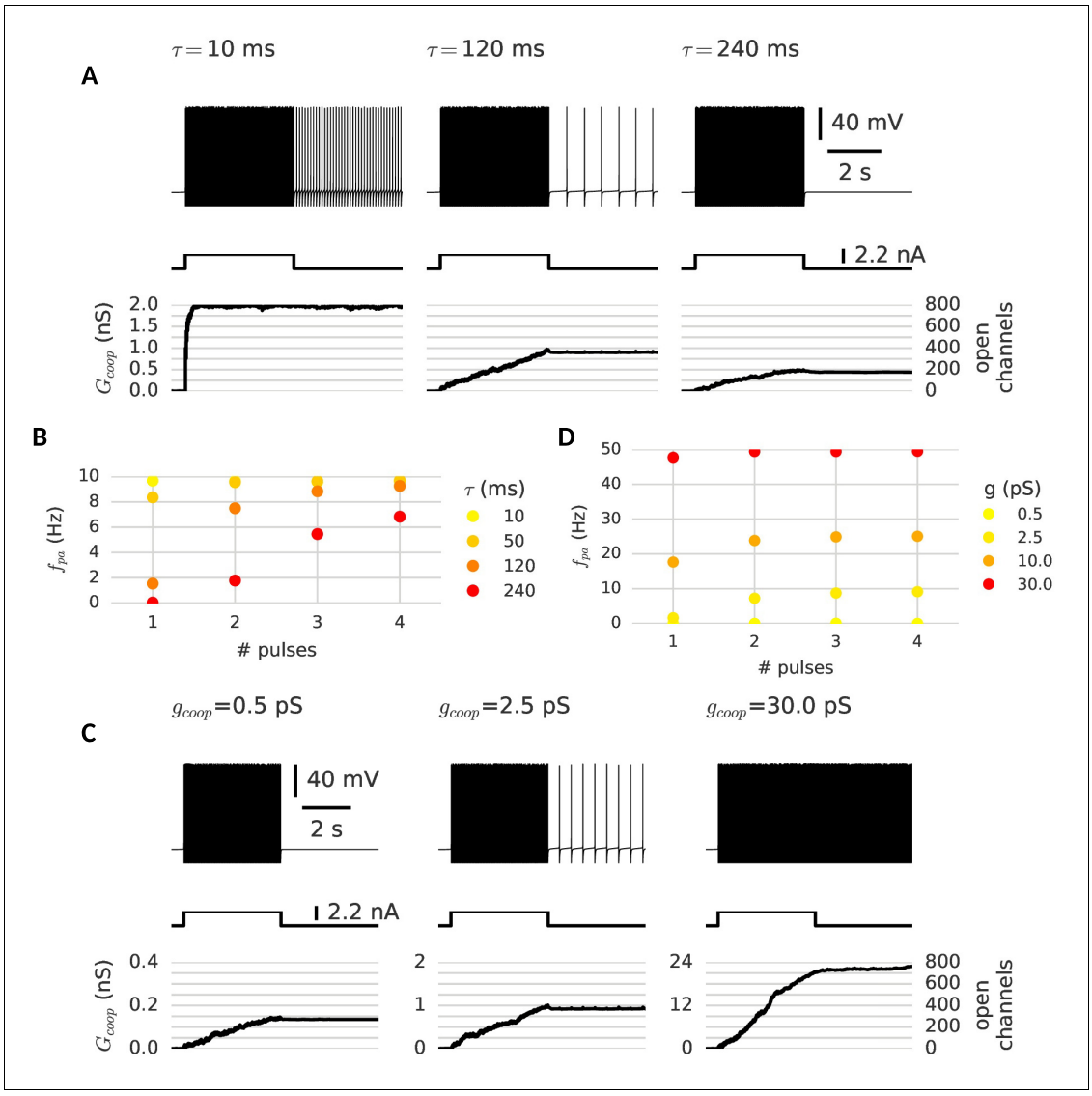

Figure 5—figure supplement 1. Memory dynamics with different properties of cooperative channels. The channel's time constant and their conductance change the memory dynamics of the neuron probed with the multi-pulse protocol for graded persistent activity. (**A**) Variation of the time constant: When channels are fast (left, τ = 10 ms), the neuron is already maximally active after the first pulse - a few spikes suffice to open all clusters and there is only one level of persistent activity. Slower channels allow for a graded opening of channels and intermediate levels of persistent activity (middle, τ = 120 ms). If the channels are too slow and too few clusters open during the first pulse, the neuron remains silent (right, τ = 240 ms). (**B**) Frequency of persistent activity after each pulse for different time constants. (**C**) Variation of the channel conductance: When channels are low conducting, the persistent current remains subthreshold and is thus insufficient to drive persistent activity (left). At an intermediate conductance, the clusters mediate low frequency persistent activity (middle). When the provided conductance is too large, the high frequency persistent activity can open further clusters and is no longer stable. (**D**) Frequency of persistent activity after each pulse for different channel conductances. Other cluster parameters are summarized in ***Table 1***.

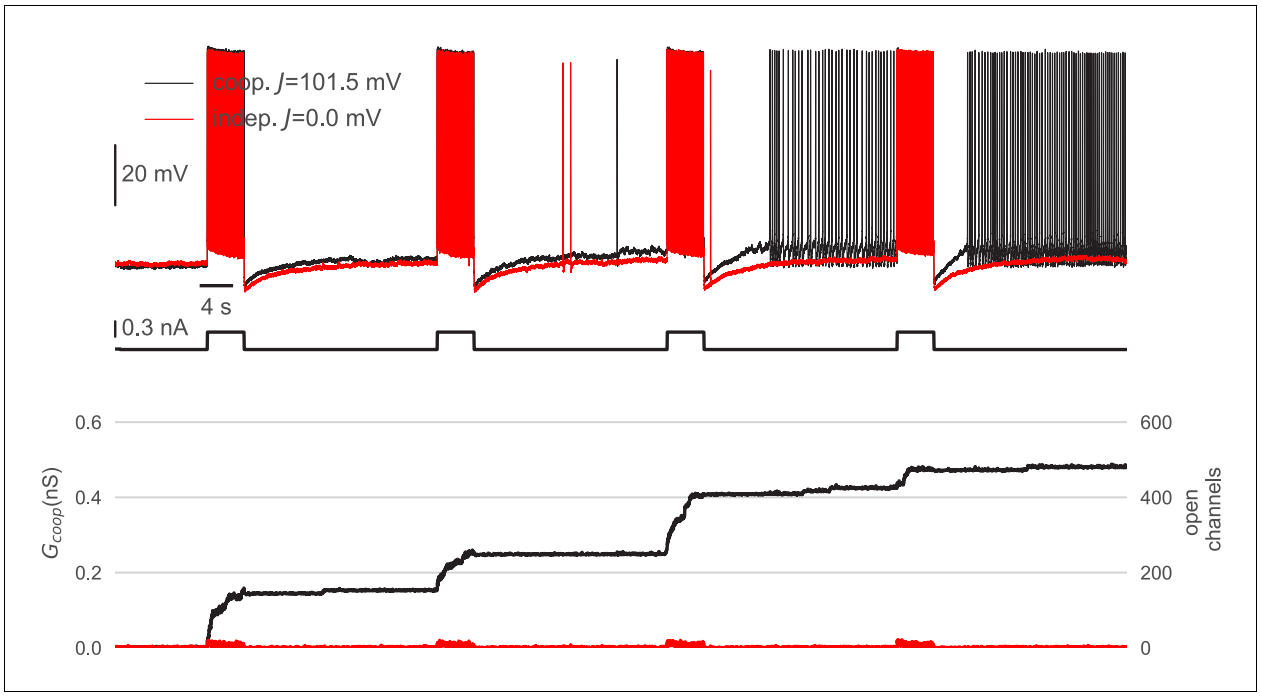

Figure 6—figure supplement 1. Cooperative interactions are necessary to mediate graded persistent activity. Control experiment to demonstrate the requirement of cooperative channel interactions for graded persistent activity in a perirhinal cortex neuron. *Top*: When the channels gated independently (red, J=0 mV), the neuron only fired during the stimulating pulses and otherwise remained silent. When, in contrast, the channels cooperate strongly (black, J=101.5 mV), the cell produced graded persistent activity (this trace is the full trace of the extract shown in ***Figure 6***). *Bottom*: The independent channels reacted to spiking activity only in a transient way and remained closed after the stimulus. In contrast, cooperative channels opened and facilitated their neighbors to open as well. In this way, spiking could open whole clusters, which remained open after the stimulus and drove persistent activity. A detailed description of the dynamic clamp experiment is given in Material and methods. Cluster parameters are summarized in ***Table 1***.

4.2 CAPCLAMP – A dynamic clamp protocol to artificially modify cell capacitance

Paul Pfeiffer, Federico José Barreda Tomás, Jiameng Wu, Jan-Hendrik Schleimer, Imre Vida, and Susanne Schreiber (Apr. 2022). "A Dynamic Clamp Protocol to Artificially Modify Cell Capacitance". In: *eLife* 11. Ed. by Ronald L. Calabrese and Jorge Golowasch, e75517. ISSN: 2050-084X. DOI: 10.7554/eLife.75517

Supplementary figure(s) follow directly after the main article.

eLife

TOOLS AND RESOURCES

A dynamic clamp protocol to artificially modify cell capacitance

Paul Pfeiffer[1,2], Federico José Barreda Tomás[2,3], Jiameng Wu[2,4], Jan-Hendrik Schleimer[1,2], Imre Vida[2,3], Susanne Schreiber[1,2]*

[1]Institute for Theoretical Biology, Humboldt-Universität zu Berlin, Berlin, Germany; [2]Bernstein Center for Computational Neuroscience, Humboldt-Universität zu Berlin, Berlin, Germany; [3]Institute for Integrative Neuroanatomy, Charité - Universitätsmedizin Berlin, Corporate Member of Freie Universität Berlin, Humboldt-Universität zu Berlin, and Berlin Institute of Health, Berlin, Germany; [4]Einstein Center for Neurosciences Berlin, Charité - Universitätsmedizin Berlin, Corporate Member of Freie Universität Berlin, Humboldt-Universität zu Berlin, and Berlin Institute of Health, Berlin, Germany

Abstract Dynamics of excitable cells and networks depend on the membrane time constant, set by membrane resistance and capacitance. Whereas pharmacological and genetic manipulations of ionic conductances of excitable membranes are routine in electrophysiology, experimental control over capacitance remains a challenge. Here, we present capacitance clamp, an approach that allows electrophysiologists to mimic a modified capacitance in biological neurons via an unconventional application of the dynamic clamp technique. We first demonstrate the feasibility to quantitatively modulate capacitance in a mathematical neuron model and then confirm the functionality of capacitance clamp in in vitro experiments in granule cells of rodent dentate gyrus with up to threefold virtual capacitance changes. Clamping of capacitance thus constitutes a novel technique to probe and decipher mechanisms of neuronal signaling in ways that were so far inaccessible to experimental electrophysiology.

Editor's evaluation

The manuscript introduces a new enhancement to the dynamic clamp technique, CapClamp that, analogous to the artificial conductances of standard Dynamic Clamp, allows the experimenter to adjust the somatic time constant by setting a new membrane artificial capacitance independent of any change in input resistance. The technique is shown to have application for studying temporal integration, energetic costs of spiking and bifurcations. The technique is rigorously tested in model and physiological application and is robust when sampling frequency of the feedback (clamp) loop is fast compared to the fastest electrical event in a neuron (usually action potentials), and for vertebrate neurons it should be 20KHz or faster and yet faster for fast spiking neurons.

***For correspondence:** s.schreiber@hu-berlin.de

Funding: See page 21

Received: 12 November 2021
Preprinted: 13 November 2021
Accepted: 17 March 2022
Published: 01 April 2022

Reviewing Editor: Ronald L Calabrese, Emory University, United States

Introduction

Membrane capacitance is a major biophysical parameter in neurons and other excitable cells, which determines how fast the membrane potential changes in response to a current (***Golowasch et al., 2009***; ***White and Hooper, 2013***). How capacitance impacts electrical signaling and neuronal processing, however, can rarely be observed experimentally, because besides reduced values in myelinated axons (***Hartline and Colman, 2007***) most membranes appear to have a specific membrane capacitance in the range of 0.7–1.0 µF/cm2 (***Gentet et al., 2000***). The effects of capacitance changes

can, therefore, so far only be compared via mathematical simulations, where capacitance is simple to control. Such modeling, for example, suggests that the reduced membrane capacitance observed in human pyramidal cells can serve to increase synaptic efficacy or propagation speed of action potentials (***Eyal et al., 2016***, but see ***Beaulieu-Laroche et al., 2018***). In contrast, experimental manipulation of capacitance remains challenging; in particular because changes in membrane area, thickness and lipid composition that affect capacitance might influence other membrane functions, such as the embedding of ion channels, with potentially unintended and uncontrolled consequences for electrical behavior. Here, we address this technical challenge by introducing capacitance clamp (CapClamp): an intracellular recording mode based on the dynamic clamp that emulates altered capacitance values in biological neurons (***Robinson, 1994***; ***Sharp et al., 1993***). Via CapClamp, the voltage dynamics governed by the actual biophysics of a cell – active ion channels and synaptic inputs – can thus be flexibly probed under multiple 'virtual' capacitance conditions, which provides precise experimental control over this hitherto inaccessible parameter.

In addition to the analysis of biological capacitance adaptations, control over capacitance offers a distinct way to probe cellular electrical dynamics. Capacitance has a unique temporal role, because its direct effects are restricted to the membrane time constant whilst leaving the steady state I-V function unaltered. In this way, capacitance differs from leak conductance, the other determinant of the time constant, as the latter also alters steady-state response amplitudes. For this reason, theoretical studies preferentially vary capacitance to investigate ion channel dynamics (***Jaffe and Brenner, 2018***; ***Franci et al., 2018***) and qualitative switches (bifurcations) in neural excitability (***Kirst et al., 2015***; ***Hesse et al., 2017***). Furthermore, effects of an altered capacitance can be informative about more complex, time scale-related parameters like temperature or ion concentrations (***Contreras et al., 2020***). Such computational predictions, however, often rely on simplified neuron models, so a similar experimental control over capacitance would be desirable to test them in biological cells.

The proposed CapClamp alters capacitance in a virtual manner, combining the simplicity of computational control with the complex biophysics of a real neuron. It is inspired by the dynamic clamp technique, which has originally been developed to simulate the presence of additional conductances in a biological neuron relying on a fast feedback loop between intracellular recording and a computational model (***Robinson, 1994***; ***Sharp et al., 1993***; ***Prinz et al., 2004***; ***Economo et al., 2010***). The precise control over these virtual conductances enables electrophysiological experiments that are more difficult or even impossible with traditional pharmacological or genetic means (***Turrigiano et al., 1996***; ***Svirskis et al., 2004***; ***Prescott et al., 2008b***; ***Hasenstaub et al., 2010***; ***Szűcs et al., 2017***; ***Pfeiffer et al., 2020***). Here, we demonstrate how the dynamic clamp can be extended to enable manipulations of the apparent membrane capacitance by currents designed to speed up or slow down dynamics of the membrane potential. We derive a simple expression for these CapClamp currents, which can be applied in all excitable cells and only requires the experimenter to specify the original cell and the desired target capacitance. In an experiment based on a hardware-implemented RC circuit, we verify that the CapClamp indeed correctly modifies the time constant. Via numerical simulations, we confirm that a clamped model neuron exhibits the same pronounced changes of firing and spike shape as a control cell with an altered capacitance. For an experimental demonstration, we clamp the near-somatic capacitance of rat dentate gyrus granule cells and analyze how the induced local capacitance change affects their spiking behavior. Finally, we illustrate how the CapClamp can be used to probe signal integration and energy consumption of excitable cells in ways that so far were experimentally inaccessible.

Results

Capacitance clamp: A dynamic clamp protocol to mimic capacitance changes

Dynamic clamp relies on a fast feedback loop between an intracellular recording of a neuron and a computer that simulates virtual cellular or circuit components online. Originally, the dynamic clamp has been developed to study how a membrane conductance alters the neuron's voltage dynamics (***Sharp et al., 1993***; ***Robinson, 1994***). In each sampling interval (i.e. time interval between two voltage samplings), a digital model of the conductance receives the sampled membrane potential, updates the conductance state and sends the corresponding current value back to the amplifier. Given a

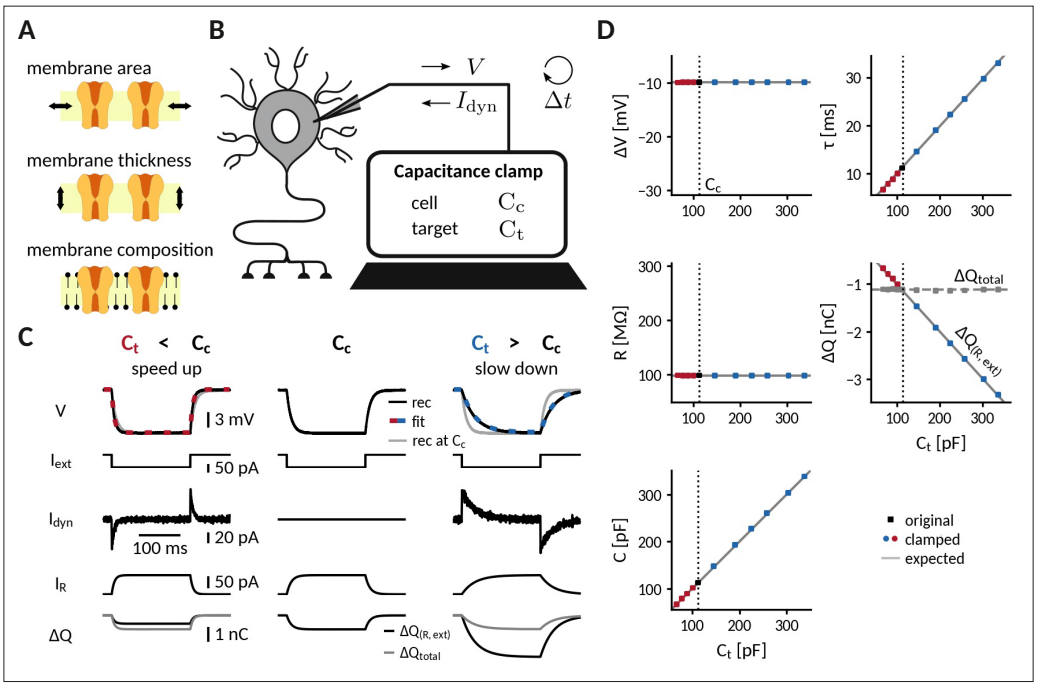

Figure 1. Adding or removing artificial capacitance via the CapClamp. (**A**) Physically, membrane capacitance varies with surface area, thickness and lipid composition (**B**) Virtual capacitance modification via the CapClamp is a form of dynamic clamp, a fast feedback loop between intracellular voltage sampling and computer-controlled current injection: given the measured cell capacitance C_c, the target capacitance C_t, recorded membrane potentials and the sampling interval Δt, the computer calculates clamping currents required to mimic the desired change of capacitance (see ***Equation 1***). (**C**) Clamping a hardware-implemented model cell (RC circuit) at a decreased (left) or increased (right) capacitance leads to faster respectively slower charging of the 'membrane potential' V to the same steady-state voltage response (top row, black: recordings, dashed red and blue: exponential fits $\Delta V\left(1-e^{-\frac{t}{\tau}}\right)$, gray: recording at original C_c) in response to a step current I_{ext} (2nd row) due to the clamping currents I_{dyn} (3rd row). As a result, the current through the resistance $I_R=-\frac{V}{R}$ (4th row) has a different profile and the apparently deposited charge $\Delta Q(R,\mathrm{ext})=\int \mathrm{d}t I_R+I_{ext}$ (bottom row, black) by the 'cellular' transmembrane currents decreases, respectively, increases as expected for a capacitance change. The real deposited charge ΔQ_{total} (bottom row, gray), taking into account the clamping currents, has the same steady-state amplitude in all three cases, because the physical capacitance did not change. (**D**) Measured time constant τ, voltage responses ΔV, resistance R, deposited charge ΔQ (apparent and total) and capacitance C versus target capacitances.

The online version of this article includes the following figure supplement(s) for figure 1:

Figure supplement 1. Impedance analysis of an RC circuit coupled to the capacitance clamp.

sufficiently high update rate f_{dyn} (often ≥10 kHz), this current injected via the recording electrode makes the dynamics of the neuron appear as if the virtual channels represented by the conductance model were physically present in the membrane.

Whereas conductances gate ionic currents across the membrane, the capacitance determines how fast these currents can change the membrane potential. Every altered membrane property that results in a modified capacitance value, such as membrane area, thickness or lipid composition, affects this rate of change of the membrane potential (***Figure 1A***). To artificially mimic a modified capacitance, we therefore first asked whether a dynamic clamp protocol with its fast feedback loop between voltage sampling and current injection could adjust the 'speed' of a cell's membrane potential (***Figure 1B***). Using the current balance equation, the basic mathematical description of membrane voltage dynamics, we derived a capacitance clamp (CapClamp) scheme with a simple expression for the clamping current I_{dyn} (see "Derivation of the CapClamp current" in Methods),

$$I_{\mathrm{dyn},i}=\frac{C_c-C_t}{C_t}\left(C_c\frac{V_i-V_{i-1}}{\Delta t}-I_{\mathrm{dyn},i-1}\right), \quad (1)$$

which only requires the experimenter to measure the cell capacitance C_c in order to set a new target capacitance C_t. In every sampling interval $\Delta t = f_{\mathrm{dyn}}{}^{-1}$, the CapClamp uses the measured cell capacitance value C_c and the voltage derivative $\frac{V_i - V_{i-1}}{\Delta t}$ to estimate the present membrane current and then increases ($C_t < C_c$) or decreases ($C_c < C_t$) the net current by insertion of a correction current in the next time bin. In this way, despite a physically unaltered capacitance, the membrane potential changes faster or, respectively, slower – as if the clamped cell actually had the different capacitance C_t selected by the experimenter. In the following, we will demonstrate the CapClamp in simulated and experimental scenarios with increasing complexity ranging from a passive RC circuit up to biological neurons with a spatially extended morphology.

Clamping capacitance in a passive cell

The simplest scenario to apply the CapClamp is a single compartment passive cell, equivalent to an RC circuit. In the absence of active conductances, the effects of a capacitance change can be precisely formulated: the capacitance C sets the membrane time constant $\tau = RC$, determining how fast the membrane potential changes in response to a current. Note that, in contrast to the resistance R, the change in capacitance leaves the voltage amplitude of the steady-state response unaltered. To quantitatively confirm the effects of clamping capacitance and the ability of an exclusively temporal control, we measured time constant and capacitance of a clamped RC circuit in experiment and analyzed the temporal filtering properties of a modeled clamped circuit using mathematical analysis.

To experimentally characterize a clamped passive cell, we implemented the CapClamp scheme in a dynamic clamp setup (see "Dynamic clamp setup" in Methods) and recorded voltage responses to current pulses from the simplest possible model cell, that is, a hardware implemented RC circuit, while clamping it at a range of target capacitances (***Figure 1C***). As expected for an RC circuit, the charging curve of the unclamped model cell was fit well by a single exponential, whose time constant (τ = 11.1ms) and voltage amplitude (ΔV = −9.9 mV) allowed us to determine the circuit's resistance R=99.4 MΩ and capacitance C=112.3 pF. This capacitance value was then used as the cell capacitance C_c input for the CapClamp. Clamped at a decreased capacitance, the time constant shortened (C_t = 67.4 pF: τ=6.6ms) and at an increased capacitance, it lengthened (C_t = 336.9 pF: τ=33.0ms), but in both cases the steady state voltage amplitude remained the same. Accordingly, the measured capacitance of the clamped circuit confirmed the chosen target capacitance for the whole tested range from a 0.6- up to a 3-fold change with respect to the original capacitance (e.g. C_t=67.4 pF: C=67.5 pF; C_t=336.9 pF: C=338.1 pF), whereas the measured resistance remained constant (***Figure 1D***).

As a consequence of the correctly transformed voltage response, the leak current in the clamped RC circuit also behaved as if the capacitance had changed. When the circuit was clamped, the leak current through the resistance, $I_R = \frac{V}{R}$, exhibited a shorter ($C_t < C_c$) or longer ($C_t > C_c$) transient until reaching steady state. Further, the charge $\Delta Q(I_R, I_{\mathrm{ext}})$ deposited on the capacitance by the apparent 'transmembrane' current, the sum of leak and external stimulus current, reduced ($C_t < C_c$) or increased ($C_t > C_c$) to the extent expected for an altered capacitance (***Figure 1C***). In contrast, the overall deposited charge $\Delta Q(I_R, I_{\mathrm{ext}}, I_{\mathrm{dyn}})$, including the clamping current, attained the same steady-state amplitude in the clamped and the original circuit, reflecting that the physical capacitance did not change. For the simple RC circuit considered here, the distinction between the clamping current and the intrinsic 'cellular' currents might appear artificial, because all currents use the same charge carrier. In a biological neuron, however, this distinction becomes relevant, because the clamping currents through the recording electrode might rely on other charge carriers (depending on the used intracellular solution) than the cellular currents governed by multiple ion selective channel types.

For more complex stimuli than a simple current pulse, the temporal filtering properties of a clamped membrane determine how well the CapClamp mimics the chosen capacitance change. To generally assess these filtering properties, we analytically derived the frequency-dependent impedance of a modeled clamped RC circuit using linear control theory (***Figure 1—figure supplement 1b*** A, see "Impedance of a capacitance-clamped RC circuit" in Appendix 1). The derived impedance profiles confirmed the experimentally observed altered time constants. For example, an RC circuit clamped at an increased capacitance further attenuated non-zero frequencies reflecting its longer time constant. Overall, impedance amplitudes of a clamped RC and the corresponding target circuit fit well up to a tenth of the dynamic clamp frequency f_{dyn}, that is up to ≈2 kHz for a 20 kHz dynamic clamp system as used here (***Figure 1—figure supplement 1B and C***). As high frequencies are heavily attenuated

by the low pass filter of a cell's membrane, these differences lead to relatively small deviations in the voltage responses. The mathematical analysis thus suggests that for a fast dynamic clamp system (> 20 kHz), the CapClamp is expected to work well for most stimuli with time scales in the physiological range.

Simulation of the capclamp in a biophysical neuron model

In neurons with active spike-generating conductances, capacitance changes impact neuronal firing via the interplay of the altered membrane time constant and the gating kinetics of the channels involved. As gating dynamics can be in the sub-millisecond range, for example for transient sodium channels, the CapClamp is expected to require a sufficiently high dynamic clamp frequency to accurately reproduce changes of spike shape or firing rate. To understand these requirements and lay the ground for investigations of capacitance changes in biological neurons, we simulated the CapClamp in a neuron model with biophysical channel dynamics and a single-compartment morphology (see "Biophysical neuron model" in Methods). The simulation allowed us to compare the firing of the clamped neuron to the expected firing at this modified capacitance.

Specifically, we inspected the spiking responses to a depolarizing current for the original 150 pF, a decreased 90 pF and an increased 210 pF capacitance, for the latter two comparing clamped and expected dynamics (***Figure 2A***). Capacitance changes exerted a notable influence on both firing frequency and spike shape, which was mostly well-captured by the simulated CapClamp (***Table 1***). When the capacitance was decreased to 90 pF, spiking became faster and action potentials had a larger peak amplitude, a decreased duration and an increased afterhyperpolarization (AHP). When the capacitance was increased to 210 pF, the effects were opposite: spiking became slower and action potentials had a smaller peak amplitude, an increased duration and a reduced AHP. At decreased capacitances, spike amplitudes of the clamped neuron were larger than in the respective control simulation, a consequence of the limited tracking of the fast sodium current at the dynamic clamp frequency used (***Figure 2B and C***). Except for this brief overshoot, the CapClamp overall forced the membrane potential on the expected trajectory and correctly adjusted the resulting ionic currents and the gating variable dynamics of the active conductances. For example, at a reduced capacitance of 90 pF, sodium channels inactivated less during the fast rise of the AP and therefore the sodium current exhibited a second peak during AP repolarization (see the sodium inactivation variable h at AP peak time in ***Figure 2B***).

A subsequent comparison of simulated spiking for the whole range of tested target capacitances from 75 pF to 225 pF confirmed that the CapClamp reliably reproduced the main effects of a modified capacitance on spike shape (***Figure 2D***) and firing frequency (***Figure 2E***). Furthermore, the obtained frequency-current curves fit well with the theoretically expected reduction of excitability at higher capacitance: a decrease of gain proportional to $\frac{1}{C}$ and a constant rheobase current (see "Analytically expected effect of capacitance on the form of the f-I curve" in Methods). A crucial factor for the CapClamp, especially for a good quantitative fit of the spike shape, is the dynamic clamp frequency – observable differences at a 20 kHz sampling frequency were strongly reduced for a sampling frequency of 100 kHz (***Figure 2C and D***). In this regard, the chosen neuron model is especially demanding because its rapid gating dynamics are fit to a fast spiking interneuron (***Wang and Buzsáki, 1996***). Taken together, our simulations show that capacitance impacts neuronal spiking from firing frequency to action potential shape and that the CapClamp is well-suited to study these effects.

Experimental demonstration of the CapClamp in rat dentate gyrus granule cells

Biological neurons differ from the simple 'cells' considered so far, that is RC circuit and single compartment neuron model, in one major aspect: they can have complex morphologies, where the membrane potential varies between different compartments and membrane capacitance is distributed across the neuronal structure. As the CapClamp in contrast operates locally through the recording electrode, the emulated capacitance change is expected to be localized to the recorded compartment instead of affecting all compartments. To demonstrate such localized capacitance changes and study their effects on neuronal spiking, we applied the CapClamp in in vitro patch-clamp recordings of rat dentate gyrus granule cells (DGGCs). Among morphologically complex cells, DGGCs appear well-suited to test the CapClamp, because their morphological structure, consisting of a central soma and

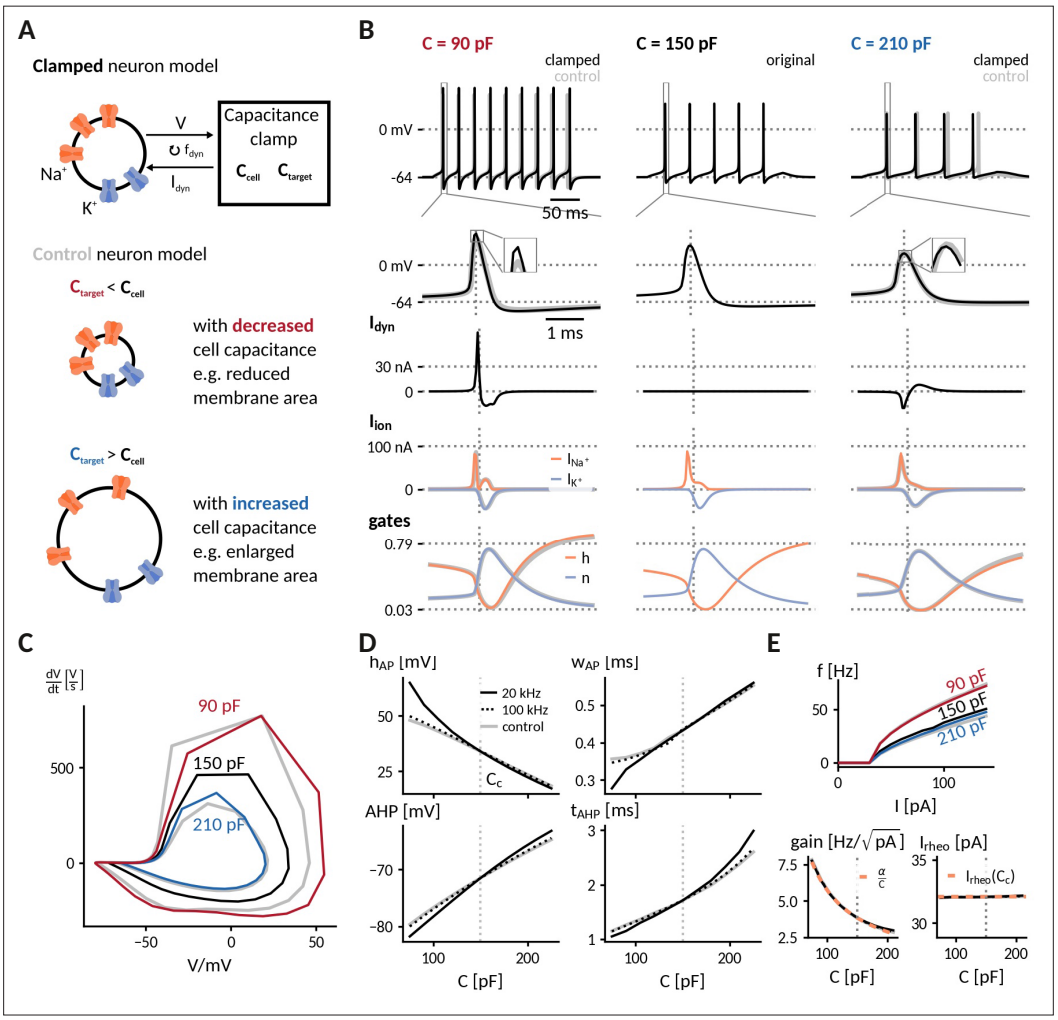

Figure 2. Simulation of the capacitance clamp in a conductance based neuron model. (**A**) Neurons coupled to the CapClamp are compared with control neurons with an altered capacitance (depicted as a difference in membrane area). (**B**) Spiking at 0.6-fold decreased (90 pF), original (150 pF) and 1.4-fold increased capacitance (210 pF) with from top to bottom: spike shape, dynamic clamp current, ionic currents (Na^+, K^+) and gating states (h: sodium inactivation gate, n: potassium activation gate). Clamped and original traces in black or color, control in gray. All currents are shown with the sign they appear with in the current-balance equation (***Equation 2***). (**C**) Comparison of spike shapes in the V-$\frac{dV}{dt}$-plane (black: original, red and blue: clamped, gray: control). (**D**) Comparison of spike amplitude h_{AP} (top left), spike width w_{AP} (top right), after hyperpolarization amplitude AHP (lower left) and timing t_{AHP} (lower right) across different capacitances with two dynamic clamp frequencies (solid: 20 kHz, dotted: 100 kHz, gray:control). (**E**) *Top*: Comparison of f-I curves for capacitances in B. *Bottom*: Gain and rheobase current of the f-I curves across capacitances (solid: 20 kHz, dotted: 100 kHz, gray: control) compared with the theoretical predictions (orange, dashed) of a decreasing $\text{gain}(C) = \frac{\alpha}{C}; \alpha = \text{gain}(C_c)C_c$ and a constant rheobase (see "Analytically expected effect of capacitance on the form of the f-I curve" in Methods).

one to four primary apical dendrites as shown in ***Figure 3A*** (***Rihn and Claiborne, 1990***), translates to a relatively compact electrotonic structure (***Schmidt-Hieber et al., 2007***; ***Wybo et al., 2019***).

Measurement of local near-somatic capacitance

Most capacitance measurements aim to provide an accurate estimate of the *global* capacitance of a neuron (***Golowasch et al., 2009***; ***White and Hooper, 2013***). To correctly infer the transmembrane and axial current, however, the CapClamp requires the *local* capacitance value of the compartment where the electrode is placed at. For the somatic DGGC recordings, we exploit that the current clamp step method – fitting charging curves via a sum of exponential terms – can also provide local capacitance

Table 1. Spike shape and firing frequency in a biophysical neuron model at 60 pA as well as f-I curve gain and local gain reduction for a decreased, the original and an increased capacitance, comparing simulations of an actually altered capacitance with the CapClamp.
Values are shown as actual(clamped).

C (pF)	f (Hz)	h_{AP}(mV)	w_{AP}(ms)	AHP (mV)	Gain (Hz/$\sqrt{pA}$)	Δ Gain (Hz/$\sqrt{pA}$ per 10 pF)
decreased 90	34.9 (34.3)	45.7 (55.0)	0.30 (0.30)	–77.8 (-79.7)	6.5 (6.5)	–0.67 (-0.67)
original 150	22.1	33.9	0.39	–71.5	3.8	–0.22
increased 210	17.8 (18.9)	21.4 (20.1)	0.48 (0.48)	–66.0 (-64.7)	2.9 (2.9)	–0.11 (-0.10)

information (***Golowasch et al., 2009***). DGGC charging curves consisted of a slow (τ_0: 15.1 ± 4.8 ms, R_0: 127 ± 45 MΩ) and a fast (τ_1: 0.77 ± 0.24 ms, R_1: 35 ± 15 MΩ) component. Such a response can be understood in terms of a two compartment circuit consisting of a *near* compartment, comprising the patched soma and its surrounding, coupled to a *far*, mostly dendritic, compartment as depicted in ***Figure 3A*** (for details on the mapping, see "Capacitance measurements" in Methods). Importantly, the slow and fast components can be mapped to the corresponding five circuit parameters: near capacitance C_n (21.0 ± 9.4 pF), near resistance R_n (854 ± 394 MΩ), coupling resistance R_a (53 ± 20 MΩ), far capacitance C_f (106 ± 33 pF), and far resistance R_f (156 ± 60 MΩ) (***Figure 3C***). Accordingly, this near-somatic capacitance C_n represents the summed capacitance of the membrane area that is electrotonically close to the recording site and thus is the value that the CapClamp requires as input and should be able to modify.

Altered near-somatic capacitance in DGGCs

To confirm the localized effect of the CapClamp, we repeated the above capacitance measurement while clamping DGGCs at values ranging from 0.6 to 3 times the original near capacitance. ***Figure 3B*** depicts how the charging of the membrane potential in an exemplary cell changed its shape in reaction to the clamp. Both slow and fast time constant lengthened with capacitances, whereas the associated resistances increased and decreased, respectively, such that their sum, the total input resistance (which is expected to be independent of capacitance), remained constant. These measured time constants and amplitudes matched the predicted ones for a two compartment circuit with a near capacitance at the chosen target values and all other circuit parameters at their original values. In a multicompartment simulation of a morphologically reconstructed DGGC, we could reproduce both the two compartment structure of DGGCs and the isolated modification of the near capacitance, further confirming the local control via the CapClamp.

Across 18 recorded cells, the CapClamp robustly altered DGGC charging curves and modified their charging time constants. Within the tested capacitance range, the slow time constant τ_0 decreased by –0.8 (-1.0 to -0.6) ms, median and interquartile range in parentheses, and increased up to 3.0 (2.4 to 3.9) ms, whereas the fast time constant τ_1 changes ranged from –0.24 (-0.29 to -0.20) ms up to 0.60 (0.36 to 0.86) ms (***Figure 3D***). To quantify how well these changes reflected an altered near capacitance, we evaluated the goodness of fit between the observed and expected time constants and resistances. In the majority of cells, R-squared values were close to 1, indicating that the CapClamp induced the expected changes (τ_0: 0.87 (0.76 to 0.92), R_0: 0.77 (0.56 to 0.89), τ_1: 0.76 (0.32 to 0.97), R_1: 0.85 (0.75 to 0.91)). The largest mismatches occurred for the fast time constant, especially at high capacitances, where the measured time constant was often shorter than predicted (***Figure 3D***). A small bias toward a shorter fast component is to be expected and also present in the multicompartment simulation, because this time constant was only about ten times longer than the sampling interval of 50 µs limiting its slowing-down by the CapClamp currents. Larger deviations of τ_1 however could not be reproduced in numerical simulations and likely result from other error sources, such as the difficulty of fitting this small and short time constant in the presence of noise or imprecise estimates of the original near capacitance (see "Online measurement of capacitance" in Methods). Overall, in terms of circuit parameters, the capacitance measurements confirmed the targeted near capacitance change for 12 out of 18 cells within an average error of 10% (***Figure 3E***). In summary, the CapClamp achieved an isolated change of the near-somatic capacitance in DGGCs and thereby allows to control the time constants of their passive voltage dynamics.

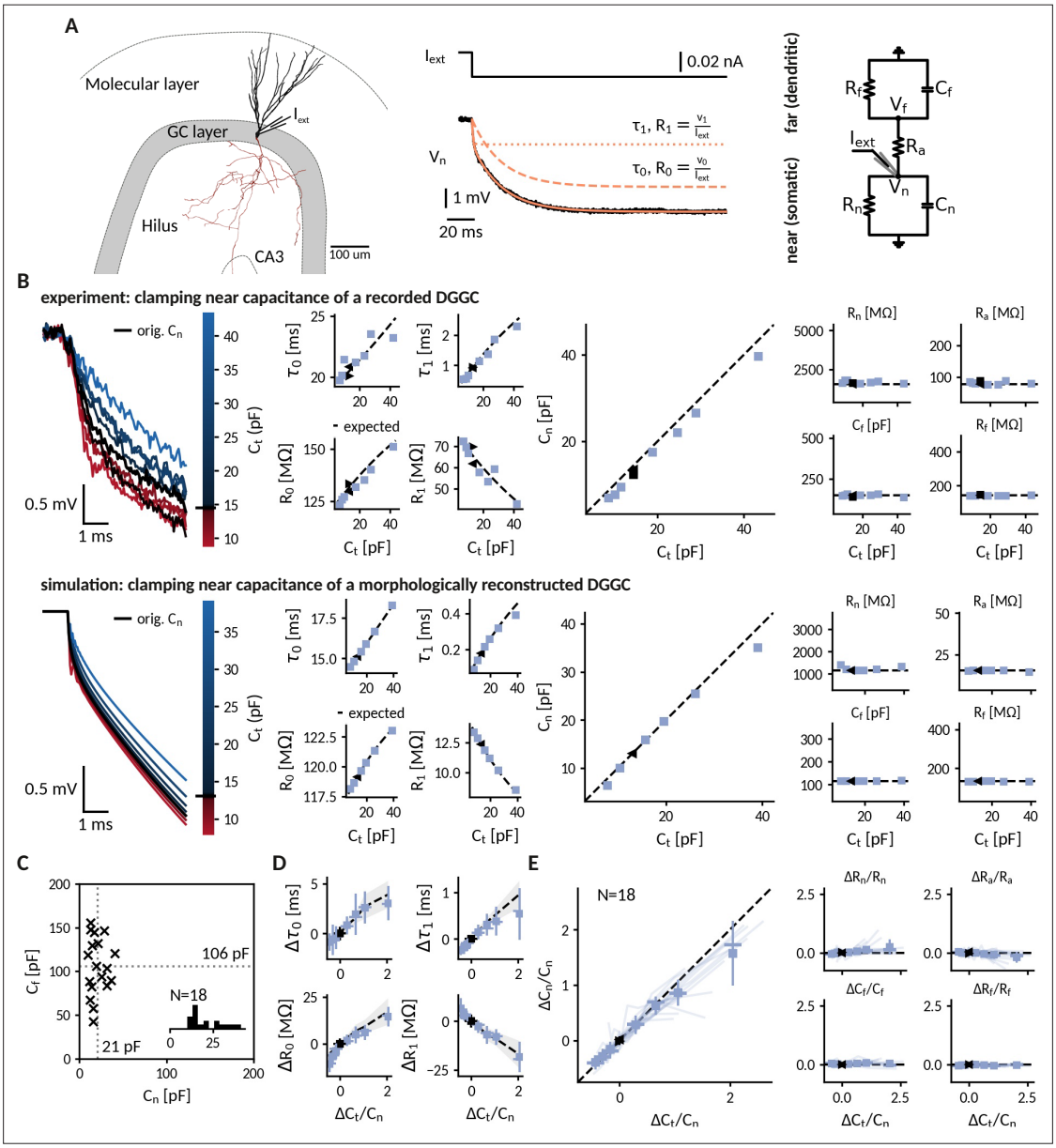

Figure 3. Clamping capacitance in rat dentate gyrus granule cells (DGGCs). (**A**) Morphology of a DGGC (left) and response to a hyperpolarizing current injected at the soma, fit via a sum of exponential terms with a slow τ_0, v_0 and a fast component τ_1, v_1 (middle), which can be mapped to two resistively coupled RC-circuits (right) with a near (somatic) compartment C_n and R_n, resistive coupling R_a and a far (dendritic) compartment C_f and R_f. (**B**) *Left*: Voltage responses of a recorded (top) and a simulated morphologically-reconstructed (bottom) DGGC to a current pulse (exp: –27 pA, sim: –50 pA) clamped at 0.6- to 3-fold the cell's near capacitance (black: original near capacitance, color: target near capacitances). *Middle*: Slow and fast components versus target capacitance. *Right*: Circuit parameters versus target capacitance. ◀, ▶: before and after clamping, blue square: clamped, dashed line: expected values. (**C**) Measured near C_n and far C_f capacitances for 18 DGGCs (gray dotted: mean). Inset: histogram of near capacitances. (**D**) Changes of slow and fast components in all recorded cells versus relative targeted change of near capacitance (squares: mean, horizontal line: median, vertical line: std, shaded area: std of expected changes). (**E**) Relative changes of circuit parameters versus relative targeted change of near capacitance. Legend same as in *D* and individual cells shown with transparent blue lines.

Near-somatic capacitance governs action potential shape and firing frequency in dentate gyrus granule cells

In neurons such as the recorded DGGCs, where the axon directly emerges from the soma, the ability to clamp the near-somatic capacitance provides control over the major capacitive load for the action potential generating site in the axon initial segment. Consequently, the CapClamp, although acting locally, is expected to impact action potential (AP) dynamics and excitability of a morphologically complex DGGC as demonstrated earlier for the simplified single-compartment neuron model (***Figure 2***). To illustrate how the CapClamp can be applied to characterize neuronal firing, we compared spiking responses and f-I curves across near capacitances ranging from 0.6 to 3 times the original value, corresponding to a range from 10 pF to 60 pF for the near and from 110 pF to 160 pF for the total (near and far) capacitance.

Clamping the near-somatic capacitance in DGGCs, we observed pronounced changes in the spiking response to depolarizing current step, clearly visible in the raw voltage traces (***Figure 4A***). The most apparent change was an altered AP shape (***Figure 4B***) – a continuous reduction of AP peak amplitude (from 60 ± 10 mV at 0.6 C_n to 22 ± 17 mV at 3 C_n for 9 DGGCs) and a simultaneous broadening of AP width (from 0.78 ± 0.15 ms at 0.6 C_n to 1.33 ± 0.48 ms at 3 C_n) with increasing capacitance (***Figure 4C and D***). In addition, fast afterhyperpolarization (fAHP) was diminished and disappeared in the majority of cells after increasing capacitance (fAHP in 8/9 cells at 0.6 C_n and 2/9 at 3 C_n). Importantly, the observed disappearance of fAHP cannot be explained by increased capacitive filtering alone, as an increased capacitance would reduce the fAHP amplitude, but not abolish it. Thus, our data suggests that the somatic capacitive load in DGGCs is able to influence the AP generating currents.

To illustrate the interplay of capacitance and the AP generating currents, we compared the observed spikes with hypothetical ones obtained by assuming unaltered currents with respect to those at the original capacitance (see "Protocol 2: Analysis of f-I curves and spike shapes" in Methods). Recorded and hypothetical spike shapes exhibited marked differences (***Figure 4B***). At 0.6-fold decreased capacitances, for example, the recorded AP amplitude was significantly smaller than the hypothetical one (rec.: 60 ± 10 mV, hyp.: 94 ± 19 mV, one-sided Wilcoxon signed-rank Z=0, p<0.001), presumably reflecting a reduction of the driving force for the sodium current when the AP peak approaches the reversal potential of sodium. Furthermore, at threefold increased capacitance, as noted above the recorded spikes exhibited no fAHP in most cells while the hypothetical ones still did (fAHP rec: 2/9, hyp: 8/9) – potentially a result of a reduced activation of potassium channels due to lower AP amplitudes and/or earlier closing during the slowed AP repolarization. In contrast to driving force and gating dynamics, the channel kinetics, for example their activation curves, cannot be altered by capacitance. Correspondingly, the spike threshold, which reflects the voltage where sodium channels start to massively open, was not significantly correlated with near capacitance (Pearson correlation r = 0.10, p = 0.42). Taken together, our analysis indicates that an altered somatic capacitance affects both sodium and potassium currents underlying APs in DGGCs.

Near-somatic capacitance also impacted DGGC excitability. With increasing capacitance, DGGCs became less excitable and firing frequencies significantly decreased (***Figure 4D and F***). From 0.6- to 3-fold of the original near capacitance, the decrease was modest for low firing rates close to threshold (from 9.7 ±3.2 Hz to 7.8 ±3.9 Hz, Wilcoxon signed-rank Z=45, p=0.002) and became more pronounced for high firing rates at the largest injected currents (from 23.3 ±6.4 Hz to 18,6 ±4.8 Hz, Z=45, p=0.002). In terms of the firing rate-current (f-I) curves, the gain of the DGGCs significantly decreased with capacitance (from 1.82 ± 0.40 Hz/$\sqrt{\text{pA}}$ at 0.6 C_n to 1.48 ± 0.34 Hz/$\sqrt{\text{pA}}$ at 3 C_n, Z=45, p=0.002), whereas the rheobase current remained relatively constant (from 185 ±82 pA at 0.6 C_n to 184 ±77 pA at 3 C_n, two-sided, Z=12, p=0.25). Across cells, the gain reduction obtained by linear regression was –0.10 (-0.13 to -0.06) Hz/$\sqrt{\text{pA}}$ per 10 pF near capacitance (median and interquartile range, significant slope in 8/9 cells, p < 0.1). Compared to the simulated neuron with a gain reduction of –0.22 Hz/$\sqrt{\text{pA}}$ per 10 pF over the same capacitance range as in the DGGC experiments (see ***Figure 2D***), DGGCs thus exhibit a weaker gain dependence on near capacitance. A biological factor for this reduced effect in the DGGCs is their overall smaller gain – reflecting the different set of ionic conductances compared to the Wang-Buzsáki model designed to mimic a fast-spiking cortical interneuron. Assuming a scaling of gain with 1/C (as predicted theoretically for neurons with a continuous f-I curve, see "Analytically expected effect of capacitance on the form of the f-I curve" in Methods), the gain reduction is expected to be -gain(C_c)/C_c, which is approximately twice as high for the model

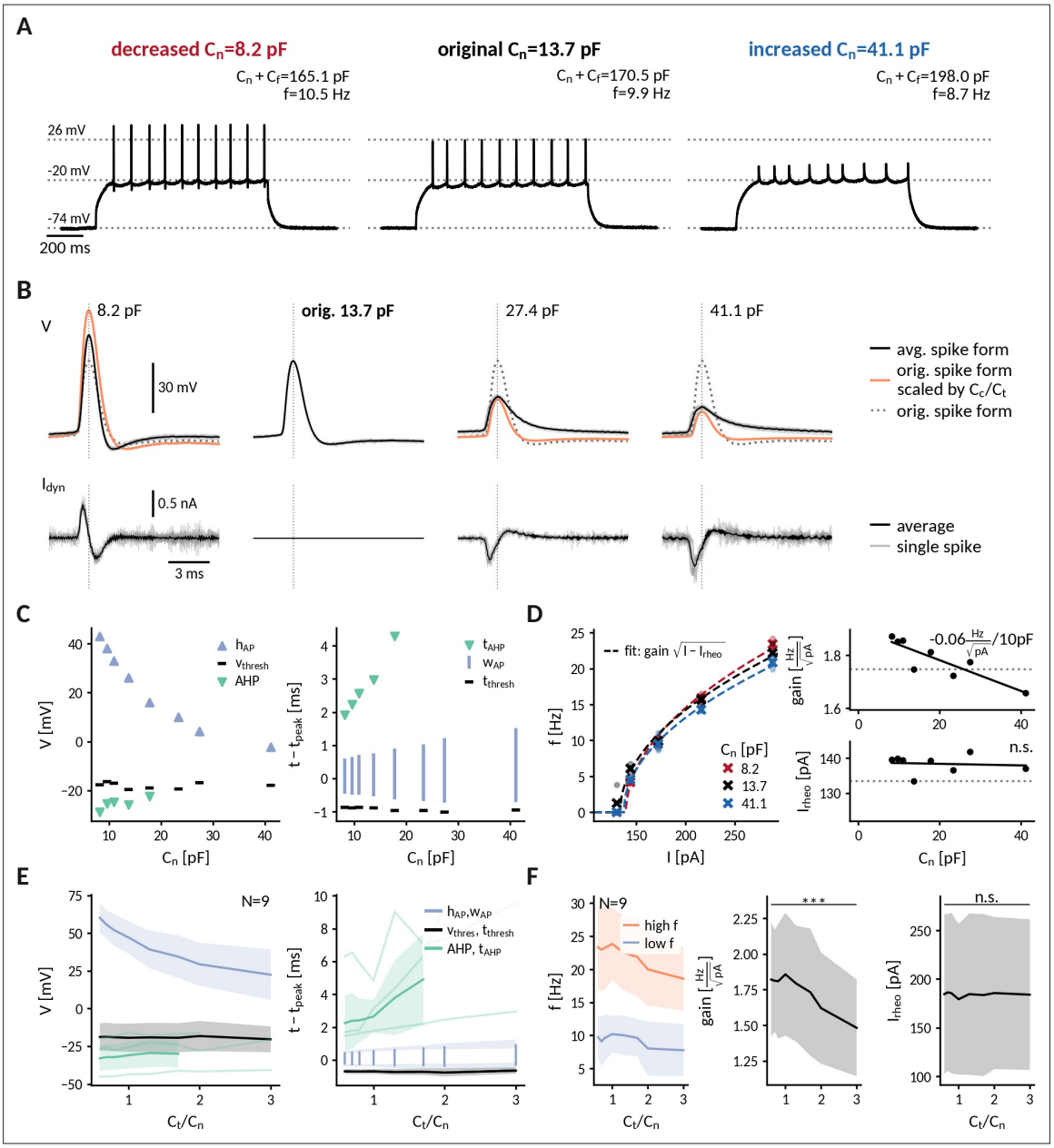

Figure 4. Repetitive spiking and action potential shapes in DGGCs clamped at different capacitances. (**A**) Spiking at decreased 0.6-fold (left), original (middle) and increased 3-fold (right) near capacitance C_n. (**B**) Spike shapes (top) and capacitance clamp currents (bottom) for increasing capacitances from 0.6 to 3-fold of the original near capacitance (black: mean, light gray: single spikes, orange: expected spike shape for unaltered intrinsic currents as described in protocol-2-analysis-of-f-i-curves-and-spike-shapesMethods, dotted: spike shape at original capacitance). (**C**) Comparison of spike shape (left) and temporal structure (right) across tested near capacitances. (**D**) Measured f-I curve at 0.6-, 1- and 3-fold near capacitance with fit $f = \text{gain}\sqrt{I - I_{\text{rheo}}}$ (dashed lines). Extracted gain and rheobase for all tested near capacitances (dotted line: values at original capacitance 13.7 pF, solid line: linear regression with slope value reported if significantly different from zero p<0.1). (**E**) Effect of near capacitance changes on spike shape (left) and temporal structure (right) for all recorded DGGCs (solid: mean, shaded: std). To compare different cells, the capacitance is shown relative to the original near capacitance and spikes were compared at 1.2-fold of the cell's rheobase. (**F**) Effect of near capacitance changes on firing frequency, low firing (blue) at 1.2 fold rheobase and high firing (red) at 2.0-fold rheobase (left), gain (middle) and rheobase (right) for all recorded DGGCs (solid: mean, shaded: std).

($\approx -\frac{3.8\frac{\text{Hz}}{\sqrt{\text{pA}}}}{150\text{pF}} = -0.25\ \text{Hz}/\sqrt{\text{pA}}$ per 10 pF) compared to the average DGGC ($\approx -\frac{1.8\frac{\text{Hz}}{\sqrt{\text{pA}}}}{127\text{pF}} = -0.14\ \text{Hz}/\sqrt{\text{pA}}$ per 10 pF). A further technical factor for a weaker effect in the DGGCs is the local nature of the capacitance modification. Depending on the particular location and geometry of the axon initial segment, the influence of the clamped somatic compartment on AIS excitability can differ (***Goethals and Brette, 2020***). The altered excitability in the majority of DGGCs, however, demonstrates that clamping their near capacitance was sufficient to affect the capacitive load of their AIS. We conclude that a somatic capacitance clamp, altering perisomatic capacitance alone, is able to modify the input-output relationship of a real neuron.

Applications of the CapClamp

The CapClamp lends itself to either test hypotheses on the impact of capacitance or to exploit the control over the membrane time constant in order to to alter neuronal dynamics in informative ways. In the following, we briefly illustrate applications of the CapClamp from these two fields, applying the

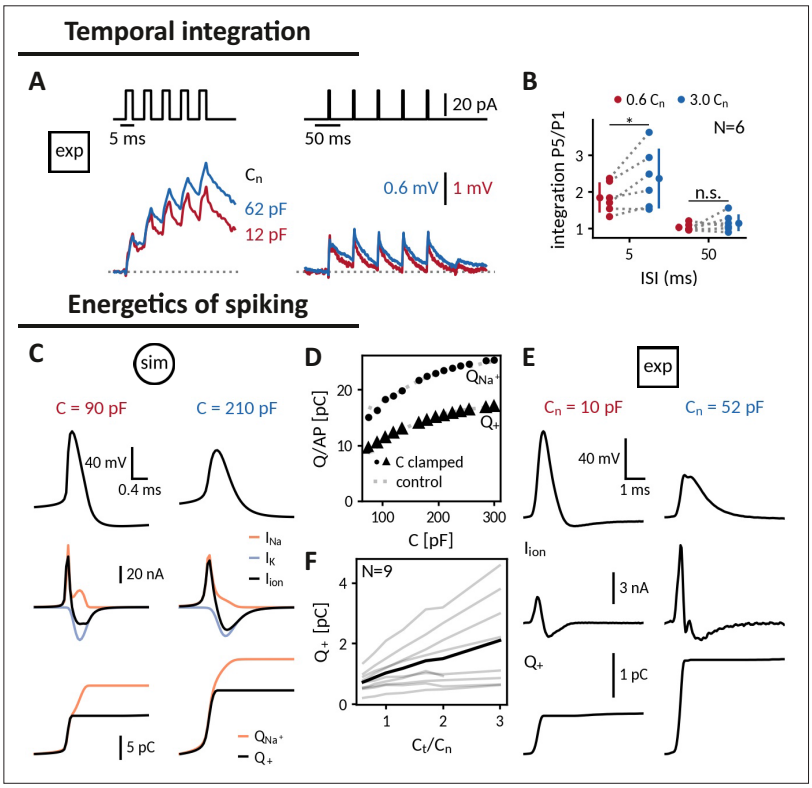

Figure 5. Applying the capacitance clamp to study neuronal signaling and physiology. Temporal integration: (**A**) Brief current pulses of 3ms length with interstimulus intervals of 5ms and 50ms (top) and voltage responses of an exemplary DGGC at a decreased (12 pF) and an increased (62 pF) near capacitance (voltage scale adapted to first response height). (**B**) Ratio of fifth and first response as a measure of temporal integration for a 0.6-fold decreased capacitance in comparison to a threefold increased one at 5ms and 50ms ISI. Energetics of spiking: (**C**) Spike shape (top), sodium, potassium and total ionic current (middle, shown with the sign they appear with in the current-balance equation, see ***Equation 2***) and deposited sodium Q_{Na_+} as well as depolarizing Q_+ charge (bottom) in the Wang-Buzsáki neuron model for a 90 pF and a 210 pF capacitance. (**D**) Sodium Q_{Na_+} and depolarizing Q_+ charge per action potential versus capacitance (dot and triangle: clamped from an original capacitance of 150 pF, gray: control). (**E**) Spike shape and depolarizing charge for a dentate gyrus granule cell clamped at decreased 10 pF and increased 52 pF near capacitance. (**F**) Deposited depolarizing charge versus relative change of near capacitance in recorded DGGCs (black: mean, gray: individual cells).

technique to experimentally explore effects of capacitance on temporal integration and energetic costs of spiking.

Temporal integration

A basic processing step in neuronal computation is temporal integration, the summation of time-separated synaptic inputs (***Krueppel et al., 2011***; ***Athilingam et al., 2017***). An upper limit for temporal integration, at least in the absence of dedicated active channels, is set by the membrane time constant $\tau = RC$, which is directly proportional to the cell's capacitance. Hence, increasing the capacitance of a cell should make it a better integrator: if two brief inputs arrive separated by less than the membrane time constant, the cell will summate the responses so that the membrane potential after the second is higher than after the first one. Indeed, when we compared the responses of DGGCs clamped at decreased and increased near-somatic capacitances to current pulse trains, increasing the capacitance allowed the cell to better "sum" 3ms pulses at an inter stimulus interval (ISI) of 5 ms as apparent by the stair-like voltage response with a higher ratio of last to first pulse response. (***Figure 5A and B***). At an ISI of 50ms, in contrast, neither capacitance was sufficient for temporal integration. The biological relevance of tailoring capacitance to temporal processing can, for example, be observed in auditory cells of the barn-owl, which have no dendrites to reduce capacitive and resistive load and hence shorten their time constant such that they can perform sub-millisecond coincidence detection (***Ashida et al., 2007***).

Energy consumption during spiking

Action potentials are energetically expensive, because the contributing sodium and potassium ions need to be pumped back using ATP (***Laughlin et al., 1998***; ***Hasenstaub et al., 2010***). The minimal amount of ionic charge required for an action potential is dictated by the capacitance as $Q = C\Delta V_{AP}$, suggesting that a smaller capacitance is energetically favorable. In order to gauge how capacitance affects charge accumulation and energy consumption, we reexamined spike shapes for a fixed current input at different capacitances both in the simulated neuron and in the recorded DGGCs (***Figure 5C and E***). We found that despite a reduced amplitude at larger capacitances, these smaller spikes still required more depolarizing charge $Q_+ = C\Delta V_{AP}$ (***Figure 5D and F***). In the model, we tested whether this depolarizing charge provided a reliable indication of the sodium charge $Q_{\mathrm{Na^+}}$, which finally determines pump activity and energy consumption (***Figure 5D***). Due to the overlap of sodium and potassium currents, the sodium charge exceeded the net depolarizing charge, but as this overlap remained roughly constant, both charge measures increased by the same amount with capacitance. Taken together, in the tested model and the recorded DGGCs, energy consumption per action potential appears to be reduced at smaller capacitances. In line with this observation, it has been reported that perineuronal nets could decrease membrane capacitance of fast-spiking interneurons, thereby facilitating high-frequency firing, while keeping energetic costs at bay (***Tewari et al., 2018***).

Discussion

The dynamic clamp is a valuable tool in intracellular recordings to examine the diverse roles of ionic conductances in excitable cells (***Sharp et al., 1993***; ***Prinz et al., 2004***; ***Wilders, 2006***; ***Economo et al., 2010***). In this study, we introduced the capacitance clamp (CapClamp), an application of the dynamic clamp that allows electrophysiologists to mimic a modified membrane capacitance in a biological neuron. Via simulations of a biophysical neuron model, we confirmed that the CapClamp correctly captures how capacitance affects spike shapes and firing frequency. In recordings of rat dentate gyrus granule cells, we further verified that the CapClamp could accurately control the capacitance of the recorded somatic compartments. Moreover, we clamped this near-somatic capacitance of DGGCs during spiking and found that, as predicted by our simulations, capacitance can modify the fI curve and alter the course of the spike generating currents. CapClamp can serve as a new probe to neuronal signaling and physiology. In the following, we highlight requirements for the CapClamp and discuss how this experimental control over capacitance can benefit the study of cellular electrical behavior.

Precise, flexible and local control over capacitance in all excitable cells

To our knowledge, the CapClamp is the first tool to experimentally study capacitance changes in a precise and flexible manner. The CapClamp owes its precision and flexibility to the virtual nature of the altered capacitance. In contrast, methods to physically modify the capacitance are affected by various undesired side effects. Dendritic pinching, decoupling dendrites from the soma, for instance greatly reduces membrane area and thereby capacitance, but also removes all dendritic conductances (***Bekkers and Häusser, 2007***). Capacitance alterations have also been reported after application of mefloquine, a drug binding to membrane phospholipids, but it also blocks gap junctions (***Szoboszlay et al., 2016***). A notable exception is the recent demonstration of engineered polymer synthesis in neuronal cell membranes, which alters their capacitance, but not their input resistance (***Liu et al., 2020***). In comparison, however, the CapClamp provides more accurate and dynamic control by allowing experimenters to test multiple selected capacitance values in a single cell (***Figures 3 and 4***), while being significantly simpler to implement.

The CapClamp can be applied in every excitable cell. Here, we focused on neurons, but the proposed clamping currents can also be used to study capacitance changes in other cells, including for example heart cells (***Wilders, 2006***; ***de Oliveira et al., 2015***). In particular, no prior knowledge about the ionic or external currents in the clamped cell is required, so that the capacitance can be clamped during any experimental protocol (step current, ramp current, etc.) or during synaptic input. Furthermore, capacitance can be clamped in both electrotonically compact cells like oocytes (***Ori et al., 2020***) and non-compact cells like most neurons (***Wybo et al., 2019***), although in the latter case the CapClamp is limited locally to the capacitance of the recorded compartment (***Figure 3***). Consequently, the effects of clamping capacitance depend on the cell's morphology and the recording site. The soma, for example, represents the major capacitive load for spike generation in vertebrate neurons, where the axon predominantly emerges close to the soma (***Figure 4***), but it is expected to exert less influence in neurons, where the axon comes out of the dendritic tree, a common feature of invertebrate neurons (***Hesse and Schreiber, 2015***), but also seen in mammalian neurons (***Martina et al., 2000***; ***Thome et al., 2014***).

The major prerequisite to apply the CapClamp is a reliable capacitance measurement of the clamped compartment, which can be challenging, especially for electrotonically complex cells (***Golowasch et al., 2009***; ***White and Hooper, 2013***). An imprecise capacitance estimate leads to erroneous clamping currents, which increase high-frequency noise for small errors and might even induce instabilities for larger errors. The measurement method presented for the recorded DGGCs, that is mapping the charging response to a two compartment circuit, could in principle be extended to cells with a larger number of compartments e.g. pyramidal cells (***Edwards and Mulloney, 1984***; ***Wybo et al., 2021***). Yet, accurate multi-exponential fitting is demanding and the assumption of uniform membrane properties underlying the mapping is a simplification, shown to be violated in some cells, such as GABAergic interneurons (***Nörenberg et al., 2010***). As an alternative, measurement protocols could be exploited that inherently yield local capacitance estimates, including fast voltage ramps (***Golowasch et al., 2009***) or sampling of voltage responses to fast fluctuating currents (***Badel et al., 2008***). Reliable capacitance measurements can further be used to compare measured and target capacitance of the clamped cell, which can serve as a first simple test to ensure the quality of the CapClamp.

A CapClamp on every rig

As a novel application of the established dynamic clamp technique, the CapClamp is an accessible and low-cost extension of a standard electrophysiology stack (***Prinz et al., 2004***; ***Economo et al., 2010***). For an existing dynamic clamp setup, the sole requirement is to implement the calculation of the clamping currents (see ***Equation 5***). Otherwise, multiple open source frameworks exist that only require a dedicated computer with a data acquisition card to enable the dynamic clamp in a conventional electrophysiology setup (***Dorval et al., 2001***; ***Benda et al., 2007***; ***Kemenes et al., 2011***; ***Linaro et al., 2015***; ***Patel et al., 2017***; ***Desai et al., 2017***; ***Amaducci et al., 2019***). To facilitate the usage of the technique, we provide code for the CapClamp scheme in the RELACS and RTXI frameworks (see "Data and software availability" in Appendix 1).

In CapClamp recordings, as in all dynamic clamp applications, a high sampling frequency and accurate voltage monitoring are key (***Bettencourt et al., 2008***). Whether a sampling frequency is

sufficiently high can be tested by assuring that the observed voltage dynamics for example the spike amplitudes are invariant when the sampling frequency is decreased from the maximal possible value (**Robinson, 1994**). For the simulated fast-spiking interneuron, we found a satisfactory clamp at a frequency of 20 kHz, which we expect to also be sufficient for most excitatory neurons, because they tend to have slower voltage dynamics (**Hasenstaub et al., 2010**). In our single electrode recordings, we focused on careful electrode compensation to avoid electrode artifacts in the recorded voltages which would lead to incorrectly estimated membrane currents and eventually instabilities. To improve voltage monitoring, future applications could either apply active electrode compensation (**Brette et al., 2008**; **Bal and Destexhe, 2009**) or resort to two electrode recordings, where current injection and voltage recordings are separated.

Modifying capacitance as a probe for cellular electrical dynamics

Via the CapClamp, experimenters can ask a question that was previously accessible only in theoretical work: What if capacitance was different? In contrast to the theoretical approach, the answers to this question do not have to rely on models of channel dynamics or other membrane properties, because the latter are provided by the biological cell itself (**Sharp et al., 1993**). Modifying capacitance with the CapClamp can serve either to investigate changes in this biophysical parameter or, more broadly, to alter the membrane time constant of a cell as a way to characterize its electrical dynamics.

Understanding the role of capacitance

The virtual capacitance changes induced by the CapClamp could serve to address two crucial questions about actual membrane biophysics: why capacitance appears to be biologically mostly constant (**Gentet et al., 2000**) and how exceptions to this rule can facilitate or deter neuronal function (**Amzica and Neckelmann, 1999**; **Hartline and Colman, 2007**; **Eyal et al., 2016**; **Tewari et al., 2018**). Capacitance is for example rarely tested for optimality - a common question in ion channel kinetics, which appear optimized for function and energy expenditure (**Hasenstaub et al., 2010**; **Sengupta et al., 2010**). Regarding energy consumption, our CapClamp experiments in DGGCs indicate that action potentials become energetically cheaper at lower capacitances (**Figure 5E and F**). Interestingly, reports of exceptional capacitance values mostly find reductions e.g. for myelinated axons ($C_m \approx 0.05$ uF/cm^2 for a 10-fold wrapped myelin sheath, see **Castelfranco and Hartline, 2015**) or human pyramidal cells ($C_m \approx 0.5$ uF/cm^2, see **Eyal et al., 2016**) suggesting that indeed the metabolic cost of AP generation could have been a contributing factor to capacitance adaptations. In addition, the recent hypothesis that perineuronal nets can reduce capacitance of interneurons in a similar way as myelination of axons suggests that capacitance adaptation could be more widespread in the brain than often assumed (**Tewari et al., 2018**). Moreover, understanding the role of capacitance can contribute to an improved understanding of infrared (**Shapiro et al., 2017**; **Carvalho-de-Souza et al., 2018**) and ultrasonic (**Krasovitski et al., 2011**; **Plaksin et al., 2014**) stimulation of neural activity, whose effects are assumed to rely on rapid alteration of the capacitance.

Another application of the CapClamp might be to investigate changes of excitability associated with neuronal growth. During development, cell size can increase considerably, necessarily accompanied by a larger membrane capacitance (**McComb et al., 2003**). To maintain neural function, neurons need to compensate for this altered capacitance via a corresponding regulation of ionic conductances – a homeostatic process that is hypothesized to involve activity-dependent channel expression (**Gorur-Shandilya et al., 2020**). To disentangle the contributions of capacitance in this concurrent alteration with ionic conductances, the CapClamp could be combined with the 'classic' dynamic clamp, for example parallel changes of both capacitance and a leak conductance.

Altering the membrane time constant

A key contribution of the CapClamp is the isolated experimental control of the membrane time constant via changes in capacitance while leaving the ion channel conductances unaffected. In neuron models, monitoring response properties when changing the membrane time constant has been used to characterize a cell's dynamical repertoire (**Kirst et al., 2015**; **Hesse et al., 2017**; **Franci et al., 2018**). As an experimental analogue, the CapClamp introduces this option for the characterization of biological neurons.

To optimally support neural processing, nerve cells exhibit qualitatively different response properties, which in some cases can be flexibly adapted to context. For example, neurons with class 2 excitability (marked by a jump of the f-I curve to non-zero frequencies when exceeding threshold) can be switched to class 1 excitability (marked by a smooth transition with arbitrarily low frequencies) via neuromodulation (***Stiefel et al., 2008***; ***Stiefel et al., 2009***), transforming them from resonators to integrators. These qualitative differences in response and processing properties can be characterized by bifurcation analysis (***Izhikevich, 2006***; ***Prescott et al., 2008a***; ***Kirst et al., 2015***; ***Hesse et al., 2017***). Capacitance as a canonical parameter can induce transitions between excitability classes and the underlying bifurcation types, including the switch of neuronal dynamics from class 1 excitability (with regularly spiking neurons) to dynamics that include bistable firing with stochastic switches between spiking and rest (***Hesse et al., 2017***). Because computational properties can be expected to change with such qualitative switches in dynamics, it may be of interest to determine how close the dynamics of a given cell is to a transition. An estimate of this proximity to switches that can be obtained via the CapClamp by monitoring firing properties and qualitative changes thereof as a function of membrane capacitance. Dynamics in the vicinity of capacitance-induced switches are likely to be also susceptible to switches induced by other parameters with similar temporal effects, such changes in temperature (***Hesse et al., 2017***) or ionic concentrations (***Contreras et al., 2020***). As such switches can involve regimes of exceptionally fast dynamics, for such measurements extra care should be given to ensure that the temporal resolution of the dynamic clamp is sufficiently high.

In addition to such qualitative changes of dynamics, the broad impact of the time constant (and therefore the capacitance) on firing frequency and spike shape could be applied for more quantitative studies of neuronal activity. On the one hand, observations of neural activity at different capacitances could for example be used to further constrain and improve fitting of conductance-based neuron models (***Podlaski et al., 2017***; ***Gouwens et al., 2018***; ***Franci et al., 2018***). On the other hand, it could serve to examine activity-dependent physiological processes such as ion concentration dynamics (***Contreras et al., 2020***) or calcium controlled channel homeostasis (***O'Leary et al., 2014***; ***Temporal et al., 2014***; ***Santin and Schulz, 2019***).

Conclusion

Taken together, the presented CapClamp enables an accurate and flexible control over capacitance in biological neurons, a basic determinant of cellular excitability, that so far has been inaccessible in experiment. We expect that the CapClamp will, therefore, broaden and enrich the electrophysiological study of neurons and other excitable cells. With expanding techniques to sense and manipulate neural activity, the combination of modeling and targeted closed-loop feedback that underlies the CapClamp (and more generally the dynamic clamp ***Chamorro et al., 2012***) will further unlock experimental control over other previously inaccessible aspects of single neuron (***Ullah and Schiff, 2009***; ***Rivera et al., 2015***; ***Harrigan et al., 2018***) and network dynamics (***Newman et al., 2015***; ***Hocker and Park, 2019***).

Materials and methods

Key resources table

Reagent type (species) or resource	Designation	Source or reference	Identifiers	Additional information
Strain, strain background (*Rattus norvegicus, male and female*)	Wistar Rat (wild type)	Wistar Institute of Philadelphia, Pennsylvania		
Peptide, recombinant protein	Avidin conjugated AlexaFluor-647	Thermo Fisher Scientific	RRID:AB_2336066	
Software, algorithm	Fiji distribution of ImageJ software	imagej.net	RRID:SCR_003070	
Software, algorithm	Neutube	neutracing.com	https://doi.org/10.1523/ENEURO.0049-14.2014	
Software, algorithm	RELACS	relacs.sourceforge.net	RRID:SCR_017280	

Continued on next page

Continued

Reagent type (species) or resource	Designation	Source or reference	Identifiers	Additional information
Software, algorithm	RELACS CapClamp	This paper	https://doi.org/10.5281/zenodo.6322768	Capacitance clamp code for RELACS, see "Data and software availability" in Appendix 1
Software, algorithm	RTXI	rtxi.org	https://doi.org/10.1371/journal.pcbi.1005430	
Software, algorithm	RTXI CapClamp	This paper	https://doi.org/10.5281/zenodo.5553946	Capacitance clamp code for RTXI, see "Data and software availability" in Appendix 1
Software, algorithm	Brian 2	brian-team/ brian2	https://doi.org/10.7554/eLife.47314	

Derivation of the capclamp current

In order to derive a dynamic clamp feedback scheme for the CapClamp, we compare the actual membrane potential dynamics at the original capacitance C_c with the target dynamics at the chosen capacitance C_t. The actual dynamics of the cell, which for the moment is assumed to be isopotential, is given by the current-balance equation of a single compartment

$$\frac{\mathrm{d}V}{\mathrm{d}t} = \frac{I(V,t)+I_{\mathrm{dyn}}(t)}{C_c}, \tag{2}$$

with capacitance C_c, membrane currents $I(V,t)$ (comprising all ionic and synaptic currents, as well as external stimuli) and the dynamic clamp current $I_{\mathrm{dyn}}(t)$. Note that ionic and synaptic contributions to the membrane currents $I(V,t)$ are voltage-dependent, both with respect to driving force and gating dynamics, so that a voltage trajectory governed by a different capacitance also leads to a modified shape of the membrane currents. In the target dynamics, the dynamic clamp current is absent and the capacitance is modified to the desired value

$$\frac{\mathrm{d}V}{\mathrm{d}t} = \frac{I(V,t)}{C_t}. \tag{3}$$

Both membrane potential trajectories would coincide, if we chose a dynamic clamp current such that the right-hand sides of actual (***Equation 2***) and target dynamics (***Equation 3***) become identical,

$$I_{\mathrm{dyn}}(t) = \frac{C_c-C_t}{C_t} I(V,t).$$

Generally, an exact model for the membrane currents $I(V,t)$ will not be available, as it would require knowledge about all active conductances and incoming synaptic inputs. Instead, the membrane current can be estimated from the stream of incoming voltage data using the discrete version of ***Equation 2***

$$I(V_{i-1},t_{i-1}) \approx C_c \frac{V_i-V_{i-1}}{\Delta t} - I_{dyn,i-1} \tag{4}$$

where Δt is the sampling interval. A prerequisite is the measurement of the cell capacitance C_c. Furthermore, for the estimation to be accurate, the samplin ginterval needs to be shorter than the fastest time scales of changes in the membrane currents for example sodium gating time constants. With this estimated membrane current, the complete expression for the CapClampcurrent reads

$$I_{\mathrm{dyn},i} = \frac{C_c-C_t}{C_t}\left(C_c \frac{V_i-V_{i-1}}{\Delta t} - I_{\mathrm{dyn},i-1}\right). \tag{5}$$

The above derivation assumes that the cell is isopotential. In the case of an electrotonically non-compact cell, the steps are identical, but the cell capacitance C_c has to be replaced by the capacitance of the compartment where the recording electrode is located. Consequently, in a non-isopotential neuron, the mimicked capacitance modification is restricted to the compartment at the tip of the

recording electrode - a constraint known as the space clamp that is shared by all clamping techniques (**Prinz et al., 2004**; **Bar-Yehuda and Korngreen, 2008**).

The indexing above assumes a voltage sampling $V_i = V(i\Delta t)$ and a quasi-immediate current injection $I_{\mathrm{dyn},i} = I_{\mathrm{dyn}}(i\Delta t)$. However, sampling can take a non-negligible amount of time, so that depending on the sampling system the currently available voltage actually represents the voltage from the previous cycle $V_i = V((i-1)\Delta t)$. In this case, for a correct estimation of the membrane currents, the dynamic clamp current index has to be shifted correspondingly to $I_{\mathrm{dyn},i} = \frac{C_c - C_t}{C_t}\left(C_c \frac{V_i - V_{i-1}}{\Delta t} - I_{\mathrm{dyn},i-2}\right)$.

Capacitance measurements

To apply the CapClamp, a prerequisite is to measure the capacitance of the recorded local compartment. Here, we use the current clamp protocol, which estimates the capacitance from the voltage response to a current step with amplitude I_{ext},

$$V(t) = \sum_i v_i \left(1 - e^{-\frac{t}{\tau_i}}\right) = I_{ext} \sum_i R_i \left(1 - e^{-\frac{t}{\tau_i}}\right), \tag{6}$$

where an ordering in terms of these time scales is assumed i.e. $\tau_0 > \tau 1 > \ldots$. Depending on the morphology, this sum can have a large number of components (**Major et al., 1993**), but in practice often only two or three components can be reliably extracted. As described in **Golowasch et al., 2009**, the slowest component τ_0 is the membrane time constant and allows to infer the total capacitance of a neuron by $C = \frac{\tau_0}{R_0} = \frac{\tau_0}{v_0} I_{ext}$. In the case of an isopotential cell, the membrane time constant is the only component in the charging curve and the total capacitance can be used for the CapClamp.

Measurement of near capacitance

For the case of two components τ_0, R_0 and τ_1, R_1 in the charging curve (**Equation 6**), an equivalent two compartment circuit can be identified comprising a near compartment with capacitance C_n and resistance R_n connected via a coupling resistance R_a to a far compartment with capacitance C_f and resistance R_f (**Golowasch et al., 2009**). With the additional assumption of a uniform membrane time constant $\tau_m = R_n C_n = R_f C_f$, the fitted two components can be mapped to the values of these five circuit parameters, which in particular provides the near capacitance C_n required for the CapClamp

$$C_n = \frac{\tau_0 \tau_1}{\tau_1 R_0 + \tau_0 R_1}. \tag{7}$$

When the capacitance is subsequently clamped to a k-fold different value, $C_t = kC_n$, the uniformity assumption has to be correspondingly adjusted to $R_n C_n = k R_f C_f$ (see "Mapping between a charging curve with two components and a two compartment circuit" in Appendix 1).

CapClamp in dentate gyrus granule cells

Electrophysiology

Acute brain slices were produced as described earlier (**Booker et al., 2014**). Briefly, rats were anesthetized (3% Isoflurane, Abbott, Wiesbaden, Germany) and then decapitated. Brains were removed quickly and transferred to carbogenated (95% O_2 / 5% CO_2) ice-cold sucrose-ACSF containing (in mM): 87 NaCl, 2.5 KCl, 25 $NaHCO_3$, 1.25 NaH_2PO_4, 25 glucose, 75 sucrose, 7 $MgCl_2$, 0.5 $CaCl_2$, 1 Na-pyruvate, 1 ascorbic acid. Horizontal brain slices of 300 µm thickness were cut using a Vibratome (VT1200 S, Leica, Wetzlar, Germany). Hippocampal tissue slices, were collected and placed in a submerged holding chamber filled with carbogenated sucrose ACSF at 32-34 °C for 30 min and then at room temperature for 15 min before recording. Experiments were alternated between left and right hemisphere slices to prevent bias due to slice condition.

For recording, slices were transferred to a submerged chamber and superfused with pre-warmed, carbogenated ACSF containing (in mM): 125 NaCl, 2.5 KCl, 25 $NaHCO_3$, 1.25 NaH_2PO_4, 25 glucose, 1 $MgCl_2$, 2 $CaCl_2$, 1 Na-pyruvate, 1 ascorbic acid. The bath temperature was set to 32-34 °C with a perfusion rate of 12-13 ml/min. Slices were visualized using an upright microscope (AxioScope; Zeiss) equipped with infrared differential inference contrast optics and a digital camera (Retiga EX QImaging CCD, Teledyne Photometrics, AZ, USA). Granule cells from the DG were chosen based on their anatomical location within the cell body layer as well as their morphological appearance.

Whole-cell patch-clamp electrodes were produced from borosilicate glass capillaries (outer diameter , inner diameter 1 mm, Hilgenberg, Germany) using a horizontal puller (P-97, Sutter Instruments, CA, USA) and filled with an intracellular solution consisting of (in mM): K-gluconate 130, KCl 10, HEPES 10, EGTA 10, $MgCl_2$ 2, Na_2ATP 2, Na_2GTP 0.3, $Na_2Creatine$ 1 and 0.1% biocytin (adjusted to pH 7.3 and 315 mOsm), giving a series resistance of 2.5-4 MΩ. All recordings were performed with a SEC LX10 amplifier (npi electronic, Germany), filtered online at 20 kHz with the built-in Bessel filter, and digitized at 20 kHz (National Instruments, UK). Following breakthrough into whole-cell configuration, we adjusted the bridge and capacitance compensation before switching to the dynamic clamp mode for recording. Cells were excluded if resting membrane potential was more depolarized than -45 mV. The liquid junction potential was not corrected.

Table 2. Multi-exponential fit and corresponding circuit parameters in the recorded dentate gyrus granule cells (N = 18) and a multicompartment model based on a reconstructed DGGC morphology (see "Multicompartment model of a dentate gyrus granule cell" in Methods).

	DGGCs (mean ± std)	Multicomp. model
Exp. fit		
τ_0	15.1±4.8 ms	15.1 ms
R_0	127.1±44.6 MΩ	119.2 MΩ
τ_1	0.77±0.24 ms	0.18 ms
R_1	34.5±14.7 MΩ	12.3 MΩ
Circuit		
C_n	21.0±9.4 pF	13.0 pF
R_n	854.2±394.0 MΩ	1158.0 MΩ
R_a	52.5±19.8 MΩ	15.5 MΩ
C_f	105.8±33.0 pF	113.7 pF
R_f	155.5±59.9 MΩ	132.8 MΩ

Neuronal visualization and immunohistochemistry

Following recording, selected cells were immersion fixed in 4% paraformaldehyde (PFA) in 0.1 M phosphate buffer (PB, pH 7.4) at 4 °C for 24–48 hr, slices were then transferred to fresh PB. Prior to immunohistochemical processing, slices were rinsed in PB, followed by PB buffered saline (PBS, 0.9% NaCl). Slices were then rinsed in PBS and incubated in a fluorescent-conjugated streptavidin (Alexa Fluor-647, 1:1000, Invitrogen, UK) in PBS solution containing 3% NGS, 0.1% TritonX-100 and 0.05% NaN3 for 24 hr at 4 °C. Slices were rinsed in PBS and then desalted in PB before being mounted (Fluoromount-G, Southern Biotech) on 300-µm-thick metal spacers, cover-slipped, sealed, and stored at 4 °C prior to imaging.

Confocal imaging and reconstruction

DGGCs were imaged on a laser scanning confocal microscope (FV1000, Olympus, Japan). First, a low magnification (4 x, Olympus, Japan) overview image was taken to confirm the cellular type and localization to the DG, then high resolution z-stacks were obtained with a 30x silicone oil immersion objective (N.A. 1.05, UPlanSApo, Olympus) over the whole extent of the cell (1 µm axial steps). Image stacks were stitched offline using the FIJI software package (https://imagej.net/software/fiji/imagej.net), then the cells were reconstructed and volume filled using Neutube (https://www.neutracing.com/neutracing.com) (***Feng et al., 2015***).

Dynamic clamp setup

Data acquisition and dynamic clamp loop were controlled by RELACS, V0.9.8, RRID:SCR_017280 using a dedicated computer with a Linux-based real time operating system (https://www.rtai.org/rtai.org). The sampling frequency was set to 20 kHz and the recordings were performed in discontinuous current clamp with a duty cycle of 16.5 µs. We implemented a CapClamp procedure for RELACS that allows the user to online specify the measured capacitance C_c and the desired target capacitance C_t (for documentation and installation instruction, see "Data and software availability" in Appendix 1).

Online measurement of capacitance

For the online measurement of the local capacitance, DGGCs were subjected to twenty hyperpolarizing pulses of $200\,\mathrm{ms}$ length with $400\,\mathrm{ms}$ pauses and an amplitude chosen to produce a response of $-5\,\mathrm{mV}$ in order to minimize interference from active ionic currents. Responses were averaged and the resulting mean trajectory was fit with a sum of exponentials using the Levenberg-Marquardt method

from the python library scipy (***Virtanen et al., 2020***). Fits were performed with one, two and three components and were compared via the F-statistic (***Bardsley et al., 1986***). In all recorded DGGCs, the two component fit was significantly better than the one exponential fit ($p < 0.05$, 18/18), whereas no cell exhibited a significant third component ($p < 0.05$, 0/18). Finally, the extracted two components were mapped to a two compartment circuit as explained above and the near capacitance was then used in the subsequent CapClamp (***Table 2***).

An offline reexamination revealed that in several recorded cells the above fitting procedure yielded inaccurate estimates of the exponential components, e.g. very short fast components due to an artefactual voltage dip *before* pulse onset. To circumvent these problems, improved offline fits were performed for the artifact-free recharging at the pulse end (see "Adapted fitting procedure of dentate gyrus charging curves" in Appendix 1). In 8/18 cells, the offline and the original online estimate of the near capacitance differed by less than 20%, but overall the offline measurement yielded higher capacitance values than originally used for the CapClamp (offline: $21.0 \pm 9.4\,\mathrm{pF}$/, online: $14.9 \pm 4.8\,\mathrm{pF}$/). In contrast to the online measurement, the offline procedure reported a better fit with three components for a subset of cells ($p < 0.05$, 7/18), but for the analysis presented here the result of the two component fit is used in all cells.

Protocol 1: Verification of altered capacitance

After online measurement of the capacitance, each DGGC was clamped at a range of capacitances from 60% to 300% of the original near capacitance. For each clamped capacitance, the above offline capacitance measurement protocol was repeated to see how the CapClamp altered the slow and fast components. These time scale and amplitude changes were then mapped to the corresponding two compartment circuit parameters to compare them to the target capacitance (see Measurement of near capacitance). Due to the difference between online and offline estimate of the original near capacitance, we corrected the original target capacitance to $C_t^{\mathrm{corr}} = C_c^{\mathrm{off}} + \Delta C_t$, which preserves the targeted capacitance change $\Delta C_t = C_t - C_c^{\mathrm{on}}$. Equally, the clamping factors in the mapping were updated to $k = \frac{C_t^{\mathrm{corr}}}{C_c^{\mathrm{off}}}$.

Protocol 2: Analysis of f-I curves and spike shapes

In a subset of cells, after measuring near capacitance, an fI curve was obtained for the original capacitance and for target capacitances in the above range. Current pulses were 1 s long and repeated three times, at amplitudes ranging from 90% to 200% of an estimated rheobase. This rheobase was estimated by the first occurrence of spiking in response to a ramp (length: 5 s, height: 250 pA). For a quantitative comparison, the resulting fI curves were fit by a square-root function

$$f(I) = \Theta(I - I_{\mathrm{rheo}})\mathrm{gain}\sqrt{I - I_{\mathrm{rheo}}} \tag{8}$$

which captured their type 1 firing with a continuous frequency-current relationship (***Izhikevich, 2006***, p. 168). Cells with more than 30% varying input resistance within the protocol and/or a non-monotonically increasing fI curves were excluded from the analysis.

Spikes were detected as a minimum 10 mV elevation over the average depolarization during the pulse. For the mean action potential (AP) shape, varying spike forms from the initial (< 300 ms) part of the pulse were discarded. The extracted AP features were peak amplitude, threshold voltage and threshold time to peak (voltage derivative crossing 10 mV/ms), height (difference between peak and threshold), temporal width at half of the height and fast afterhyperpolarization (fAHP; a voltage dip of –0.5 mV or larger within 10 ms after the spike). For threshold and fAHP detection, the spike shape was filtered with a digital 4th order Butterworth filter with critical frequencies 3.3 kHz, respectively 1 kHz.

To detect, whether changes in capacitance affect the action potential generating currents, we compared the recorded spikes with hypothetical ones obtained by assuming unaltered currents with respect to the original near capacitance. For a target capacitance C_t, such a hypothetical spike would be a scaled version of the original spike,

$$V_{hypo}(t) = V_c(t_0) + \frac{C_c}{C_t}\left(V_c(t) - V_c(t_0)\right),$$

where $V_c(t)$ is the spike form at the original cell capacitance C_c and the initial time t_0 was chosen to be $t_{spike} - 3\text{ms}$ short before onset of the spike generating currents. Changes in the measured spike shape compared to this hypothetical shape signal a change of the underlying currents.

Simulations of the CapClamp

Simulations of neuron models coupled to the CapClamp were implemented using the neuron simulator Brian2 (***Stimberg et al., 2019***) and the CapClamp was realized using the Brian2 provided NetworkOperation that updated the clamp current every sampling interval using ***Equation 5*** with zero delay between voltage sampling and current injection (for links to the available code, see "Data and software availability" in Appendix 1).

Biophysical neuron model

In order to test the CapClamp in the presence of active ionic conductances, a Wang-Buzsáki (WB) neuron, a single compartment model of hippocampal interneurons, was used (***Wang and Buzsáki, 1996***). Gating dynamics and peak conductances of the transient sodium current and the delayed rectifier potassium current were modeled as described earlier (***Hesse et al., 2017***, Appendix A). The specific membrane capacitance was chosen as $C_m = 0.75\ \frac{\mu\text{F}}{\text{cm}^2}$ and the membrane area was set to $A = 20000\,\mu m^2$, so that the original cell capacitance was 150 pF. When the capacitance is varied, the WB neuron undergoes a well-characterized series of bifurcations; in particular it exhibits a saddle-node loop (SNL) bifurcation at $C_m = 1.47\ \frac{\mu\text{F}}{\text{cm}^2}$ accompanied by an abrupt doubling of the firing rate (***Hesse et al., 2017***). For the demonstration of the CapClamp here, we decided to restrict the tested capacitances to the regime below this critical value, but we confirmed via additional simulations that the CapClamp continues to work beyond the bifurcation (data not shown).

Simulations were performed with the second order Runge-Kutta method, a time step of 1 μs and dynamic clamp loop frequencies up to 100 kHz. Analysis of spike shapes and f-I curves was performed in the same way as for the recorded cells.

Analytically expected effect of capacitance on the form of the f-I curve

How the form of the f-I curve depends on capacitance can be analytically calculated for a single-compartment conductance-based neuron model undergoing a saddle-node on a limit cycle bifurcation at spiking onset like the WB model considered here (***Izhikevich, 2006***), pp. 162–168; (***Schleimer and Schreiber, 2018***). In this case, the time between two spikes T_{isi} is dominated by the slow traversal T_2 of the saddle node, which close to threshold is multiple times longer than the brief duration T_1 of the spike and can be derived by considering solely local dynamics

$$T_{\text{isi}} = T_1 + T_2 \approx T_2 = \frac{\pi}{\sqrt{ac\left(I - I_{\text{rheo}}\right)}}$$

where a and c parametrize the normal form of the dynamics around the saddle node and $I_{\text{rheo}} = I_{\text{sn}}$ is the current value where the saddle node bifurcation occurs. Inverting the inter spike interval to get the frequency then gives the square root form of the f-I curve (see ***Equation 8***). Under the assumption of fast gating kinetics, the $\text{gain} = \frac{\sqrt{ac}}{\pi}$ is expected to be proportional to the inverse of the capacitance $\frac{1}{C}$, because the relevant time scale for the local slow dynamics around the saddle node is the membrane time constant implying that the traversal duration scales as $T_2 \propto \tau \propto C$. The rheobase current in contrast is expected to remain constant, because equilibrium points are independent of the time scales of the dynamics. Formally calculating the normal form parameters a and c confirms these expectations (see "Formal derivation of f-I curve gain and rheobase dependence oncapacitance" in Appendix 1).

The $\frac{1}{C}$ dependence of the gain allows to estimate an expected gain reduction for small capacitance changes around the original capacitance C_c by Taylor expansion

$$\Delta\text{gain} = \text{gain}(C_c) - \text{gain}(C_c + \Delta C) \approx -\frac{\text{gain}(C_c)}{C_c}\Delta C$$

which we compare for both simulated neuron and DGGCs to the observed gain reduction.

Multicompartment model of a dentate gyrus granule cell

For a controlled test of the CapClamp in an electrotonically non-compact cell, a morphologically reconstruction of a recorded DGGC was used as the basis for a multicompartment simulation. Soma and the two dendritic trees had a total area of 14,126 μm^2. The axon was removed for the simulation. Membrane properties were assumed to be uniform and chosen such that they reproduced the average values of the total capacitance and the membrane time constant observed in the experiments: $C_m = \frac{\overline{C_n + C_f}}{A} \approx 0.9 \frac{\mu F}{cm^2}$ and $R_m = \frac{\tau_0}{C_m} \approx 16800\,\Omega cm^2$. The axial resistivity was chosen as $R_{axial} = 300\,\Omega cm$. Simulations were performed with exponential Euler integration, a time step of 10 μs and a dynamic clamp sampling frequency of 20 kHz. Capacitance measurement and clamp procedure were the same as in the recorded DGGCs (***Table 2***).

Acknowledgements

We thank Jan Benda and Lukas Sonnenberg for their dedicated support with dynamic clamp and fruitful discussions. We are grateful to Eve Marder and Ekaterina Morozova for being able to test the RTXI implementation of the CapClamp and apply the CapClamp in neurons of the crustacean stomatogastric ganglion. We thank Robert Gowers and Philipp Norton for valuable feedback on the manuscript.

This project has received funding from the European Research Council (ERC) under the European Union's Horizon 2020 research and innovation program (grant agreement No 864243). The article processing charge was funded by the Deutsche Forschungsgemeinschaft (DFG, German Research Foundation) – 491192747 and the Open Access Publication Fund of Humboldt-Universität zu Berlin.

Additional information

Funding

Funder	Grant reference number	Author
Bundesministerium für Bildung und Forschung	01GQ1403	Jan-Hendrik Schleimer Susanne Schreiber
Deutsche Forschungsgemeinschaft	GRK 1589/2	Paul Pfeiffer Federico José Barreda Tomás
Deutsche Forschungsgemeinschaft	EXC 257	Federico José Barreda Tomás Imre Vida
Deutsche Forschungsgemeinschaft	FOR 2134	Federico José Barreda Tomás Imre Vida
H2020 European Research Council	864243	Susanne Schreiber
Einstein Stiftung Berlin	EZ-2014-224	Jiameng Wu

The funders had no role in study design, data collection and interpretation, or the decision to submit the work for publication.

Author contributions

Paul Pfeiffer, Conceptualization, Data curation, Formal analysis, Investigation, Methodology, Project administration, Software, Visualization, Writing – original draft, Writing – review and editing; Federico José Barreda Tomás, Data curation, Investigation, Methodology, Software, Validation, Visualization, Writing – review and editing; Jiameng Wu, Formal analysis, Investigation, Methodology, Software, Visualization, Writing – review and editing; Jan-Hendrik Schleimer, Conceptualization, Formal analysis, Methodology, Supervision, Writing – review and editing; Imre Vida, Funding acquisition, Project administration, Resources, Supervision, Writing – review and editing; Susanne Schreiber, Conceptualization, Funding acquisition, Project administration, Resources, Supervision, Writing – original draft, Writing – review and editing

Author ORCIDs
Paul Pfeiffer http://orcid.org/0000-0001-5324-5886
Jiameng Wu http://orcid.org/0000-0002-6266-7666
Jan-Hendrik Schleimer http://orcid.org/0000-0002-2156-330X
Imre Vida http://orcid.org/0000-0003-3214-2233
Susanne Schreiber http://orcid.org/0000-0003-3913-5650

Ethics
All procedures and animal maintenance were performaed in accordance with institutional guidelines, the German Animal Welfare Act, the European Council Directive 86/609/EEC regarding the protection of animals, and guidelines from local authorities (Berlin, T-0215/11).

Decision letter and Author response
Decision letter https://doi.org/10.7554/eLife.75517.sa1
Author response https://doi.org/10.7554/eLife.75517.sa2

Additional files

Supplementary files
- Transparent reporting form

Data availability
All data generated, analysis code as well as computational modelling code is uploaded on https://zenodo.org/, see article section Data and software availability.

The following dataset was generated:

Author(s)	Year	Dataset title	Dataset URL	Database and Identifier
Pfeiffer P, Barreda Tomás F J	2021	Capacitance Clamp Demonstration in Rat Dentate Gyrus Granule Cells	https://doi.org/10.5281/zenodo.5552207	Zenodo, 10.5281/zenodo.5552207

References

Amaducci R, Reyes-Sanchez M, Elices I, Rodriguez FB, Varona P. 2019. RTHybrid: A Standardized and Open-Source Real-Time Software Model Library for Experimental Neuroscience. *Frontiers in Neuroinformatics* **13**:11. DOI: https://doi.org/10.3389/fninf.2019.00011, PMID: 30914940

Amzica F, Neckelmann D. 1999. Membrane capacitance of cortical neurons and glia during sleep oscillations and spike-wave seizures. *Journal of Neurophysiology* **82**:2731–2746. DOI: https://doi.org/10.1152/jn.1999.82.5.2731, PMID: 10561441

Ashida G, Abe K, Funabiki K, Konishi M. 2007. Passive soma facilitates submillisecond coincidence detection in the owl's auditory system. *Journal of Neurophysiology* **97**:2267–2282. DOI: https://doi.org/10.1152/jn.00399.2006, PMID: 17135480

Athilingam JC, Ben-Shalom R, Keeshen CM, Sohal VS, Bender KJ. 2017. Serotonin enhances excitability and gamma frequency temporal integration in mouse prefrontal fast-spiking interneurons. *eLife* **6**:e31991. DOI: https://doi.org/10.7554/eLife.31991, PMID: 29206101

Badel L, Lefort S, Brette R, Petersen CCH, Gerstner W, Richardson MJE. 2008. Dynamic I-V curves are reliable predictors of naturalistic pyramidal-neuron voltage traces. *Journal of Neurophysiology* **99**:656–666. DOI: https://doi.org/10.1152/jn.01107.2007, PMID: 18057107

Bal T, Destexhe A. 2009. Dynamic-Clamp: From Principles to Applications. New York, NY: Springer US. DOI: https://doi.org/10.1007/978-0-387-89279-5

Bar-Yehuda D, Korngreen A. 2008. Space-clamp problems when voltage clamping neurons expressing voltage-gated conductances. *Journal of Neurophysiology* **99**:1127–1136. DOI: https://doi.org/10.1152/jn.01232.2007, PMID: 18184885

Bardsley WG, McGinlay PB, Wright AJ. 1986. The F Test for Model Discrimination with Exponential Functions. *Biometrika* **73**:501. DOI: https://doi.org/10.2307/2336228

Beaulieu-Laroche L, Toloza EHS, van der Goes MS, Lafourcade M, Barnagian D, Williams ZM, Eskandar EN, Frosch MP, Cash SS, Harnett MT. 2018. Enhanced Dendritic Compartmentalization in Human Cortical Neurons. *Cell* **175**:643–651. DOI: https://doi.org/10.1016/j.cell.2018.08.045, PMID: 30340039

Bekkers JM, Häusser M. 2007. Targeted dendrotomy reveals active and passive contributions of the dendritic tree to synaptic integration and neuronal output. *PNAS* **104**:11447–11452. DOI: https://doi.org/10.1073/pnas.0701586104, PMID: 17592119

Benda J, Gollisch T, Machens CK, Herz AV. 2007. From response to stimulus: adaptive sampling in sensory physiology. *Current Opinion in Neurobiology* **17**:430–436. DOI: https://doi.org/10.1016/j.conb.2007.07.009, PMID: 17689952

Bettencourt JC, Lillis KP, Stupin LR, White JA. 2008. Effects of imperfect dynamic clamp: computational and experimental results. *Journal of Neuroscience Methods* **169**:282–289. DOI: https://doi.org/10.1016/j.jneumeth.2007.10.009, PMID: 18076999

Booker SA, Song J, Vida I. 2014. Whole-cell patch-clamp recordings from morphologically- and neurochemically-identified hippocampal interneurons. *Journal of Visualized Experiments*:e51706. DOI: https://doi.org/10.3791/51706, PMID: 25350149

Brette R, Piwkowska Z, Monier C, Rudolph-Lilith M, Fournier J, Levy M, Frégnac Y, Bal T, Destexhe A. 2008. High-resolution intracellular recordings using a real-time computational model of the electrode. *Neuron* **59**:379–391. DOI: https://doi.org/10.1016/j.neuron.2008.06.021, PMID: 18701064

Carvalho-de-Souza JL, Pinto BI, Pepperberg DR, Bezanilla F. 2018. Optocapacitive Generation of Action Potentials by Microsecond Laser Pulses of Nanojoule Energy. *Biophysical Journal* **114**:283–288. DOI: https://doi.org/10.1016/j.bpj.2017.11.018, PMID: 29273263

Castelfranco AM, Hartline DK. 2015. The evolution of vertebrate and invertebrate myelin: A theoretical computational study. *Journal of Computational Neuroscience* **38**:521–538. DOI: https://doi.org/10.1007/s10827-015-0552-x, PMID: 25832903

Chamorro P, Muñiz C, Levi R, Arroyo D, Rodríguez FB, Varona P. 2012. Generalization of the dynamic clamp concept in neurophysiology and behavior. *PLOS ONE* **7**:e40887. DOI: https://doi.org/10.1371/journal.pone.0040887, PMID: 22829895

Contreras SA, Schleimer JH, Gulledge AT, Schreiber S. 2020. Activity-Mediated Accumulation of Potassium Induces a Switch in Firing Pattern and Neuronal Excitability Type. *Neuroscience* **1**:403782. DOI: https://doi.org/10.1101/2020.11.30.403782

de Oliveira BL, Pfeiffer ER, Sundnes J, Wall ST, McCulloch AD. 2015. Increased cell membrane capacitance is the dominant mechanism of stretch-dependent conduction slowing in the rabbit heart: A computational study. *Cellular and Molecular Bioengineering* **8**:237–246. DOI: https://doi.org/10.1007/s12195-015-0384-9, PMID: 27087858

Desai NS, Gray R, Johnston D. 2017. A Dynamic Clamp on Every Rig. *ENeuro* **4**:ENEURO.0250-17.2017. DOI: https://doi.org/10.1523/ENEURO.0250-17.2017, PMID: 29085905

Dorf R, Bishop R. 2010. Modern Control Systems. twelfth ed. Pearson.

Dorval AD, Christini DJ, White JA. 2001. Real-Time linux dynamic clamp: A fast and flexible way to construct virtual ion channels in living cells. *Annals of Biomedical Engineering* **29**:897–907. DOI: https://doi.org/10.1114/1.1408929, PMID: 11764320

Economo MN, Fernandez FR, White JA. 2010. Dynamic clamp: alteration of response properties and creation of virtual realities in neurophysiology. *The Journal of Neuroscience* **30**:2407–2413. DOI: https://doi.org/10.1523/JNEUROSCI.5954-09.2010, PMID: 20164323

Edwards DH, Mulloney B. 1984. Compartmental models of electrotonic structure and synaptic integration in an identified neurone. *The Journal of Physiology* **348**:89–113. DOI: https://doi.org/10.1113/jphysiol.1984.sp015101, PMID: 6716298

Eyal G, Verhoog MB, Testa-Silva G, Deitcher Y, Lodder JC, Benavides-Piccione R, Morales J, DeFelipe J, de Kock CP, Mansvelder HD, Segev I. 2016. Unique membrane properties and enhanced signal processing in human neocortical neurons. *eLife* **5**:e16553. DOI: https://doi.org/10.7554/eLife.16553, PMID: 27710767

Feng L, Zhao T, Kim J. 2015. neuTube 1.0: A New Design for Efficient Neuron Reconstruction Software Based on the SWC Format. *ENeuro* **2**:ENEURO.0049-14.2014. DOI: https://doi.org/10.1523/ENEURO.0049-14.2014, PMID: 26464967

Franci A, Drion G, Sepulchre R. 2018. Robust and tunable bursting requires slow positive feedback. *Journal of Neurophysiology* **119**:1222–1234. DOI: https://doi.org/10.1152/jn.00804.2017, PMID: 29357476

Gentet LJ, Stuart GJ, Clements JD. 2000. Direct measurement of specific membrane capacitance in neurons. *Biophysical Journal* **79**:314–320. DOI: https://doi.org/10.1016/S0006-3495(00)76293-X, PMID: 10866957

Goethals S, Brette R. 2020. Theoretical relation between axon initial segment geometry and excitability. *eLife* **9**:e53432. DOI: https://doi.org/10.7554/eLife.53432, PMID: 32223890

Golowasch J, Thomas G, Taylor AL, Patel A, Pineda A, Khalil C, Nadim F. 2009. Membrane capacitance measurements revisited: dependence of capacitance value on measurement method in nonisopotential neurons. *Journal of Neurophysiology* **102**:2161–2175. DOI: https://doi.org/10.1152/jn.00160.2009, PMID: 19571202

Gorur-Shandilya S, Marder E, O'Leary T. 2020. Activity-dependent compensation of cell size is vulnerable to targeted deletion of ion channels. *Scientific Reports* **10**:15989. DOI: https://doi.org/10.1038/s41598-020-72977-6, PMID: 32994529

Gouwens NW, Berg J, Feng D, Sorensen SA, Zeng H, Hawrylycz MJ, Koch C, Arkhipov A. 2018. Systematic generation of biophysically detailed models for diverse cortical neuron types. *Nature Communications* **9**:710. DOI: https://doi.org/10.1038/s41467-017-02718-3, PMID: 29459718

Harrigan P, Madhani HD, El-Samad H. 2018. Real-Time Genetic Compensation Defines the Dynamic Demands of Feedback Control. *Cell* **175**:877–886. DOI: https://doi.org/10.1016/j.cell.2018.09.044, PMID: 30340045

Hartline DK, Colman DR. 2007. Rapid conduction and the evolution of giant axons and myelinated fibers. *Current Biology* **17**:R29–R35. DOI: https://doi.org/10.1016/j.cub.2006.11.042, PMID: 17208176
Hasenstaub A, Otte S, Callaway E, Sejnowski TJ. 2010. Metabolic cost as a unifying principle governing neuronal biophysics. *PNAS* **107**:12329–12334. DOI: https://doi.org/10.1073/pnas.0914886107, PMID: 20616090
Hesse J, Schreiber S. 2015. Externalization of neuronal somata as an evolutionary strategy for energy economization. *Current Biology* **25**:R324–R325. DOI: https://doi.org/10.1016/j.cub.2015.02.024, PMID: 25898099
Hesse J, Schleimer JH, Schreiber S. 2017. Qualitative changes in phase-response curve and synchronization at the saddle-node-loop bifurcation. *Physical Review. E* **95**:052203. DOI: https://doi.org/10.1103/PhysRevE.95.052203, PMID: 28618541
Hocker D, Park IM. 2019. Myopic control of neural dynamics. *PLOS Computational Biology* **15**:e1006854. DOI: https://doi.org/10.1371/journal.pcbi.1006854, PMID: 30856171
Izhikevich EM. 2006. Dynamical Systems in Neuroscience: The Geometry of Excitability and Bursting. The MIT Press. DOI: https://doi.org/10.7551/mitpress/2526.001.0001
Jaffe DB, Brenner R. 2018. A computational model for how the fast afterhyperpolarization paradoxically increases gain in regularly firing neurons. *Journal of Neurophysiology* **119**:1506–1520. DOI: https://doi.org/10.1152/jn.00385.2017, PMID: 29357445
Kemenes I, Marra V, Crossley M, Samu D, Staras K, Kemenes G, Nowotny T. 2011. Dynamic clamp with StdpC software. *Nature Protocols* **6**:405–417. DOI: https://doi.org/10.1038/nprot.2010.200, PMID: 21372819
Kirst C, Ammer J, Felmy F, Herz A, Stemmler M. 2015. Fundamental Structure and Modulation of Neuronal Excitability: Synaptic Control of Coding, Resonance, and Network Synchronization. *Neuroscience*. . 1 :022475. DOI: https://doi.org/10.1101/022475
Krasovitski B, Frenkel V, Shoham S, Kimmel E. 2011. Intramembrane cavitation as a unifying mechanism for ultrasound-induced bioeffects. *PNAS* **108**:3258–3263. DOI: https://doi.org/10.1073/pnas.1015771108, PMID: 21300891
Krueppel R, Remy S, Beck H. 2011. Dendritic integration in hippocampal dentate granule cells. *Neuron* **71**:512–528. DOI: https://doi.org/10.1016/j.neuron.2011.05.043, PMID: 21835347
Laughlin SB, de Ruyter van Steveninck RR, Anderson JC. 1998. The metabolic cost of neural information. *Nature Neuroscience* **1**:36–41. DOI: https://doi.org/10.1038/236, PMID: 10195106
Linaro D, Couto J, Giugliano M. 2015. Real-time Electrophysiology: Using Closed-loop Protocols to Probe Neuronal Dynamics and Beyond. *Journal of Visualized Experiments* **1**:e52320. DOI: https://doi.org/10.3791/52320, PMID: 26132434
Liu J, Kim YS, Richardson CE, Tom A, Ramakrishnan C, Birey F, Katsumata T, Chen S, Wang C, Wang X, Joubert LM, Jiang Y, Wang H, Fenno LE, Tok JBH, Paşca SP, Shen K, Bao Z, Deisseroth K. 2020. Genetically targeted chemical assembly of functional materials in living cells, tissues, and animals. *Science (New York, N.Y.)* **367**:1372–1376. DOI: https://doi.org/10.1126/science.aay4866, PMID: 32193327
Major G, Evans JD, Jack JJB. 1993. Solutions for transients in arbitrarily branching cables: I. Voltage recording with a somatic shunt. *Biophysical Journal* **65**:423–449. DOI: https://doi.org/10.1016/S0006-3495(93)81037-3, PMID: 8369447
Martina M, Vida I, Jonas P. 2000. Distal initiation and active propagation of action potentials in interneuron dendrites. *Science (New York, N.Y.)* **287**:295–300. DOI: https://doi.org/10.1126/science.287.5451.295, PMID: 10634782
McComb C, Meems R, Syed N, Lukowiak K. 2003. Electrophysiological differences in the CPG aerial respiratory behavior between juvenile and adult Lymnaea. *Journal of Neurophysiology* **90**:983–992. DOI: https://doi.org/10.1152/jn.00263.2003, PMID: 12711713
Newman JP, Fong M, Millard DC, Whitmire CJ, Stanley GB, Potter SM. 2015. Optogenetic feedback control of neural activity. *eLife* **4**:e07192. DOI: https://doi.org/10.7554/eLife.07192, PMID: 26140329
Nörenberg A, Hu H, Vida I, Bartos M, Jonas P. 2010. Distinct nonuniform cable properties optimize rapid and efficient activation of fast-spiking GABAergic interneurons. *PNAS* **107**:894–899. DOI: https://doi.org/10.1073/pnas.0910716107, PMID: 20080772
Ori H, Hazan H, Marder E, Marom S. 2020. Dynamic clamp constructed phase diagram for the Hodgkin and Huxley model of excitability. *PNAS* **117**:3575–3582. DOI: https://doi.org/10.1073/pnas.1916514117, PMID: 32024761
O'Leary T, Williams AH, Franci A, Marder E. 2014. Cell types, network homeostasis, and pathological compensation from a biologically plausible ion channel expression model. *Neuron* **82**:809–821. DOI: https://doi.org/10.1016/j.neuron.2014.04.002, PMID: 24853940
Patel YA, George A, Dorval AD, White JA, Christini DJ, Butera RJ, Poisot T. 2017. Hard real-time closed-loop electrophysiology with the Real-Time eXperiment Interface (RTXI. *PLOS Computational Biology* **13**:e1005430. DOI: https://doi.org/10.1371/journal.pcbi.1005430, PMID: 28557998
Pfeiffer P, Egorov AV, Lorenz F, Schleimer JH, Draguhn A, Schreiber S. 2020. Clusters of cooperative ion channels enable a membrane-potential-based mechanism for short-term memory. *eLife* **9**:e49974. DOI: https://doi.org/10.7554/eLife.49974, PMID: 32031523
Plaksin M, Shoham S, Kimmel E. 2014. Intramembrane Cavitation as a Predictive Bio-Piezoelectric Mechanism for Ultrasonic Brain Stimulation. *Physical Review X* **4**:011004. DOI: https://doi.org/10.1103/PhysRevX.4.011004
Podlaski WF, Seeholzer A, Groschner LN, Miesenböck G, Ranjan R, Vogels TP. 2017. Mapping the function of neuronal ion channels in model and experiment. *eLife* **6**:e22152. DOI: https://doi.org/10.7554/eLife.22152, PMID: 28267430

Prescott SA, De Koninck Y, Sejnowski TJ. 2008a. Biophysical basis for three distinct dynamical mechanisms of action potential initiation. *PLOS Computational Biology* **4**:e1000198. DOI: https://doi.org/10.1371/journal.pcbi.1000198, PMID: 18846205

Prescott SA, Ratté S, De Koninck Y, Sejnowski TJ. 2008b. Pyramidal neurons switch from integrators in vitro to resonators under in vivo-like conditions. *Journal of Neurophysiology* **100**:3030–3042. DOI: https://doi.org/10.1152/jn.90634.2008, PMID: 18829848

Prinz AA, Abbott LF, Marder E. 2004. The dynamic clamp comes of age. *Trends in Neurosciences* **27**:218–224. DOI: https://doi.org/10.1016/j.tins.2004.02.004, PMID: 15046881

Rihn LL, Claiborne BJ. 1990. Dendritic growth and regression in rat dentate granule cells during late postnatal development. *Brain Research. Developmental Brain Research* **54**:115–124. DOI: https://doi.org/10.1016/0165-3806(90)90071-6, PMID: 2364540

Rivera CM, Kwon HJ, Hashmi A, Yu G, Zhao J, Gao J, Xu J, Xue W, Dimitrov AG. 2015. Towards a dynamic clamp for neurochemical modalities. *Sensors (Basel, Switzerland)* **15**:10465–10480. DOI: https://doi.org/10.3390/s150510465, PMID: 25946635

Robinson HP. 1994. Conductance injection. *Trends in Neurosciences* **17**:147–148. DOI: https://doi.org/10.1016/0166-2236(94)90088-4, PMID: 7517591

Santin JM, Schulz DJ. 2019. Membrane Voltage Is a Direct Feedback Signal That Influences Correlated Ion Channel Expression in Neurons. *Current Biology* **29**:1683–1688. DOI: https://doi.org/10.1016/j.cub.2019.04.008, PMID: 31080077

Schleimer JH, Schreiber S. 2018. Phase-response curves of ion channel gating kinetics. *Mathematical Methods in the Applied Sciences* **41**:8844–8858. DOI: https://doi.org/10.1002/mma.5232

Schmidt-Hieber C, Jonas P, Bischofberger J. 2007. Subthreshold dendritic signal processing and coincidence detection in dentate gyrus granule cells. *The Journal of Neuroscience* **27**:8430–8441. DOI: https://doi.org/10.1523/JNEUROSCI.1787-07.2007, PMID: 17670990

Sengupta B, Stemmler M, Laughlin SB, Niven JE. 2010. Action potential energy efficiency varies among neuron types in vertebrates and invertebrates. *PLOS Computational Biology* **6**:e1000840. DOI: https://doi.org/10.1371/journal.pcbi.1000840, PMID: 20617202

Shapiro MG, Homma K, Villarreal S, Richter CP, Bezanilla F. 2017. Corrigendum: Infrared light excites cells by changing their electrical capacitance. *Nature Communications* **8**:16148. DOI: https://doi.org/10.1038/ncomms16148, PMID: 29125141

Sharp AA, O'Neil MB, Abbott LF, Marder E. 1993. The dynamic clamp: artificial conductances in biological neurons. *Trends in Neurosciences* **16**:389–394. DOI: https://doi.org/10.1016/0166-2236(93)90004-6, PMID: 7504352

Stiefel KM, Gutkin BS, Sejnowski TJ. 2008. Cholinergic neuromodulation changes phase response curve shape and type in cortical pyramidal neurons. *PLOS ONE* **3**:e3947. DOI: https://doi.org/10.1371/journal.pone.0003947, PMID: 19079601

Stiefel KM, Gutkin BS, Sejnowski TJ. 2009. The effects of cholinergic neuromodulation on neuronal phase-response curves of modeled cortical neurons. *Journal of Computational Neuroscience* **26**:289–301. DOI: https://doi.org/10.1007/s10827-008-0111-9, PMID: 18784991

Stimberg M, Brette R, Goodman DF. 2019. Brian 2, an intuitive and efficient neural simulator. *eLife* **8**:e47314. DOI: https://doi.org/10.7554/eLife.47314, PMID: 31429824

Svirskis G, Kotak V, Sanes DH, Rinzel J. 2004. Sodium along with low-threshold potassium currents enhance coincidence detection of subthreshold noisy signals in MSO neurons. *Journal of Neurophysiology* **91**:2465–2473. DOI: https://doi.org/10.1152/jn.00717.2003, PMID: 14749317

Szoboszlay M, Lőrincz A, Lanore F, Vervaeke K, Silver RA, Nusser Z. 2016. Functional Properties of Dendritic Gap Junctions in Cerebellar Golgi Cells. *Neuron* **90**:1043–1056. DOI: https://doi.org/10.1016/j.neuron.2016.03.029, PMID: 27133465

Szűcs A, Rátkai A, Schlett K, Huerta R. 2017. Frequency-dependent regulation of intrinsic excitability by voltage-activated membrane conductances, computational modeling and dynamic clamp. *The European Journal of Neuroscience* **46**:2429–2444. DOI: https://doi.org/10.1111/ejn.13708, PMID: 28921695

Temporal S, Lett KM, Schulz DJ. 2014. Activity-dependent feedback regulates correlated ion channel mRNA levels in single identified motor neurons. *Current Biology* **24**:1899–1904. DOI: https://doi.org/10.1016/j.cub.2014.06.067, PMID: 25088555

Tewari BP, Chaunsali L, Campbell SL, Patel DC, Goode AE, Sontheimer H. 2018. Perineuronal nets decrease membrane capacitance of peritumoral fast spiking interneurons in a model of epilepsy. *Nature Communications* **9**:4724. DOI: https://doi.org/10.1038/s41467-018-07113-0, PMID: 30413686

Thome C, Kelly T, Yanez A, Schultz C, Engelhardt M, Cambridge SBB, Both M, Draguhn A, Beck H, Egorov AVV. 2014. Axon-carrying dendrites convey privileged synaptic input in hippocampal neurons. *Neuron* **83**:1418–1430. DOI: https://doi.org/10.1016/j.neuron.2014.08.013, PMID: 25199704

Turrigiano GG, Marder E, Abbott LF. 1996. Cellular short-term memory from a slow potassium conductance. *Journal of Neurophysiology* **75**:963–966. DOI: https://doi.org/10.1152/jn.1996.75.2.963, PMID: 8714669

Ullah G, Schiff SJ. 2009. Tracking and control of neuronal Hodgkin-Huxley dynamics. *Physical Review. E, Statistical, Nonlinear, and Soft Matter Physics* **79**:1–4. DOI: https://doi.org/10.1103/PhysRevE.79.040901, PMID: 19518166

Virtanen P, Gommers R, Oliphant TE, Haberland M, Reddy T, Cournapeau D, Burovski E, Peterson P, Weckesser W, Bright J, van der Walt SJ, Brett M, Wilson J, Millman KJ, Mayorov N, Nelson ARJ, Jones E, Kern R, Larson E, Carey CJ, et al. 2020. Author Correction: SciPy 1.0: fundamental algorithms for scientific

computing in Python. *Nature Methods* **17**:352. DOI: https://doi.org/10.1038/s41592-020-0772-5, PMID: 32094914

Wang XJ, Buzsáki G. 1996. Gamma oscillation by synaptic inhibition in a hippocampal interneuronal network model. *The Journal of Neuroscience* **16**:6402–6413 PMID: 8815919.,

White WE, Hooper SL. 2013. Contamination of current-clamp measurement of neuron capacitance by voltage-dependent phenomena. *Journal of Neurophysiology* **110**:257–268. DOI: https://doi.org/10.1152/jn.00993.2012, PMID: 23576698

Wilders R. 2006. Dynamic clamp: A powerful tool in cardiac electrophysiology. *The Journal of Physiology* **576**:349–359. DOI: https://doi.org/10.1113/jphysiol.2006.115840, PMID: 16873403

Wybo WAM, Torben-Nielsen B, Nevian T, Gewaltig MO. 2019. Electrical Compartmentalization in Neurons. *Cell Reports* **26**:1759–1773. DOI: https://doi.org/10.1016/j.celrep.2019.01.074, PMID: 30759388

Wybo WA, Jordan J, Ellenberger B, Marti Mengual U, Nevian T, Senn W. 2021. Data-driven reduction of dendritic morphologies with preserved dendro-somatic responses. *eLife* **10**:e60936. DOI: https://doi.org/10.7554/eLife.60936, PMID: 33494860

Appendix 1

Impedance of a capacitance-clamped RC circuit

The impedance of a cell captures its linear response to the whole range of input frequencies (see ***Figure 1—figure supplement 1b***). In the following, we derive the impedance of a passive membrane, an RC circuit, with capacitance C_c coupled to the CapClamp and compare it to the impedance of an RC circuit with the target capacitance C_t.

Analysis of the dynamic clamp via the Z-transform

In general, the dynamic clamp technique forms a digital filter, mapping the incoming sampled voltages to injected currents. For a sampling interval Δt, a linear mapping such as the CapClamp has the form

$$I_{\mathrm{dyn}}(i\Delta t) = \sum_{j=0}^{N} \nu_j V\left((i-j)\Delta t\right) + \sum_{k=1}^{M} \gamma_k I_{\mathrm{dyn}}\left((i-k)\Delta t\right), \tag{9}$$

where N and M determine history of voltage and current values, respectively, taken into account. For the CapClamp, the coefficients depend on cell capacitance C_c, target capacitance C_t and the sampling interval (see ***Equation 5***),

$$\begin{aligned} \nu_0 &= \frac{C_C - C_t}{C_t}\frac{C_C}{\Delta_t}, \\ \nu_1 &= -\nu_0, \\ \gamma_1 &= -\frac{C_C - C_t}{C_t}. \end{aligned} \tag{10}$$

This linear mapping can be represented and analyzed using the Z-transform (***Dorf and Bishop, 2010***, Ch. 13),

$$\hat{I}(z) = F_{\mathrm{dyn}}(z)\hat{V}(z), \tag{11}$$

$$F_{\mathrm{dyn}}(z) = \frac{\sum_{j=0}^{N} \nu_j z^{-j}}{1 - \sum_{k=1}^{M} \gamma_k z^{-k}}. \tag{12}$$

where the transfer function follows from the properties of the Z-transform: linearity $\lambda X_i \xrightarrow{Z} \lambda\hat{X}(z)$ and delay transformation $X_{i-1} \xrightarrow{Z} z^{-1}\hat{X}(z)$ (***Dorf and Bishop, 2010***, Table 13.2),

If the cell also forms a linear system, like the RC circuit, the transfer function of the coupled system ***Appendix 1—figure 1*** is given by ***Dorf and Bishop, 2010***, Table 2.6.

$$H_{\mathrm{cell+dyn}}(z) = \frac{H_{\mathrm{cell}}(z)}{1 - H_{\mathrm{cell}}(z)F_{\mathrm{dyn}}(z)}, \tag{13}$$

where $H_{\mathrm{cell}}(z)$ is the Z-transform of the membrane filter, e.g. $H_{\mathrm{cell}}(z) = H_{\mathrm{RC}}(z)$.

The transfer function of the coupled system $H_{\mathrm{cell+dyn}}(z)$ can then be compared with the one of the target system $H_{\mathrm{target}}(z)$ (***Appendix 1—figure 1***). Additionally, the frequency-dependent impedance can be retrieved from the transfer function by

$$Z_{\mathrm{cell+dyn}}(f) = H_{\mathrm{cell+dyn}}(e^{i2\pi f\Delta t}). \tag{14}$$

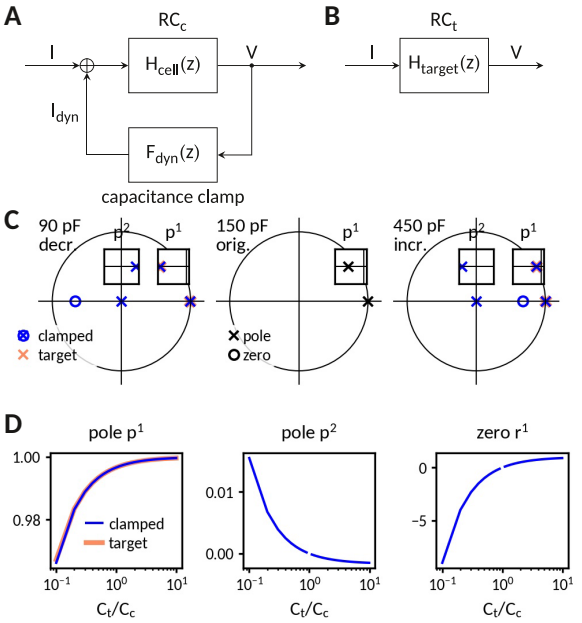

Appendix 1—figure 1. Analysis of the capacitance clamp as a discrete feedback filter. (**A**) Block diagram of the coupled system: RC circuit with original capacitance Cc and capacitance clamp feedback current. (**B**) Block diagram of the target system: RC circuit with target capacitance Ct. (**C**) Pole-zero plot of the transfer functions at a decreased (left), the original and an increased capacitance. In addition to mimicking the pole of the target system, the clamped system has an additional pole and an additional zero. (**D**) Pole and zero position versus capacitance.

Transfer function of the CapClamp

The Z-transform of the CapClamp filter can be read directly from the general form of the transfer function (***Equation 12***) and the CapClamp feedback coefficients (***Equation 10***),

$$F_{\mathrm{dyn}}(z) = \frac{C_c - C_t}{C_t} \frac{C_c}{\Delta t} \frac{1 - z^{-1}}{1 + \frac{C_c - C_t}{C_t} z^{-1}}. \tag{15}$$

Transfer function of the RC circuit

In an RC circuit, the dynamics of the voltage are

$$C \frac{\mathrm{d}V}{\mathrm{d}t} = -\frac{V}{R} + I.$$

Thus, in a single time step Δt, when the current is fixed, the voltage evolves as

$$V(k\Delta t) = V((k-1)\Delta t) e^{-\frac{\Delta t}{\tau}} + RI\left(1 - e^{-\frac{\Delta t}{\tau}}\right),$$

where $\tau = RC$ is the time constant. Applying the Z-transform results in the transfer function

$$H_{RC}(z) = R\left(1 - e^{-\frac{\Delta t}{\tau}}\right) \frac{1}{z - e^{-\frac{\Delta t}{\tau}}}, \tag{16}$$

which is subsequently used as the cell's transfer function $H_{\mathrm{cell}}(z) = H_{\mathrm{RC}}(z)$.

Transfer function of the clamped RC circuit

Introducing $K = \frac{C_c - C_t}{C_t}$ and $h_c = \frac{\Delta t}{\tau_c}$, the RC circuit (***Equation 16***) and CapClamp (***Equation 15***) transfer functions can be combined using ***Equation 13*** to get the transfer function of the combined system

$$H_{\mathrm{cell+dyn}}(z) = R\left(1 - e^{-h_c}\right) \frac{z + K}{z^2 + \left(K - e^{-h_c} - \frac{1}{h_c} K\left(1 - e^{-h_c}\right)\right) z - K\left(e^{-h_c} - \frac{1}{h_c}\left(1 - e^{-h_c}\right)\right)}. \tag{17}$$

In comparison, the transfer function of the target RC circuit reads

$$H_{\text{target}}(z) = R\left(1 - e^{-h_t}\right)\frac{1}{z - e^{-h_t}}$$

with $h_t = \frac{\Delta t}{\tau_t} = \frac{\Delta t}{RC_t}$ reflecting the different target capacitance.

Figure 1—figure supplement 1b compares the resulting impedances for decreased and increased capacitances. As discussed in the "Results" section , the impedance amplitudes fit well up to a tenth of the dynamic clamp frequency. A closer look at the transfer function explains the fit at low frequencies and the deviations at higher frequencies.

Input resistance is preserved

The input resistance is equal to the impedance at zero frequency, that is at $z = e^{i2\pi 0} = 1$, which for both coupled and target system is the original resistance,

$$H_{\text{cell+dyn}}(1) = H_{\text{target}}(1) = R. \tag{18}$$

Poles and zeros

For a further comparison, poles and zeros of the transfer functions are calculated. To simplify the expressions, it is assumed that the time constant of the original and target circuits are much larger than the sampling interval, that is $h_c \ll 1$ and $h_t \ll 1$.

Target circuit

The target circuit has no zero and a single pole located at

$$p_t^{(1)} = e^{-h_t} = 1 - h_t + \ldots \tag{19}$$

Capacitance clamped circuit

The coupled system has one zero at

$$r_c^{(1)} = -K = 1 - \frac{C_c}{C_t}. \tag{20}$$

The clamped circuit has two poles at

$$p_c^{(1)} = 1 - (1 + K)h_c + \ldots \tag{21}$$

and

$$p_c^{(2)} = \frac{K}{2}h_c + \ldots \tag{22}$$

Comparison of poles

All poles and zeros for an RC circuit in its original state and clamped at decreased and increased capacitances are shown in ***Appendix 1—figure 1***. The first pole of the clamped circuit coincides with the one of the target circuit: $p_c^{(1)} = 1 - \frac{C_c}{C_c}\frac{\Delta t}{RC_c} = 1 - h_t = p_t^{(1)}$. As these pole lies close to $z = 1$, they determine the lower frequency response, which explains why the impedance amplitudes fit so well in this range.

In addition to moving the existent pole of the cell circuit to the one of the target circuit, the CapClamp creates an additional pole $p_c^{(2)} \approx \frac{h_c}{2}(\frac{C_c}{C_t} - 1)$ and a new zero $r_c^{(1)} = 1 - \frac{C_c}{C_t}$. Thus, at an increased capacitance $C_t > C_c$, the new pole lies in the left half of the unit circle and thereby increases the impedance at higher frequencies. In contrast, at a decreased capacitance, the additional zero moves into the left half of the complex plane and thereby decreases the impedance at higher frequencies.

Stability

For the investigated RC circuit with R=100 MΩ and C = 150 pF and a sampling interval of 50 us, both poles of the capacitance clamped system remain within the unit circle (***Appendix 1—figure 1***) for the tested range from 0.1 to 10 times the original capacitance. As the coupled system is naturally causal, this implies that the transfer function of the clamped circuit is stable for this range of target capacitances, i.e. there are no unstable oscillations.

Mapping between a charging curve with two components and a two compartment circuit

In the following, we explain how a charging curve of a cell with two components can be mapped to the parameters of a two compartment circuit, which we used to extract the local capacitance in the recorded dentate gyrus granule cells (see ***Figure 3***). We first report the approach and results derived earlier (***Golowasch et al., 2009***) and then explain how to extend the mapping when the capacitance is clamped to a modified value.

Golowasch et al. derived expressions for the near capacitance and the other circuit parameters by comparing the impedance of a two compartment circuit in ***Figure 3A***

$$Z(s) = \frac{1}{\frac{1}{R_n}+sC_n+\frac{1}{R_a+\frac{1}{\frac{1}{R_f}+sC_f}}} \tag{23}$$

with the impedance of a system whose response to a step currents is a sum of two exponentials

$$Z(s) = R_0 \frac{1}{1+s\tau_0} + R_1 \frac{1}{1+s\tau_1}. \tag{24}$$

The comparison of these two impedances gives four equations linking the circuit parameters and the two components of the charging curve:

$$R_0 + R_1 = \frac{R_aR_n + R_fR_n}{R_a + R_f + R_n}, \tag{25}$$

$$R_0\tau_0 + R_1\tau_1 = \frac{R_aR_nR_fC_f}{R_a + R_f + R_n}, \tag{26}$$

$$\tau_0 + \tau_1 = \frac{(R_a + R_n)C_fR_f + (R_a + R_f)C_nR_n}{R_a + R_f + R_n}, \tag{27}$$

$$\tau_0\tau_1 = \frac{R_aC_nR_nC_fR_f}{R_a + R_f + R_n}. \tag{28}$$

To solve this set of equations, they assume that the membrane time constant is the same in all compartments $C_nR_n = C_fR_f = \tau_c$. However in a clamped neuron, where the near capacitance is targeted to be modified to a k-fold different value, this equation becomes

$$C_nR_n = kC_fR_f, \tag{29}$$

where $k = \frac{C_{n,clam.}}{C_{n,orig.}}$.

For the unclamped case, $k = 1$, the mapping from the two components to the circuit parameters is

$$R_n = R_0 + \frac{\tau_0}{\tau_1}R_1, \tag{30}$$

$$C_n = \frac{\tau_0\tau_1}{\tau_1R_0 + \tau_0R_1}, \tag{31}$$

$$R_f = \frac{R_0\tau_1}{R_1\tau_0}\left(R_0 + \frac{\tau_0}{\tau_1}R_1\right) \tag{32}$$

$$C_f = \frac{R_1\tau_0}{R_0\tau_1}\frac{\tau_0\tau_1}{\tau_1R_0 + \tau_0R_1} \tag{33}$$

$$R_a = \frac{\tau_1}{\tau_0 - \tau_1}\left(R_0 + \frac{\tau_0}{\tau_1}R_1\right)\left(1 + \frac{R_0\tau_1}{R_1\tau_0}\right). \tag{34}$$

For the clamped case, $k \neq 1$, we used the python package sympy to solve the equations.

Adapted fitting procedure of dentate gyrus charging curves

The initial online capacitance measurement was based on fitting the charging curve at the beginning of the current pulse. Posterior analysis showed an artefactual voltage drop of –0.2 mV starting about 0.2ms before pulse onset (probably due to coupling of the DAQ measurement card and the motherboard of the dynamic clamp computer), which limited the reliability of the online fit for cells with a small fast component. As no such artifact was observed for the recharging at the end of the pulse, this part was used in an improved offline fit. Additional measures to improve the fit were: cut of the first 0.2ms after pulse end to minimize electrode artifacts, limiting the fit to the first 60 ms (3–4 times τ_0) after the pulse to prioritize the early part of the charging curve and a switch to the python package lmfit for better evaluation of parameter confidence bounds (https://lmfit.github.io/lmfit-py/). Furthermore, the finite rise time of the current injection by the amplifier was taken into account by adapting the original form of the charging curve (***Equation 6***) to

$$V(t) = I_{ext} \left[\sum_{i;\tau_i \neq \tau_a} \frac{R_i}{\tau_i - \tau_a} \left(\tau_i \left(1 - e^{-\frac{t}{\tau_i}} \right) - \tau_a \left(1 - e^{-\frac{t}{\tau_a}} \right) \right) + \sum_{i;\tau_i = \tau_a} R_i \left(1 - e^{-\frac{t}{\tau_i}} - \frac{t}{\tau_i} e^{-\frac{t}{\tau_i}} \right) \right], \tag{35}$$

where the current rise time of the amplifier τ_a ($87 \pm 2\,\mu$s) was obtained by fitting the recorded injected current for the current step command by a simple exponential. A comparison of the two exponential components and the resulting circuit parameters for the online and offline fitting procedures is show in ***Appendix 1—table 1***.

For the charging curves under capacitance clamp, the fitting procedure for the charging curve with two exponentials was initialized with values as expected for the targeted capacitance change: mapping the fitting results of the unclamped response to a two compartment circuit, changing the near capacitance to the targeted value and finally mapping this altered circuit back to the expected time scale and amplitudes. This initialization improved the fits especially at increased near capacitances, where the amplitude of the fast component becomes smaller.

Formal derivation of f-I curve gain and rheobase dependence on capacitance

To confirm the expectations of gain and rheobase dependence on capacitance in a single compartment neuron model (see "Analytically expected effect of capacitance on the form of the f-I curve" in Methods), we here sketch the calculation of the normal form parameters a and c following ***Izhikevich, 2006***, pp. 162–163. In principle, a and c can be calculated for arbitrary gating kinetics by projecting the dynamics on the center manifold (***Schleimer and Schreiber, 2018***). For the assumption

Appendix 1—table 1. Comparison of online and offline fits to charging curves in the recorded dentate gyrus granule cells (N = 18).

	Online fit (mean ± std)	Offline fit (mean ± std)
Two comp.		
τ_0	14.9±4.8 ms	15.1±4.8 ms
R_0	136.9±47.5 MΩ	127.1±44.6 MΩ
τ_1	0.41±0.23 ms	0.77±0.24 ms
R_1	25.1±14.1 MΩ	34.5±14.7 MΩ
Circuit		
C_n	14.9±4.7 pF	21.0±9.4 pF
R_n	1106.3±519.3 MΩ	854.2±394.0 MΩ
R_a	34.9±19.9 MΩ	52.5±19.8 MΩ
C_f	99.1±33.7 pF	105.8±33.0 pF
R_f	159.6±58.1 MΩ	155.5±59.9 MΩ

of small gating time constants, however, they can be expressed in simpler terms using the steady state I-V relation of the neuron divided by its membrane capacitance

$$\mathbf{I}(V,I) = \frac{1}{C}\left(I - I_\infty(V)\right) = \frac{1}{C}\left(I - \sum_{i=1}^{N} g_i \prod_{j=1}^{M_i} x_{ij,\infty}(V)^{p_{ij}}(V - E_i)\right)$$

taking the form $a = \frac{1}{2}\frac{\partial^2 \mathbf{I}(V,I)}{\partial V^2}\Big|_{V=V_{\mathrm{sn}},I=I_{\mathrm{sn}}}$ and $c = \frac{\partial \mathbf{I}(V,I)}{\partial I}\Big|_{V=V_{\mathrm{sn}},I=I_{\mathrm{sn}}}$, where the saddle node voltage V_{sn} and current I_{sn} are given by the equations

$$\mathbf{I}(V,I)|_{V=V_{\mathrm{sn}},I=I_{\mathrm{sn}}} = 0,$$
$$\frac{\partial \mathbf{I}(V,I)}{\partial V}\Big|_{V=V_{\mathrm{sn}},I=I_{\mathrm{sn}}} = 0.$$

In summary, both a and c are proportional to $\frac{1}{C}$ and the rheobase current $I_{\mathrm{rheo}} = I_{\mathrm{sn}} = I_\infty(V_{\mathrm{sn}})$ is independent of capacitance, thus confirming the expected scaling.

Data and software availability

- Electrophysiological recordings of capacitance clamped dentate gyrus granule cells: Pfeiffer, P., & Tomás F. J. B. (2021). Capacitance clamp demonstration in rat dentate gyrus granule cells. https://doi.org/10.5281/zenodo.5552207
- Project repository with capacitance clamp module for https://scicrunch.org/resolver/RRID:SCR_017280RELACS and custom analysis/simulation in python: Pfeiffer, P., Tomás, F. J. B., Wu, J., Schleimer, J.-H., Vida, I., & Schreiber, S. (2021). Software for: A dynamic clamp protocol to artificially modify cell capacitance. https://doi.org/10.5281/zenodo.6322768
- Capacitance clamp plugin for http://rtxi.org/RTXI, a real-time data-acquistion and control application for biological research that allows to extend a conventional electrophysiology setup for dynamic clamp experiments (***Patel et al., 2017***). Capacitance_clamp_rtxi_module: https://doi.org/10.5281/zenodo.5553946

Supplementary figures for Publication CAPCLAMP

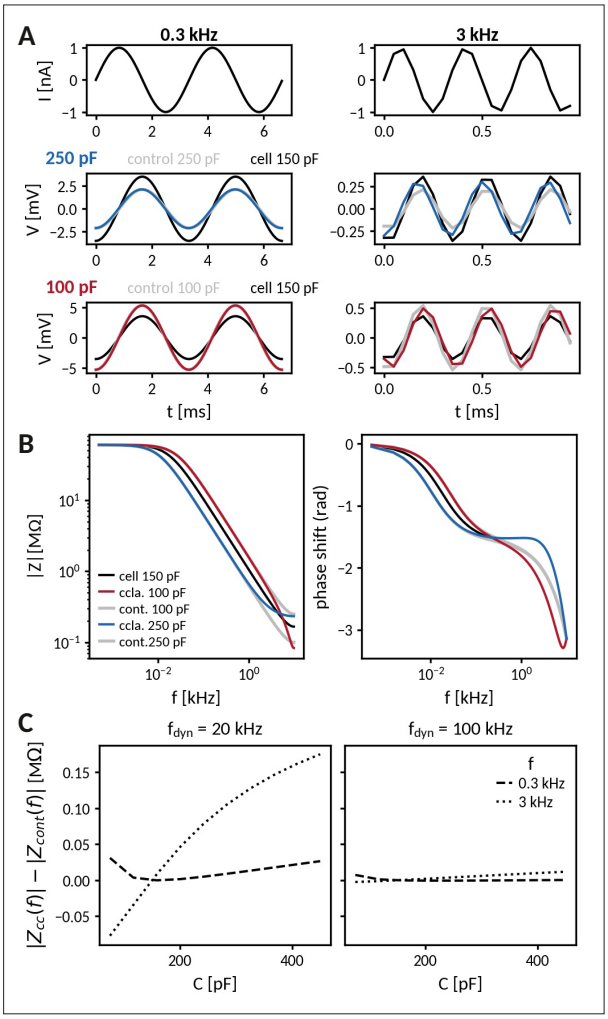

Figure 1—figure supplement 1. Impedance analysis of an RC circuit coupled to the capacitance clamp. (**A**) Injection of an oscillating current at 300 Hz (left) and at 3 kHz (right) to a passive cell (RC-circuit) with voltage responses clamped at an increased (middle) and a decreased capacitance (bottom). Black lines indicate the response of the cell at the original capacitance and gray lines those of the corresponding control cells. (**B**) Comparison of frequency-dependent impedance and phase shift of a cell at the above capacitances (black: cell capacitance, blues: clamped, gray: control). (**C**) Difference of impedances at 300 Hz (dotted) and 3 kHz (dashed) for clamped and control cell across different capacitances and for dynamic clamp frequencies of 20 kHz (left) and 100 kHz (right).

5 Discussion

5.1 Summary

This cumulative thesis investigated the role of cooperative ion channels (Publication COOPMEM) and variations in cell capacitance (Publication CAPCLAMP) for the electrical dynamics of neurons and other excitable cells. In studying these experimentally observed, but rarely considered aspects of excitable membranes, these two lines of research explored neuronal dynamics beyond the standard modeling assumptions of independent channel gating and membrane capacitance as a biological constant. The main results of this exploration are a new model-based hypothesis for the function of ion channel cooperativity in cell-autonomous short-term memory and the first experimental technique to artificially modify cell capacitance in biological neurons.

1. Small clusters of strongly-coupled cooperative ion channels have been shown to act as bistable conductances, whose memory capabilities can mediate persistent spiking – a firing mode suited to maintain information on past activity in a single neuron.

2. A new dynamic clamp protocol able to mimic a cell capacitance change in an intracellularly recorded neuron has been proposed and demonstrated to affect spike shape, ionic currents, and firing frequency in dentate gyrus granule cells.

In Publication COOPMEM, cooperative channels were analyzed in a model combining two central factors: the observed clustering of interacting channels and a potential regime of strong coupling. Strong coupling between channels has previously been suggested as a mechanism for highly synchronous opening of channels, but the potential of such positive feedback for cellular short-term memory has remained unnoticed. The central model prediction established here is that a cluster of strongly coupled channels acts like a bistable conductance – a macro-channel that keeps track of recent electrical activity.

The robustness of this memory was evaluated by relating the bistability to cluster size, coupling strength, and channel kinetics. The critical coupling strength required for bistability could be derived from the steepness of the single

channel activation curve and the cluster size. Smaller clusters were observed to be prone to channel noise. But already at about ten channels, the expected lifetimes of the open and closed cluster configuration could be shown to exceed the single channel time constant in the millisecond range by multiple orders of magnitude up to several seconds and more. Consequently, cooperativity suggests itself as a cellular mechanism for a membrane-based second-long short-term memory.

Finally, ion channel cooperativity was demonstrated to offer an alternative mechanism for cell-autonomous graded persistent activity (GPA). GPA has been difficult to explain and is thought to rely on forms of indirect calcium-mediated feedback between independently-gating channels. Cooperative channels, however, assembled into an ensemble of bistable clusters were observed to also equip a modeled cell with the graded, stable, and activity-modulated conductance required for GPA. The mechanism is robust enough to mediate GPA in biological neurons as confirmed by dynamic clamp injection of cooperative channels. Combined, the results of Publication COOPMEM demonstrate that cooperative interactions hidden in a small subset of spatially-clustered channels, different from the populations directly involved in action potential generation, can increase the functional repertoire of a neuron and contribute, in interaction with the surrounding network, to working memory.

In Publication CAPCLAMP, the established dynamic clamp technique to insert virtual conductances was developed further to enable virtual capacitance changes. The protocol – termed capacitance clamp (CapClamp) – is the first tool to precisely and flexibly alter capacitance in biological neurons. This neuronal modification, so far not accessible in experiments, is shown to enable a different approach to study neuronal excitability and the role of biologically observed exceptions to the rule of constant membrane capacitance.

Capacitance alteration exploits the closed loop of the dynamic clamp in a new way. Different from classical conductance injection, where a current is added to mimic the presence of the modeled channel, capacitance alteration relies on a clamping current that estimates the rate of change of the membrane potential and dynamically adjusts it to the value expected for the chosen target capacitance. For this estimation, as shown in the derivation of the clamping currents, the proposed protocol requires a measurement of the original *local capacitance of the clamped compartment*[1]. In this regard, the capacitance clamp

[1]Note that if the capacitance physically changes during a capacitance clamp experiment, this is not automatically detected by the protocol and an updated capacitance measurement is needed to correctly adjust the clamping currents. In this way, the expression of "clamp" in capacitance clamp differs from the one in voltage and current clamp, which fix the corresponding physical variables at a given value. The term capacitance clamp is instead

inherits a constraint common to all patch clamp techniques, the space clamp, namely that they operate locally at the recording site.

Thorough testing and analysis of the CapClamp in a series of simulations and experiments ensured that the technique is practical and robust. In a simple passive cell model (RC circuit), the CapClamp achieved the expected changes in the membrane time constant. Simulations of a biophysical neuron model with active sodium and potassium channels coupled to the CapClamp showed that practically available dynamic clamp frequencies of 20 kHz are sufficient to accurately capture the effects of capacitance on spike shape and firing frequency.

Finally, experiments with rat dentate gyrus granule cells (DGGCs) confirmed that the CapClamp allows electrophysiologists to alter capacitance in biological electrotonically complex neurons. A local capacitance measurement method was presented to estimate the near-somatic capacitance and then verify its alteration upon clamping. In the tested range from 60% to 300%, measured and targeted capacitance values matched well. Effects on spiking and firing frequency were also found to be consistent with the results from the simulated neuron, indicating that in DGGCs the capacitative load of the soma affects the site of action potential initiation.

In a set of illustrative applications, the CapClamp was used to alter temporal integration in DGGCs and to study energy consumption during spiking at different capacitances. These proof-of-principle experiments recaptured the two-fold motivation for developing the capacitance clamp. First, via control over capacitance, the CapClamp sets the membrane time constant and thereby integrative properties of a neuron. This clean temporal modification of voltage dynamics, not possible via conductance changes, has been exploited in theory-driven approaches to understand neuronal firing types and might prove useful in experiments. Second, against its reputation as being a biological constant, capacitance can vary both in physiological contexts as well as with new neural stimulation techniques like infrared or ultrasound. As shown in the DGGCs experiments the functional consequences of such alterations, like for example a reduced energetic cost per action potential at a decreased capacitance, can be elucidated via the CapClamp.

In the following discussion, a critical assessment of these two works is presented and future research questions building on their results are sketched, beginning with Publication COOPMEM.

---

inspired by the "conductance clamp", an alternative name for the original dynamic clamp (Reyes, Rubel, and Spain 1996).

5.2 Cellular short-term memory by cooperative ion channel gating

The assessment of Publication COOPMEM starts with a more detailed examination of the biological plausibility of bistable gating by cooperativity, leading to questions about how the strong coupling regime affects channels with more complex gating schemes. Next, cooperativity is compared to the other major mechanism for cellular short-term memory, calcium-mediated feedback on channel activity, followed by a brief outlook on how these two feedback mechanisms could potentially be combined. After this inspection of mechanisms, the long-standing question of the function of cell-autonomous memory in networks and working memory is discussed. Finally, the subchapter concludes with ideas for future modeling studies on cooperativity, including dendritic memory and heterogeneous clusters.

5.2.1 Biological plausibility

The central prediction of Publication COOPMEM is a cluster bistability for strongly cooperating channels. As discussed in the article, it relies on biologically plausible assumptions for the cluster sizes and suggests concrete voltage clamp experiments to test whether candidate cooperative channels like calcium or TRP channels are coupled sufficiently strong for the bistable regime. Here, the robustness of the proposal is further examined concerning the physiologically relevant modeling assumptions of basic channel kinetics with only two states and the linear voltage-shift model of cooperativity.

The role of channel inactivation An obvious way to interfere with the bistability of a cluster is channel inactivation. If cooperative channels have an inactivated state in addition to the open and closed one considered in Publication COOPMEM, open channels might – despite mutual facilitation with their coupled neighbors – first inactivate and then return to the closed state. Whether the conductance of such cooperative inactivating channels can still be bistable and which effects are expected for the membrane potential dynamics (that could involve other channel populations) depends on the gating scheme and the nature of the coupling.

How inactivation can interfere with the conductance bistability is illustrated by the case of strongly-coupled inactivating sodium channels, proposed as a mechanism for rapid spike onset in cortical neurons (Naundorf, Wolf, and Volgushev 2006; Huang, Volgushev, and Wolf 2012). As activation is strongly cooperative for these channels, their activation curve is expected to have the

same "S"-formed shape as the one reported in Publication COOPMEM[2]. Still, the conductance of these channels would not be bistable and should not exhibit a hysteresis with respect to voltage, because the open state is destabilized by voltage-independent inactivation as apparent in their gating scheme:

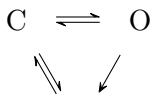

Considering the implications for membrane potential dynamics, another difference is that the all-to-all coupled population of sodium channels studied by Naundorf, Wolf, and Volgushev is directly involved in the generation of the action potential. In this way, the synchronous opening of these channels achieves the desired rapid onset of the spike. To terminate the spike, however, inactivation becomes important, because it circumvents the bistability and allows the channels to close again. The further consequences for firing are difficult to judge because their analysis only focused on the first generated spike. Repetitive firing, for example, is only mentioned in a later version of the model where the sodium channel population is split into a cooperative and a non-cooperative fraction (Öz, Huang, and Wolf 2015). In Publication COOPMEM, in contrast, interference between spike generation and the effects of strong coupling is avoided by placing cooperative interactions in a separate channel population. Concluding, even in the absence of bistability, the regime of strong might still be exploited by inactivating channels, e.g., for synchronous gating. To further guarantee functional spiking in the presence of strong coupling, it appears that cooperative and AP-generating populations should not (completely) overlap.

There are scenarios, where inactivating cooperative channels could retain bistable gating dynamics and potentially still support cell-intrinsic memory. On the one hand, cooperative interactions in the above gating scheme could additionally affect the transition to the inactivated state (Hichri, Selimi, and Kucera 2020). Otherwise, the bistability of a cluster is also expected to be preserved, when the inactivating gate is independent of the activation gate(s) (independence in the sense that except for the indirect coupling via the membrane potential they do not interact). This is for example the case in the classical description of the sodium channel in the Hodgkin-Huxley model (Koch 1999) (simplified to a single closed state instead of three)

[2]Naundorf, Wolf, and Volgushev, however, display the activation curve as a step function with a sudden jump from the closed to the open state (as they are interested in the synchronous opening of these channels) and do not consider the potentially bistable regime.

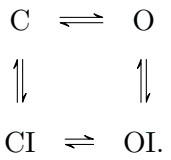

With such a gating scheme, it is possible that a cooperative inactivating population (separate from the spike generating channels like in Publication COOPMEM) could still mediate graded persistent activity. Channels in an open state (O) might inactivate (OI) during a spike, but the open activation gates would continue to mutually facilitate each other. Back at the resting membrane potential, the channels would return to the non-inactivated open state (O) and drive the membrane potential back to the spike threshold.

To summarize, whether cluster bistability occurs in the presence of inactivating channels depends on the channel kinetics as well as the coupling. The scenarios discussed above could be quantitatively analyzed by extending the cluster model from Publication COOPMEM. To constrain such cluster models with complex single channel kinetics, more experimental data is needed, because these clusters have a large state space and many transitions can be affected by cooperativity (Hichri, Selimi, and Kucera 2020).

The role of the cooperativity model Cluster bistability requires a strong coupling regime, but it is not expected to depend on a specific form of interaction. Generally, the main requirement is that the mutual facilitation between the channels can outweigh the activation set by the membrane potential. In Publication COOPMEM, these requirements are quantified for the theoretically convenient linear voltage-shift model. Although a heuristic description, it can be shown to obey microscopic reversibility, a condition for any physically valid cooperativity model as specified by Hichri, Selimi, and Kucera (in other words, the altered transition rates can in principle be mapped to a modified energy landscape, as demonstrated in the Appendix).

While physically consistent, the voltage-shift model so far has not been fit to any of the experimentally observed instances of cooperative gating. To account for experimental data, the model might need adjustments like a saturation of the coupling when multiple neighboring channels are in the open state (corresponding to a non-linear form for the shift function in Equation 2.7) or a more sparse interaction graph instead of all-to-all coupling. If the coupling strength is still sufficient, such a generalized voltage-shift model should allow for bistability just like the simplified linear version.

5.2.2 Comparison to calcium-based mechanisms of cell-intrinsic short-term memory

Direct positive feedback by ion channel cooperativity offers an additional mechanism for cell-intrinsic short-term memory. The experimental question about the still unknown nature of the channels underlying graded persistent activity, including the possibility that they are cooperative, has been discussed in Publication COOPMEM. Here, cooperativity and the major alternative mechanism, calcium-mediated feedback between channels are compared from a model-driven perspective, focusing on functional differences, mathematical similarities, potential complementary roles, and external modulation.

Differences and similarities to the calcium-based model of graded persistent activity A long-standing hypothesis on the mechanism of GPA by Fransén et al. is based on calcium control of a channel-regulating protein (Fransén et al. 2006). Although based on a physiologically different mechanism from the cooperativity hypothesis, the Fransén model exploits a similar mathematical pattern to achieve the multistability in firing required for GPA. It proposes the existence of a regulatory protein X whose availability depends on intracellular calcium and determines the amount of active I_{CAN} carrying channel. The number of available X proteins (or equivalently the number of activated CAN channels) hence corresponds to the number of open clusters in the cooperativity proposal. While the clusters are bistable with respect to the membrane potential, the availability of the X protein is bistable with respect to the intracellular calcium concentration. Therefore, the availability of X proteins, similar to the number of open clusters, remains constant at low firing frequencies but can be increased during periods of high firing and decreased during periods of hyperpolarization.

Comparing both proposals, a strength of the Fransén model is the bistability with respect to the calcium concentration. In this way, the concentration of the X protein (or equivalently the ratio of active CAN channels) is expected to remain truly constant during the self-sustained low firing with intracellular calcium concentration in the bistable regime. For the clusters, in contrast, a few channels are transiently opening during the high membrane potential values of a spike. As a result, long channel time constants are required to reduce the chance of a cluster switching to the open state during low firing.

A conceptual advantage of the presented cooperativity model is that it specifies the mechanism underlying the central bistability – namely the positive autofeedback between the coupled channels. As a result, the cooperativity model can make concrete predictions on the extent of the bistable regime and

the expected memory robustness. For the bistability of protein X with respect to the calcium concentration, in contrast, a mechanistic understanding is missing. It is an interesting parallel that one potential feedback loop implementing the bistability in the Fransén model could be the cooperative binding of calcium ions to an intermediate signaling molecule, a system that could be modeled in a similar way as the cluster of cooperative channels.

Combined feedback loops Calcium- and cooperativity-mediated feedback loops, so far regarded separately, might also act together. In a combined model of calcium-dependent cooperativity, spiking could trigger calcium inflow, which either directly or through a secondary messenger unlocks the cooperative gating mode. The increased activation of the coupled channels leads to an additional current that drives self-sustained firing and calcium inflow, closing the feedback cycle. Evidence for parts of such a combined feedback cycle has been reported for CaV1.3 channels. During spiking, calcium inflow induced coupling of previously independent channels. In turn, artificially coupling channels increased the spontaneous firing of hippocampal neurons (Moreno et al. 2016). In a combined feedback cycle, weak channel cooperativity might suffice for persistent activity, because clusters are not required to be bistable, but solely need to have a steeper activation curve.

Modulation of cell-intrinsic memory mechanisms An interesting functional dimension for cell-intrinsic memory mechanisms is how the memory mode can be modulated externally. GPA, for example, is only observed in the presence of carbachol, a substance mimicking the action of acetylcholine (Egorov et al. 2002) – a neuromodulator fittingly implicated in working memory (Newman et al. 2012). It remains an open question how acetylcholine, which triggers a variety of downstream signaling by activating muscarinic receptors, modulates the ion channels underlying persistent activity.

Within the class of calcium-based models, acetylcholine appears to close the feedback cycle by activating calcium-regulation of the channels that set the excitability of the cell. An example of such a controlled cellular memory mechanism is the Ether-a-go-go-related gene (ERG) potassium channel (Cui and Strowbridge 2018). These channels close in response to high calcium concentrations, but due to an unidentified molecular AND logic only in the presence of acetylcholine. If the channels are allowed to close, this leads to a second-long increase in subthreshold excitability after a period of activity. For the cooperativity proposal, a corresponding control mechanism could be envisioned by which channels only link and interact when acetylcholine prepares

the corresponding intracellular environment. A case of external regulation of cooperativity is the coupling of CaV1.3 channels, which is conditioned on a mechanistic link between two channel proteins via calmodulin, a calcium-activated messenger protein (Moreno et al. 2016).

5.2.3 Role of persistently active neurons in networks and working memory

A cell-autonomous persistent activity like GPA suggests a role for flexible short-term storage and accumulation of information required for cognitive processes like working memory. Neurons capable of self-sustained firing are part of brain networks implicated in short-term memory functions such as path integration in the entorhinal cortex (Egorov et al. 2002; Egorov, Unsicker, and Von Bohlen Und Halbach 2006) or evidence accumulation and decision making in the prefrontal cortex (Winograd, Destexhe, and Sanchez-Vives 2008). To date, models of persistent activity in these networks, however, focus mostly on synapse-based memory (Durstewitz, Seamans, and Sejnowski 2000; Compte 2006; Zylberberg and Strowbridge 2017). To underline the relevance of cell-intrinsic mechanisms such as ion channel cooperativity proposed here, ideas on how they might complement existent network models are discussed in the following.

Network models of short-term memory A major class of network models of persistent activity is built on the hypothesis of synaptic reverberation (Amit 1995). Similar to the cluster of cooperative channels, the network acquires bistability through the positive feedback between connected neurons whose intrinsic memory is limited to several milliseconds. A model system to study synaptic reverberation are neurons from the oculomotor system, which integrate movements of the eyes into persistent activity encoding the eye position (Seung et al. 2000). For such an essential and stereotyped task, the recurrent connectivity could be genetically predetermined, although the required precision speaks in favor of other mechanisms to make this network more robust (Goldman et al. 2003)

The enormous flexibility of more general short-term memory is however hard to reconcile with the idea of pre-wired neuronal ensembles or slowly learned ones by long-term synaptic plasticity. Thus, such fixed neuronal ensembles have been proposed to underlie expert "crystallized" forms of short-term memory, whereas novice "liquid" forms require other mechanisms such as chaotic dynamics in random networks (Barak et al. 2013).

Flexibility and robustness via cell-intrinsic memory Cell-autonomous memory could offer an alternative for a more flexible formation of neuronal ensembles. Among a set of weakly connected neurons, each capable of persistent activity, any combination of neurons can become a persistently firing ensemble (Compte 2006). Similarly, in the more realistic case of a broadly connected network, a persistent increase of excitability could select stimulated neurons into newly forming ensembles. Such a cell-intrinsically driven sustained activity is for example observed in the dentate gyrus (Larimer and Strowbridge 2010; Walker, Pavlov, and Kullmann 2010). As these ensembles are not synaptically preconfigured, the network might store stimuli that it has not yet encountered. An interesting observation in this regard is a recent study on the formation of cellular assemblies for long-term memory by Alejandre-García et al. (Alejandre-García et al. 2022). They tried to artificially "imprint" new cellular assemblies into a network via prolonged optogenetic stimulation. Afterwards, contrary to the classic model of synaptic ensemble formation, neurons in these artificial assemblies were not stronger connected than before. Instead, the stimulated neurons exhibited increased intrinsic excitability. This observation emphasizes the need to study networks with hybrid memory mechanisms combining synaptic connectivity and cell-intrinsic properties.

Another role of cell-autonomous memory could be to stabilize network-based delay activity. Exploring the conditions for robust synaptic reverberation, Wang observed that persistent activity in a simulated network connected by fast AMPS synapses alone tends to vanish over time and that slower NMDA synapses are needed to stabilize it (Wang 1999). Focusing on synaptic time scales, this study considered pyramidal cells whose integration time was limited by their membrane time constant. Longer cell-intrinsic time scales provided by calcium- or cooperativity-mediated feedback loops might be a further robustness measure to prevent reverberatory activity from dying out (Compte 2006). Neuronal and dendritic bistabilities have indeed been shown to make delay activity more robust against perturbations and imprecise connectivity, but this demonstration was limited to rate-based model neurons (Camperi and Wang 1998; Goldman et al. 2003). In conductance-based spiking neuron models, slow calcium-activated currents were observed to act in a similar stabilizing fashion complementing the role of NDMA synapses, yet the considered levels were not sufficient for cellular bistability (Tegnér, Compte, and Wang 2002). How biologically realistic cell-intrinsic memory integrates into a network of spiking neurons remains to be further explored.

Studying larger networks of neurons with complex cellular memory like the ensemble of clusters of cooperative channels will get computationally expensive. For such explorations, simplified models of persistent activity might be better

suited (Rodriguez et al. 2018).

5.2.4 Future directions and further roles of cooperative gating

Spatial distribution of clusters One future direction to explore is the question of where to strategically place clusters of cooperative channels in a neuron to exploit their memory function. Even in the simple one-compartment neuron model studied so far, the enlarged memory capacity implicitly depends on a spatial property, namely the arrangement of channels into clusters. In more realistic morphologies, the distribution of bistable clusters throughout the dendritic tree may further enhance cell-autonomous memory capabilities. Especially, in large neurons, where dendritic sites are electrically decoupled, clusters might represent the recent synaptic activity on a specific dendritic branch and persistently alter the response to further inputs at the same site. Such dendritic attenuation or boosting could be another way to complement synaptic short-term plasticity mechanisms (Debanne, Inglebert, and Russier 2019).

Cooperativity in heterogeneous clusters

As demonstrated in Publication COOPMEM, a cluster of identical channels exhibits emerging dynamics, qualitatively different from those of its constituents. What if clusters were composed of various channels, maybe with opposing functions?

The majority of experimental evidence of cooperativity is for homogeneous channel ensembles, but interactions have also been observed between different channel types, for example in clusters of BK potassium and CaV1.3 calcium channels (Vivas et al. 2017). Channels might, as in this case, differ in their activation profiles and carry opposing currents. This makes it difficult to preview how heterogeneous clusters behave and how they contribute to neuronal dynamics. A quantitative approach to these questions can make use of the here presented cluster modeling, which can accommodate heterogeneity, for example, via different channel activation functions.

Concerning the potential of heterogeneous clusters, an interesting thought experiment is in what could be termed counterfactual biology: cooperative gating between the two main channel types underlying the typical action potential in the Hodgkin-Huxley model – the depolarizing sodium and the delayed-rectifier potassium channel. Admittedly, coupling between these two channels has not been observed and appears unlikely given the long history of research on their gating behavior. So why even consider such a coupling?

An aspect of spike generation that has received significant attention is the energetically costly overlap of sodium and potassium currents (Sengupta et al. 2010). Some mammalian axons exhibit a close to optimal reduction of overlap. But for independent channels, it has been shown that the underlying tuning of time constants comes at a cost, for example, the maximum firing frequency that can be obtained (Hasenstaub et al. 2010). At first sight, negative cooperativity appears as an ideal candidate to further minimize this overlap, reducing the simultaneous opening of sodium and potassium channels.

Although purely speculative, a "counterfactual" model neuron with negative Na^+-K^+ coupling might yield insights into the question of why some channels cooperate and others do not. Given that these channels are observed to operate independently, it is expected that such an examination unveils why cooperativity has not emerged as a solution to the overlapping current problem. Is action potential generation even possible with coupled Na^+-K^+ clusters? And if this were the case, could the overlap be minimized given that any interactions would be local, so that in one cluster sodium channels could be open while in another one potassium channels are open?

Future work addressing the role of cooperativity in heterogeneous clusters can build on the modeling techniques applied in Publication COOPMEM. The applications of the other resource developed in this thesis, the capacitance clamp, are discussed next.

5.3 Capacitance clamp – a novel tool to probe neural dynamics

Major limitations and hardware requirements of the capacitance clamp technique are addressed in the discussion provided in Publication CAPCLAMP. The following section, therefore, elaborates on how the technique can be applied, including ideas like the vision to characterize bifurcations in neuronal dynamics, studying neuronal homeostasis, and a potential extension to emulating a capacitance varying in time. Finally, an outlook on future model-driven closed-loop experiments is provided from the dynamic clamp for single cells to the opto-clamp for whole networks.

5.3.1 Ideas for further applications of the capacitance clamp

A firing pattern map in capacitance-conductance-current C-g-I space The capacitance clamp might enrich experimental characterization protocols of neurons. An fI curve, the canonical way to characterize a cell, maps how a

neuron reacts to stimulation, but it provides no information on how a neuron reacts to modulation. Neuronal modulation, however, can profoundly change the input-output function of a neuron – changes that in one case are crucial for flexible context-dependent computation, but that in another case provoke pathological brain activity. A general map of modulatory influences is impossible to obtain given their diverse origins from environmental factors like temperature (Roemschied et al. 2014; Ratliff et al. 2021), or network activity (Chance, Abbott, and Reyes 2002), to targeted neuromodulation (Stiefel, Gutkin, and Sejnowski 2008). Theory-driven explorations of neuronal excitability, however, suggest that a basic informative map of modulations, can be obtained by characterizing how firing patterns respond to capacitance C and leak conductance g_L changes (Kirst et al. 2015; Hesse, Schleimer, and Schreiber 2017). Experimentally, the combination of the here presented capacitance clamp and the "classic" dynamic clamp can realize such a mapping, which might provide a basis to predict responses to other modulatory factors.

Searching for critical capacitances Modulatory influences on neuronal firing are especially interesting if they can switch the dynamical type of firing in a neuron. It is currently unclear if neurons try to actively stay away from such critical switches or even tune into them in order to exploit their functional consequences. In this regard, the demonstration of the capacitance clamp in the dentate gyrus granule cells can be viewed as a proof-of-principle experiment to identify how "close" or "far" neurons are from such switches. At their original capacitance, DGGCs exhibited a continuous fI curve indicating a SNIC-type spike onset. According to modeling, increasing the capacitance of such a cell over a critical value is predicted to change the spike onset to the less extensively studied, but computationally interesting HOM-type as determined by the underlying (technically codimension-two) saddle-node-loop (SNL) bifurcation (Hesse, Schleimer, and Schreiber 2017; Hesse et al. 2022). In a reexamination of the capacitance clamp experiments in DGGC, the following discussion provides preliminary results on this prediction.

One hallmark of the SNL transition is that a neuron firing close to the current threshold is expected to double its firing frequency when crossing a critical capacitance value (see Fig. 5.1). Simulations confirmed that a capacitance-clamped neuron exhibits this doubling of the firing frequency at the theoretically expected capacitance values – confirming that the capacitance clamp can induce and locate the transition. Among the clamped DGGCs, however, all cells decreased their firing rates when capacitance was increased (see Publication CAPCLAMP Fig. 4). This observation indicates that the critical capacitance

values of DGGCs lie above the tested range.

This distance from the SNL transition in capacitance space could reflect that DGGCs, at least in a brain slice environment, are not operating "close" to this switch. Based on the argument that capacitance approximates effects of other parameters which change the relative timescales of the membrane potential and channel gating, the firing type of DGGCs would then be expected to also exhibit a degree of robustness against, for example, an increased temperature.

Further experiments are required to confirm the robustness of the DGGC firing type against capacitance changes. For a demonstration that the transition can be experimentally induced, further attempts should aim at increasing the tested capacitance range. Robust recordings at higher capacitances than reported in Publication CAPCLAMP were possible and can potentially be improved further by investing in capacitance measurements and more accurate voltage monitoring.

If neurons remain at their firing type even within such an increased capacitance range, another measure could be to modulate them into a regime, where they are closer to the transition, e.g., by altering the temperature or adding a leak conductance via the classic dynamic clamp. Furthermore, the search could be complemented by measuring other fingerprints of crossing the SNL bifurcation like the bistability between firing and resting state, detectable in the noise-driven spiking statistics (Schleimer, Hesse, and Schreiber 2019).

In the interpretation of the distance to a firing type measured by the capacitance clamp, it is important to note that the technique only controls the near-somatic capacitance. The comparably large dendritic capacitative load remains constant – a scenario whose effects on the distance and nature of the possible transitions have to be further investigated. The prediction of the SNL transition is based on point neurons without a spatial dimension (Hesse, Schleimer, and Schreiber 2017). To test how the locality of the capacitance changes affects the SNL transition, analysis and simulations of multicompartmental models should be used (Gowers and Schreiber 2021).

Probing neuronal homeostasis Perturbation of neuronal firing by modifying capacitance could contribute to testing hypotheses on how neurons self-organize into a functional regime. During development or in response to environmental changes, neurons and networks adjust their properties to achieve or respectively maintain function. The homeostatic mechanisms behind the resilience of neural systems (Turrigiano and Nelson 2004; Turrigiano 2011; Wu et al. 2020), as well as their failure in several brain disorders (O'Leary 2018; Mizusaki and O'Donnell 2021), remain only partially understood (Davis 2006; Niemeyer, Schleimer, and

Schreiber 2021).

A specific question in this regard is how neurons control the combination of ion channels determining their firing type (Turrigiano, Abbott, and Marder 1994; Schulz et al. 2008; Goaillard and Marder 2021). Levels of ion channel expression in neurons of the same type vary significantly, suggesting that neurons regulate firing behavior rather than channel numbers (Schulz, Goaillard, and Marder 2006). To maintain a firing property, like the average firing rate, neurons could sense activity, e.g., via intracellular calcium levels, and correspondingly adjust channel function (Stemmler and Koch 1999) or expression (Liu et al. 1998; O'Leary et al. 2014). Complementary to such activity-dependent mechanisms, direct feedback between proteins could link the expression of different channel types to provide functional combinations (Kulik et al. 2019; Tyssowski et al. 2019). One way to experimentally distinguish contributions of activity-dependent mechanisms of channel homeostasis from other forms is to electrophysiologically control membrane potential dynamics, for example via enforcing a voltage trajectory by the voltage clamp and monitoring its long-term effects on channel expression (Santin and Schulz 2019). Extending this direction, capacitance clamp and dynamic clamp experiments could test whether and how neurons compensate for altered cell capacitance, additional ionic conductances, or combinations thereof. Such an approach has the advantage that it isolates the activity-dependent part of homeostasis, because the actual cellular environment does not change.

Another natural growth scenario, interesting for channel homeostasis, that can be mimicked via the dynamic clamp is the emergence of a dendritic branch. One could approximate the additional capacitative and resistive load via a combination of capacitance and dynamic clamp. Such an approach, however, remains approximative because the impedance of a dendrite cannot be captured by a simple RC circuit due to its spatial extent (Koch 1999). A more accurate alternative would consist in simulating the entire dendrite and connecting it to the biological neuron via the axial currents flowing at the connection point.

Emulation of dynamic cell capacitance In addition to the permanent capacitance alteration considered so far, the capacitance clamp can be extended to mimic a capacitance varying in time. Technically, this amounts to replacing the target capacitance by a time-dependent function $C_t(t)$ and adding the usually neglected part of the capacitative current $-\dot{C_t}(t)V$ (see Eq. 2.1). This current is simple to implement via the dynamic clamp because it only depends on the recorded membrane potential and the selected capacitance shape. It thus has the same form as the current through an ionic conductance with a 0 mV reversal

potential and a conductance given by the rate of capacitance change.

If capacitance changes are fast and of sufficient amplitude, the associated capacitative currents can evoke relevant voltage responses and might even elicit action potentials. From the known cases of a dynamic capacitance in physiological scenarios, the associated currents are expected to be relatively small[3]. Stronger capacitative currents are supposed to underlie two novel neural stimulation techniques based on infrared light and ultrasound. Infrared stimulation is hypothesized to excite the firing of neurons by fast temperature-induced changes in membrane capacitance (Shapiro et al. 2017). In ultrasound stimulation, the oscillating pressure could induce rapid capacitance changes by modulating membrane thickness (Plaksin, Shoham, and Kimmel 2014).

A capacitance clamp extended to emulate a dynamic capacitance could provide a way to test such hypotheses in a controlled fashion. An important limitation that would need to be tested for is the maximum frequency of time-varying capacitance that could be reliably captured. One advantage of an emulated capacitance change is the ability to separate the role of the altered capacitance value from the capacitative current by either emulating both or only a single one.

5.3.2 Dynamic clamp of capacitance and other cellular parameters beyond conductances

The dynamic clamp has been applied in many variations since its introduction in 1992. The large majority of applications exploited the underlying closed-loop current injection to insert virtual conductances as originally suggested. The capacitance clamp is a demonstration that the dynamic clamp can be useful to study neuronal parameters different from conductances. The following outlook discusses the potential of closed-loop model-guided protocols in neurons and networks.

A closer look at studying conductances via the dynamic clamp In the realm of conductances, it is important to emphasize that the dynamic clamp goes beyond the insertion of ion channels modeled according to the Hodgkin-Huxley

[3] In a study of anesthetized cats, for example, cell capacitance of cortical neurons was measured to undergo a $\approx$ 1 Hz oscillation with an amplitude of 50-150 pF in correspondence with the membrane potential switching between an up- and a down state produced by the surrounding network (Amzica and Neckelmann 1999). These capacitance oscillations were hypothesized to stem from cell swelling in response to altered ionic concentrations during the phases of high activity or from altered gap junction functioning. Given a resting membrane potential of around -75 mV, the capacitative current amounts to 50 pF $\cdot$ 1 Hz $\cdot$ 75 mV $\approx$ 4 pA.

description. One example was the insertion of clusters of cooperative channels with stochastic dynamics in Publication COOPMEM. In these experiments, cluster size and coupling strength were varied at will, a degree of control missing for real cooperative channels.

But the dynamic clamp cannot only insert additional conductances. It also can modulate currents already present in the cell's membrane. Peak conductances, for example, can be directly reduced or abolished by inverting the injected current. However, to avoid destabilizing the dynamics with this inverted current, an accurate model of the channel in question is required (Vervaeke et al. 2006). An approximate but more stable solution is to pharmacologically block the conductance of interest and then "re-inject" it virtually with the desired conductance level.

Another advantage of this "block"-"reinsert" approach is that it allows the experimenter to explore aspects of an existent ionic current that cannot be directly modified via the dynamic clamp. Replacing sodium channels in fast-spiking interneurons with virtual ones, Hasenstaub et al. for example tested how half activation voltage or gating time constant affects the energetic costs of spiking (Hasenstaub et al. 2010). In this way, the dynamic clamp could serve to screen the effects of channel phosphorylation or genetic mutations. A parameter apparently not yet studied in dynamic clamp experiments, but accessible in this approach is the reversal potential of a conductance.

Mimicking ionic concentration dynamics via the dynamic clamp Reversal potentials set the driving force of a current and have widespread effects on the electrical dynamics of a cell. As the reversal potential depends on the extra- and intracellular concentrations of the conducted ionic species, varying the reversal potential of a virtual conductance via the dynamic clamp would correspond to studying cellular excitability under different concentration conditions.

Actual concentration conditions and the associated reversal potentials, however, are dynamic. During strong spiking activity, potassium flows outside of the cell, temporarily exceeding the restorative activity of the Na^+-K^+ pump, and accumulates in the extracellular space. As a result, the reversal potential of potassium increases, cells become more excitable and potentially switch their excitability type (Contreras et al. 2021). Accounting for these concentration dynamics in the dynamic clamp is challenging because it would require additional electrodes to measure the concentrations and provide them to the running conductance model (Fröhlich et al. 2008; Heiny, Cannon, and DiFranco 2019).

An interesting theoretical proposal to circumvent the need for additional measurements is to infer the concentrations in real time from the recorded

membrane potential. Ullah and Schiff demonstrated accurate online estimation of the extracellular potassium concentration via a Kalman filter, but so far this demonstration remains restricted to a simulated neuron (Ullah and Schiff 2009). As the Kalman filter technique relies on a model of the whole dynamics of the recorded neuron, it is questionable whether it can be used in practice. Still, a further advantage of this online running digital copy of the real neuron would be that it provides other not directly observable variables like the membrane currents or the state of the gating variables.

Ways to improve the capacitance clamp protocol In principle, using Kalman filtering might further improve the capacitance clamp. It could reduce noise in the estimate of the transmembrane current and shorten the delay in the injection of the clamping current by relying on the predicted value. Practically, however, the value of this online estimation depends on how robust the technique is with respect to the neuron model, for example, the number of included ionic currents – a question that requires further investigation.

If a digital twin of the biological neuron was required, this would defy the original purpose of developing the capacitance clamp, namely probing the role of capacitance in the unknown physiology of a real cell. The proposed capacitance clamp protocol in contrast is suited for this purpose because it only requires measuring the cell capacitance, but no knowledge about the present ionic currents.

Designing subthreshold processing of neurons by shaping their impedance profile Subthreshold processing of neurons – how they react to small inputs – is determined by their electrical impedance profile. The mathematical impedance analysis of a clamped neuron demonstrated in Publication CAPCLAMP suggests a way to directly imprint a desired target impedance on a recorded neuron – extending the capacitance clamp to a form of "impedance clamp". Provided with a measurement of the cell impedance, for example via a ZAP current covering a large range of input frequencies (Schreiber et al. 2004), and given a target impedance, the coefficients of a linear dynamic clamp protocol could be optimized to minimize the distance between the two. As impedance is complex-valued, capturing both amplitude and phase of the linear response, an important non-trivial step in this minimization is the choice of an adequate distance measure.

Although more of a playful idea, such an "impedance clamp" might for example be useful to study links of subthreshold properties and spiking in a general fashion independent of the specific membrane components (conductances

and capacitance).

Closed-loop techniques to investigate and control network dynamics The dynamic clamp as an intracellular recording technique is bound to investigate the biophysical properties of one or up to a few neurons. With recent optical means to interact with large ensembles of neurons, however, the closed-loop principle behind the dynamic clamp could also be used on the network level. In all-optical neuroscience, experimenters monitor spiking activity and even the membrane potential with novel fluorescent indicators (Jin et al. 2012), while at the same time stimulating neurons via genetically implanting light-sensitive ion channels (Emiliani et al. 2015; Rost et al. 2022). While technically still challenging, optical monitoring and stimulation of neural activity can be combined for closed-loop paradigms – a form of an optical dynamic clamp. Called an 'opto-clamp' such systems can keep a network at a chosen firing frequency (Newman et al. 2015) and maintain average membrane potentials of neurons at desired levels (Bergs et al. 2022). In the future, opto-clamp applications might be possible that act more in a dynamic clamp manner, emulating neuronal or synaptic changes within the biological network.

In addition to providing new research tools, closed-loop stimulation paradigms on the network level are a promising route for therapeutic applications. The dynamic clamp, as well as the capacitance clamp, are related to model reference control, whose objective is to ensure that a system follows a given target dynamics (Hocker and Park 2019). Model reference control has been proposed as a theoretical framework for designing closed-loop brain stimulation that returns a network with pathological dynamics, e.g., with a detrimental oscillatory state, back to its functional physiological dynamics. In addition to precise monitoring and manipulation of neural activity, such control relies on good models of the system to be controlled – another reason among many for a thorough understanding of neuronal dynamics.

5.4 Conclusion

This thesis analyzed the consequences of revising two experimentally questionable assumptions of single neuron modeling, independent channel gating and membrane capacitance as a universal constant.

The results of this thesis demonstrate how to incorporate ion channel cooperativity and altered capacitance into neuronal models, and how to study them in biological neurons via closed-loop electrophysiology. The proposed role of cooperative channels in cell-autonomous memory gives further credence to the

emerging picture that cooperativity is not a by-product of the highly interactive nature of channels, but that these interactions serve functional adaptations. The novel capacitance clamp is expected to complement the electrophysiologist's toolbox, both to specifically shine a light on cases of varying capacitance and more generally as a way to study modulation of neuronal dynamics.

Concluding, this thesis provides predictions and tools to guide further investigations into the functional role of cooperative ion channels and varying membrane capacitance. It emphasizes the role of the variable properties of neurons, unlikely to be captured by a single standard model, to create the wide range of dynamics, which makes the brain such a powerful and adaptive organ.

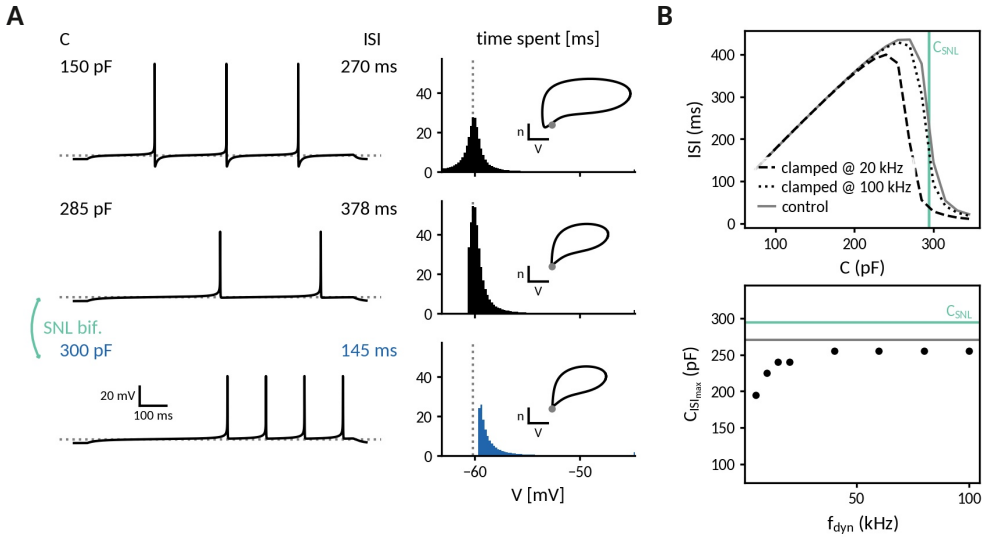

Figure 5.1: **Detecting bifurcations with the capacitance clamp. A** *Left*: In a simulated neuron model, spiking slows down when increasing capacitance (here up to 285 pF), but a further small increase to 300 pF abruptly doubles the firing frequency, a signature of the saddle-node-loop (SNL) bifurcation. *Right*: Histograms of the time spent at different membrane potentials between two spikes illustrate the origin of the frequency doubling, namely that beyond the critical capacitance the altered spike skips the slow approach to the "ghost" of the previous rest state (gray dashed line). This altered approach is also apparent in the insets showing the spike dynamics in the potassium gating n-voltage V plane. **B** The capacitance clamp can induce the SNL bifurcation and locate the critical capacitance C_{SNL}. *Top*: Frequency doubling, or equivalently halving of the interspike interval (ISI), is also observed when modifying capacitance via a simulated capacitance clamp at 20 kHz (dashed) and 100 kHz (dotted) dynamic clamp frequency (control simulation with actually altered capacitance parameter in gray and the expected critical capacitance C_{SNL} indicated in green). *Bottom*: Capacitance at maximal ISI against f_{dyn} shows that frequencies ≥ 40 kHz are required to correctly locate the bifurcation. For smaller frequencies, the bifurcation happens at a reduced capacitance value. Adapted from the preprint version of Publication CAPCLAMP, available at biorxiv.org/content/10.1101/2021.11.12.468368v1.

6 Appendix

6.1 Microscopic reversibility of the linear voltage-shift model

The voltage-shift model of cooperative gating is a heuristic description. In particular, it is a priori unclear whether this description is physically consistent and which interaction energies between channels are required for a given value of the coupling j. The following section confirms the physical consistency of the voltage shift-model and shows how to estimate these interaction energies.

Consider a dimer consisting of two identical coupled channels with an open state O and a closed state C. The channels have an activation curve $m(V)$ and a gating time $\tau(V)$. According to the voltage-shift model, the transition rates from the all closed CC state to the OC or OC state are just the single channel opening $\alpha(V) = \frac{m(V)}{\tau}$ and closing rates $\beta(V) = \frac{m(V)}{\tau}$, whereas the rates between the states with one open channel OC or OC and all open OO are correspondingly shifted by the coupling coefficient $\alpha(V + j)$ and $\beta(V + j)$.

To demonstrate that the voltage-shift model is compatible with microscopic reversibility, the altered transition rates have to be consistent with a modified energy landscape, either by a change in the energy of the states or the barriers between them (see Fig. 6.1). For the involved states and barriers, these modifications can be derived as:

- the state energy E_{OC} remains unaltered, because otherwise the closing rate back to the all closed state CC would be affected,
- the height of the energy barrier $\Delta_{\mathrm{OC}\leftrightarrow\mathrm{OO}}$ has to change by an amount $\delta\Delta_{\mathrm{OC}\leftrightarrow\mathrm{OO}}$ to obtain the altered opening rate $\alpha(V+j) = e^{-\frac{\delta\Delta_{\mathrm{OC}\leftrightarrow\mathrm{OO}}}{kT}}\alpha(V) \Rightarrow \delta\Delta_{\mathrm{OC}\leftrightarrow\mathrm{OO}} = -kT\log\frac{\alpha(V+j)}{\alpha(V)}$,
- so that the state energy E_{OO} has to change by an amount δE_{OO} to obtain the altered closing rate, which is already affected by the modified energy barrier $\beta(V + j) = e^{\delta E_{\mathrm{OO}}/kT}e^{-\delta\Delta_{\mathrm{OC}\leftrightarrow\mathrm{OO}}/kT}\beta(V) \Rightarrow \delta E_{\mathrm{OO}} = kT\log\frac{\beta(V+j)}{\beta(V)} + \delta\Delta_{\mathrm{OC}\leftrightarrow\mathrm{OO}}$.

As an illustration, assume that the channels are half-activated at the current membrane potential $m(V) = 0.5$ and that the activity is increased to $m(V+j) =$

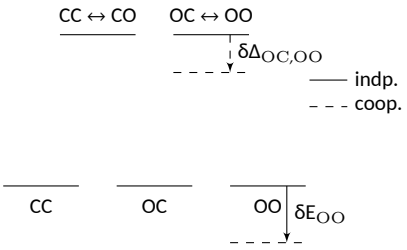

Figure 6.1: Energy levels (bottom) and barriers between states (top) of a cluster of two independent channels and the corresponding alterations to realize the cooperative interactions in the voltage-shift model.

0.75 when a neighboring channel opens. Consequently, the ratio of transition rates are $\frac{\alpha(V+j)}{\alpha(V)} = 1.5$ and $\frac{\beta(V+j)}{\beta(V)} = 0.5$ and the corresponding energy changes are $\delta\Delta_{\mathrm{OC}\leftrightarrow\mathrm{OO}} \approx -0.4kT$ and $\delta E_{\mathrm{OO}} \approx -1.1kT$. Thus such positive coupling would both lower the energy barrier – increasing the opening rate – and at the same time further decrease the energy of the all open state – reducing the closing rate. Energetic modifications on the order of kT appear plausible and are also found to be required to explain the altered gating behavior of dimers of cooperative sodium channel (Hichri, Selimi, and Kucera 2020).

For clusters that contain more than two channels, the same argument can be used iteratively to demonstrate that also interactions between multiple channels are physically consistent . Starting from the altered energy level of the state with n open channels, to obtain the desired opening rate $\alpha(V + nj)$, the height of the energy barrier to the state with $n + 1$ open channels is modified. Then the energy level of this state has to be adapted to get the closing rate $\beta(V + nj)$. This iterative procedure provides a well-defined series of changes to barriers and state energies. Whether these changes remain in the physiologically plausible regime depends on the number of involved channels and the coupling coefficient.

Bibliography

Aldrich, R. W., D. P. Corey, and C. F. Stevens (Dec. 1983). "A Reinterpretation of Mammalian Sodium Channel Gating Based on Single Channel Recording". In: *Nature* 306.5942, pp. 436–441. ISSN: 1476-4687. DOI: 10.1038/306436a0.

Alejandre-García, Tzitzitlini et al. (May 2022). "Intrinsic Excitability Mechanisms of Neuronal Ensemble Formation". In: *eLife* 11. Ed. by Lisa Giocomo, Ronald L Calabrese, and Christian Hansel, e77470. ISSN: 2050-084X. DOI: 10.7554/eLife.77470.

Amit, Daniel J. (Dec. 1995). "The Hebbian Paradigm Reintegrated: Local Reverberations as Internal Representations". In: *Behavioral and Brain Sciences* 18.4, pp. 617–626. ISSN: 1469-1825, 0140-525X. DOI: 10.1017/S0140525X00040164.

Amzica, Florin and Dag Neckelmann (1999). "Membrane Capacitance of Cortical Neurons and Glia During Sleep Oscillations and Spike-Wave Seizures". In: *Journal of Neurophysiology* 82.5, pp. 2731–2746. ISSN: 0022-3077. DOI: 10.1152/jn.1999.82.5.2731.

Anderson, David F., Bard Ermentrout, and Peter J. Thomas (2015). "Stochastic Representations of Ion Channel Kinetics and Exact Stochastic Simulation of Neuronal Dynamics". In: *Journal of Computational Neuroscience* 38.1, pp. 67–82. ISSN: 15736873. DOI: 10.1007/s10827-014-0528-2. arXiv: 1402.2584.

Bal, Thierry and Alain Destexhe, eds. (2009). *Dynamic-Clamp: From Principles to Applications*. New York, NY: Springer US. ISBN: 978-0-387-89278-8 978-0-387-89279-5. DOI: 10.1007/978-0-387-89279-5.

Barak, Omri et al. (2013). "From Fixed Points to Chaos: Three Models of Delayed Discrimination". In: *Progress in Neurobiology* 103, pp. 214–222. ISSN: 03010082. DOI: 10.1016/j.pneurobio.2013.02.002.

Beniaguev, David, Idan Segev, and Michael London (Sept. 2021). "Single Cortical Neurons as Deep Artificial Neural Networks". In: *Neuron* 109.17, 2727–2739.e3. ISSN: 0896-6273. DOI: 10.1016/j.neuron.2021.07.002.

Bergs, Amelie C. F. et al. (June 2022). *All-Optical Closed-Loop Voltage Clamp for Precise Control of Muscles and Neurons in Live Animals*. DOI: 10.1101/2022.06.03.494532.

Bettencourt, Jonathan C. et al. (2008). "Effects of Imperfect Dynamic Clamp: Computational and Experimental Results". In: *Journal of Neuroscience Methods* 169.2, pp. 282–289. ISSN: 08966273. DOI: 10.1016/j.jneumeth.2007.10.009.

Brette, Romain (Dec. 2013). "Sharpness of Spike Initiation in Neurons Explained by Compartmentalization". In: *PLoS Computational Biology* 9.12. Ed. by Nicolas Brunel, e1003338. ISSN: 1553-7358. DOI: 10.1371/journal.pcbi.1003338.

Brette, Romain and Alain Destexhe (2012). "Intracellular Recording". In: *Handbook of Neural Activity Measurement*. Ed. by Alain Destexhe and Romain Brette. Cambridge: Cambridge University Press, pp. 44–91. ISBN: 978-0-521-51622-8. DOI: 10.1017/CBO9780511979958.003.

Brette, Romain et al. (Aug. 2008). "High-Resolution Intracellular Recordings Using a Real-Time Computational Model of the Electrode". In: *Neuron* 59.3, pp. 379–391. ISSN: 08966273. DOI: 10.1016/j.neuron.2008.06.021.

Brunel, Nicolas, Vincent Hakim, and Magnus JE Richardson (Apr. 2014). "Single Neuron Dynamics and Computation". In: *Current Opinion in Neurobiology* 25, pp. 149–155. ISSN: 09594388. DOI: 10.1016/j.conb.2014.01.005.

Burrill, Devin R. and Pamela A. Silver (2010). "Making Cellular Memories". In: *Cell* 140.1, pp. 13–18. DOI: 10.1016/j.cell.2009.12.034.

Camperi, Marcelo and Xiao Jing Wang (1998). "A Model of Visuospatial Working Memory in Prefrontal Cortex: Recurrent Network and Cellular Bistability". In: *Journal of Computational Neuroscience* 5.4, pp. 383–405. ISSN: 09295313. DOI: 10.1023/A:1008837311948.

Castelfranco, Ann M. and Daniel K. Hartline (June 2015). "The Evolution of Vertebrate and Invertebrate Myelin: A Theoretical Computational Study". In: *Journal of Computational Neuroscience* 38.3, pp. 521–538. ISSN: 0929-5313, 1573-6873. DOI: 10.1007/s10827-015-0552-x.

Chance, Frances S, L.F Abbott, and Alex D Reyes (Aug. 2002). "Gain Modulation from Background Synaptic Input". In: *Neuron* 35.4, pp. 773–782. ISSN: 08966273. DOI: 10.1016/S0896-6273(02)00820-6.

Choi, Kee Hyun (2014). "Cooperative Gating between Ion Channels". In: *General Physiology and Biophysics* 33.1, pp. 1–12. ISSN: 02315882. DOI: 10.4149/gpb_2013076.

Choi, Kee-Hyun and Stuart Licht (May 2012). "ATP-Sensitive Potassium Channels Exhibit Variance in the Number of Open Channels below the Limit Predicted for Identical and Independent Gating". In: *PLOS ONE* 7.5, e37399. ISSN: 1932-6203. DOI: 10.1371/journal.pone.0037399.

Clatot, Jérôme et al. (2017). "Voltage-Gated Sodium Channels Assemble and Gate as Dimers". In: *Nature Communications* 8.1, p. 2077. ISSN: 2041-1723. DOI: 10.1038/s41467-017-02262-0.

Cohen, Charles C.H. et al. (Jan. 2020). "Saltatory Conduction along Myelinated Axons Involves a Periaxonal Nanocircuit". In: *Cell* 180.2, 311–322.e15. ISSN: 00928674. DOI: 10.1016/j.cell.2019.11.039.

Compte, Albert (Apr. 2006). "Computational and in Vitro Studies of Persistent Activity: Edging towards Cellular and Synaptic Mechanisms of Working Memory". In: *Neuroscience* 139.1, pp. 135–151. ISSN: 03064522. DOI: 10.1016/j.neuroscience.2005.06.011.

Contreras, Susana Andrea et al. (May 2021). "Activity-Mediated Accumulation of Potassium Induces a Switch in Firing Pattern and Neuronal Excitability Type". In: *PLOS Computational Biology* 17.5, e1008510. ISSN: 1553-7358. DOI: 10.1371/journal.pcbi.1008510.

Crick, Francis (Nov. 1984). "Neurobiology: Memory and Molecular Turnover". In: *Nature* 312.5990, pp. 101–101. ISSN: 0028-0836, 1476-4687. DOI: 10.1038/312101a0.

Cui, Edward D. and Ben W. Strowbridge (2018). "Modulation of Ether-à-Go-Go Related Gene (ERG) Current Governs Intrinsic Persistent Activity in Rodent Neocortical Pyramidal Cells". In: *The Journal of Neuroscience* 38.2, pp. 423–440. ISSN: 0270-6474. DOI: 10.1523/JNEUROSCI.1774-17.2017.

Davie, Jenny T et al. (Aug. 2006). "Dendritic Patch-Clamp Recording". In: *Nature Protocols* 1.3, pp. 1235–1247. ISSN: 1754-2189, 1750-2799. DOI: 10.1038/nprot.2006.164.

Davis, Graeme W. (July 2006). "Homeostatic Control of Neural Activity: From Phenomenology to Molecular Design". In: *Annual Review of Neuroscience* 29.1, pp. 307–323. ISSN: 0147-006X, 1545-4126. DOI: 10.1146/annurev.neuro.28.061604.135751.

Debanne, Dominique, Yanis Inglebert, and Michaël Russier (2019). "Plasticity of Intrinsic Neuronal Excitability". In: *Current Opinion in Neurobiology* 54, pp. 73–82. ISSN: 09594388. DOI: 10.1016/j.conb.2018.09.001.

Destexhe, Alain, Michael Rudolph, and Denis Paré (2003). "The High-Conductance State of Neocortical Neurons in Vivo." In: *Nature reviews. Neuroscience* 4.9, pp. 739–751. ISSN: 1471-003X. DOI: 10.1038/nrn1289.

Dixon, Rose E. et al. (July 2022). "Mechanisms and Physiological Implications of Cooperative Gating of Clustered Ion Channels". In: *Physiological Reviews* 102.3, pp. 1159–1210. ISSN: 0031-9333. DOI: 10.1152/physrev.00022.2021.

Dorval, Alan D, David J Christini, and John A White (2001). "Real-Time Linux Dynamic Clamp: A Fast and Flexible Way to Construct Virtual Ion Channels in Living Cells". In: *Annals of Biomedical Engineering* 29, p. 11.

Dufour, Martial A et al. (Oct. 2014). "Non-Linear Developmental Trajectory of Electrical Phenotype in Rat Substantia Nigra Pars Compacta Dopaminergic Neurons". In: *eLife* 3. Ed. by Ronald L Calabrese, e04059. ISSN: 2050-084X. DOI: 10.7554/eLife.04059.

Durstewitz, Daniel, Jeremy K. Seamans, and Terrence J. Sejnowski (2000). "Neurocomputational Models of Working Memory". In: *Nature Neuroscience* 3.11, pp. 1184–1191. ISSN: 1097-6256. DOI: 10.1038/81460.

Egorov, Alexei V et al. (Nov. 2002). "Graded Persistent Activity in Entorhinal Cortex Neurons." In: *Nature* 420.6912, pp. 173–8. ISSN: 0028-0836. DOI: 10.1038/nature01171.

Egorov, Alexei V., Klaus Unsicker, and Oliver Von Bohlen Und Halbach (2006). "Muscarinic Control of Graded Persistent Activity in Lateral Amygdala Neurons". In: *European Journal of Neuroscience* 24.11, pp. 3183–3194. ISSN: 0953816X. DOI: 10.1111/j.1460-9568.2006.05200.x.

Emiliani, Valentina et al. (Oct. 2015). "All-Optical Interrogation of Neural Circuits". In: *Journal of Neuroscience* 35.41, pp. 13917–13926. ISSN: 0270-6474, 1529-2401. DOI: 10.1523/JNEUROSCI.2916-15.2015.

Eyal, Guy et al. (2016). "Unique Membrane Properties and Enhanced Signal Processing in Human Neocortical Neurons". In: *eLife* 5, pp. 1–18. ISSN: 2050084X. DOI: 10.7554/eLife.16553.

Franci, Alessio, Guillaume Drion, and Rodolphe Sepulchre (Mar. 2018). "Robust and Tunable Bursting Requires Slow Positive Feedback". In: *Journal of Neurophysiology* 119.3, pp. 1222–1234. ISSN: 0022-3077, 1522-1598. DOI: 10.1152/jn.00804.2017.

Fransén, Erik et al. (2006). "Mechanism of Graded Persistent Cellular Activity of Entorhinal Cortex Layer V Neurons". In: *Neuron* 49.5, pp. 735–746. ISSN: 08966273. DOI: 10.1016/j.neuron.2006.01.036.

Fröhlich, Flavio et al. (Oct. 2008). "Potassium Dynamics in the Epileptic Cortex: New Insights on an Old Topic". In: *The Neuroscientist* 14.5, pp. 422–433. ISSN: 1073-8584. DOI: 10.1177/1073858408317955.

Gentet, Luc J., Greg J. Stuart, and John D. Clements (July 2000). "Direct Measurement of Specific Membrane Capacitance in Neurons". In: *Biophysical Journal* 79.1, pp. 314–320. ISSN: 00063495. DOI: 10.1016/S0006-3495(00)76293-X.

Gidon, Albert et al. (Jan. 2020). "Dendritic Action Potentials and Computation in Human Layer 2/3 Cortical Neurons". In: *Science* 367.6473, pp. 83–87. ISSN: 0036-8075, 1095-9203. DOI: 10.1126/science.aax6239.

Goaillard, Jean-Marc and Eve Marder (July 2021). "Ion Channel Degeneracy, Variability, and Covariation in Neuron and Circuit Resilience". In: *Annual Review of Neuroscience* 44.1, annurev-neuro-092920–121538. ISSN: 0147-006X, 1545-4126. DOI: 10.1146/annurev-neuro-092920-121538.

Goldman, Mark S. et al. (Nov. 2003). "Robust Persistent Neural Activity in a Model Integrator with Multiple Hysteretic Dendrites per Neuron". In: *Cerebral Cortex* 13.11, pp. 1185–1195. ISSN: 1047-3211. DOI: 10.1093/cercor/bhg095.

Goldman-Rakic, P. S. (1995). "Cellular Basis of Working Memory". In: *Neuron* 14.3, pp. 477–485. ISSN: 08966273. DOI: 10.1016/0896-6273(95)90304-6.

Golowasch, J. et al. (2009). "Membrane Capacitance Measurements Revisited: Dependence of Capacitance Value on Measurement Method in Nonisopotential Neurons". In: *Journal of Neurophysiology* 102.4, pp. 2161–2175. ISSN: 0022-3077. DOI: 10.1152/jn.00160.2009.

Gorur-Shandilya, Srinivas, Eve Marder, and Timothy O'Leary (Dec. 2020). "Activity-Dependent Compensation of Cell Size Is Vulnerable to Targeted Deletion of Ion Channels". In: *Scientific Reports* 10.1, p. 15989. ISSN: 2045-2322. DOI: 10.1038/s41598-020-72977-6.

Gouwens, Nathan W. et al. (July 2019). "Classification of Electrophysiological and Morphological Neuron Types in the Mouse Visual Cortex". In: *Nature Neuroscience* 22.7, pp. 1182–1195. ISSN: 1097-6256, 1546-1726. DOI: 10.1038/s41593-019-0417-0.

Gowers, Robert and Susanne Schreiber (Sept. 2021). "How Morphology Affects Neuronal Excitability Type". In: *Bernstein Conference*. G-Node. DOI: 10.12751/NNCN.BC2021.P036.

Grage, Stephan L. et al. (2011). "Bilayer-Mediated Clustering and Functional Interaction of MscL Channels". In: *Biophysical Journal* 100.5, pp. 1252–1260. ISSN: 15420086. DOI: 10.1016/j.bpj.2011.01.023.

Gutkin, Boris and G. Bard Ermentrout (2006). "Spikes Too Kinky in the Cortex?" In: *Nature* 440.7087, pp. 999–1000. ISSN: 14764687. DOI: 10.1038/440999a.

Hartline, D.K. and D.R. Colman (Jan. 2007). "Rapid Conduction and the Evolution of Giant Axons and Myelinated Fibers". In: *Current Biology* 17.1, R29–R35. ISSN: 09609822. DOI: 10.1016/j.cub.2006.11.042.

Hasenstaub, A. et al. (July 2010). "Metabolic Cost as a Unifying Principle Governing Neuronal Biophysics". In: *Proceedings of the National Academy of Sciences* 107.27, pp. 12329–12334. ISSN: 0027-8424, 1091-6490. DOI: 10.1073/pnas.0914886107.

Heiny, Judith A., Stephen C. Cannon, and Marino DiFranco (Sept. 2019). "A Four-Electrode Method to Study Dynamics of Ion Activity and Transport in Skeletal Muscle Fibers". In: *The Journal of General Physiology* 151.9, pp. 1146–1155. ISSN: 1540-7748. DOI: 10.1085/jgp.201912398.

Herculano-Houzel, Suzana (2009). "The Human Brain in Numbers: A Linearly Scaled-up Primate Brain". In: *Frontiers in Human Neuroscience* 3. ISSN: 1662-5161.

Hesse, Janina, Jan Hendrik Schleimer, and Susanne Schreiber (2017). "Qualitative Changes in Phase-Response Curve and Synchronization at the Saddle-Node-Loop Bifurcation". In: *Physical Review E* 95.5. ISSN: 24700053. DOI: 10.1103/PhysRevE.95.052203. arXiv: 1606.07398v2.

Hesse, Janina et al. (July 2022). "Temperature Elevations Can Induce Switches to Homoclinic Action Potentials That Alter Neural Encoding and Synchronization". In: *Nature Communications* 13.1, p. 3934. ISSN: 2041-1723. DOI: 10.1038/s41467-022-31195-6.

Hichri, Echrak, Zoja Selimi, and Jan P. Kucera (2020). "Modeling the Interactions Between Sodium Channels Provides Insight Into the Negative Dominance of Certain Channel Mutations". In: *Frontiers in Physiology* 11, p. 1423. ISSN: 1664-042X. DOI: 10.3389/fphys.2020.589386.

Hille, Bertil (2001). *Ion Channels of Excitable Membranes*. 3rd ed. Sunderland, Mass: Sinauer. ISBN: 978-0-87893-321-1.

Hocker, David and Il Memming Park (Mar. 2019). "Myopic Control of Neural Dynamics". In: *PLOS Computational Biology* 15.3. Ed. by Daniele Marinazzo, e1006854. ISSN: 1553-7358. DOI: 10.1371/journal.pcbi.1006854.

Hodge, Rebecca D. et al. (Sept. 2019). "Conserved Cell Types with Divergent Features in Human versus Mouse Cortex". In: *Nature* 573.7772, pp. 61–68. ISSN: 0028-0836, 1476-4687. DOI: 10.1038/s41586-019-1506-7.

Hodgkin, A. L. (1948). "The Local Electric Changes Associated with Repetitive Action in a Non-Medullated Axon". In: *The Journal of Physiology* 107.2, pp. 165–181. ISSN: 1469-7793. DOI: 10.1113/jphysiol.1948.sp004260.

Hodgkin, A. L. and A. F. Huxley (Aug. 1952). "A Quantitative Description of Membrane Current and Its Application to Conduction and Excitation in Nerve." In: *The Journal of Physiology* 117.4, pp. 500–44. ISSN: 0022-3751.

Huang, Min, Maxim Volgushev, and Fred Wolf (2012). "A Small Fraction of Strongly Cooperative Sodium Channels Boosts Neuronal Encoding of High Frequencies". In: *PLOS ONE* 7.5. DOI: 10.1371/journal.pone.0037629.

Iwasa, K. et al. (1986). "Evidence for Interactions between Batrachotoxin-Modified Channels in Hybrid Neuroblastoma Cells." In: *Biophysical journal* 50.3, pp. 531–7. ISSN: 0006-3495. DOI: 10.1016/S0006-3495(86)83491-9.

Izhikevich, E.M. (Sept. 2004). "Which Model to Use for Cortical Spiking Neurons?" In: *IEEE Transactions on Neural Networks* 15.5, pp. 1063–1070. ISSN: 1045-9227. DOI: 10.1109/TNN.2004.832719.

Izhikevich, Eugene M. (2006). *Dynamical Systems in Neuroscience: The Geometry of Excitability and Bursting*. The MIT Press. ISBN: 978-0-262-27607-8. DOI: 10.7551/mitpress/2526.001.0001.

Jin, Lei et al. (Sept. 2012). "Single Action Potentials and Subthreshold Electrical Events Imaged in Neurons with a Fluorescent Protein Voltage Probe". In: *Neuron* 75.5, pp. 779–785. ISSN: 0896-6273. DOI: 10.1016/j.neuron.2012.06.040.

Keleshian, A.M. et al. (Aug. 1994). "Superposition Properties of Interacting Ion Channels". In: *Biophysical Journal* 67.2, pp. 634–640. ISSN: 00063495. DOI: 10.1016/S0006-3495(94)80523-5.

Keleshian, Asbed M. et al. (Jan. 2000). "Evidence for Cooperativity Between Nicotinic Acetylcholine Receptors in Patch Clamp Records". In: *Biophysical Journal* 78.1, pp. 1–12. ISSN: 0006-3495. DOI: 10.1016/S0006-3495(00)76568-4.

Keller, Dagmar I. et al. (Aug. 2005). "Brugada Syndrome and Fever: Genetic and Molecular Characterization of Patients Carrying SCN5A Mutations". In: *Cardiovascular Research* 67.3, pp. 510–519. ISSN: 0008-6363. DOI: 10.1016/j.cardiores.2005.03.024.

Kim, Grace E. et al. (Dec. 2014). "Human Slack Potassium Channel Mutations Increase Positive Cooperativity between Individual Channels". In: *Cell Reports* 9.5, pp. 1661–1672. ISSN: 2211-1247. DOI: 10.1016/j.celrep.2014.11.015.

Kirst, Christoph et al. (July 2015). "Fundamental Structure and Modulation of Neuronal Excitability: Synaptic Control of Coding, Resonance, and Network Synchronization". In: *BioRxiv*. DOI: 10.1101/022475.

Koch, Christof (Dec. 1999). *Biophysics of Computation: Information Processing in Single Neurons*. Computational Neuroscience. Oxford University Press. ISBN: 978-0-19-518199-9.

Koch, Christof, Moshe Rapp, and Idan Segev (Mar. 1996). "A Brief History of Time (Constants)". In: *Cerebral Cortex* 6.2, pp. 93–101. ISSN: 1047-3211. DOI: 10.1093/cercor/6.2.93.

Kulik, Yelena et al. (Apr. 2019). "Dual Separable Feedback Systems Govern Firing Rate Homeostasis". In: *eLife* 8, e45717. ISSN: 2050-084X. DOI: 10.7554/eLife.45717.

Larimer, Phillip and Ben W. Strowbridge (Feb. 2010). "Representing Information in Cell Assemblies: Persistent Activity Mediated by Semilunar Granule Cells". In: *Nature Neuroscience* 13.2, pp. 213–222. ISSN: 1546-1726. DOI: 10.1038/nn.2458.

Lisman, J E (May 1985). "A Mechanism for Memory Storage Insensitive to Molecular Turnover: A Bistable Autophosphorylating Kinase." In: *Proceedings of the National Academy of Sciences* 82.9, pp. 3055–3057. DOI: 10.1073/pnas.82.9.3055.

Liu, Jia et al. (Mar. 2020). "Genetically Targeted Chemical Assembly of Functional Materials in Living Cells, Tissues, and Animals". In: *Science* 367.6484, p. 1372. DOI: 10.1126/science.aay4866.

Liu, Y and J P Dilger (1993). "Application of the One- and Two-Dimensional Ising Models to Studies of Cooperativity between Ion Channels." In: *Biophysical journal* 64.1, pp. 26–35. ISSN: 0006-3495. DOI: 10.1016/S0006-3495(93)81337-7.

Liu, Zheng et al. (Apr. 1998). "A Model Neuron with Activity-Dependent Conductances Regulated by Multiple Calcium Sensors". In: *The Journal of Neuroscience* 18.7, pp. 2309–2320. ISSN: 0270-6474, 1529-2401. DOI: 10.1523/JNEUROSCI.18-07-02309.1998.

Lundqvist, Mikael, Pawel Herman, and Earl K. Miller (2018). "Working Memory: Delay Activity, Yes! Persistent Activity? Maybe Not". In: *The Journal of Neuroscience* 38.32, pp. 7013–7019. ISSN: 0270-6474. DOI: 10.1523/JNEUROSCI.2485-17.2018.

Major, Guy and David Tank (2004). "Persistent Neural Activity: Prevalence and Mechanisms". In: *Current Opinion in Neurobiology* 14.6, pp. 675–684. ISSN: 09594388. DOI: 10.1016/j.conb.2004.10.017.

McCormick, David A., Yousheng Shu, and Yuguo Yu (Jan. 2007). "Hodgkin and Huxley Model — Still Standing?" In: *Nature* 445.7123, E1–E2. ISSN: 1476-4687. DOI: 10.1038/nature05523.

Mizusaki, Beatriz E.P. and Cian O'Donnell (Oct. 2021). "Neural Circuit Function Redundancy in Brain Disorders". In: *Current Opinion in Neurobiology* 70, pp. 74–80. ISSN: 09594388. DOI: 10.1016/j.conb.2021.07.008.

Moreno, Claudia M et al. (May 2016). "Ca2+ Entry into Neurons Is Facilitated by Cooperative Gating of Clustered CaV1.3 Channels". In: *eLife* 5, e15744. ISSN: 2050-084X. DOI: 10.7554/eLife.15744.

Morozova, Ekaterina, Peter Newstein, and Eve Marder (Feb. 2022). "Reciprocally Inhibitory Circuits Operating with Distinct Mechanisms Are Differently Robust to Perturbation and Modulation". In: *eLife* 11. Ed. by Ronald L Calabrese et al., e74363. ISSN: 2050-084X. DOI: 10.7554/eLife.74363.

Murthy, Mala and Glenn Turner (Feb. 2013). "Whole-Cell In Vivo Patch-Clamp Recordings in the *Drosophila* Brain". In: *Cold Spring Harbor Protocols* 2013.2, pdb.prot071704. ISSN: 1940-3402, 1559-6095. DOI: 10.1101/pdb.prot071704.

Naundorf, Björn, Fred Wolf, and Maxim Volgushev (2006). "Unique Features of Action Potential Initiation in Cortical Neurons". In: *Nature* 440.7087, pp. 1060–1063. ISSN: 0028-0836. DOI: 10.1038/nature04610.

Navedo, Manuel F. et al. (2010). "Increased Coupled Gating of L-type Ca2+ Channels during Hypertension and Timothy Syndrome". In: *Circulation Research* 106.4, pp. 748–756. ISSN: 00097330. DOI: 10.1161/CIRCRESAHA.109.213363.

Neumcke, B. and R. Stämpfli (Jan. 1983). "Alteration of the Conductance of Na+ Channels in the Nodal Membrane of Frog Nerve by Holding Potential and Tetrodotoxin". In: *Biochimica et Biophysica Acta (BBA) - Biomembranes* 727.1, pp. 177–184. ISSN: 00052736. DOI: 10.1016/0005-2736(83)90382-6.

Newman, Ehren L. et al. (2012). "Cholinergic Modulation of Cognitive Processing: Insights Drawn from Computational Models". In: *Frontiers in Behavioral Neuroscience* 6.June, pp. 1–19. ISSN: 1662-5153. DOI: 10.3389/fnbeh.2012.00024.

Newman, Jonathan P et al. (July 2015). "Optogenetic Feedback Control of Neural Activity". In: *eLife* 4, e07192. ISSN: 2050-084X. DOI: 10.7554/eLife.07192.

Niemeyer, Nelson, Jan-Hendrik Schleimer, and Susanne Schreiber (Oct. 2021). "Biophysical Models of Intrinsic Homeostasis: Firing Rates and Beyond". In: *Current Opinion in Neurobiology* 70, pp. 81–88. ISSN: 0959-4388. DOI: 10.1016/j.conb.2021.07.011.

Niles, W.D., R.A. Levis, and F.S. Cohen (Mar. 1988). "Planar Bilayer Membranes Made from Phospholipid Monolayers Form by a Thinning Process". In: *Biophysical Journal* 53.3, pp. 327–335. ISSN: 00063495. DOI: 10.1016/S0006-3495(88)83110-2.

Nörenberg, A. et al. (Jan. 2010). "Distinct Nonuniform Cable Properties Optimize Rapid and Efficient Activation of Fast-Spiking GABAergic Interneurons". In: *Proceedings of the National Academy of Sciences* 107.2, pp. 894–899. ISSN: 0027-8424, 1091-6490. DOI: 10.1073/pnas.0910716107.

Nusser, Zoltan (June 2012). "Differential Subcellular Distribution of Ion Channels and the Diversity of Neuronal Function". In: *Current Opinion in Neurobiology* 22.3, pp. 366–371. ISSN: 09594388. DOI: 10.1016/j.conb.2011.10.006.

O'Leary, Timothy (Apr. 2018). "Homeostasis, Failure of Homeostasis and Degenerate Ion Channel Regulation". In: *Current Opinion in Physiology* 2, pp. 129–138. ISSN: 24688673. DOI: 10.1016/j.cophys.2018.01.006.

O'Leary, Timothy et al. (2014). "Cell Types, Network Homeostasis, and Pathological Compensation from a Biologically Plausible Ion Channel Expression Model". In: *Neuron* 82.4, pp. 809–821. ISSN: 10974199. DOI: 10.1016/j.neuron.2014.04.002.

Öz, Pinar, Min Huang, and Fred Wolf (Aug. 2015). "Action Potential Initiation in a Multi-Compartmental Model with Cooperatively Gating Na Channels in the Axon Initial Segment". In: *Journal of Computational Neuroscience* 39.1, pp. 63–75. ISSN: 1573-6873. DOI: 10.1007/s10827-015-0561-9.

Patel, Yogi A. et al. (2017). "Hard Real-Time Closed-Loop Electrophysiology with the Real-Time eXperiment Interface (RTXI)". In: *PLOS Computational Biology* 13.5, e1005430. ISSN: 1553-7358. DOI: 10.1371/journal.pcbi.1005430.

Pauling, Linus (Apr. 1935). "The Oxygen Equilibrium of Hemoglobin and Its Structural Interpretation". In: *Proceedings of the National Academy of Sciences* 21.4, pp. 186–191. DOI: 10.1073/pnas.21.4.186.

Perez-Nieves, Nicolas et al. (Oct. 2021). "Neural Heterogeneity Promotes Robust Learning". In: *Nature Communications* 12.1, p. 5791. ISSN: 2041-1723. DOI: 10.1038/s41467-021-26022-3.

Pfeiffer, Paul et al. (Feb. 2020). "Clusters of Cooperative Ion Channels Enable a Membrane-Potential-Based Mechanism for Short-Term Memory". In: *eLife* 9, e49974. ISSN: 2050-084X. DOI: 10.7554/eLife.49974.

Pfeiffer, Paul et al. (Apr. 2022). "A Dynamic Clamp Protocol to Artificially Modify Cell Capacitance". In: *eLife* 11. Ed. by Ronald L. Calabrese and Jorge Golowasch, e75517. ISSN: 2050-084X. DOI: 10.7554/eLife.75517.

Plaksin, Michael, Shy Shoham, and Eitan Kimmel (Jan. 2014). "Intramembrane Cavitation as a Predictive Bio-Piezoelectric Mechanism for Ultrasonic Brain Stimulation". In: *Physical Review X* 4.1, p. 011004. ISSN: 2160-3308. DOI: 10.1103/PhysRevX.4.011004.

Prescott, Steven A. et al. (Dec. 2008). "Pyramidal Neurons Switch From Integrators In Vitro to Resonators Under In Vivo-Like Conditions". In: *Journal of Neurophysiology* 100.6, pp. 3030–3042. ISSN: 0022-3077, 1522-1598. DOI: 10.1152/jn.90634.2008.

Prinz, Astrid A., L. F. Abbott, and Eve Marder (2004). "The Dynamic Clamp Comes of Age". In: *Trends in Neurosciences* 27.4, pp. 218–224. ISSN: 01662236. DOI: 10.1016/j.tins.2004.02.004.

Prinz, Astrid A., Dirk Bucher, and Eve Marder (2004). "Similar Network Activity from Disparate Circuit Parameters". In: *Nature Neuroscience* 7.12, pp. 1345–1352. ISSN: 10976256. DOI: 10.1038/nn1352.

Ratliff, Jacob et al. (Apr. 2021). "Neuronal Oscillator Robustness to Multiple Global Perturbations". In: *Biophysical Journal* 120.8, pp. 1454–1468. ISSN: 0006-3495. DOI: 10.1016/j.bpj.2021.01.038.

Reyes, A. D., E. W. Rubel, and W. J. Spain (Feb. 1996). "In Vitro Analysis of Optimal Stimuli for Phase-Locking and Time-Delayed Modulation of Firing in Avian Nucleus Laminaris Neurons". In: *The Journal of Neuroscience* 16.3, pp. 993–1007. ISSN: 0270-6474, 1529-2401. DOI: 10.1523/JNEUROSCI.16-03-00993.1996.

Robinson, Hugh P.C. (Jan. 1994). "Conductance Injection". In: *Trends in Neurosciences* 17.4, p. 147. ISSN: 01662236. DOI: 10.1016/0166-2236(94)90088-4.

Rodriguez, Guillaume et al. (2018). "Conditional Bistability, a Generic Cellular Mnemonic Mechanism for Robust and Flexible Working Memory Computations". In: *The Journal of Neuroscience* 38.22, pp. 5209–5219. DOI: 10.1523/JNEUROSCI.1992-17.2017.

Roemschied, Frederic A. et al. (2014). "Cell-Intrinsic Mechanisms of Temperature Compensation in a Grasshopper Sensory Receptor Neuron". In: *eLife* 2014.3, pp. 1–23. ISSN: 2050084X. DOI: 10.7554/eLife.02078.

Rost, Benjamin R. et al. (July 2022). "Optogenetics at the Presynapse". In: *Nature Neuroscience*. ISSN: 1097-6256, 1546-1726. DOI: 10.1038/s41593-022-01113-6.

Santin, Joseph M. and David J. Schulz (May 2019). "Membrane Voltage Is a Direct Feedback Signal That Influences Correlated Ion Channel Expression in Neurons". In: *Current Biology* 29.10, 1683–1688.e2. ISSN: 09609822. DOI: 10.1016/j.cub.2019.04.008.

Sato, Daisuke et al. (2018). "A Model for Cooperative Gating of L-type Ca 2 + Channels and Its Effects on Cardiac Alternans Dynamics". In: *Plos Computational Biology* 14.1, pp. 1–18. DOI: 10.1371/journal.pcbi.1005906.

Sato, Daisuke et al. (Aug. 2019). "A Stochastic Model of Ion Channel Cluster Formation in the Plasma Membrane". In: *Journal of General Physiology* 151.9, pp. 1116–1134. ISSN: 0022-1295. DOI: 10.1085/jgp.201912327.

Schindler, H., F. Spillecke, and E. Neumann (Oct. 1984). "Different Channel Properties of Torpedo Acetylcholine Receptor Monomers and Dimers Reconstituted in Planar Membranes". In: *Proceedings of the National Academy of Sciences* 81.19, pp. 6222–6226. ISSN: 0027-8424, 1091-6490. DOI: 10.1073/pnas.81.19.6222.

Schleimer, Jan-Hendrik, Janina Hesse, and Susanne Schreiber (2019). "Spike Statistics of Stochastic Homoclinic Neuron Models in the Bistable Region". In: pp. 1–16. arXiv: 1902.00951.

Schreiber, Susanne et al. (2004). "Subthreshold Resonance Explains the Frequency-Dependent Integration of Periodic as Well as Random Stimuli in the Entorhinal Cortex". In: *Journal of Neurophysiology* 92.1, pp. 408–415. ISSN: 00223077. DOI: 10.1152/jn.01116.2003.

Schulz, D J et al. (2008). "Mechanisms of Voltage-Gated Ion Channel Regulation: From Gene Expression to Localization". In: 65, p. 17.

Schulz, David J, Jean-Marc Goaillard, and Eve Marder (Mar. 2006). "Variable Channel Expression in Identified Single and Electrically Coupled Neurons in Different Animals". In: *Nature Neuroscience* 9.3, pp. 356–362. ISSN: 1097-6256, 1546-1726. DOI: 10.1038/nn1639.

Schutter, Erik D E and Paul Smolen (1999). "Calcium Dynamics in Large Neuronal Models". In: *Methods in Neuronal Modeling: From Ions to Networks*. Ed. by Christof Koch and Idan Segev. ISBN: 0585375879 (electronic bk.) DOI: 10.1017/CBO9781107415324.004. arXiv: 1011.1669v3.

Sender, Ron, Shai Fuchs, and Ron Milo (Aug. 2016). "Revised Estimates for the Number of Human and Bacteria Cells in the Body". In: *PLOS Biology* 14.8, e1002533. ISSN: 1545-7885. DOI: 10.1371/journal.pbio.1002533.

Sengupta, Biswa et al. (July 2010). "Action Potential Energy Efficiency Varies Among Neuron Types in Vertebrates and Invertebrates". In: *PLOS Computational Biology* 6.7. Ed. by Karl J. Friston, e1000840. ISSN: 1553-7358. DOI: 10.1371/journal.pcbi.1000840.

Seung, H. Sebastian et al. (Apr. 2000). "Stability of the Memory of Eye Position in a Recurrent Network of Conductance-Based Model Neurons". In: *Neuron* 26.1, pp. 259–271. ISSN: 0896-6273. DOI: 10.1016/S0896-6273(00)81155-1.

Shapiro, Mikhail G. et al. (2017). "Infrared Light Excites Cells by Changing Their Electrical Capacitance". In: *Nature communications* 8, p. 16148. ISSN: 20411723. DOI: 10.1038/ncomms16148.

Sharp, Andrew A. et al. (1993). "The Dynamic Clamp: Artificial Conductances in Biological Neurons". In: *Trends in Neurosciences* 16.10, pp. 389–394. ISSN: 01662236. DOI: 10.1016/0166-2236(93)90004-6.

Sidiropoulou, Kyriaki, Eleftheria Kyriaki Pissadaki, and Panayiota Poirazi (Sept. 2006). "Inside the Brain of a Neuron". In: *EMBO Reports* 7.9, pp. 886–892. ISSN: 1469-221X. DOI: 10.1038/sj.embor.7400789.

Sigworth, F. J. (1980). "The Variance of Sodium Current Fluctuations at the Node of Ranvier". In: *The Journal of Physiology* 307.1, pp. 97–129. ISSN: 1469-7793. DOI: 10.1113/jphysiol.1980.sp013426.

Stemmler, Martin and Christof Koch (June 1999). "How Voltage-Dependent Conductances Can Adapt to Maximize the Information Encoded by Neuronal Firing Rate". In: *Nature Neuroscience* 2.6, pp. 521–527. ISSN: 1546-1726. DOI: 10.1038/9173.

Stemmler, Martin et al. (2011). "Energetically Optimal Action Potentials". In: *Advances in neural information processing systems* 24.

Stiefel, Klaus M., Boris S. Gutkin, and Terrence J. Sejnowski (Dec. 2008). "Cholinergic Neuromodulation Changes Phase Response Curve Shape and Type in Cortical Pyramidal Neurons". In: *PLOS ONE* 3.12. Ed. by Bard Ermentrout, e3947. ISSN: 1932-6203. DOI: 10.1371/journal.pone.0003947.

Swadlow, Harvey A. and Stephen G. Waxman (June 2012). "Axonal Conduction Delays". In: *Scholarpedia* 7.6, p. 1451. ISSN: 1941-6016. DOI: 10.4249/scholarpedia.1451.

Taylor, Adam L. (2012). "What We Talk about When We Talk about Capacitance Measured with the Voltage-Clamp Step Method". In: *Journal of Computational*

Neuroscience 32.1, pp. 167–175. ISSN: 09295313. DOI: 10.1007/s10827-011-0346-8.

Tegnér, Jesper, Albert Compte, and Xiao-Jing Wang (Dec. 2002). "The Dynamical Stability of Reverberatory Neural Circuits". In: *Biological Cybernetics* 87.5-6, pp. 471–481. ISSN: 03401200. DOI: 10.1007/s00422-002-0363-9.

Tripathy, Shreejoy J. et al. (Apr. 2014). "NeuroElectro: A Window to the World's Neuron Electrophysiology Data". In: *Frontiers in Neuroinformatics* 8, p. 40. ISSN: 1662-5196. DOI: 10.3389/fninf.2014.00040.

Turrigiano, G, L. Abbott, and E Marder (May 1994). "Activity-Dependent Changes in the Intrinsic Properties of Cultured Neurons". In: *Science* 264.5161, pp. 974–977. ISSN: 0036-8075, 1095-9203. DOI: 10.1126/science.8178157.

Turrigiano, Gina (July 2011). "Too Many Cooks? Intrinsic and Synaptic Homeostatic Mechanisms in Cortical Circuit Refinement". In: *Annual Review of Neuroscience* 34.1, pp. 89–103. ISSN: 0147-006X, 1545-4126. DOI: 10.1146/annurev-neuro-060909-153238.

Turrigiano, Gina G, Eve Marder, and L F Abbott (1996). "Cellular Short-Term Memory from a Slow Potassium Conductance." In: *Journal of Neurophysiology* 75.2, pp. 963–6. ISSN: 0022-3077. DOI: 10.1152/jn.1996.75.2.963.

Turrigiano, Gina G. and Sacha B. Nelson (Feb. 2004). "Homeostatic Plasticity in the Developing Nervous System". In: *Nature Reviews Neuroscience* 5.2, pp. 97–107. ISSN: 1471-0048. DOI: 10.1038/nrn1327.

Tyssowski, Kelsey M. et al. (Dec. 2019). "Firing Rate Homeostasis Can Occur in the Absence of Neuronal Activity-Regulated Transcription". In: *The Journal of Neuroscience* 39.50, pp. 9885–9899. ISSN: 0270-6474, 1529-2401. DOI: 10.1523/JNEUROSCI.1108-19.2019.

Tytgat, Jan and Peter Hess (Oct. 1992). "Evidence for Cooperative Interactions in Potassium Channel Gating". In: *Nature* 359.6394, pp. 420–423. ISSN: 1476-4687. DOI: 10.1038/359420a0.

Ullah, Ghanim and Steven J. Schiff (2009). "Tracking and Control of Neuronal Hodgkin-Huxley Dynamics". In: *Physical Review E - Statistical, Nonlinear, and Soft Matter Physics* 79.4, pp. 1–4. ISSN: 15393755. DOI: 10.1103/PhysRevE.79.040901.

Ursell, Tristan et al. (2007). "Cooperative Gating and Spatial Organization of Membrane Proteins through Elastic Interactions". In: *PLoS Computational Biology* 3.5, pp. 0803–0812. ISSN: 1553734X. DOI: 10.1371/journal.pcbi.0030081. arXiv: q-bio/0702031.

van Rossum, M.c.w., B. J. O'Brien, and R. G. Smith (May 2003). "Effects of Noise on the Spike Timing Precision of Retinal Ganglion Cells". In: *Journal of Neurophysiology* 89.5, pp. 2406–2419. ISSN: 0022-3077. DOI: 10.1152/jn.01106.2002.

Vervaeke, Koen et al. (Jan. 2006). "Contrasting Effects of the Persistent Na+ Current on Neuronal Excitability and Spike Timing". In: *Neuron* 49.2, pp. 257–270. ISSN: 08966273. DOI: 10.1016/j.neuron.2005.12.022.

Vivas, Oscar et al. (2017). "Proximal Clustering between BK and CaV 1.3 Channels Promotes Functional Coupling and BK Channel Activation at Low Voltage". In: *eLife* 6. ISSN: 2050-084X. DOI: 10.7554/eLife.28029.

Walker, Matthew C., Ivan Pavlov, and Dimitri M. Kullmann (Feb. 2010). "A 'sustain Pedal' in the Hippocampus?" In: *Nature Neuroscience* 13.2, pp. 146–148. ISSN: 1546-1726. DOI: 10.1038/nn0210-146.

Wang, Xiao-Jing (1999). "Synaptic Basis of Cortical Persistent Activity: The Importance of NMDA Receptors to Working Memory". In: *The Journal of Neuroscience* 19.21, pp. 9587–9603. ISSN: 0270-6474. DOI: 10.1523/JNEUROSCI.19-21-09587.1999.

White, John A., Jay T. Rubinstein, and Alan R. Kay (2000). "Channel Noise in Neurons". In: *Trends in Neurosciences* 23.3, pp. 131–137. ISSN: 01662236. DOI: 10.1016/S0166-2236(99)01521-0.

White, W. E. and S. L. Hooper (2013). "Contamination of Current-Clamp Measurement of Neuron Capacitance by Voltage-Dependent Phenomena". In: *Journal of Neurophysiology* 110.1, pp. 257–268. ISSN: 0022-3077. DOI: 10.1152/jn.00993.2012.

Winograd, Milena, Alain Destexhe, and Maria V Sanchez-Vives (2008). "Hyperpolarization-Activated Graded Persistent Activity in the Prefrontal Cortex." In: *PNAS* 105.20, pp. 7298–7303. ISSN: 0027-8424. DOI: 10.1073/pnas.0800360105.

Wu, Yue Kris et al. (Sept. 2020). "Homeostatic Mechanisms Regulate Distinct Aspects of Cortical Circuit Dynamics". In: *Proceedings of the National Academy of Sciences* 117.39, pp. 24514–24525. DOI: 10.1073/pnas.1918368117.

Yeramian, E., A. Trautmann, and P. Claverie (Aug. 1986). "Acetylcholine Receptors Are Not Functionally Independent". In: *Biophysical Journal* 50.2, pp. 253–263. ISSN: 00063495. DOI: 10.1016/S0006-3495(86)83459-2.

Zarubin, Dmitry, Ekaterina Zhuchkova, and Susanne Schreiber (2012). "Effects of Cooperative Ion-Channel Interactions on the Dynamics of Excitable Membranes". In: *Phys. Rev. E.C* 85.6. ISSN: 15393755. DOI: 10.1103/PhysRevE.85.061904.

Zylberberg, Joel and Ben W. Strowbridge (July 2017). "Mechanisms of Persistent Activity in Cortical Circuits: Possible Neural Substrates for Working Memory". In: *Annual Review of Neuroscience* 40.1, pp. 603–627. ISSN: 0147-006X. DOI: 10.1146/annurev-neuro-070815-014006.

Acknowledgements

First and foremost, I would like to thank Susanne Schreiber for her dedicated scientific and personal mentorship. As a theoretical neuroscientist, she taught me to look for principles in neural dynamics and at the same time never cease to appreciate and consider the beautiful quirks of real neurons. I am thankful for the clear advice, the continued support to explore and be curious, and the warm atmosphere of togetherness in the lab.

During all projects, I strongly profited from the always encouraging and knowledgeable conceptual and technical input of Jan-Hendrik Schleimer. I remember that the seed for the capacitance clamp was laid on the whiteboard in our office during one of our (typically never-ending, but deeply enjoyable) excursions into neuroscience and everything beyond (that unfortunately become so much rarer during the last years of the pandemic).

I am further grateful for the opportunity to have worked with so many knowledgeable and motivated colleagues on the projects in this cumulative thesis.

During my first winter as a PhD student, Andreas Draguhn kindly invited me to Heidelberg and gave us the opportunity to study virtual cooperative channels via the dynamic clamp. In fun recording days with patch magicians Franziska Lorenz and Alexei V. Egorov, I got the privilege to see and even hear real neurons spiking (persistently in a graded form), a valuable experience that motivated the continued combination of modeling and experiment in this thesis.

For the capacitance clamp, a decisive phase was the initial theoretical exploration by the wonderful Jiameng Wu during her lab rotation. The capacitance clamp would however not have come to life without the experimental expertise and generous support of Federico Barreda Jose Tomas, Imre Vida, and the other members of the Neuroanatomy lab (as well as roughly a hundred Pizza Campanola at Ristorante Roma). An excitable follow-up chapter of this collaboration was the project on Interneuron morphology together with Moritz Drangmeister, Yangfan Peng, and Jörg Geiger. I am also deeply indebted to Ekaterina Morozova and Eve Marder for the amazing lab exchange at Brandeis University, where we could test the technique in the same crab neurons that about thirty years earlier had served to develop the original dynamic clamp. Finally, in both experimental ventures, I am particularly thankful to Prof. Jan Benda who introduced me to the technical side of the dynamic clamp and tirelessly supported me in my struggles with RELACS and real-time Linux kernels.

Great support for writing the thesis came from early readers. I am thankful to Natalie, Fabian, Thomas, Robert, Martina, Philipp, Jana, and Friedhelm as

well as the collaborative writing group organized by Mahraz for helpful feedback on drafts and careful proofreading.

I would like to thank all my colleagues and fellow students at the Institute of Theoretical Biology (ITB) and at the Bernstein Center of Computational Neuroscience (BCCN) for creating such an enjoyable and interesting working environment. I am thankful for scientific discourse and happy chitchatting at coffee breaks, "PhD help desks", and exciting conference trips with both current "ITBlers" Nelson, Liz, Mahraz, Fabian, Philipp, Friedrich, Robert, Lousianne, Paula, Naomi, Gaspar, and Rike as well as Katha, Fred, Pia, Thomas, Erik, Roberta, Tiziano, Martina, Nikolai, Michiel, André, Rahul and José from earlier days. An especially memorable time was the organization of ENCODS2018 with Roberta, my fellow pirates Natalie and Susanne, and the other great people from the ENCODS crew.

At the ITB and the BCCN, I relied on invaluable administrative and technical support of Lisa Velosi, Magret Franke, Robert Martin, Elvira Lauterbach, Karin Winklhöfer, Angela Piater, Rike-Benjamin Schuppner and Andreas Hantschmann. I am further grateful for the funding and network provided by the SmartStart (Volkswagen foundation) and the BCCN graduate program (GRK 1589/2). I sincerely thank the organizers, lecturers, and other participants of the 2018 CAJAL course for a great summer month in Lisbon full of neuroscience. Last, not a single line of code in this PhD thesis would have been possible without open-source software.

A special round of thanks goes to all my friends who accompanied me during this wonderful time in Berlin. I also thank my family who has been a safe haven of laughter and kindness in good times and of care and support in difficult ones. My final thanks go to Jana for her loving company in so many small and big adventures.